# Effect of Saline and Non-Specific Insulin Binding on the Phase Behavior of Poly(Ethylene Glycol)-Grafted Phosphoethanolamine-Succinyl Model Membranes

*Muhammad Naeem Shahid*

**A Dissertation Submitted to the Faculty of Graduate Studies in Partial Fulfillment of the Requirements for the Degree of**

**Doctor of Philosophy**

**Graduate Program in Chemistry**

**York University**

**Toronto, Ontario**

**Canada**

September 2013

# Abstract

Poly (ethylene glycol)-grafted membrane-mimetic surfaces bearing negatively charged phospholipid headgroups have gained significant attention due to their promising contributions in numerous biomedical applications. The conformational properties of PEG chains have been mainly studied at the air/water interface, which does not elucidate much about its behavior at the physiological pH ~ 7.4. In this contribution, binary mixtures of a phosphoethanolamine-Succinyl bearing $C_{16}$ aliphatic chains, DPPE-Succinyl, and a PEG-phospholipid conjugate bearing a PEG chain of 2000 Da, DPPE-PEG2000, have been used as ideal models of bio-nonfouling membrane-mimetic surfaces. The effect of PBS with pH ~7.4 as well as each of its individual constituents including $Na_2HPO_4$, KCl, $KH_2PO_4$, and NaCl on the biophysical properties of model membrane was examined. Our findings suggest that saline and each of its individual constituents play a pivotal role in the phase and conformational behavior of PEG-grafted membrane models. Insulin as a model protein was then selected to further investigate the effect of phase and conformation behavior of PEG-grafted membrane models on protein/membrane interactions. The insulin/membrane interactions were quantified in terms of monolayer area expansion, $\Delta A$, penetration area, $A_p$, as well as protein binding degree, $\chi_p$. To the best of our knowledge, this study provides the first insight into mechanistic aspects of protein interactions with model negatively charged PEG-grafted membranes. This knowledge, may aid in understanding the in-vivo performance of advanced targeted therapeutic carriers.

*Dedicated to my Beloved Parents, Siblings, Wife and Lovely Daughter Ezzah*

# Acknowledgements

I would like to express my sincere gratitude to my supervisor, Dr. Valeria Tsoukanova for providing me this wonderful opportunity to work in her research group and complete this project. She has been really supportive and cooperative throughout this project and helped me achieve my goals in every step of the way. I would also like to take this opportunity to thank all my colleagues for their valuable help and moral support.

I would also like to thank my committee members Dr. Rene Fournier and Dr. Gerald F. Audette, for their continuing support and positive feedback throughout this project.

In addition, I am very thankful to Dr. Zoya Leonenko and Dr. Roger Lew for their valuable time and cooperation.

I also like to thank Dr. Howard Hunter and Dr. Derek Wilson for their support and cooperation in conducting the NMR and ESI-MS experiments, as well as Peter Liuni and Tamanna Rob for their help in ESI-MS analysis. Further, a sincere thanks to Dr. Logan WF Donaldson for using his CD instrument.

This dissertation would not be completed without thanking my parents and siblings whose prayers, encouragements and motivations have made this journey possible.

Most importantly, a special thanks to my wife, Kanwal, who helped me in the best way possible to complete this dissertation.

# Table of Contents

**Abstract** ii

**Dedication** iii

**Acknowledgements** iv

**Table of Contents** v

**List of Tables** ix

**List of Figures** x

**Symbols and Abbreviations** xv

**Chapter1: Introduction.....…….…… 1**

1.1 Grafted PEG Chains and Bio-Nonfouling…… 01
1.2 Conformation of PEG Chains Grafted onto Membrane-Mimetic Surfaces……... 05
1.3 Grafting Density of PEG Chains on Membranes-mimetic Surfaces…… 06
1.4 Interactions of Membrane-Mimetic Surfaces with Dissolved Proteins..... 07
1.5 Phase State of Membrane-mimetic Surfaces in the Non-specific interactions with Dissolved Biomolecules……..... 08
1.6 Phase Behavior of PEG-grafted Membrane-mimetic Surfaces……..... 09
1.7 Properties of Dissolved Biomolecules in the Non-Specific Interactions with PEG-grafted Membrane-Mimetic Surfaces……..... 10
1.8 Objectives…….... 12
1.8.1 Model Membranes and proteins…… 12
1.8.2 Langmuir Monolayers as Model Membrane-Mimetic Surfaces… 13
1.8.3 The Matrix Phospholipid for Model Membrane-Mimetic Surfaces…..... 16
1.8.4 The PEG-Phospholipid for Membrane-Mimetic Surface…….. 19
1.8.5 The Model Protein…… 21
1.8.6 Significance of Physiological pH ~7.4…….. 24
1.9 Methodology of the Study…..…… ..... 26
1.9.1 Monolayer Study at Air/Water Interface…….. . 26
1.9.2 Monolayer Study on PBS Subphase…….. 26
1.9.3 In-Situ Imaging of Monolayer Phase Behavior and PEG Distribution using EFM……..... 27
1.9.4 Synthesis of DPPE-PEG2000-FITC as a Fluorescent Probe……. 27
1.9.5 In-Situ Imaging of Insulin/Membrane Interactions by EFM……. 28
1.9.6 Quantification of Insulin/Monolayer Interaction Study……. 28

1.9.7 CD analysis of insulin structure upon Interactions with SUVs…. 29
1.10 References……. 30

**Chapter2: Experimental……..... 36**

2.1 Materials..... 36
2.2 Experimental Techniques……..... 38
2.2.1 Langmuir Technique…….. 38
2.2.1.1 Area per Phospholipid Molecule……. 41
2.2.1.2 Mean Molecular Area……..... 42
2.2.1.3 Surface Pressure Sensor/Wilhelmy Plate..... 44
2.2.1.4 Surface Pressure – Area ($\pi - A$) Isotherm..... 48
2.2.1.5 Preparation of Langmuir Monolayers and $\pi - A$ Isotherm Measurements..... 51
2.2.2 Surface Potential Measurements..... 52
2.2.3 In-Situ Epifluorescence Microscopy Imaging..... 56
2.2.3.1 Principle and Technical Specifications of EFM..... 56
2.2.3.2 Two-Channel EFM in Visualizing the Membrane Morphology and Insulin/Membrane Interactions..... 61
2.2.3.2.1 Phase State Imaging..... 61
2.2.3.2.2 PEG-Phospholipid Distribution Imaging..... 64
2.2.3.2.3 Insulin/Membrane Interaction Imaging..... 65
2.2.3.3 Low-Intensity Imaging in the FITC Channel..... 66
2.2.4 Basic Principle of Circular Dichroism Spectroscopy, CD..... 70
2.3 References..... 73

**Chapter3: Synthesis and Characterization of DPPE-PEG2000-FITC……..... 75**

3.1 Synthesis of FITC Labeled DPPE-PEG2000..... 78
3.2 Results and Discussion..... 81
3.2.1 Nuclear Magnetic Resonance (NMR) Spectroscopy Analysis of DPPE-PEG2000-FITC..... 81
3.2.2 ESI- Mass Spectroscopy (ESI-MS) Analysis of synthesized DPPE-PEG2000-FITC..... 87
3.2.3 Monolayer Properties of the DPPE-PEG2000-FITC Probe..... 90
3.2.4 In-Situ EFM Imaging of DPPE-PEG2000 and DPPE-PEG2000-FITC Monolayers..... 93
3.3 Conclusion..... 95
3.4 References..... 96

**Chapter 4: Phase Behaviour of DPPE-Succinyl Monolayers..... 97**

4.1 Results..... 98
4.1.1 Surface Pressure – Area ($\pi - A$) Isotherms of DPPE-Succinyl monolayers on water and PBS..... 98

4.1.2 Surface Pressure – Area ($\pi - A$) Isotherms of DPPE-Succinyl Monolayers on Basic Constituents of PBS..... 101
4.1.3 In-Situ Imaging of DPPE-Succinyl Monolayer Morphology on Water and PBS..... 104
4.1.4 In-Situ Imaging of DPPE-Succinyl Monolayer Morphology on the PBS Constituents..... 107
4.1.5 $\Delta V$, and $\psi_0$ – Potential for DPPE-Succinyl Monolayer..... 110
4.2 Discussion..... 112
4.2.1 PBS-Induced Changes in Monolayer Properties of DPPE-Succinyl..... 113
4.2.2 Effect of Saline: Contribution of Individual PBS Constituents to the Monolayer Behaviour of DPPE-Succinyl..... 115
4.3 Conclusion..... 119
4.4 References..... 120

**Chapter 5: Phase Behaviour of Binary Mixtures of DPPE-Succinyl/DPPE-PEG2000 Monolayers..... 122**

5.1 Results..... 122
5.1.1 Surface Pressure –Molecular Area ($\pi - A$) Isotherms for DPPE-PEG2000..... 123
5.1.2 In-Situ EFM Imaging of DPPE-PEG2000 Monolayers on Water and PBS..... 127
5.1.3 Surface Pressure – Mean Molecular Area ($\pi - A$) Isotherms for Mixed DPPE-Succinyl/DPPE-PEG2000 monolayers..... 129
5.1.4 Miscibility Analysis for Mixed DPPE-Succinyl/DPPE-PEG2000 Monolayers..... 132
5.1.5 In-Situ EFM Imaging of Mixed DPPE-Succinyl/DPPE-PEG2000 Monolayers on Water..... 135
5.1.6 In-Situ EFM Imaging of DPPE-Succinyl/DPPE-PEG2000 Monolayers on PBS..... 142
5.1.7 Surface Potential Measurements for Mixed DPPE-Succinyl/DPPE-PEG2000 Monolayers..... 147
5.2 Discussion..... 150
5.2.1 Lateral Compressibility in Identified Transitions in Mixed DPPE-Succinyl/DPPE-PEG2000 Monolayers..... 151
5.2.2 Effect of Saline on Phase and Conformational Transitions in DPPE-Succinyl/DPPE-PEG2000 Binary Mixtures..... 159
5.3 Conclusion..... 165
5.4 References..... 166

**Chapter 6: Binding Parameters of Insulin with Pure and Mixed DPPE-Succinyl/DPPE-PEG2000 Monolayers..... 168**

6.1 Results..... 169

6.1.1 Area Expansion Measurements for Insulin/Monolayer Interactions..... 169
6.1.1.1 Methodology for Area Expansion Measurements..... 169
6.1.1.2 Area Expansion Measurements for DPPE-Succinyl and Mixed DPPE-Succinyl/DPPE-PEG2000 Monolayers upon Interactions with Insulin..... 170
6.1.2 In-Situ Imaging of Insulin/Monolayer Interactions..... 181
6.1.2.1 Methodology for In-Situ Imaging by EFM..... 181
6.1.2.2 In-Situ Imaging of Insulin/DPPE-Succinyl Monolayer Interactions..... 182
6.2 Discussion..... 191
6.2.1 Insulin Penetration Area, $A_p$, for DPPE-Succinyl and Mixed DPPE-Succinyl/DPPE-PEG2000 Monolayers..... 192
6.2.2 Binding Degree of Insulin, $\chi_p$, for DPPE-Succinyl and Mixed DPPE-Succinyl/DPPE-PEG2000 Monolayers..... 197
6.2.3 Effect of Grafted PEG2000 Chains on Insulin/Monolayer Interactions..... 200
6.3 Conclusion..... 202
6.4 References..... 203

**Chapter 7: Insulin Conformation in Non-Specific Interactions with DPPE-Succinyl/DPPE-PEG2000 Model Membranes: CD Spectroscopy Study..... 205**

7.1.1 Molecular Dimensions of Insulin Molecule..... 205
7.1.2 Conformational Dynamics of Insulin Molecule..... 207
7.1.3 CD Spectroscopy for Insulin-Membrane Interactions..... 210
7.1.4 Preparation of Small Unilamellar Vesicles (SUVs)..... 213
7.1.5 Methodology of CD Measurements..... 213
7.2 Results and Discussion..... 214
7.2.1 In-Situ EFM Visualization of Insulin Interactions with DPPE-Succinyl/DPPE-PEG2000 Vesicles..... 214
7.2.2 Far-UV CD Spectrum of Native Insulin Molecule..... 217
7.2.3 Monitoring Changes in the Secondary Structure of Insulin upon Interactions with DPPE-Succinyl/DPPE-PEG2000 Membrane (SUVs) by CD..... 220
7.3 Conclusion..... 226
7.4 References..... 227

**Summary..... 229**

**Future Directions..... 231**

# List of Tables

**Table** **Page**

**5.1** Excess area, $\boldsymbol{A_{exc}}$, calculated using equation 5.1 for mixed monolayers containing 1, 3, 6 and 9 mol% DPPE-PEG2000 in DPPE-Succinyl at the air/water interface at various surface pressures..... 134

**5.2** Excess area, $\boldsymbol{A_{exc}}$, calculated using equation 5.1 for mixed monolayers containing 1, 3, 6 and 9 mol% DPPE-PEG2000 in DPPE-Succinyl at the air/PBS interface at various surface pressures..... 134

**6.1** Degree of insulin binding, $\chi_p$, for DPPE-Succinyl and mixed DPPE-Succinyl/DPPE-PEG2000 monolayers calculated from $\Delta A_{ss}$ data by using equation 6.4..... 199

**7.1** Changes in the α-helical structure content of insulin due to PEG increment in vesicles..... 225

# List of Figures


**Figure** **Page**

**1.1** Chemical structure of poly (ethylene glycol) monomer..... 04

**1.2** Schematic diagram of a pure and PEGylated phospholipid monolayer as membrane model demonstrating the non-specific binding of protein..... 04

**1.3** Schematics diagram of a typical liposome/vesicle illustrating the phospholipid arrangements in a bilayer..... 15

**1.4** Chemical structure of DPPE-Succinyl molecule displaying hydrophobic aliphatic chains and hydrophilic headgroup connected by a phosphate group..... 18

**1.5** Chemical structure of DPPE-PEG2000 molecule displaying hydrophobic aliphatic chains and hydrophilic headgroup attached to PEG2000 and a phosphate group..... 20

**1.6** Crystal structure of bovine insulin molecule..... 23

**2.1** Schematics depicting a Langmuir trough with two teflon barriers..... 40

**2.2** Schematic diagram of phospholipid molecules at the air/water interface in a Langmuir trough..... 40

**2.3** A Schematic diagram of a whilhelmy plate illustrating the dimensions of a rectangular plate, when submerged in an aqueous medium..... 47

**2.4** Schematics diagram of a $\pi - A$ isotherm illustrating the various phase transitions of phospholipid molecules on air/water interface..... 50

**2.5** Schematics illustrating the principle of vibrating electrode method for surface potential measurements..... 55

**2.6** Schematic diagram of an EFM interfaced with the NIMA trough depicting its principle using excitation filter, emission filter, and dichroic mirror..... 58

**2.7** **a)** Spectral profile of TRITC fluorophore **b)** Spectral profile of FITC fluorophore..... 59

**2.8** Spectral profile of a) FITC fluorophore depicting blue line as an efficient excitation profile from 465 -495 nm and red line as emission intensity spectrum from 510 – 560 nm. b) Spectral profile of TRITC probe exhibiting blue line as an efficient excitation profile from 530 – 560 nm and red line as emission intensity spectrum from 590 – 650 nm.... 60

**2.9** Chemical structure of fluorescent probe, DOPE-Rh..... 63

**2.10** Image A of the monolayer was captured through TRITC channel using HBO lamp; Image B was captured by EFM via FITC channel using HBO lamp; Image C of the monolayer was captured using FIITC channel with X-Cite (120W) lamp; Image D was captured through the FITC channel using the Laser Glow Technology, laser and a lens focusing directly on the area of interest..... 69

**2.11** Schematics of a laser arm with a focusing lens coupled with EFM..... 69

**2.12** Schematics illustrating the principle of Circular Dichroism Spectrophotometer..... 72

**3.1** Chemical Structures of (**a**) DPPE-PEG2000 and (**b**) DPPE-PEG2000-FITC..... 77

**3.2** A chemical reaction scheme depicting the synthesis of DPPE-PEG2000-FITC by reacting DPPE with NHS-PEG2000-FITC..... 80

**3.3** Chemical structure and $^{1}H$ NMR Spectrum of DPPE-PEG2000-FITC in $CD_2Cl_2$. The letters on each peak corresponds to the protons present in the chemical structures of DPPE-PEG2000-FITC shown above..... 84

**3.4** 2D $^{1}H$ -$^{1}H$ COSY Spectrum of DPPE-PEG2000-FITC in $CD_2Cl_2$ displaying the proton correlation with their adjacent proton..... 85

**3.5** 2D $^{1}H$ – $^{13}C$ HMBC Spectrum of DPPE-PEG2000-FITC in $CD_2Cl_2$ exhibiting the proton correlation with their attached $^{13}C$..... 86

**3.6** The ESI-MS spectrum of DPPE-PEG2000-FITC analyzed over an area of 400 to 3000 m/z. The peak area from 700 – 1050 m/z indicates a +3 charge distribution and from 1100 to 1500 m/z exhibits +2 charge distributions..... 88

**3.7** An enlarged view of the ESI-MS spectrum of DPPE-PEG2000-FITC analyzed over an area of 1100 to 1500 m/z..... 89

**3.8** $\pi - A$ isotherms of (red dotted line) DPPE-PEG2000, (black solid line) DPPE-PEG2000-FITC and (green dashed line) NHS-PEG2000-FITC measured on water as a subphase..... 92

**3.9** EFM images of DPPE-PEG2000 monolayer containing 0.5 mol % DPPE-PEG2000-FITC. Images were captured at 25 mN/m on water (*a*) and at 42 mN/m on PBS (*b*) at 20 ± 1 °C. Image size 250 x 250 $\mu m^2$. The scale bar is 50 $\mu m$..... 94

**4.1** $\pi -$ *A* isotherms of DPPE-Succinyl monolayer on water and PBS as a subphase..... 100

**4.2** $\pi -$ *A* isotherms of DPPE-Succinyl monolayer on PBS (black dashed curve), NaCl (Blue), $Na_2HPO_4$ (Brown), KCl (green), $KH_2PO_4$ (Pink) and water (gray dashed curve) as a subphase, respectively..... 103

**4.3** EFM images of DPPE-Succinyl monolayer captured on water (*a, b, c*) and PBS (*d, e, f*) at 20 ± 1°*C*..... 106

**4.4** EFM images of DPPE-Succinyl monolayer containing 1 mol % DOPE-Rh as fluorescent probe, Images (*a, b)* captured at 9 and 15 mN/m on $KH_2PO_4$, (*c, d*) at 18 and 29 mN/m on KCl, (*e, f*) at 21 and 47 mN/m on $Na_2HPO_4$ , (*g, h*) at 24 and 49 mN/m on NaCl, respectively as subphases at 20 ± 1 °*C*..... 109

**5.1** $\pi - A$ isotherms of DPPE-PEG2000 monolayer on water and PBS as a subphase.... 125

**5.2** The schematics of PEG-phospholipid molecules conformational transition from pancake to pseudo-brush..... 126

**5.3** The schematics of PEG-phospholipid molecules arrangement, showing partially submerged PEG2000 chains in the subphase..... 126

**5.4** EFM images of DPPE-PEG2000 monolayer containing 1 mol % DOPE-Rh. Images were captured at 25 mN/m on water (*a*) and at 42 mN/m on PBS (*b*) at 20 ± 1 °C. Image size 250 x 250 $\mu m^2$. The scale bar is 50 $\mu m$..... 128

**5.5** **(a)** $\pi$ - *A* isotherms of mixed DPPE-Succinyl/DPPE-PEG2000 monolayers on water (a) and PBS (b) subphase at 20 ± 1 °C..... 131

**5.6** EFM images of 1 mol % DPPE-PEG2000 in DPPE-Succinyl monolayer on water as a subphase at 20 ± 1 °C..... 139

**5.7** EFM images of 3 mol % DPPE-PEG2000 in DPPE-Succinyl monolayer on water as a subphase at 20 ± 1 °C..... 139

**5.8** EFM images of 6 mol % DPPE-PEG2000 in DPPE-Succinyl monolayer on water as a subphase at 20 ± 1 °C..... 140

**5.9** EFM images of 9 mol % DPPE-PEG2000 in DPPE-Succinyl on water as a subphase at 20 ± 1 °C..... 140

**5.10** Percentage of Dark DOPE-Rh-excluded LC phase domains plotted against surface pressure for DPPE-Succinyl and mixed DPPE-Succinyl/DPPE-PEG2000 monolayers on water at 20 ± 1 ºC. ..... 141

**5.11** EFM images of 1 mol % DPPE-PEG2000 in DPPE-Succinyl monolayer on PBS as a subphase at 20 ± 1 °C..... 144

**5.12** EFM images of 3 mol % DPPE-PEG2000 in DPPE-Succinyl monolayer on PBS as a subphase at 20 ± 1 °C..... 144

**5.13** EFM images of 6 mol % DPPE-PEG2000 in DPPE-Succinyl monolayer on PBS as a subphase at 20 ± 1 °C..... ..... 145

**5.14** EFM images of 9 mol % DPPE-PEG2000 in DPPE-Succinyl monolayer on PBS as a subphase at 20 ± 1 °C..... 145

**5.15** Percentage of Dark DOPE-Rh-excluded LC phase domains plotted against surface pressure for DPPE-Succinyl and mixed DPPE-Succinyl/DPPE-PEG2000 monolayers on PBS at 20 ± 1 ºC..... 146

**5.16** Surface potential, $\Delta V$, as a function of mol % PEG for monolayers spread on water ($\Delta V_{H2O}$) and PBS ($\Delta V_{PBS}$) at 20 ± 1°C..... 149

**5.17** Lateral compressibility curves , *C*, with respect to surface pressure, $\pi$, for DPPE-Succinyl, DPPE-PEG2000 as well as their binary mixtures containing 1, 3, 6, and 9 mol % DPPE-PEG2000 in DPPE-Succinyl..... 157

**5.18** Lateral compressibility , *C*, with respect to surface pressure, $\pi$, for DPPE-Succinyl, DPPE-PEG2000 as well as their binary mixtures containing 1, 3, 6, and 9 mol % DPPE-PEG2000 in DPPE-Succinyl..... 158

**5.19** Phase diagrams for the binary DPPE-Succinyl/DPPE-PEG2000 mixtures at the air/water interface (A) and on PBS subphase (B)..... 164

**6.1** A schematics illustrating the area expansion data analysis..... 174

**6.2** Insulin-induced changes in the pure DPPE-Succinyl monolayers mean molecular area as a function of time..... 175

**6.3** Insulin-induced changes in the 1 mol% DPPE-PEG2000 in DPPE-Succinyl monolayers mean molecular area as a function of time..... 176

**6.4** Insulin-induced changes in the 3 mol% DPPE-PEG2000 in DPPE-Succinyl monolayers mean molecular area as a function of time..... 177

**6.5** Insulin-induced changes in the 6 mol% DPPE-PEG2000 in DPPE-Succinyl monolayers mean molecular area as a function of time..... 178

**6.6** Insulin-induced changes in the 9 mol% DPPE-PEG2000 in DPPE-Succinyl monolayers mean molecular area as a function of time..... 179

**6.7** **S**ummarized data of the $\Delta A_{ss}$ values obtained for monolayers plotted with respect to $\pi$ with different mol% PEG..... 180

**6.8** (A) EFM image displaying the monolayer morphology of DPPE-Succinyl monolayer on PBS subphase at $\pi \approx$ 15mN/m. Typical EFM images captured through TRITC (B) and FITC (C) channel for the Pure DPPE-Succinyl monolayer at a preset $\pi$ of 15mN/m... 185

**6.9** EFM image displaying the monolayer morphology of DPPE-Succinyl monolayer on PBS subphase at $\pi \approx$ 25mN/m..... 186

**6.10** EFM image displaying the monolayer morphology of DPPE-Succinyl monolayer on PBS subphase at $\pi \approx$ 35mN/m..... 187

**6.11** Typical EFM images captured through TRITC (A, B) and FITC (C) channel for the mixed DPPE-Succinyl/DPPE-PEG2000 monolayer containing 9 mol% PEG at a preset $\pi$ of 15mN/m..... 188

**6.12** Typical EFM images captured through TRITC (A, B, C) and FITC (D, E) channel for the mixed DPPE-Succinyl/DPPE-PEG2000 monolayer containing 9 mol% PEG at a preset $\pi$ of 25mN/m..... 189

**6.13** Typical EFM images captured through TRITC (A, B, C) and FITC (D, E) channel for the mixed DPPE-Succinyl/DPPE-PEG2000 monolayer containing 9 mol% PEG at a preset $\pi$ of 35mN/m..... 190

**6.14** A Semilogariphmic plot of $\Delta A_{ss}/A$ with respect to surface pressure, $\pi$, with different mol % PEG..... 196

**7.1** Secondary structure of an insulin monomer indicating the hydrophobic region containing mostly α−helices and β−strand (red line) as well as hydrophilic region bearing mostly α−helices (yellow line)..... 209

**7.2** Spectral Regions of CD and Chromospheres contributions from proteins..... 212

**7.3** A typical CD spectra of polypeptide indicating α−helix, β−sheet and random coil.... 212

**7.4** Snapshots of DPPE-Succinyl small unilamellar vesicles (SUV) (A) before the insulin (B) 2 hr after the insulin injection. The images were captured before and after CD measurements were performed. T = 20 ºC..... 216

**7.5** Snapshots of binary mixture containing 9 mol% DPPE-PEG2000 and DPPE-Succinyl small unilamellar vesicles (SUV) (A) before the insulin (B) 2 hr after the insulin injection. The images were captured before and after CD measurements were performed. T = 20 ºC..... 216

**7.6** Far-UV CD spectrum of native insulin in PBS, pH~7.4 at 20 ˚C..... 219

**7.7** Far-UV CD spectra beginning from (♦) 9 mol% (▲) 6 mol%, (■) 3 mol%, (●) 1 mol%, (○) DPPE-Succinyl and (--) the native insulin interacting with DPPE-Succinyl/DPPE-PEG2000 vesicles in PBS..... 224

# Symbols and Abbreviations

**DPPE-Succinyl** = 1, 2-Dipalmitoyl-sn-Glycero-3-Phosphoethanolamine-N-(Succinyl) (sodium salt)

**DPPE-PEG2000** = 1, 2-Dipalmitoyl-sn-Glycero-3-Phosphoethanolamine-N-[Methoxy(Polyethylene glycol)-2000

**DPPE** = 1, 2-Dipalmitoyl-sn-Glycero-3-Phosphoethanolamine

**DOPE-Rh =** 1, 2-Dioleoyl-sn-Glycero-3-phophoethanolamine-N-Lissamine Rhodamine B Sulfonyl (ammonium Salt)

**NHS-PEG2000-FITC** = N-hydroxysuccinimidyl-ester- N-(Polyethylene glycol)-2000-fluorescein-isothiocyanate

**PBS** = Phosphate buffered saline

**FITC-insulin** = Fluorescein isothiocyanate conjugate of human insulin

**Rh- insulin** = insulin labelled with rhodamine

**PEG** = Poly (ethylene glycol)

**LE** = Liquid expanded phase of monolayer

**LC** = Liquid condensed phase of monolayer

$\boldsymbol{L_O}$ = Liquid ordered phase

$\boldsymbol{L_D}$ = Liquid disordered phase

**G** = Gaseous phase of monolayer

**LE/LC** = Liquid expanded/Liquid condensed phase coexistence of monolayer

**C** = Collapse point for monolayer

**EFM** = Epifluorescence microscopy

**AFM** = Atomic Force Microscopy

**CD =** Circular Dichroism Spectroscopy

**ESI-MS** = Electrospray ionization mass spectrometry

**NMR** = Nuclear magnetic resonance spectroscopy

**SUVs** = Small unilamellar vesicles

$\boldsymbol{\pi}$ **=** Surface Pressure

$\boldsymbol{A}$ **=** Area per molecule

$\boldsymbol{\Delta V}$ = Surface potential

$\boldsymbol{A_p}$ = Penetration area of insulin

$\boldsymbol{\chi_p}$ = Binding degree of insulin

$\boldsymbol{\Delta A}$ = Change in area

**t** = time

$\boldsymbol{\pi - A}$ **=** Change in surface pressure with respect to area

$\boldsymbol{\Delta A - t}$ = Change in area with respect to time

$\boldsymbol{\Delta A_{ss}}$ = Steady-state value of change in area

**mol%** = mole percent

**mN/m** = Milli newton per meter

$\mathbf{nm^2}$ = Nano-meter square

**TRITC** = Texas red-isothiocyanate

**FITC** = Fluorescein-isothiocyanate

$\boldsymbol{N_A}$ = Avogadro's constant

$\boldsymbol{MW}$ = Molecular weight

**h** = Hour

**min** = Minutes

# Chapter 1: Introduction

There is a need to develop a variety of membrane-mimetic surfaces for tissue-contacting layers on implantable devices, biosensor platforms, microfluidic chips as well as drug delivery vesicles. Lipids in particular phospholipids are a natural choice; they are native to the body [Berg 2002; Tien 2000], can self-assemble in various structures including, monolayers, bilayers, liposomes, micelles, vesicles etc and incorporate various other molecules to suit the needs of various biomedical applications. Phospholipid membrane-mimetic surfaces are also considered most effective due to their reduced toxicity, enhanced bioavailability, and biocompatibility with promising targeted delivery options [Immordino 2006; Jesorka 2008; Mfuh 2011]. However, the major setback associated with these membrane-mimetic surfaces is the biofouling since they face a substantial resistance from serum proteins, platelets, thrombocytes, macrophages and numerous other bio-molecules. This may subsequently damage and/or reduce the efficiency of biomedical applications up to a threshold level [Dhruv 2009; Immordino 2006; Jebrail 2008; Jesorka 2008; Ratner 2004]. To overcome this problem various strategies can be used including grafting polymeric chains, in particular PEG-chains to the lipids.

## 1.1 Grafted PEG Chains and Bio-Nonfouling

A variety of approaches have been adopted to systematically develop membrane-mimetic surfaces with bio-nonfouling properties to mimic non-specific binding of dissolved biomolecules. Poly (ethylene glycol) (PEG), also known as poly (ethylene oxide) (PEO), is considered to be one of the best synthetic bio-nonfouling materials and has been studied extensively for its cell and protein resistance characteristics [Chen 2005; Ratner 2004]. The

chemical structure of PEG contains repeating units of ethylene oxide connected through oxygen atoms is shown in Figure 1.1. PEG chains are believed to be bio-nonfouling by creating a steric repulsive and entropic barrier upon forming a "hydration shell" with water molecules that H-bond with its ether oxygen [Allen 2002; Immordino 2006; Naumann 1999; Stepniewski 2011; Vermette 2003]. This repelling capacity of PEG chains is also described as an osmotic repulsion where PEG chains swell with water and form a water barrier to suppress the protein adsorption [Albertorio 2005; Merian 2012]. A schematic diagram illustrating the non-specific adsorption of protein on phospholipid monolayer as a model membrane is sketched in Figure 1.2 to better comprehend the protein binding degree prior to and after the incorporation of PEG as a bio-nonfouling material.

It has been reported that the number of water molecules bounded per PEG monomer unit in a free state in a PEG2000 chain is ~3.1, where the water molecules surround the polymer chain in a well-structured manner [Allen 2002; Albertorio 2005]. PEG has also been selected due to its characteristic behavior of bio-compatibility, hydrophilicity, non toxicity, chemically inertness, and steric stabilization. Other great features of PEG include its neutral, non-immunogenic, non-antigenic behaviour, and its solubility in both organic solvents and water [Allen 2002; Benhabbour 2008; Harris 1997; Lasic 1997; Ostuni 2001; Wu 2010].

Several methodologies can be adopted to graft PEG onto membrane-mimetic surface. These include the (i) physical adsorption or interpenetration of PEG onto the surface, (ii) covalently attaching to the reactive groups on the surface, and (iii) incorporation of PEG-phospholipid conjugate during preparation [Dalsin 2003; Immordino 2006; Ratner 2004]. The latter is considered as the most effective and efficient approach that can resist non-specific protein

binding for a longer period of time [Dalsin 2003; Immordino 2006; Ratner 2004] and hence will be used in our study. The resistance of PEG-grafted membranes towards non-specific protein binding is largely due to the high hydration of PEG-chains with water that creates a steric hindrance effect for the membrane-mimetic surfaces [Immordino 2006]. These unique properties have enabled PEG to be used in a variety of bio-medical and nano-medicine applications such as protein (antibodies, antigens, enzymes) immobilizations, microfluidic devices, lipoparticles, biosensors, drug modifications and designing of bio-nonfouling surfaces [Benhabbour 2008; Dhruv 2009; Harris 1991; Lasic 1997]. A wide range of PEGs with different molecular weights are commercially available. However, it has been reported that the non-fouling characteristics of PEG are mainly dependent on its surface chain density as well as the molecular weight of PEG in the membrane mimetic surfaces [Dhruv 1997; Harris 1992; Ostuni 2001; Ratner 2004; Sheth 1997]. Hence, there is a great need for designing a sufficiently thick and dense layer of PEG brushes to shield the membrane surface.

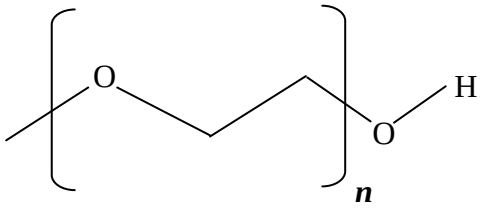


**Figure 1.1**: Chemical structure of poly (ethylene glycol) monomer.

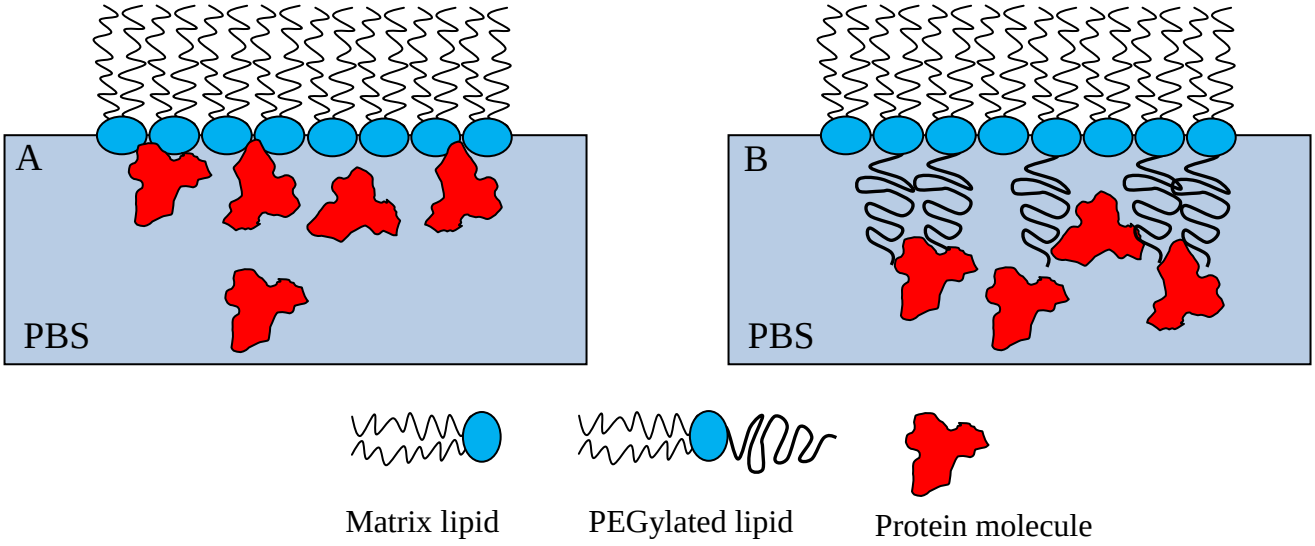


**Figure 1.2:** Schematic diagram of a pure and PEGylated phospholipid monolayer as a membrane model demonstrating the non-specific binding of protein. Part A shows a continuous binding of protein molecules at the hydrophilic/headgroup portion of the monolayer; however, Part B depicts a substantial resistance caused by the PEG chains and eventually repels the protein molecules away from the phospholipid layer.

### 1.2 Conformation of PEG Chains Grafted onto Membrane-Mimetic Surfaces

As stated above that there is a great need for creating a thick and dense layer of PEG brushes for optimal suppression of non-specific binding of dissolved biomolecules. A lot of research has been performed to figure out the type of polymer chains, in terms of MW and chain length, that have to be grafted to achieve the best non-fouling performance [Albertorio 2005; Allen 1991; Allen 2002; Hristova 1995; Immordino 2006; Kenworthy 1995b; Luna 2011; Shahid 2011; Stepniewski 2011; Tanwir 2012; Tsoukanova 2008]. For instance, incorporation of short PEG chains (i.e. 750 Da) in the stabilized plasmid-lipid particles has shown great transfection potency for non-viral gene transfer system [Mok 1999]. Medium PEG chains in the range of 1000 – 5000 Da are usually good for phospholipid therapeutic carriers as they have been shown to improve the blood residence time and reduce the non-specific adsorption of proteins [Immordino 2006; Luna 2011]. It has been reported that liposomes containing PEG of longer chains (i.e. 1900 and 5000 Da) remained in blood for longer period of time than the ones with shorter PEG chains (i.e. 120 and 750 Da) [Allen 1991; Immordino 2006]. Most importantly, PEG with molecular weight of 2000 Da doubled the liposome residence time as compared to PEG with smaller chains [Allen 2002; Allen 1991]. Moreover, it has also been reported that polymer chains with medium length (i.e. 2000 – 5000) increase the blood circulation time of liposomes, depending on the graft density of the polymer, since they are in stretched brush conformation [Kenworthy 1995a]. Conversely, chains larger than 5000 Da are not suitable for self-assembled phospholipid aggregates or structures due to entanglement of bulky polymer chains, which causes phase separation and thus destabilize the membrane-mimetic surfaces [Bedu-Addo 1996; Maruyama 1991]. Some studies have also suggested that PEG chains larger than 2000 Da do not provide

sufficient resistance against protein adsorption [Benhabbour 2008]. Moreover, a study performed on immunoliposomes containing PEG2000 has shown optimal performance for target binding as compared to the ones containing PEG5000 [Mori, 1991]. Hence, the most universal size for PEG to be used in membrane-mimetic surface studies is considered to be 2000 Da and this is why we decided to use PEG2000 for our membrane model studies.

### 1.3 Grafting Density of PEG Chains on Membranes-mimetic Surfaces

Grafting density of PEG is another important factor along with the MW in determining the optimum bio-nonfouling performance. Grafting density is a measure of the PEG-phospholipid conjugate that can be incorporated into the self-assembled phospholipid aggregates without compromising its structural integrity. According to a study by Lasic, liposomes can incorporate up to 10 mol% PEG2000 or $\leq$ 7 mol% of PEG5000 in their formulation for optimum performance [Bedu-Addo 1996; Lasic 1995; Maruyama 1991; Vermette 2003]. Micelles can incorporate up to 10 mol% PEG [Vermehren 1998]. Stable bilayers containing $C_{16}$ aliphatic chain length can be obtained by incorporating up to 7 mol% PEG2000 whereas bilayer with $C_{18}$ aliphatic chain length can contain up to 10 mol% PEG2000 [Belsito 1998; Hristova 1995; Kuhl 1994; Rex 1998; Stepniewski 2011]. Hence, it can be deduced that both MW and grafting density of PEG chains are key factors to achieve maximum stability for PEG-grafted membrane mimetic surfaces.

As suggested by the literature, most applications use PEG-phospholipids grafted with PEG2000 in a range of 1 to 9 mol%, [Allen 2002; Bedu-Addo 1996; Blume 1990; Lasic 1995; Luna 2011; Stepniewski 2011; Tanwir 2012; Vermette 2003], hence, we mainly focus on those mol% in our study. However, at this point it is not entirely clear which mol% PEG2000 is the most efficient

for optimum bio-nonfouling properties for membrane-mimetic surfaces. Some reports have suggested that PEG2000 as low as 2 mol% and as high as 20 mol% can be added to enhance the bio-non-fouling properties of membrane-mimetic surfaces without losing the structural stability [Luna 2011; Rossi 2007; Xu 2001]. Thus, it will be of great interest to determine the optimal mixture composition containing PEG2000 that can be used to for efficient and enhanced membrane-mimetic surfaces.

Further, PEG conformation, in fact, may not be the only factor determining the bio-nonfouling properties of PEG-grafted membrane-mimetic surfaces. Other factors may include the membrane phase state and distribution of the PEG chains. There have been a few reports looking into the effect of PEG-phospholipid on the phase behavior of membrane-mimetic surfaces [Baekmark 1995; Lozano 2009a; Wiesenthal 1999]. However, there have been conflicting reports concerning the distribution of PEG chains [Kim 2004; Majewski 1997]. The precise knowledge of phase behavior as well as PEG distribution may be important for understanding the interactions of PEG-grafted membrane-mimetic surfaces with dissolved biomolecules, i.e. proteins, as discussed below.

### 1.4 Interactions of Membrane-Mimetic Surfaces with Dissolved Proteins

Non-specific adsorption of proteins onto the membrane-mimetic surfaces is known to be the first step to foreign body reaction, which further triggers the recognition of membrane-mimetic surfaces by various other dissolved bio-molecules [Benhabbour 2008; Dhruv 2009; Ratner 2004]. Non-specific interaction of proteins is described as the accumulation and/or penetration of dissolved proteins on to the membrane-mimetic surfaces without any covalent interactions [Dhruv 2009; Kiess 1997]. Non-specific protein interactions can eventually lead to a

considerable malfunctioning of the membrane-mimetic surface [Dhruv 2009]. The protein adsorption mechanism is primarily divided into three stages (i) initial stage (ii) the intermediate stage also known as the reversible bound stage and (iii) final stage considered as the irreversible stage which develops an adsorbed protein layer [Dhruv 2009; Krisdhasima 1992; Rabe 2007]. The overall driving forces involved during protein/membrane interactions include electrostatic interactions, intermolecular forces, hydrophobic interactions and hydrogen bonding. The outcome of these interactions mainly depends on (i) the membrane properties such as phase state, electrostatic properties as well as (ii) dissolved biomolecules (protein, enzymes) properties such as size, hydrophobic/hydrophilic domains, flexibility of protein structure, and local electrostatic properties [Andrade 1986; Dhruv 2009; Leckband 2000]. Hence, a comprehensive understanding of the biophysical properties of proteins such as size, structural conformation and charge distribution as well as the phase characterization of PEG grafted membrane-mimetic surfaces can play a key role in designing biocompatible bio-medical surfaces [Andrade 1986; Dhruv 2009].

### 1.5 Phase State of Membrane-Mimetic Surfaces in the Non-specific Interactions with Dissolved Biomolecules

Non-specific binding of dissolved biomolecules occurs at the molecular level, at some locations on the membrane-mimetic surface. It has been reported that proteins and enzyme mainly bind to the liquid-disordered (LE) phase. For example, proteins such as the surfactant protein C (SP-C), the lectins concanavalin A (Con A) and the glycoprotein fibronectin (Fn) tend to occupy the fluid phase of the phosphocholine membrane models [Baneyx 1999; Haas 1989; Nag 1996]. Some proteins have also been shown to interact through the boundary or bind directly to the liquid-

ordered (LC) phase. These proteins include small proteins such as streptavidin, Retinis Pigmentosa 2 (RP2) as well as poly(L-arginine) (PLA) [Boisselier 2012; Netz 1996; Schwieger 2009]. Hence, the non-specific binding appears to be highly localized and confined to certain domains of the membrane-mimetic surface, e.g. the LE phase domains because it is easier for proteins to fit in there [Baneyx 1999; Haas 1989; Netz 2008].

### 1.6 Phase Behavior of PEG-grafted Membrane-mimetic Surfaces

Although it is clear from the above discussion that the phase state plays a key role in non-specific interactions, the phase behavior of PEG-grafted membranes has not yet been systematically studied. Many reports suggest that the phase state may vary across PEG-grafted membranes. Images reported by Lozano et al. for vesicles suggest the coexistence of liquid-disordered ($L_d$) and gel ($L_\beta$ or $L_{\beta`}$) phase domains [Lozano 2009a; Lozano 2009b]. A similar coexistence has also been observed for other PEG-grafted membrane models, in particular monolayer [Lozano 2009b; Shahid 2011; Tanwir 2012]. In monolayer terms, $L_d$ phase is called the LE phase whereas $L_\beta$ phase refers to LC phase. According to a recent study by Tanwir et al., many factors affect the phase behavior of model PEG-grafted membranes [Tanwir 2012]. For example, an increase in PEG content and temperature increases the $L_d$ (LE) phase in PEG-grafted membranes, such an increase in LE phase may favor the non-specific binding of some dissolved biomolecules. However, it has never been looked at and an aim of our study is to address this issue.

## 1.7 Properties of Dissolved Biomolecules in the Non-Specific Interactions with PEG-grafted Membrane-Mimetic Surfaces

Several properties of dissolved biomolecules (i.e proteins and enzymes) may affect the non-specific interactions with PEG-grafted membrane-mimetic surfaces. These properties include size, hydrophobic/hydrophilic domains, flexibility of protein structure, and electrostatics.

Protein size is one of the major factors when it comes to the non-specific interactions with membrane-mimetic surfaces. Large proteins are likely to be repelled by the PEG chains but small proteins might cross through the repulsive barrier and penetrate the PEG-grafted membrane-mimetic surfaces [Halperin 2007; Rahmati 2008].

Hydrophobic interaction of proteins with PEG-grafted membrane-mimetic surfaces is also considered to play a key role in non-specific interactions. The non-specific binding of proteins may be driven by the tendency for hydrophobic residues on the outer surface of the proteins to minimize their exposure to the aqueous environment by inserting themselves into hydrophobic aliphatic chain region [Birdi 1976]. Furthermore, protein charge can also play an important role in non-specific interactions with PEG-grafted membrane-mimetic surfaces. The large negative charge on the protein and membrane may result in introducing a repulsive electrostatic interaction between them [Brehmer 2012; Farias, 1989; Schwieger 2009; Taneva 1995]. However, small negative charges on both protein and membrane may result in attraction [Wang 1998]. Moreover, some previous studies have also reported that grafted polymeric chains in the outer segment of the membrane may not always be efficient in repelling proteins but in contrast might attract proteins by changing their confirmation from the *trans-gauche-trans* (protein-repulsive) to *gauche* (protein-attractive) configuration [Allen 2002; Efremova 2000; Sheth 1997; Vermette 2003; Xu 2000]. In addition, the effect of aqueous medium, in particular its

temperature, pH and ionic strength, is also an important factor in the non-specific binding of proteins to membrane-mimetic surfaces [Dhruv 2009; Nieto-Suarez 2008].

As discussed above, most of the studies have used large proteins as their models including albumin, haemoglobin, immunoglobulin, fibrinogen as well as lysozyme and they were indeed repelled by the PEG-grafted membrane-mimetic surfaces [Efremova 2000; Liu 2007; Rahmati 2008; Vermette 2003]. However, only a few studies have investigated the interactions of PEG-grafted surfaces with small proteins, these studies showed that small proteins might aid in destabilizing the PEG-grafted membrane-mimetic surfaces [Halperin 2007; Rahmati 2008; Zhao 2002]. Thus, an understanding of the mechanistic nature of small proteins is really important to analyze their non-specific interactions with PEG-grafted membrane-mimetic surfaces. A lot of studies used zwitterionic membranes with small mol% PEG and negligible charge on the membrane that showed a repulsion behavior against proteins [Allen 2002; Kozarac 1987; Xu 2000]. However, some studies did report an increased non-specific binding onto charged PEG surfaces, regardless of the charge on the protein and membrane, opposite or the same [Farias 1989; Mohwald 1990; Peschke 1987; Zhao 2002]. It remains largely unclear and hence, the aim of our study is to elucidate the mechanism responsible for the non-specific binding of proteins. However, none of the studies have focused on the conformational changes in the protein upon binding to the PEG-grafted membrane-mimetic surfaces. Thus, we have also looked into the conformational changes of small protein upon interaction, in particular if unfolding occurs, upon binding to the membrane model.

## 1.8 Objectives

The motivation behind this project is to design fundamental guidelines to engineer sterically stabilized membranes including monolayers and vesicles with optimum incorporation of PEG-grafted phospholipids. This rationale can then serve as unique experimental models to develop and engineer efficient and controlled bio-nonfouling membrane mimetic surfaces. Furthermore, these membrane models can also provide comprehensive knowledge about different ways proteins can adsorb to destabilize and reduce the efficiency of membranes-mimetic surfaces. For this, the main objective of our study is to examine the effect of PEG content on the phase behavior of PEG-grafted membrane-mimetic surfaces in aqueous media of physiological relevance. The effect of the phase behavior of PEG-grafted membrane-mimetic surfaces on non-specific binding of proteins will also be studied. Then, the effect of the non-specific interactions with PEG-grafted phospholipid membranes on the conformational and structural properties of proteins will also be examined. Hence, a comprehensive analysis of phase behavior of PEG-grafted membrane models can play a significant role in selecting mixture compositions to achieve optimum performance of membrane-mimetic surfaces for various biomedical applications.

### 1.8.1 Model Membranes and proteins

To achieve the goals set out above, the choice of PEG-grafted membrane and protein model is crucial. For this study, we have selected negatively-charged PEG-grafted monolayers and small unilamaller vesicles (SUVs) as model PEG-grafted membrane-mimetic surfaces. These models were prepared by introducing a PEG-phospholipid, DPPE-PEG2000, into the matrix of an

anionic phospholipid, DPPE-Succinyl. Both are synthetic phospholipids and will be discussed in detail below. Human insulin has been selected as the model protein.

### 1.8.2 Langmuir Monolayers as Model Membrane-Mimetic Surfaces

Monolayers of phospholipid spread onto the surface of aqueous medium (referred to as the subphase) have proven to provide ideal models for biological membranes and various membrane-mimetic surfaces [ Eeman 2010; Gaines 1966; Lozano 2009a; Vermette 2003]. Monolayers are useful for various studies due to their stability, homogeneity as well as planar geometry [Zhao 2012]. The monolayers are conventionally prepared in a Langmuir trough and are called Langmuir monolayers. The phospholipid monolayer is held together by cohesive interactions between aliphatic chains whereas its headgroup region is exposed to the aqueous medium. Such a structure thus generally resembles the outer layer of liposome/vesicle membrane, solid-supported bilayers, phospholipid-coated microbubbles, and etc. [Eeman 2010; Gaines 1966; Lozano 2009a; Vermette 2003]. Moreover, there is a direct thermodynamic relationship between bilayers and monolayers since it is considered as an unzipped half of a typical bilayer as can be seen in Figure 1.3 [Baekmark 1999; Faure 1999]. Phospholipid monolayers have been proven useful in the studies of lipid-lipid and lipid-protein interactions since this membrane model allows precise control over several important parameters including the surface pressure, mean molecular area, density of lipids, subphase content and lipid composition [Allen 2002; Eeman 2010; Gaines 1966; Naumann 2001; Tanwir 2012; Vermette 2003; Zhao 2002]. A great number of challenges are often involved in visualizing the biomolecular interactions of membrane-mimetic surfaces, which can be overcome using monolayers and supported bilayers as membrane model systems [Moy 1986; Zhao 2012].

Several imaging techniques such as atomic force microscopy (AFM), EFM and electron microscopy can be used to study the biomolecular interactions of membrane models [Attwood 2013; Gozen 2011; Lozano 2009b; Mulligan 2011; Shahid 2011; Zhao 2012]. However, one of the major setbacks associated to study classical supported lipid bilayers using AFM is the proximity of membrane to the solid substrate, which may affect the properties of system including the mobility of membrane components as well as inclusion of transmembrane proteins [Mulligan 2011; Zhao 2012]. Recently, tethered lipid bilayers are being prepared by incorporating spacer molecules, such as polymers, carbohydrates, peptides and polyelectrolyte layers, which connect the lipid headgroups with the solid substrate [Mulligan 2011; Zhao 2012; Jackman 2012]. Each type of tether has their own advantages and disadvantages depending on the application including ruggedness and lack of aqueous layer [Jackman 2012]. Electron microscopy is also considered as a high resolution technique to study membrane models at a single atom level [Gozen 2011; Mueller 2000]. However, one of the major drawbacks with this technique is the difficulty to perform structural analysis in aqueous environment [Dorn 2010; Gozen 2011]. EFM can, hence, be used to study the biomolecular interactions of membrane models on aqueous phase [Boisselier 2012; El-Khouri 2011; Shahid 2011; Tanwir 2008]. In this study, monolayers were used as membrane models for our in-situ imaging study in particular in aqueous media of physiological relevance.

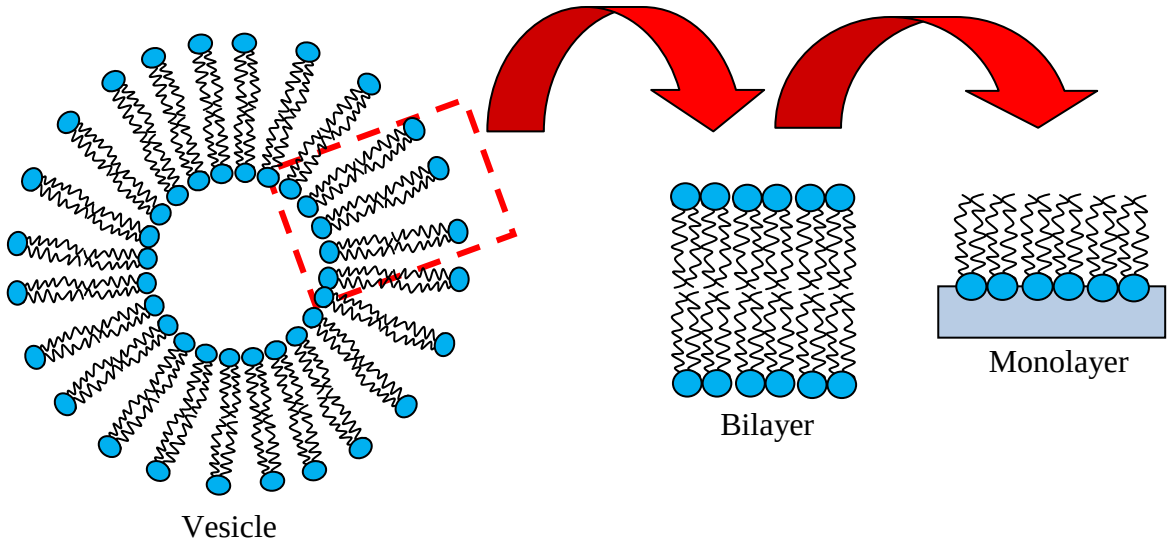


**Figure 1.3:** Schematics diagram of a typical liposome/vesicle illustrating the phospholipid arrangements in a bilayer. The blue circles represent the hydrophilic headgroup whereas the tails depict the hydrophobic region of the phospholipid molecules. The diagram is sketched based on the reference of [Biswas 2011]

### 1.8.3 The Matrix Phospholipid for Model Membrane-Mimetic Surfaces

A synthetic anionic phospholipid, dipalmitoyl phosphoethanolamine-succinyl (DPPE-Succinyl) has been selected as the matrix phospholipid for our study. DPPE-Succinyl, bearing a negatively-charged headgroup with $C_{16}$ aliphatic chains, belongs to the family of *N-c*arboxyacylamido-PEs (Figure 1.4). DPPE-Succinyl is the only phospholipid among the family of *N*-carboxyacylamido-PEs that closely resembles the phospholipid part of DPPE-PEG2000, a PEG-phospholipid most commonly used in various biomedical applications [Belsito 1998; Karve 2010; Tsoukanova 2008]. The negatively-charged headgroup of DPPE-Succinyl makes it pH-sensitive and this may be of great interest for the design of patterned PEG-lipid surfaces and tunable *pH*-sensitive colloidal lipid carriers for targeted delivery of therapeutic and diagnostic agents to tumors, metastatsis and various other inflammation sites [Cordeiro 2000; Immordino 2006; Karve 2010; Kung 1986; Lewis 2000; Nayar 1985; Shahid 2011; Vermette 2003; Zwaal 1998]. Some of the liposomal formulations containing negatively charged phospholipids have indeed reached the market and/or being tested in various clinical trials [Immordino 2006]. Furthermore, DPPE-Succinyl includes the immobilization capacity of various ligands on its headgroup via covalent coupling to the *N*-carboxyacylamido-PE group [Immordino 2006; Kung 1986; Shahid 2011]. For instance, a study by Lee et al. has conjugated poly(vinyl pyrrolidone) with DOPE-Succinyl to be used for lipid nano-particles drug delivery system [Lee 2007]. Another study by Soenen et al. has also successfully prepared magnetoliposomes using DPPE-Succinyl headgroup as a linker molecule to attach cationic tetrapeptide moiety for improved cellular uptake and reduced cytotoxic effects [Soenen 2009]. DPPE-Succinyl has a lot of good properties that may be used in various biomedical applications but its properties as a phospholipid for membrane-mimetic surfaces have never been systematically studied. This can be achieved using the monolayer as a

membrane model system. Binary mixtures of DPPE-Succinyl and DPPE-PEG2000 phospholipids were selected as ideal monolayer models to begin such a study. Hence, understanding the phase behavior of PEG grafted negatively charged membranes in an aqueous medium of biological relevance can play an essential role for numerous biomedical applications. This dissertation will highlight some of the important aspects related to negatively charged membrane model system that can aid in engineering efficient membrane mimetic surfaces.

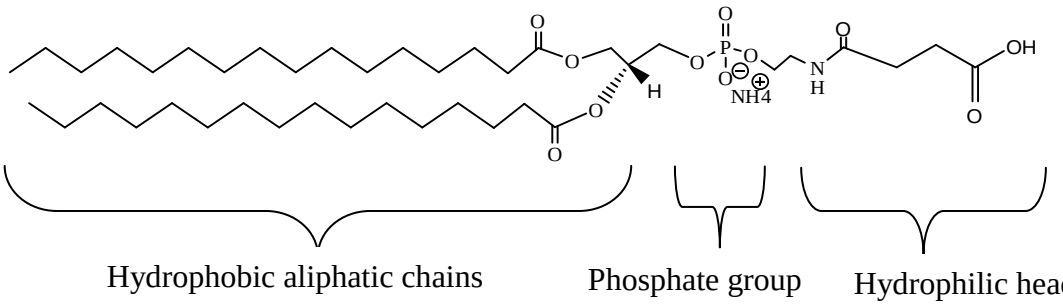


**Figure 1.4** Chemical structures of DPPE-Succinyl displaying hydrophobic aliphatic chains and hydrophilic headgroup connected by a phosphate group.

### 1.8.4 The PEG-Phospholipid for Membrane-Mimetic Surface

A synthetic PEG-grafted phospholipid, DPPE-PEG2000 has been selected to be incorporated in the matrix of DPPE-Succinyl for our study. DPPE-PEG2000 contains $C_{16}$ aliphatic chain length with 45 PEG monomers covalently attached to its headgroup (Figure 1.5). DPPE-PEG2000 is among the components commonly used in the model membrane studies for various biomedical applications including biosensor platforms and therapeutic delivery systems (Belsito 1998; Lasic 1995; Naumann 1999]. Various aspects of DPPE-PEG2000 behaviour in phospholipid membranes have been studied in detail. For instance Naumann and Coffman et al. studied the rheological properties of PEG chains in particular the formation of physical network between adjacent PEG chains and water molecules via hydrogen bonding [Coffman 2002; Naumann 1999]. A lot of studies were also aimed at understanding the conformational behavior of PEG2000 in monolayers at air/water interface [Albertorio 2005; Baekmark 1995; Faure 1999; Lozano 2009b; Majewski 1997; Vermehren 1998]. Further, a few studies have also looked at the high pressure transitions of DPPE-PEG2000 in monolayers at air/water interface [Ahrens 2001; Jebrail 2008]. However, none of the studies ever investigated the effect of DPPE-PEG2000 onto the phase behaviour of the host phospholipid matrix in particular, in the aqueous media of biological relevance. Thus, our main goal is to understand the effect of DPPE-PEG2000, on the phase properties of DPPE-Succinyl membranes at air/PBS interface.

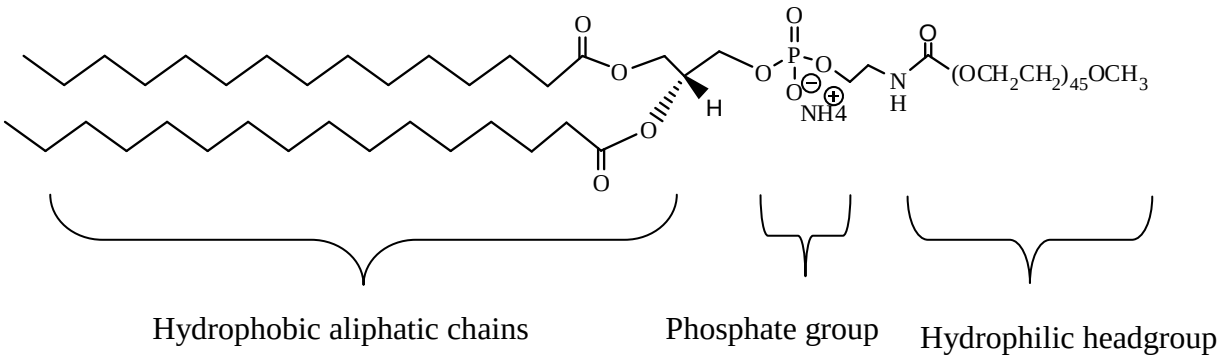


**Figure 1.5:** Chemical structures of DPPE-PEG2000 displaying hydrophobic aliphatic chains and hydrophilic headgroup attached to PEG2000 and a phosphate group.

### 1.8.5 The Model Protein

Human insulin has been selected as the model protein primarily because of its relatively small size. Insulin consists of 51 amino acids ($\alpha$-helix of 21 and $\beta$-helix of 30), bearing two disulphide linkage with a molecular formula of $C_{257}H_{383}N_{65}O_{77}S_6$ and molecular weight of 5808 Da (Figure 1.6) [Miller 2000; Yin 2005]. Chain A consisting of 21 residues is mainly hydrophilic and forms two antiparallel α−helices. It also bears two negative charges at pH of ~7. Conversely, chain B made up of 30 amino acid residues is hydrophobic and forms α−helix, turn, as well as β−strand conformation [Hong 2012; Nieto-Suarez 2008; Perez-Lopez 2011; Zlatica 1998]. Due to the small size and hydrophobic characteristics, it is believed to show high affinity towards hydrophobic surfaces [Birdi 1976; Kapishon 2008]. A study by Nieto-Suarez reported that at air/water interface, insulin hydrophilic chain A tends to submerge in the subphase whereas hydrophobic chain B stays at the surface [Nieto-Suarez 2008], similar to the hydrophobic aliphatic chains of phospholipids. Insulin is also considered to possess greater adsorption tendency towards the PEG-grafted surfaces as compared to large proteins i.e human serum albumin (HSA) [Rahmati 2008]. Moreover, our previous study has also reported that insulin injection underneath the PEG-grafted phospholipid monolayer causes a sudden increase in surface pressure, which is likely due to insulin penetration into the monolayer [Rahmati 2008]. Insulin is known to be negatively charged at physiological pH of ~7.4, yet it is known to significantly bind onto various negatively charged surfaces [Farias 1989; Lenz 1995; Nieto-Suarez 2008]. This makes it a good model for our study to figure out this "mysterious" mechanism. Understanding this mechanism may be of great importance for predicting the bio-fouling of PEG-grafted delivery of liposomes/vesicles in blood stream since insulin is present in blood at varying concentration range of 0.1 – 3 *ng/mL* [Browne 1973; Horwitz 1975].

Furthermore, understanding the mechanism can also be helpful for the development of oral, intranasal and pulmonary delivery systems for diabetes treatment as well as other biomedical applications [Cui 2006; Peng 2012].

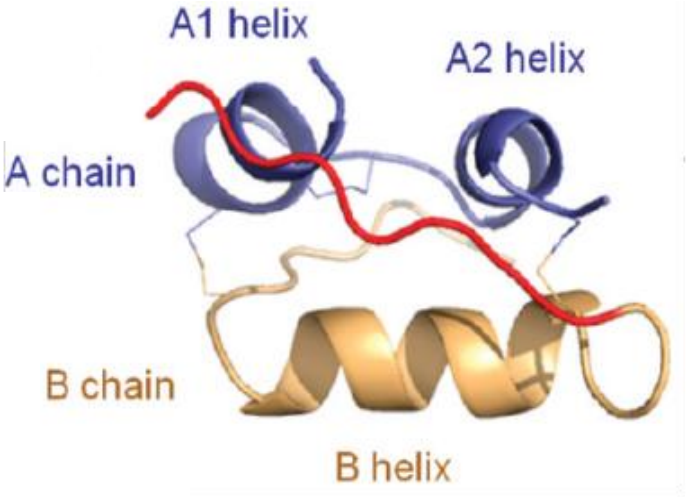


**Figure 1.6:** Crystal structure of bovine insulin molecule. Adopted from Hong et. al 2012. PDB ID: 2ZP6.

### 1.8.6 Significance of Physiological pH ~7.4

The selection of optimal experimental conditions (i.e physiological conditions) is one of the fundamental requirements in characterizing the properties of membrane-mimetic surfaces such as the miscibility of various components, phase and conformational transitions as well as biomolecular interactions. In fact, studies on many model systems such as bilayers, micelles, liposomes and etc. have been performed under physiological conditions, i.e PBS with pH ~7.4. Phosphate buffered saline (PBS) is a buffer with pH of ~7.4, containing different proportions of salts such as NaCl, KCl, $Na_2HPO_4$, $KH_2PO_4$ and can be used as a subphase for membrane model studies.

There is a need to directly visualize (image) the lipid/lipid and lipid/protein interactions at the molecular level that can be very challenging with micelles, liposomes and even bilayers as discussed above. For visualization studies, it would be ideal to use monolayers as membrane model system. In fact, a significant work has been done to observe the phase and conformational behavior of monolayers on air/water interface [Baekmark 1995; Faure 1999; Jebrail 2008; Karve 2010; Lozano 2009b; Majewski 1997; Naumann 1999; Rossi 2007; Tsukanova 2004; Tsoukanova 2008]. Many zwitterionic, PEG grafted monolayers made of DPPC, DPPE, DSPC, DSPE, etc as matrix phospholipids exhibited similar monolayer behavior both on water and PBS [Rossi 2007; Tanwir 2008]. Charged lipids, however, are known to be sensitive to the pH and/or components of the subphase [Angelova 1996; Dominguez 1998; Helm 1986; Mansour 2001; Patino 1996]. Their self-assembly, phase and conformational behavior as well as miscibility can change dramatically depending on the subphase. The subphase induced change in the electrostatic interactions in the headgroup region of the phospholipid matrix may affect the miscibility, stability, packing, as well as hydration effect, which has never gained much attention

previously [Aroti 2004; Domınguez 1998; Helm 1986]. Hence, a goal of our study is to investigate the difference between water and PBS with pH ~7.4 for negatively charged PEG-grafted membranes.

It has to be stressed that the conformational transition behaviour of PEG chains have been mainly studied on water but the effect of various counter ions on the conformational changes has not gained much attention [Ahrens 2001; Albertorio 2005; Allen 2002; Faure 1999; Kenworthy 1995b; Lozano 2009b; Majewski 1997; Vermehren 1998]. This motivated us to study the phase and conformational behaviour of PEG-grafted membranes with a simple system, containing monovalent counter ions, e.g. PBS. Divalent counter ions such as $Ca^{2+}$ and $Mg^{2+}$ can affect the PEG conformational behavior more significantly due to bridging effect and metal ion size [Vermette 2003]. The mechanism of such complex ions interactions with PEG-grafted model membranes would be hard to understand without the basic knowledge obtained with relatively simple counter ions. Hence, the focus of this project was to gain insight into the mechanism involved in the interactions between simple counter ions such as $Na^{+}$ and $K^{+}$ with PEG-grafted membranes. Most of the studies on PEG-grafted membrane models have previously been performed on water or aqueous subphases containing NaCl [Ahrens 2001; Albertorio 2005; Baekmark 1995; Coffman 2002; Faure 1999; Heeb 2009; Li 2013; Lozano 2009b; Majewski 1997; Nalam 2013; Naumann 1999; Vermette 2003; Vermehren 1998]. Based on these reports, it can be concluded that the conformation of PEG chains changes in the presence of counter ions. However, the effect of counter-ions-induced changes on the conformation of PEG chains and the non-specific protein binding has never been systematically studied. Therefore, this is, to the best of our knowledge, the first attempt to undertake such a systematic study of the phase and

conformation behavior of PEG-grafted membranes in the presence of counter ions and their effect on interactions with dissolved proteins.

### 1.9 Methodology of the Study

Various methods were adopted to study pure and PEG-grafted phospholipid membranes using monolayers and vesicles as membrane models. A comprehensive characterization was then performed to systematically study the phase state, conformational transitions as well the mechanism involved during non-specific insulin/membrane interactions.

#### 1.9.1 Monolayer Study at Air/Water Interface

Monolayers as membrane models of matrix phospholipid, DPPE-Succinyl, and the PEG-phospholipid, DPPE-PEG2000 were prepared at air/water interface. Phase behavior of the DPPE-Succinyl and DPPE-PEG2000 was analyzed using a two-dimensional Langmuir technique via surface pressure – area ($\pi - A$) isotherms. The phase, conformational behavior and miscibility of binary mixtures of DPPE-Succinyl and DPPE-PEG2000 by varying PEG content were also studied at air/water interface.

#### 1.9.2 Monolayer Study on PBS Subphase

To elucidate the effect of PBS on the membrane-mimetic surfaces, monolayer behavior of DPPE-Succinyl and DPPE-PEG2000 was studied at air/PBS interface. The monolayer properties including miscibility, phase and conformational behavior of binary mixtures of DPPE-Succinyl and DPPE-PEG2000 were examined by measuring their $\pi - A$ isotherms. Moreover, the phase

and PEG conformational transitions of pure and binary mixtures of DPPE-Succinyl and DPPE-PEG2000 were also characterized using compressibility analyses. To further analyze the contributions from each PBS constituent, the phase behavior of DPPE-Succinyl monolayer on the individual salt solutions of $KH_2PO_4$, KCl, $Na_2HPO_4$ and NaCl as a subphase was also studied.

### 1.9.3 In-Situ Imaging of Monolayer Phase Behavior and PEG Distribution using EFM

The second part of the project requires an inclusive visualization of the morphology and phase state of pure and mixed DPPE-Succinyl/DPPE-PEG2000 monolayers on both water and PBS. A unique setup of two-channel epifluorescence microscopy (EFM) with the possibility of utilizing two fluorescent probes simultaneously in the mixed monolayers was designed. This enabled us to observe the phase transitions of PEG-grafted membranes while monitoring the lateral distribution of PEG-phospholipid at the same time. 1, 2-Dioleoyl-sn-Glycero-3-phosphoethanolamine-N-Lissamine Rhodamine B Sulfonyl (ammonium Salt) (DOPE-Rh) was used as the fluorescent probe to examine the phase behavior in the pure and mixed DPPE-Succinyl/DPPE-PEG2000 monolayers. However, FITC probe needed to be attached to DPPE-PEG2000 to visualize the lateral distribution of PEG-phospholipid in the membrane model and is discussed below.

### 1.9.4 Synthesis of DPPE-PEG2000-FITC as a Fluorescent Probe

To study the lateral distribution of DPPE-PEG2000 in the binary mixtures of DPPE-Succinyl/DPPE-PEG2000, fluorescein-isothiocyanate (FITC), was coupled to DPPE-PEG2000 molecule. DPPE-PEG2000-FITC was hence synthesized in our lab followed by its comprehensive characterization using the typical Langmuir technique, 1H-NMR as well as ESI-

MS. Upon a successful synthesis of DPPE-PEG2000-FITC, the PEG-phospholipid distribution in the mixed DPPE-Succinyl/DPPE-PEG2000 monolayers was examined both on water and PBS using two-channel EFM.

### 1.9.5 In-Situ Imaging of Insulin/Membrane Interactions by EFM

Based on the significant involvement and bio-fouling properties of proteins against membrane-mimetic surfaces, the nonspecific binding of insulin on pure and mixed DPPE-Succinyl/DPPE-PEG2000 monolayers was studied. Direct imaging of insulin interactions with pure and PEGylated monolayers was performed using two-channel EFM. For this, fluorescein-labeled insulin (insulin-FITC) was used to monitor the interactions of insulin with pure and mixed monolayers. Conversely, the effect of insulin interactions on the phase behavior of the monolayers was visualized simultaneously using a phase state imaging probe, DOPE-Rh.

### 1.9.6 Quantification of Insulin/Monolayer Interactions

To quantify the insulin-induced expansion in pure and mixed monolayers, insulin binding parameters including change in monolayer molecular area upon insulin binding, $\Delta A$, penetration area of insulin, $A_p$, as well as the binding degree of insulin, $\chi_p$, were calculated. Insulin/membrane interactions were first examined by the surface characterization methodology where the effect of insulin on the monolayer area, $\Delta A$, is monitored with respect to time. The penetration area of insulin was calculated based on the $\Delta A$ measurements. Moreover, the degree of protein binding, $\chi_p$, was also estimated from the $\Delta A$ measurements after determining the $A_p$.

### 1.9.7 CD analysis of insulin structure upon Interactions with SUVs

The effect of insulin/membrane interactions on the insulin structure/conformation was examined using circular dichroism spectroscopy (CD). For this, small unilamellar vesicles (SUV) of pure DPPE-Succinyl and binary mixtures of DPPE-Succinyl/DPPE-PEG2000 as membrane models were prepared and their formation was verified by EFM. Then CD analysis on insulin secondary structure was performed after 2 hours of insulin/membrane interactions. The change in the SUV size was also observed by EFM after 2 hours of insulin/membrane interactions. The change in insulin α – helical content upon interactions with SUVs was also calculated.

## 1.10 References


Ahrens, H.; Papastavrou, G.; Helm, C. A. *Langmuir* **2001**, *17*, 3113.

Albertorio, F.; Diaz, A. J.; Yang, T.; Chapa, V. A.; Kataoka, S.; Castellana, E. T.; Cremer, P. S. *Langmuir* **2005,** *21*, 7476.

Allen, C.; Dos Santos, N.; Gallagher, R.; Chiu, G. N. C.; Shu, Y.; Li, W. M.; Johnstone, S. A.; Janoff, A. S.; Mayer, L. D.; Webb, M. S.; Bally, M. B. *Biosci. Rep.* **2002**, *22(2)*, 225.

Allen, T. M.; Hansen, C.; Martin, F.; Redemann, C.; Yau-Young, A. *Biochim. Biophys. Acta* **1991**, *29*, *1066*.

Andrade, J. D.; Hlady, V. *Adv. Poly. Sci.* **1986**, *79*, 1-63.

Angelova, A.; Vollhardt, D.; Ionov, R. *J. Phys. Chem.* **1996**, *100*, 10710.

Aroti, A.; Leontidis, E.; Maltseva, E.; Brezesinski, G. *J. Phys. Chem. B* **2004**, *108*, 15238.

Attwood, S. J.; Choi, Y.; Leonenko, Z. *Int. J. Mol. Sci.***2013**, *14*, 3514.

Baekmark, T. R.; Wiesenthal, T.; Kuhn, P.; Albersdorfer, A.; Nuyken, O.; Merkel, R. *Langmuir* **1999**, *15*, 3616.

Baekmark, T. R.; Elender, G.; Lasic, D. D.; Sackmann, E. *Langmuir* **1995,** *11*, 3975.

Bedu-Addo, F. K.; Tang, P.; Xu, Y.; Huang, L. *Pharm. Res.* **1996**, *13*, 710.

Belsito, S.; Bartucci, R.; Sportelliu, L. *Biophy. Chem.* **1998**, *75*, 3343

Benhabbour, S. R.; Sheardown, H.; Adronov, A. *Macromolecules* **2008**, *41*, 4817.

Berg, J. M.; Tymoczko, J. L.; Stryer, L. *Biochemistry 5$^{th}$ Edition*, *W H Freeman*, *New York.* 2**002**.

Birdi, K. S. *J. Coll. and Inter. Sci.***1976**, *57 (2)*, 228.

Biswas, S.; Dodwadkar, N. S.; Sawant, R. R.; Torchilin, V. P. *Bioconj. Chem.* **2011**, *22*, 2005.

Blume, G.; Cevc, G. *Biochim. Biophys. Acta* **1990**, *91*, 1029.

Boisselier, E.; Calvez, P.; Demers, E.; Cantin, L.; Salesse, C. *Langmuir* **2012**, *28*, 9680.

Brehmer, T.; Kerth, A.; Graubner, W.; Malesevic, M.; Hou, B.; Bruser, T.; Blume, A. *Langmuir* **2012**, *28*, 3534.

Browne, M.; Cecil, R.; Miller, J. C. *Eur. J. Biochem.* **1973**, *33*, 233.

Chen, S.; Zheng, J.; Li. L., and Jiang, S. *J. Am. Chem. Soc.* **2005**, *127*, 14473.

Coffman, J. P.; Naumann, C. A. *Macromolecules* **2002**, *35*,1835.

Cordeiro, C.; Wiseman, D. J.; Lutwyche, P.; Uh, M.; Evans, J. C.; Finlay, B. B.; Webb, M. S. *Antimicro. Agen. and Chemo.***2000**, *44 (3)*, 533.

Dalsin, J. L.; Hu B. H.; Lee, B. P.; Messersmith, P. B. *J. Am. Chem. Soc.* **2003**, *125*, 4253.

Dhruv, H. D. PhD Dissertation, *Utah State University* **2009**.

Dominguez, M. R.; Narvaez, I. G.; Patino J. M. R. *Ind. Eng. Chem. Res.* **1998,** *37*, 936.

Dorn, J. *PhD Dissertation, University of Mainz* **2010.**

Eeman, M.; Deleu, M. *Biotechnol. Agron. Soc. Environ.* **2010**, *14(4)*, 719.

Efremova, N. V.; Bondurant, B.; O'Brien, D. F.; Leckband, D. E. *Biochemistry* **2000**, *39*, 3441.

El-Khouri, R. J.; Frey, S. L.; Szmodis, A. W.; Hall, E.; Kauffman, K. J.; Patten, T. E.; Lee, K. Y. C.; Parikh, A. N. *Langmuir* **2011**, *27(5)*, 1900.

Farias, R. N.; Vinals, A. E. L.; Posse, E.; Morero, R. D. *Biochem. J.***1989**, *264*, 285.

Faure, M. C.; Bassereau, P. *Macromolecules* **1999**, *32*, 8538.

Gaines, G. L. Jr. *Insoluble Monolayers at Liquid–Gas Interfaces; Wiley: New York* **1966**.

Gozen, I.; Jesorka, A. *Anal. Chem.* **2012**, *84*, 822.

Halperin, A.; Fragneto, G.; Schollier, A.; Sferrazza, M. *Langmuir* **2007**, *23*, 10603.

Harris, J. M.; Zalipsky, S. *Poly(ethylene glycol): Chem. and Bio. Appl.*; *Am. Chem. Soc.***1997**.

Harris, J. M., *Poly(Ethylene Glycol) Chemistry: Biotech. and Biomed. Appl. Planum Press: New York* **1992**.

Harris, J. M.; Dust, J. M.; Mcgill, R. A. ; Harris, P. A.; Edgell, M. J. Sedaghat-Herati, R. M.; Karr, L. J.; Donnely, D. L.; *Water soluble polymers* **1991**.

Heeb, R.; Lee, S.; Venkataraman, N. V.; Spencer, N. D. *Appl. Mater. Inter.* **2009**, *1(5)*, 1105.

Hong, Y.; Meng, L.; Chen, S.; Leung, C. W. T.; Da, L.-T., Faisal, M.; Silva, D-A.; Liu, J.; Lam, J. W. Y. ; Huang, X.; Tang, B. Z. *J. Am. Chem. Soc.* **2012**, *134*, 1680.

Horwitz, D. L.; Starr, J. I.; Mako, M. E; Blackard, W.G.; Rubenstein, A. H. *J. of Clin. Inves.* **1975**, *55*, 1278.

Hristova, K.; Kenworthy, A.; McIntosh, T.J. *Macromolecules* **1995**, *28(23)*, 7693.

Immordino, M. L.; Dosio, F.; Cattel, L. *Inter. J. of Nanomed.* **2006**, *1 (3)*, 297.

Jackman, J. A.; Knoll, W.; Cho, N.-J. *Materials* **2012**, *5*, 2637.

Jebrail, M.; Schmidt, R.; DeWolf, C. E.; Tsoukanova, V. *Coll. and Surf. A* **2008,** *321*, 168.

Jesorka, A.; Orwar, O. *Annu. Rev. Anal. Chem.* **2008**, *1*, 801.

Kapishon, V.; Lew, R. R. *B.Sc Thesis, York University* **2008**.

Karve, S.; Bandekar, A.; Ali, Md. R.; Sofou, S. *Biomaterials* **2010**, 866, *31*, 4409.

Kenworthy, A. K.; Simon, S. A.; McIntosh,T. J. *Biophys. J.* **1995a**, *68*, 1903.

Kenworthy, A. K.; Hristova, K.; Needham, D.; McIntosh, T. J. *Biophys. J.* **1995b**, *68*, 1921.

Kiess, M. PhD Dissertation, *Swiss Federal Institute of Technology in Lausanne* **1997.**

Kim, K.; Kim, C.; Byun, Y. *Biomaterials* **2004**, *25 (1)*, 33.

Krisdhasima, V.; McGuire, J.; Sproull, R. *J. Coll. Inter. Sci.***1992**, 154, *2*, 337.

Kozarac, Z.; Dhathathreyan, A.; Mobius, D. *Eur. Biophys. J.***1987**, *15*, 193.

Kung, V. T.; Redemann, C. T. *Biochim. Biophys. Acta* **1986**, *862*, 435.

Lasic, D. D.; Needham, D. *Chem. Rev* **1995**, *95*, 2601.

Lasic, D. D. *ACS symposium series; Am. Chem. Soc*.**1997**.

Leckband, D.; Israelachvili, J. Q. *Rev. Biophys.* **2000**, *34*(2), 105.

Lee, H. Y.; Yu, S. A.; Jeong, K. H.; Kim, Y. J. *Macromol. Res*.**2007**, *15(6)*, 547.

Lewis, A. L., *Coll. and Surf. B* **2000**, *18(3-4)*, 261.

Li, A.; Ramakrishna, S. N.; Schwarz, T.; Benetti, E. M.; Spencer, N. D. *ACS Appl. Mater. Inter.* **2013**, *5*, 4913.

Liu, G.; Chen, Y.; Zhang, G.; Yang, S. *Phys. Chem. Chem. Phys*. **2007**, *9*, 6073.

Lozano, M. M.; Longo, M. L. *Langmuir* **2009a**, *25*, 3705.

Lozano, M. M.; Longo, M. L. *Soft Matter* **2009b**, *5*, 1822.

Majewski, J.; Kuhl, T. L.; Gerstenberg, M. C.; Israelachvili, J. N.; Smith, G. S. *J. Phys. Chem. B* **1997,** *101*, 3122.

Mansour, H.; Wang, D-S.; Chen, C-S.; Zografi, G. *Langmuir* **2001,** *17*, 6622.

Maruyama, K.; Yuda, T.; Okamoto, A.; Ishikura, C.; Kojima, S.; Iwatsuru, M. *Chem. Pharm. Bull.* **1991**, 39(6), 1620.

Merian, T.; Goddard, J. M. *J. Agric. Food Chem.* **2012**, *60*, 2943.

Miller, R.; Fainerman, V. B.; Makievski, A. V.; Kragel, J.; Wustneck, R. *Coll. and Surf.* **2000**, *161*,151.

Mfuh, A. M.; Mahindaratne, M. P. D.; Quintero, M. V.; Lakner, F. J.; Bao, A.; Goins, B. A.; Phillips, W. T.; Negrete, G. R. *Langmuir* **2011**, *27*, 4447.

Mok, K. W. C.; Lam, A. M. I.; Cullis, P. R. *Biochim. Biophys. Acta* **1999**, *1419*, 137.

Mori, A.; Klibanov, A. L.; Torchilin, V. P.; Huangl, L. *Fed. Eur. Biochem. Soc. Let.***1991**, *284(2)*, 263.

Mohwald, H. *Ann. Rev. Phys. Chem.* **1990**, *41*, 441.

Mueller, H.; Butt, H.-J.; Bamberg, E. *J. Phys. Chem. B* **2000,** *104*, 4552.

Mulligan, K.; Jakubek, Z. J.; Johnston, L. J. *Langmuir* **2011**, *27*, 14352.

Nalam, P. C.; Ramakrishna, S. N.; Espinosa-Marzal, R. M.; Spencer, N. D. *Langmuir* **2013**, *29*, 10149.

Naumann, C. A.; Brooks, C. F.; Wiyatno, W.; Knoll, W.; Fuller, G. G.; Frank, C. W. *Macromolecules* **2001**, *34*, 3024.

Naumann, C. A.; Brooks, C. F.; Fuller, G. G.; Knoll, W.; Frank, C. W. *Langmuir* **1999,** *15*, 7752.

Nayar, R.; Schroit, A. J. *Biochemistry* **1985**, *24*, 5961.

Nieto-Suarez, M.; Vila-Romeu, N.; Dynarowicz-Latka, P. *Coll. and Surf. A* **2008**, *321*, 189.

Ostuni, E.; Chapman, R. C.; Holmlin, R. E.; Takayama, S. and Whitesides, G. M. *Langmuir* **2001**, *17*, 5605.

Patino, J. M. R.; Dominguez, M. R. *Physicochem. and Eng. Asp.***1996,** *114*, 287.

Peschke, J.; Mohwald, H. *Coll. and Surf.* **1987**, *27***,** 305**.**

Rabe, M.; Verdes, D.; Rankle, M.; Artus, G. R. J.; Seeger, S. *Chem. Phys. Chem.***2007**, *8(6)*, 862.

Rahmati, K.; Koifman, J.; Tsuokanova, V. *Coll. and Surf. A* **2008**, *321*, 181.

Ratner, B. D.; Bryant, S. J. *Annu. Rev. Biomed. Eng.* **2004**, *6*, 41.

Rex, S; Zuckermann, M. J.; Lafleur, M.; Silvius, J. R. *Biophys. J.* **1998,** *75*, 2900.

Rossi, J.; Giasson, S.; Khalid, M. N.; Delmas, P.; Allen, C.; Leroux, J-C. *Eur. J. Pharm. and Biopharm.* **2007,** *67*, 329.

Schwieger, C.; Blume, A. *Biomacromolecules* **2009,** *10*, 2152.

Shahid, M. N.; Tsoukanova, V. *J. Phys. Chem. B* **2011,** *115(13)*, 3303.

Sheth, S. R.; Leckband, D.; *Proc. Natl. Acad. Sci. USA* **1997**, *94*, 8399.

Soenen, S. J. H.; Illyes, E.; Vercauteren, D.; Braeckmans, K.; Majer, Z.; De Smedt, S. C.; Cuyper, M. D. *Biomaterials* **2009**, *30*, 6803.

Stepniewski, M.; Pasenkiewicz-Gierula, M.; Rog, T.; Danne, R.; Orlowski, A.; Karttunen, M.; Urtti, A.; Yliperttula, M.; Vourimaa, E.; Bunker, A. *Langmuir* **2011**, *27*, 7788.

Tien, Ti. H.; Ottova-Leitmannova. A. *Membrane Biophysics, Elsevier Science B.V.* **2000**.

Tanwir, K.; Shahid, M. N.; Thomas, A.; Tsoukanova, V. *Langmuir* **2012**, *28(39)*, 14000.

Tanwir, K.; Tsoukanova, V. *Langmuir* **2008,** *24*, 14078.

Tsoukanova, V.; Salesse, C. *Langmuir* **2008,** *24*, 13019.

Vermehren, C.; Kiebler, T.; Hylander, I. Callisen, T. H.; Jorgensen, K. *Biochim. Biophys. Acta* **1998**, *27*, 1373.

Vermette, P.; Gauvreau, V.; Pezolet, M.; Laroche, G. *Coll. and Surf. B* **2003**, *29(4)*, 285.

Wu, F-G.; Luo, J-J.;Yu, Z-W. *Langmuir* **2010**, *26(15)*, 12777.

Xu, Z.; Marchant, R. E. *Biomaterials* **2000**, *21*, 1075.

Xu, Z.; Holland, N. B.; Marchant, R. E. *Langmuir* **2001**, *17*, 377.

Yin, F.; Kafi, A. K. M.; Shin, H-K.; Kwan, Y-S. *Thin Solid Films* **2005,** *488*, 223.

Zhao, H.; Lappalainen, P. *Mol. Bio.Cell* **2012**, *23*, 2823.

Zhao, H.; Dubielecka, P. M.; Soderlund, T.; Kinnunen, P. K. J. *Biophys. J.* **2002**, *83*, 954.

Zwaal, R.F.A; Comfurius, P.; Bevers, E. M. *Biochim. Biophys. Acta* **1998**, *1376*, 433.

# Chapter 2: Experimental

Two types of PEG-grafted phospholipid membrane models were used in this study: Langmuir monolayers and small unilamellar vesicles (SUVs). They were composed of either a single phospholipid or a binary mixture of the PEG-phospholipid, DPPE-PEG2000, and the matrix phospholipid, DPPE-Succinyl. Human insulin was used as a model protein to study the non-specific interactions of PEG-grafted phospholipid membranes with dissolved biomolecules. To characterize the model membranes and their interactions with insulin, a variety of experimental techniques were employed including surface pressure and surface potential measurements, epifluorescence microscopy (EFM) and circular dichroism (CD) spectroscopy. To enable the EFM observations, fluorescent probes were introduced into model membranes such as (i) a phase state imaging probe, DOPE-Rh, (ii) a fluorescein-labelled insulin and (iii) a fluorescent analogue of the PEG-phospholipid, DPPE-PEG2000-FITC. The latter was synthesized in the present study by coupling a NHS-ester of fluorescein-labelled PEG, NHS-PEG2000-FITC, to a disaturated phosphoethanolamine, DPPE, as discussed in detail below.

## 2.1 Materials

All phospholipids, phospholipid fluorescent probes and the PEG-phospholipid were purchased from Avanti Polar Lipids. This included 1, 2-Dipalmitoyl-sn-Glycero-3-Phosphoethanolamine-N-(Succinyl) (sodium salt) (DPPE-Succinyl), 1, 2-Dioleoyl-sn-Glycero-3-phophoethanolamine-N-Lissamine Rhodamine B Sulfonyl (ammonium Salt) (DOPE-Rh), 1, 2-Dipalmitoyl-sn-Glycero-3-Phosphoethanolamine-N-[Methoxy(Polyethylene glycol)-2000] (DPPE-PEG2000), 1,

2-Dipalmitoyl-sn-Glycero-3-Phosphoethanolamine (DPPE). N-hydroxysuccinimidyl-ester- N-(Polyethylene glycol)-2000-fluorescein-isothiocyanate (NHS-PEG2000-FITC) was obtained from Creative PEGWorks, USA. Human insulin was obtained from Sigma Aldrich. Fluorescein isothiocyanate conjugate of human insulin (FITC-insulin) was purchased from Molecular Probes. Phosphate buffered saline (PBS) 0.01M phosphate salt, 0.1M NaCl and 0.0027M KCl at pH of 7.4 was purchased from Sigma Aldrich. Potassium and sodium salts including $KH_2PO_4$, KCl, $Na_2HPO_4$ and NaCl were also obtained from Sigma Aldrich. The water used in all experiments was deionized by a Milli-Q-synthesis A10 purification system with a resistivity of $18.2 M\Omega.cm$ (pH 6.2 in equilibrium with atmospheric carbon dioxide) and surface tension of $72 \pm 0.1$ mN/m at room temperature. The value for surface tension is in good agreement with the literature [Bussieres 2012]. Triethylamine ($Et_3N$), Ethanol, Methanol, and chloroform of HPLC-grade were purchased from Fisher and used as received.

The solutions of DPPE (~$6\times10^{-4}$M), DPPE-Succinyl (~$6\times10^{-4}$M), DPPE-PEG2000 (~$6\times10^{-6}$M), and DPPE-PEG2000-FITC (~$6\times10^{-6}$M) were prepared in $CHCl_3$. The molar percentage solutions containing 1, 3, 6 and 9 % of DPPE-PEG2000 in DPPE-Succinyl were prepared by mixing calculated volumes of the stock solutions. For the EFM analysis, fluorescent probes were added to the solutions of DPPE-Succinyl and DPPE-PEG2000 to image the phase state of the DPPE-Succinyl and DPPE-PEG2000 mixtures (LE and LC phases) using DOPE-Rh and/or the lateral distribution of PEG phospholipids in the DPPE-Succinyl matrix using DPPE-PEG2000-FITC. For this purpose, three different types of binary mixtures containing fluorescent probes were prepared: (i) mixtures labelled with 0.5 mol% of DOPE-Rh, (ii) mixtures where 0.5 mol% of the total PEG phospholipid content was replaced with the DPPE-PEG2000-FITC and (iii) mixtures with both DPPE-PEG2000-FITC and DOPE-Rh probes [Shahid 2011; Tanwir 2012;

Tanwir 2008]. Insulin solutions were prepared at a concentration of (~$5.2\times10^{-8}$M) by dissolving in phosphate buffer containing 0.03 M $Na_2HPO_4$ and 0.009 M $KH_2PO_4$, pH = 7.4. All solutions were stored in the dark at 4°C. All experiments were performed at a temperature of $20 \pm 1\,^{\circ}C$.

## 2.2 Experimental Techniques

The majority of the measurements were performed with Langmuir monolayers which have proven to provide ideal models of phospholipid membranes [Wiedmer 2004]. The techniques used to study the monolayer models will thus be described first. These techniques include surface pressure, surface potential measurements and epifluorescence microscopy (EFM). The discussion of the experimental techniques will be concluded with the basic principles of CD spectroscopy performed in this study for SUV models.

### 2.2.1 Langmuir Technique

Langmuir monolayer technique is a well-designed two-dimensional method which has the capacity to easily control and detect a slight change in the lateral packing of amphiphilic molecules such as phospholipids at the air/water interface [Gaines 1966]. Langmuir monolayers are generally prepared using a conventional Langmuir trough. To better illustrate the principle and design, a schematic sketch of Langmuir trough is shown in Figure 2.1. The trough is typically equipped with two moveable barriers, which allows to vary the area available for monolayer. Langmuir monolayers are formed by spreading the amphiphilic molecules, such as phospholipids, onto an aqueous subphase in the trough. Upon spreading, phospholipids orient themselves at the air/aqueous interface in a manner that their hydrophilic headgroups face the

aqueous medium whereas the hydrophobic aliphatic tails point towards the air. When the spreading is performed over a sufficiently large area, the molecules are initially in a disordered phase with almost no interactions between each other. As the barriers compress, the phospholipid molecules begin to come in contact with each other (Figure 2.2A) and subsequently form a tightly packed monolayer by aligning their hydrophilic headgroups and hydrophobic tails together (Figure 2.2B). This approach enables examining different types of packing in model membranes and their effect on interactions between the molecules, phase state as well as the membrane behaviour under different experimental conditions. Most importantly, the major advantage of the Langmuir technique is that it allows the two major parameters of phospholipid packing in the membrane, lateral (surface) pressure and area per phospholipid molecule, to be precisely measured. The change in surface pressure with respect to area per phospholipid molecule results in a two-dimensional curve, which is called the $\pi - A$ isotherm. The isotherm can eventually be used to determine the phase behaviour of the monolayer.

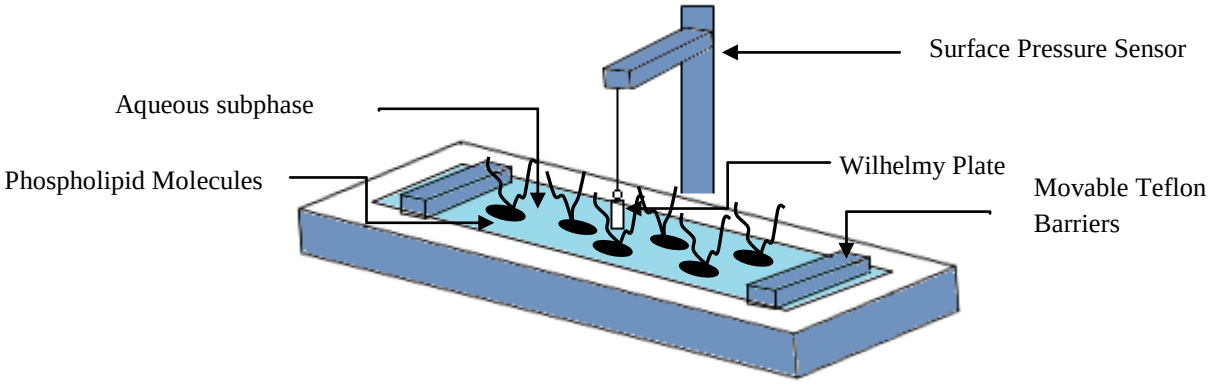


**Figure 2.1:** Schematics depicting a Langmuir trough with two teflon barriers. Surface pressure is monitored by a highly sensitive sensor measuring the force exerted on a wilhelmy plate which is suspended across the air/liquid interface.

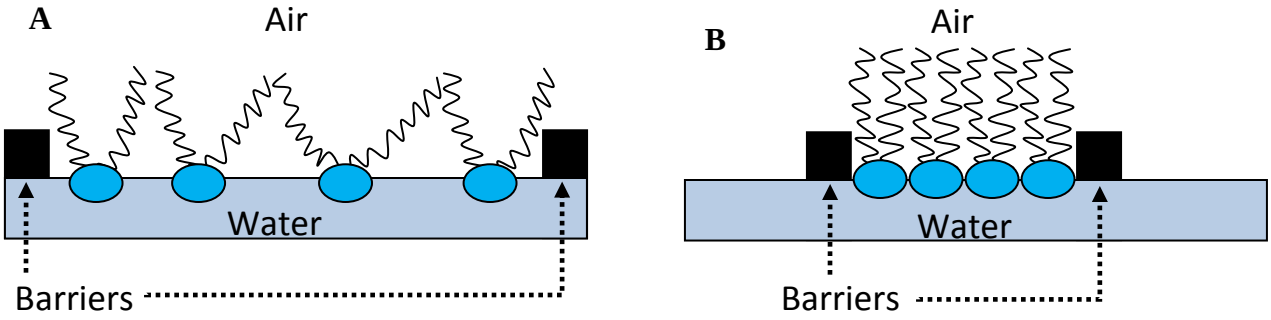


**Figure 2.2:** Schematic diagram of phospholipid molecules at the air/water interface in a Langmuir trough. Figure (A) shows that the phospholipid molecules are in the liquid expanded phase and figure (B) illustrate that the molecules come together and form condensed phase.

### 2.2.1.1 Area per Phospholipid Molecule

A typical amphiphilic molecule, such as phospholipid, is primarily composed of a hydrophilic headgroup and a hydrophobic tail portion. When spread onto the aqueous subphase, each phospholipid molecule occupies a surface area. The area occupied by each phospholipid molecule depends on the number of molecules spread and the total area of the trough available for them to spread on. The area per molecule of each phospholipid at any given surface pressure is calculated automatically by the Langmuir trough's internally built software based on the equation 2.1, as shown below.

$$A_{PL} = \frac{A_{trough}}{C \times V_{spread} \times N_A / MW} \quad \text{----------2.1}$$

where $A_{PL}$ is the area available per pure phospholipid molecule, $A_{trough}$ is the effective surface area of the trough at any given surface pressure, $C$ represents the concentration of pure phospholipid solution, $V_{spread}$ represents the volume spread on the subphase in the trough, $N_A$ is the Avogadro's constant, and $MW$ is the molecular weight of the pure phospholipid. The area available for each phospholipid molecule is usually larger before compression as compared to the actual area per phospholipid molecule since the molecules are randomly distributed over the entire surface area of the trough. Upon compression the total area occupied decreases which results in a decrease in the area per phospholipid molecule. For monolayers containing only one type of phospholipid, called in this work "pure monolayer", this area is plotted in the isotherm as area per molecule and corresponds to the actual area per molecule at which each pressure reading

is taken. In the case of phospholipid mixture, the area occupied by the components of the mixture is calculated differently and called the mean molecular area as discussed below.

### 2.2.1.2 Mean Molecular Area

In the case of binary mixtures, which contain different types and mole fractions of phospholipids, the area per molecule does not only represent the area occupied by one type of phospholipid molecule but a mean molecular area occupied by all components of the mixture at any given surface pressure. Hence, the term "mean molecular area" is generally used for a mixture to account for the area per molecule at any surface pressure. For example, a reading of 100 $nm^2$/molecule taken from the isotherm of a mixed monolayer represents the mean molecular area of both phospholipid components of the mixture at any given surface pressure. The mean molecular area of the mixture is generally calculated using the mixed concentrations and molecular weights of both lipid components at any point along the isotherm by equation 2.2.

$$A_{ML} = \frac{A_{trough}}{C_{mix} \times V_{spread} \times N_A / MW_{mix}} \quad \text{---------- 2.2}$$

where $A_{ML}$ is mean molecular area, $A_{trough}$ is the effective surface area of the trough at any given surface pressure, $C_{mix}$ represents the mixed concentration of both phospholipid components in the mixture, $V_{spread}$ represents the solution volume spread on the subphase, $N_A$ is the Avogadro's

constant, and $MW_{mix}$ is the average molecular weight of the components of the mixture. $C_{mix}$ is calculated using equation 2.3

$$C_{mix} = \frac{C_A V_A + C_B V_B}{V_{Total}} \text{ ---------- 2.3}$$

where $C_A$ and $C_B$ are the concentrations of each phospholipid component of the mixture, $V_A$ and $V_B$ are the volumes of each phospholipid component added in the mixture and $V_{Total}$ is the total volume of both components. $MW_{mix}$ in equation 2.2 is calculated using equation 2.4

$$MW_{mix} = MW_A \chi_A + MW_B \chi_B \text{ ----------2.4}$$

where $MW_A$ and $MW_B$ are the molecular weights of the components of the mixture and $\chi_A$ and $\chi_B$ are the mole fractions of each phospholipid added in the mixture.

A sample calculation is also shown below to get a better understanding of how the mean molecular area is generally calculated. The mean molecular area of 1 mol% component B (Conc: 0.2 g/L and MW: 2750 g/mol) in 99 mol% component A (Conc: 0.5 g/L and MW: 814 g/mol) is calculated from equation 2.2. The volume of the solution spread is $1^* 10^{-4}$ L whereas the effective surface area of the KSV trough is $75 \times 760$ $mm^2$. Hence, upon plugging all the values in equation 2.2, the mean molecular area of the mixture upon spreading will be 1.99$nm^2$/molecule.

$$A_{ML} = \frac{5.7 \times 10^{16} nm^2}{\frac{0.5g/L * 1 * 10^{-3} L + 0.2g/L * 8.5 * 10^{-5} L}{1.085 * 10^{-3} L} \times 1 * 10^{-4} L \times 6.02 * 10^{23} \Big/ 814g/mol * 0.99 + 2750g/mol * 0.1}$$

$\boldsymbol{A_{ML}}$ = 1.99nm$^2$/molecule

### 2.2.1.3 Surface Pressure Sensor/ Wilhelmy plate

To study various properties of the phospholipid monolayers such as lateral organization and phase behaviour, it is important to consider the relationship between surface pressure and surface tension at the air/water interface. Upon spreading the phospholipid solution onto the subphase, the teflon barriers start compressing the phospholipid molecules from both sides towards the center of the trough. The mean molecular area per phospholipid molecule begins to decrease, which eventually changes the intermolecular distance and subsequently the surface tension. This translates into changes in the surface pressure which is actually measured by the Langmuir technique. Surface pressure is defined as the difference between the surface tension of a clean liquid surface and the surface tension in the presence of a phospholipid monolayer [Aumann 2010; Gaines 1966; Jebrail 2007; Myres 1999]. Surface pressure and surface tension have the same units, mN/m, and magnitude but have inverse relationship. The change in surface tension is directly measured in the form of a change in surface pressure. This change in surface pressure with the successive compression by barriers is in fact measured by the trough's internally installed surface pressure sensor using an object partially immersed in the subphase. This object can sense the force being exerted on it. Thus, upon immersion, three forces act on the plate

including the gravitational force, surface tension acting downwards and buoyancy due to displaced water acting upward. By considering the dimensions of a rectangular plate as length, width, thickness (l × *w* × *t*), density *(ρ)*, and depth *(d)* of the portion of plate submerged in the water as shown in Figure 2.3, the net force acting downwards, *F*, can be calculated by the equation as follows:

$$Force = (\rho_P lwt).g - (\rho_L dwt).g + 2.(w+t).(ST).\cos\theta \quad \text{---------- 2.5}$$

Force = weight – upthrust + surface tension

Here, the $\rho_P$ is the density of the plate, $\rho_L$ represents the density of the liquid, *ST* is the surface tension of the liquid, $\theta$ denotes the contact angle of the liquid to the Wilhelmy plate and *g* represents the acceleration due to gravity [Birdi 1989; Jebrail 2007].

The surface pressure is always zeroed to eliminate the weight factor from equation 2.5 before spreading any phospholipid solution.

$$Force = -(\rho_L dwt).g + 2.(w+t).(ST).\cos\theta \quad \text{---------- 2.6}$$

Force = – upthrust + surface tension

Since, the wilhelmy plate is always kept at a constant level by the balance regardless of surface tension, the upthrust term can also be eradicated from equation 2.6.

$$Force = 2.(w+t).(ST).\cos\theta \text{ ---------- } 2.7$$

Further, the use of paper plate makes the contact angle of the plate with the water to 0° so the equation becomes

$$Force = 2.(w+t).(ST) \text{ ---------- } 2.8$$

Therefore, the surface tension for a paper plate can be calculated by:

$$ST = {Force}/{2.(width + thickness)} \text{ ---------- } 2.9$$

Unit for surface tension is measured in mN/m, where force is in mN and perimeter is in meters.

Thus, a thick paper plate with a 10.25 mm width, 0.25 mm thickness and 100 mg weight can create a surface pressure magnitude of 46.7 mN/m. These magnitude values are usually used to calibrate the instrument. In this study, a surface pressure sensor known as a Wilhelmy plate, made of a rectangular piece of filter paper, was used to measure the change in the surface pressure, $\pi$, of the phospholipid monolayer with an accuracy of 0.1 mN/m.

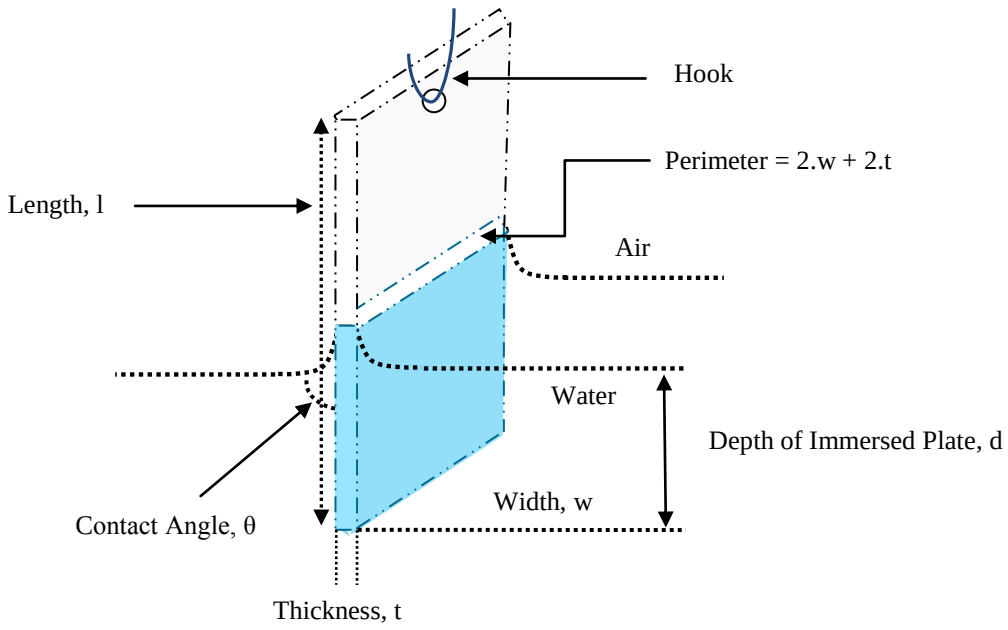


**Figure 2.3:** A Schematic diagram of a Whilhelmy plate illustrating the dimensions of a rectangular plate, when submerged in an aqueous medium. The sketch is made based on the reference [Aumann 2010].

#### 2.2.1.4 Surface Pressure – Area ($\pi - A$) Isotherm

A monolayer is usually formed by spreading the phospholipid solution on aqueous subphase followed by compressing the two moveable barriers from both sides of the trough, as sketched in Figure 2.2. The Langmuir technique measures the change in surface pressure, $\pi$, as the area per molecule of the phospholipid, $A$, decreases upon monolayer compression. This in turns produces a two-dimensional curve referred to as the $\pi - A$ isotherm [Gaines 1966]. The $\pi - A$ isotherm can provide a detailed information about the molecular dimensions of the phospholipid molecules as well as the stability and phase transition behaviour of the monolayer on air/aqueous interface (Figure 2.4). Moreover, the change in the slope of the isotherm also corresponds to different packing behaviour of the phospholipids. The $\pi - A$ isotherm of a typical monolayer can mainly be divided into several distinctive regions referred to as the gaseous phase (G), liquid expanded phase (LE), phase coexistence (LE/LC), liquid condensed phase (LC) as well as a collapse point (C), as described by the schematic diagram in Figure 2.4 [Boisselier 2012; Mohwald 1990]. Upon spreading the phospholipid solution on air/water interface, the phospholipid molecules are considered to be in a complete disordered phase where the chains are in a tilted position. Molecules are also far away with almost no interactions with each other and hence this phase is named gaseous phase (G) (Figure 2.4). Upon compression, the phospholipid molecules begin to interact with each other while keeping a high mobility between the hydrophobic chains and this is described as the liquid expanded phase (Figure 2.4). A further compression often leads to a horizontal portion of the isotherm known as the coexistence between liquid expanded and condensed phase, where about half of the phospholipid molecules get aligned with each other while the other half are still in random orientation (Figure 2.4). As the compression continues,

the monolayer forms a continuous LC phase, where the phospholipid molecules attained a tightly-packed state by aligning their hydrophilic headgroups and hydrophobic tails together (Figure 2.4). A subsequent compression of the phospholipid monolayer in the LC state eventually results in collapse (Figure 2.4) [Gaines 1966; Mohwald 1990]. Moreover, $A_{pl}$, is the effective limiting area of a phospholipid molecule in a closely packed state and can be determined from the monolayer's $\pi - A$ isotherm by extrapolating its low compressibility region to $\pi$ = 0 mN/m, (shown as a dashed line in Figure 2.4). Overall, the $\pi - A$ isotherms provide surface (lateral) pressure values corresponding to different packing of phospholipids in the model membrane, which affords relating the data obtained with monolayer models to other membrane models. $\pi - A$ isotherms have therefore become the basic characterization of monolayers that is often performed simultaneously with other measurements such as surface potential or epifluorescence microscopy (EFM).

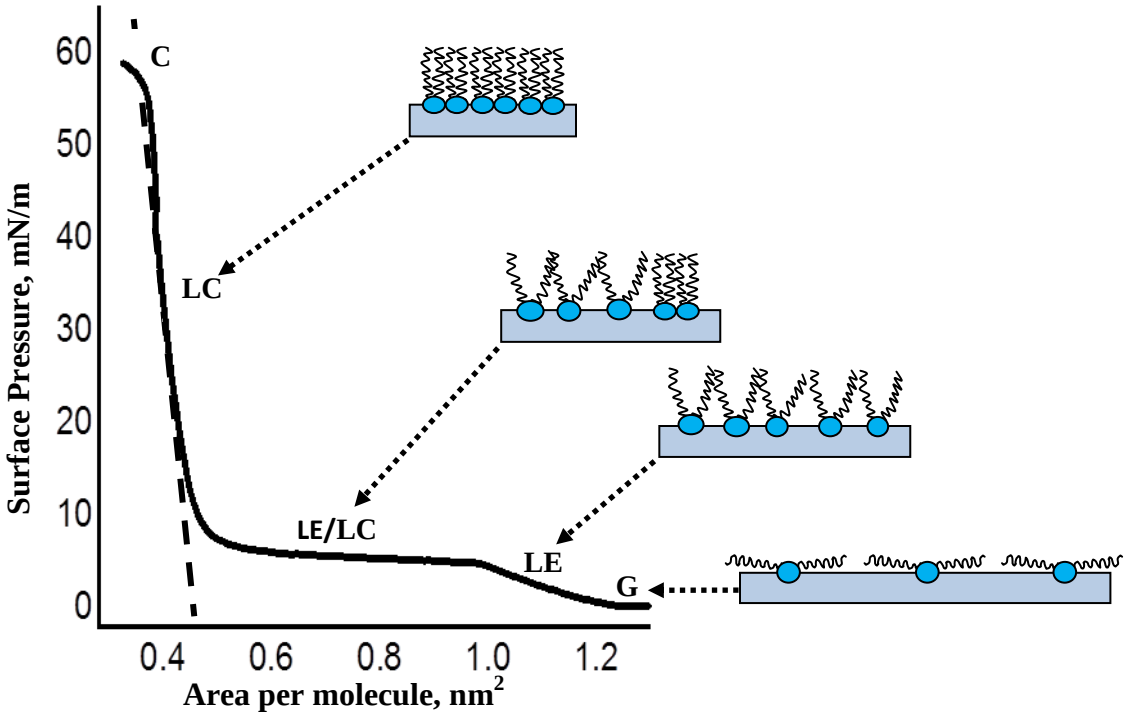


**Figure 2.4:** Schematics diagram of a $\pi - A$ isotherm illustrating the various phase transitions of phospholipid molecules on air/water interface. Upon compression, phospholipid packing in monolayer goes through several distinctive phases including: Gaseous (G), liquid expanded (LE), coexistence of liquid expanded/liquid condensed (LE/LC), liquid condensed (LC), and collapse (C) phases. The dashed line intersecting the horizontal axis (X-axis) corresponds to the effective limiting area of phospholipid molecule ($A_{pl}$). The schematic is modified from the reference [Dhruv 2009].

### 2.2.1.5 Preparation of Langmuir Monolayers and $\pi - A$ Isotherm Measurements

In this study phospholipid monolayers were prepared at the air/water and air/PBS interface by spreading from chloroform phospholipid solutions [Gaines 1966]. Two custom made Langmuir troughs were employed. The troughs are KSV2000SP (KSV Instruments Ltd., Finland) and NIMA (NIMA technology Ltd., UK). The KSV trough has an effective surface area of 75 × 760 $mm^2$ whereas NIMA trough has an effective surface area of 70 × 460 $mm^2$. Both troughs are thermostated to regulate the subphase temperature with a precision of ± 1 °C. Both KSV and Nima troughs have two movable barriers which can compress or decompress the phospholipid monolayers with a constant speed of 10 and 7 mm/min, respectively. A filter paper Wilhelmy plate was used to measure the surface pressure, $\pi$, to an accuracy of 0.1 mN/m. The KSV2000SP Langmuir trough was used to study the physical stability and phase transition behaviour of pure and mixed phospholipid monolayers. Nima trough was used to study the morphology of monolayers using EFM.

Before spreading monolayers, the same procedure was used to clean both troughs. The trough was first cleaned with ethanol followed by three rinses with milli-Q water. A reference run was then performed with water as a subphase without a phospholipid monolayer to verify the absence of any contamination on the subphase surface. In case of an increase in the surface pressure above 0.2 mN/m, the cleaning procedure was repeated. The surface pressure reading was zeroed before spreading the phospholipid solution. The required volume of phospholipid solution was spread (using microlitre syringes) drop wise on the subphase by continuously monitoring the surface pressure magnitude to avoid any undesired change in surface pressure prior to compression. After allowing the solvent to evaporate for about 15 minutes, the phospholipid

monolayer was compressed at a constant rate and the $\pi - A$ isotherm was recorded. The $\pi - A$ isotherm measurements were also performed simultaneously with surface potential and EFM. Furthermore, another mode of surface pressure and area measurement was used in protein interaction studies that will be discussed in detail in chapter 6. Each measurement was repeated at least three times. Each $\pi - A$ isotherm presented in this dissertation are the average runs of all the measurements performed.

### 2.2.2 Surface Potential Measurements

Surface potential, $\Delta V$, is generally known as the Volta potential change that occurs when an amphiphilic monolayer is spread at an air/aqueous interface [Gaines 1966]. $\Delta V$ measurements can provide useful information about the orientation and reorientation of monolayer molecules upon compression, as well as dissociation degree of an ionizable monolayer [Gaines 1966; Vogel 1988]. In this study, $\Delta V$ measurements are employed to detect the change in the interactions between the monolayer molecules in the presence of different electrolytes in the subphase.

Two types of methods are usually adopted to measure the surface potentials of a monolayer film at air/aqueous interface, ionizing electrode and vibrating plate method. The later was used in this study. A schematic of the vibrating plate setup is shown in Figure 2.5 to better illustrate the basic principle of the technique. As seen in the figure, the setup is comprised of two electrodes. The measuring electrode is usually placed in the air above the monolayer and vibrates with a set of frequencies between 100 – 180 Hz whereas the counter electrode is immersed in the subphase below the monolayer. As the vibrating plate vibrates, the capacitance between the counter

electrode and the vibrating plate leads to a current flow in the circuit. Hence, the potential difference across the gap can be measured since $\Delta V$ is directly proportional to the magnitude of the current flowing through the circuit.

For ionized monolayers, major contributions to the measured $\Delta V$ come from the components of the equation 2.10 [Mohwald 1995].

$$\Delta V = \mu_n / \varepsilon.\varepsilon_0.A \quad \text{---------- 2.10}$$

where $\mu_n$ represents the vertical component of the dipole moment, $\varepsilon$ corresponds to the subphase permittivity, $\varepsilon_0$ symbolizes the air permittivity and $A$ denotes the area per molecule. However, equation 2.10 can only be related to $\Delta V$ for unionized monolayers since, for ionized or charged monolayers additional contributions come from the electric double layer potential, $\psi_0$, as shown in equation 2.11

$$\Delta V = \frac{1}{\varepsilon_0 A}\sum\frac{\mu_i}{\varepsilon_i} + \psi_0 \quad \text{---------- 2.11}$$

where $\boldsymbol{\varepsilon_0}$ is the permittivity of vacuum, $\boldsymbol{A}$, is the mean molecular area whereas $\boldsymbol{\varepsilon_i}$ is the local effective dielectric constant. The overall dipole contributions in most phospholipid monolayer mainly comes from terminal $CH_3$ group, $\mu_{CH3}$, $C = O$ group, $\mu_{C=O}$, phospholipid headgroup, $\mu_{headgroup}$, as well as from the water molecules reorganized and polarized by the monolayer, $\mu_{H2O}$ [Burner 1994; Tocanne 1990; Tsukanova 2004; Tsukanova 2002]. The dipole contributions in

the binary mixtures of DPPE-Succinyl and DPPE-PEG2000 monolayers may also arise from the PE-group of DPPE-PEG2000, $\mu_{PE}$, and grafted PEG2000 chains, $\mu_{PEG}$ [Burner 1994; Tocanne 1990; Tsukanova 2004; Tsukanova 2002 ]. Moreover, variations in $\mu_{PEG}$ and $\mu_{H_2O}$ for mixed DPPE-Succinyl/DPPE-PEG2000 monolayers will probably be negligible for closely packed monolayers on different subphases since the polarization and reorganization of water molecules` dipoles are only limited to the first layer of molecules of the monolayer [Burner 1994; Tocanne 1990; Tsukanova 2004; Tsukanova 2002; Winterhalter 1995]. Thus, both phospholipid headgroups and grafted PEG chains remain mainly dehydrated. However, the headgroup dissociation may significantly affect the $\psi_0$ potential due to the presence of different electrolytes in the subphase [Tocanne 1990; Tsukanova 2002]. Hence, any difference in the monolayer`s surface potential measured on water and PBS, $\Delta V_{H_2O}$ and $\Delta V_{PBS}$ can be associated to the difference in $\psi_0$ potentials and will be discussed in Chapter 4.

The surface potential, $\Delta V$, of pure DPPE-Succinyl monolayer and its binary mixtures with DPPE-PEG2000 was measured with the KSV trough described above. The surface potential, $\Delta V$, was measured by a vibrating plate suspended ~2 mm above the subphase and a reference plate electrode immersed at the bottom of the KSV trough/subphase. Upon compressing the phospholipid monolayer, the surface pressure, $\pi$, and the surface potential, $\Delta V$, were recorded simultaneously with respect to the change in area per molecule. The surface potential was measured with an accuracy of ± 15 mV. A set of three consecutive measurements were performed for each monolayer to gain maximum reproducibility.

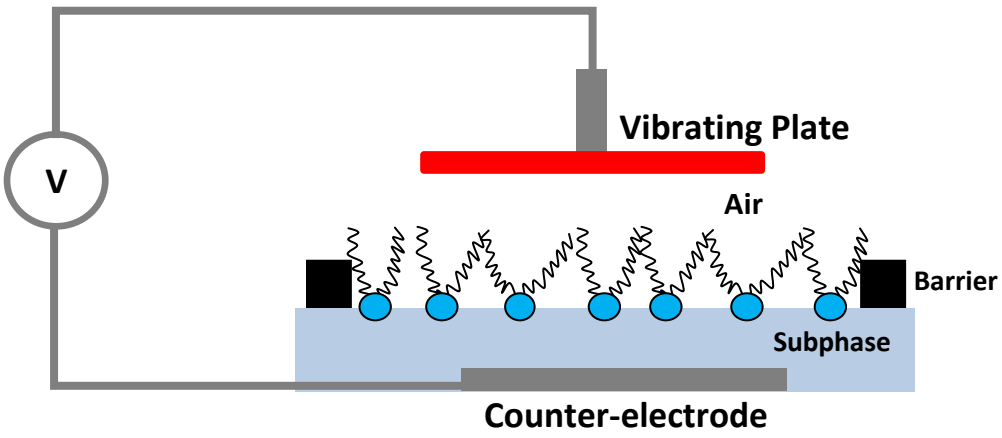


**Figure 2.5:** Schematics illustrating the principle of vibrating electrode method for Surface potential measurements [Adopted and modified from Gaines 1966].

## 2.2.3 In-Situ Epifluorescence Microscopy Imaging

### 2.2.3.1 Principle and Technical Specifications of EFM

Epifluorescence microscopy, EFM, is an imaging technique used for in-situ visualization of the morphology of phospholipid monolayers as well as for monitoring their interactions with biomolecules dissolved in the subphase. The epifluorescence microscope comprises of an excitation-emission configuration, in which both the excitation and emission light travel through the same objective while illuminating the specimen. To better illustrate the principle of an EFM, its schematic sketch is presented in Figure 2.6. As can be seen in the Figure, EFM is interfaced with the Langmuir trough on which the monolayer is prepared. The CCD camera transfers live data directly to the computer system attached to it. The images are then captured and saved in the computer system to be further analyzed.

The phenomenon of fluorescence includes the excitation of an electron of the fluorophore to a higher energy state by a photon of specific wavelength. During its transition, the electron comes back to its ground state by emitting a photon of lower energy, which in turns illuminates the specimen [Ploem 1987]. This process is known as excitation and emission. Due to the fact that most surface active substances do not fluoresce, many dyes with fluorescent properties have been developed to enhance the contrast and highlight different phases of the membrane models based on the partitioning of the fluorophore. These fluorescent dyes can be conjugated to other substances, including lipids and proteins. Such conjugates are called fluorescent probes [Gallier 2010; Chattopadhyay 1990; Maier 2002].

Most typically used fluorophores in the model membrane studies are rhodamine (Rh) and fluorescein-isothiocyanate (FITC). The excitation and emission spectral profiles of Rh and FITC are shown in Figure 2.7. The maximum fluorescence intensity of any fluorophore can be achieved by exciting the fluorophore at the wavelengths close to or at, the peak of the excitation spectrum and by selecting the widest range of wavelengths from the emission curve including the emission peak. As can be seen from Figure 2.7a, the excitation filter wavelength for TRITC ranges from 530 – 560 nm with an absorption maximum of ~545 nm and the emission intensity lies between 590 – 650 nm [Ploem 1987]. Moreover, the excitation wavelength of FITC fluorophore lies in the range of 470 – 490 nm with an absorption maximum of ~488 nm whereas the emission spectrum shows a wavelength range from 510 – 560 nm (Figure 2.7b) [Ploem 1987].

Different filter set combinations have been designed so that the two fluorophores can be used together and be selectively detected in the model membranes through the TRITC and FITC channel. TRITC channel detects fluorescence in the range of 590 – 650 nm from rhodamine (Rh) fluorophore while cutting off the fluorescence of FITC fluorophore (Figure 2.8). Conversely, FITC channel detects fluorescence from the fluorescein fluorophore in the range of 510 – 560 nm, while cutting off fluorescence of rhodamine fluorophore (Figure 2.8).

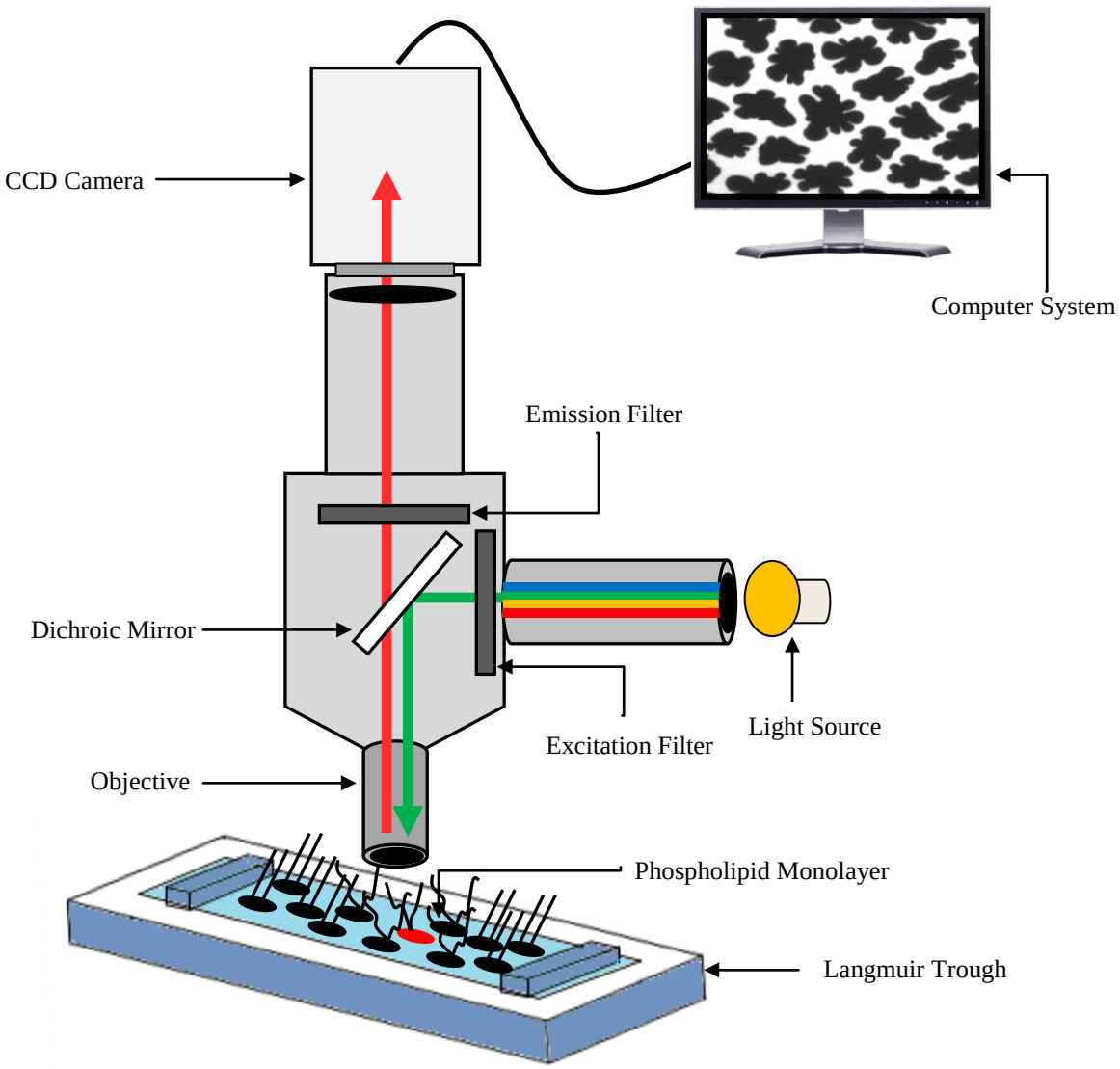


**Figure: 2.6:** Schematic diagram of an EFM interfaced with the NIMA trough depicting its principle using excitation filter, emission filter, and dichroic mirror. The diagram also shows the phospholipid monolayer as black colour spread on the Langmuir trough with the fluorescent probe as red colour. The sketch is constructed based on the reference [Na-Nakorn 2004].

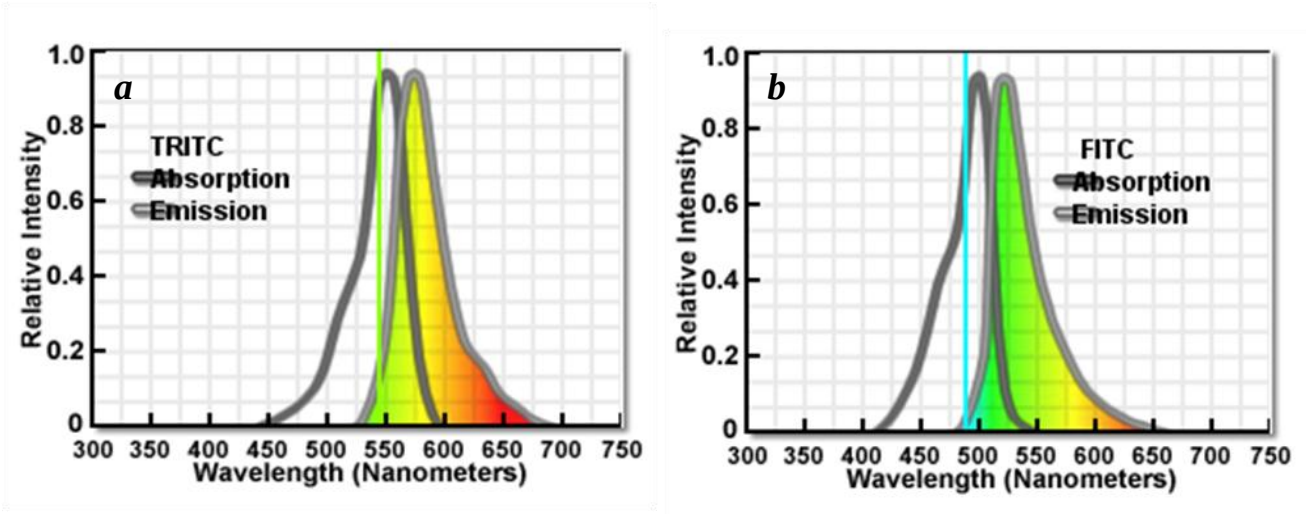


**Figure: 2.7: a)** Spectral profile of TRITC fluorophore exhibiting dark grey line as an efficient excitation profile from 530 – 560 nm and light grey line as emission intensity spectrum from 590 – 650 nm. **b)** Spectral profile of FITC fluorophore depicting dark grey line as an efficient excitation profile from 465 -495 nm and light grey line as emission intensity spectrum from 510 – 560 nm [Adapted from Olympus].

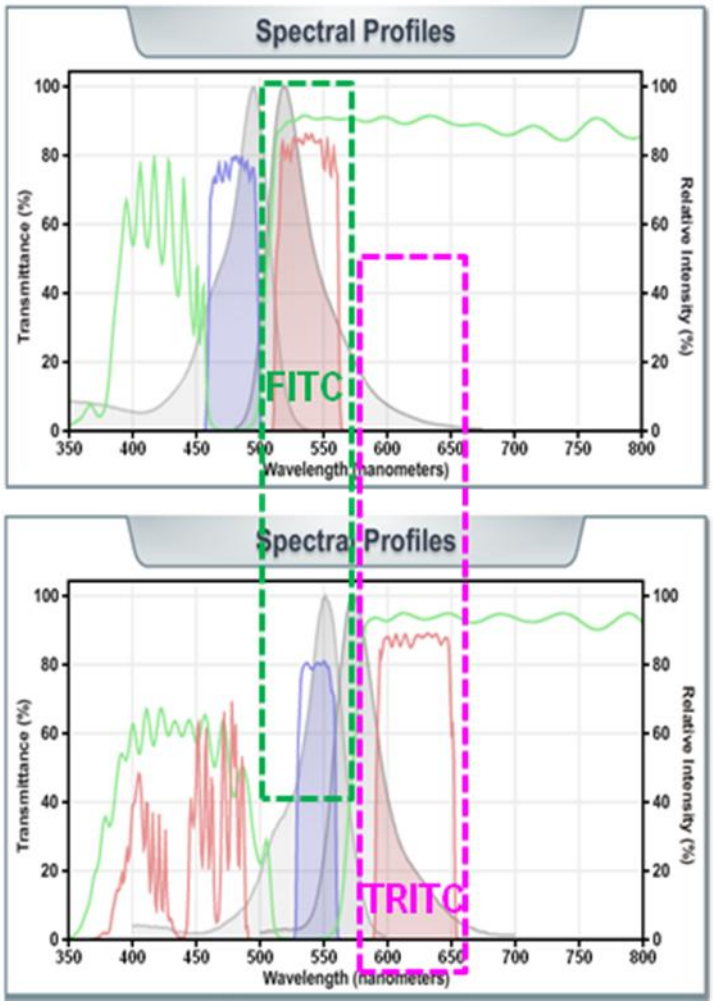


**Figure 2.8:** Spectral profile of FITC fluorophore depicting blue line as an efficient excitation profile from 465 -495 nm and red line as emission intensity spectrum from 510 – 560 nm. b) Spectral profile of TRITC probe exhibiting blue line as an efficient excitation profile from 530 – 560 nm and red line as emission intensity spectrum from 590 – 650 nm. The green dashed bar shows the emission profile of FITC fluorescence cutting off TRITC emission whereas pink dashed bar depicts the emission profile of TRITC probe fluorescence cutting off the FITC emission fluorescence [Adapted from Nikon].

#### 2.2.3.2 Two-Channel EFM in Visualizing the Membrane Morphology and Insulin/Membrane Interactions

In this study, two channel EFM was employed to (i) characterize the phase state, (ii) PEG distribution as well as (iii) monitor the insulin/membrane interactions. Characterization of phase state (LE/LC) and PEG-distribution were performed by adding DOPE-Rh and DPPE-PEG2000-FITC in the model membrane, monolayer. The insulin/membrane interactions and its effect on the membrane morphology were further examined using insulin-FITC and DOPE-Rh in the model membrane.

##### 2.2.3.2.1 Phase State Imaging

The phase state of the model membrane was visualized by using the DOPE-Rh fluorescent probe. DOPE-Rh contains unsaturated aliphatic chains and large size headgroup with a rhodamine fluorophore attached to it, as can be seen in Figure 2.9. This means it mainly stay in the LE phase and is excluded from the LC region of the model membrane [Gudheti 2007]. It is also suggested in the previously reported data that the fluorescent probes stay largely in the LE phase due to high solubility in the LE phase as well as difference in the molecular density of the coexisting phases [Kaganer 1999; Losche 1984; Mohwald 1995; Moy 1986; Shimshick 1973]. Hence, the fluorescence emission of DOPE-Rh can aid in characterizing the lateral phase states of the membrane model upon compression in particular between the LE and LC phase. The bright fluorescent areas seen in the model membrane thus corresponds to the DOPE-Rh rich

region and visualize the LE phase whereas dark areas corresponds to the DOPE-Rh excluded regions and thus identify the LC phase.

In our study, DOPE-Rh was used as a fluorescent probe to visualize the phase state of model membranes through TRITC channel. DOPE-Rh was also added in the monolayer together with the DPPE-PEG2000-FITC to characterize the phase behaviour of binary mixtures. Moreover, DOPE-Rh was used together with FITC-insulin in insulin/monolayer interaction studies to monitor changes in the monolayer morphology upon insulin binding.

**The Fluorescent Probe, DOPE-Rh**

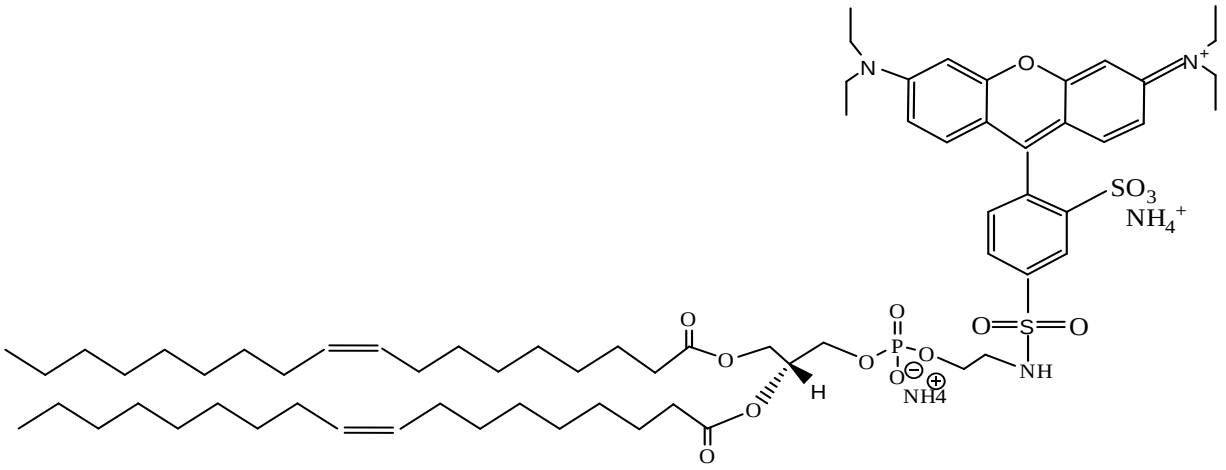


**Figure 2.9:** Chemical Structure of fluorescent probe, DOPE-Rh.

#### 2.2.3.2.2 PEG-Phospholipid Distribution Imaging

The lateral distribution of the DPPE-PEG2000 in the binary mixtures was visualized by EFM. The PEG distribution in the model membrane was monitored by attaching a FITC fluorophore to the distal end of the PEG2000 chain. For this purpose, a fluorescent analogue of DPPE-PEG2000 labelled with FITC, DPPE-PEG2000-FITC was synthesized in our lab. DPPE-PEG2000-FITC mixes ideally with DPPE-PEG2000, which will be discussed in detail in chapter 3. In model membranes, DPPE-PEG2000-FITC will thus reside where DPPE-PEG2000 is present. The DPPE-PEG2000-FITC will hence report on the location of the DPPE-PEG2000 molecules in model membrane and this region will appear stained green in the EFM images. Superimposing images from the same area of the monolayer through FITC and TRITC channels were captured. This afforded determining the location and distribution of PEG-phospholipid, between LE and LC phases.

In this study, DPPE-PEG2000-FITC was used to visualize the distribution of PEG-phospholipid via FITC channel. DPPE-PEG2000-FITC was added in the monolayer together with the DOPE-Rh to characterize the phase behaviour of binary mixtures. DPPE-PEG2000-FITC was also used together with rhodamine-labelled insulin in insulin/monolayer interaction studies to monitor changes in distribution of the PEG-phospholipid upon insulin binding. These results, however, are not presented as discussed below.

#### 2.2.3.2.3 Insulin/Membrane Interaction Imaging

Once the phase behaviour of pure and mixed monolayers has been characterized, the interactions between insulin and membrane can be studied using two-channel EFM. This was done by introducing one fluorescent probe in the monolayer and labelling the protein with another probe. The protein of interest, insulin, can be labelled with both FITC and Rh fluorophore. FITC-insulin is commercially available; the results presented in this thesis were obtained with FITC-insulin. FITC-insulin used in this study was mono-substituted species of insulin and has been specifically modified at the N-terminus of the B-chain. The substitution on B-chain has shown to retain the biological activity similar to the native insulin [Hentz 1997]. Some of the experiments were also performed with Rh-labelled (Rh-Insulin). Labelling of insulin with Rh was performed in our lab. The insulin labelled with Rh has been provided by Kanwal Tanwir. Two types of experiments were performed in our lab. In the first approach, FITC channel was used to monitor FITC-insulin whereas TRITC channel was employed to examine the changes in the LE/LC phases using DOPE-Rh, upon insulin/membrane interactions. The above procedure was also reversed by labelling insulin with Rh and DPPE-PEG2000 with FITC to study the insulin/ membrane interactions. However, there was no observable difference in the results. That is why this report will only present results obtained using FITC-insulin and DOPE-Rh in the monolayer. Importantly, proteins are known to interact with either LC or LE phase. However, non-specific interactions of proteins are generally limited to LE phase. Therefore, this study was specifically designed to examine the interaction mechanism of insulin with the LE phase of the membrane.

#### 2.2.3.3 Low-Intensity Imaging in the FITC Channel

The major difficulty associated with the monolayer models is the low-intensity and low-resolution imaging because the fluorescent probe is added at a very low concentration of ≤1 mol%. While the excitation output in TRITC channel is usually high enough to produce easily detectable fluorescence emission, a careful selection is often required for the excitation source in the FITC channel.

The light source commonly supplied with conventional EFM attachment for optical microscopes is a mercury lamp such as HBO mercury lamp supplied by Nikon, in our case. In the visible range, major bands of mercury lamp are positioned at 365, 405, 436, 546, and 579 nm. The band at 546 nm is positioned in the excitation window of the TRITC filter set. As a result, the optical output power that reaches the monolayer through the TRITC filter set is 76 $mW/cm^2$. This produces bright fluorescence from the Rh fluorophore and high contrast in images obtained through the TRITC channel as shown in image A in Figure 2.10. By contrast, no mercury band falls into the FITC excitation window. The mercury band closest to the FITC excitation range, at 436 nm, falls just outside the excitation filter set. This results in a very low excitation output through the FITC channel, at 20 $mW/cm^2$, which result in very poor contrast of images captured from the monolayers (image B in Figure 2.10). Thus, to improve the resolution in the FITC channel, we had to explore two other options.

The X-Cite technology by EXFO Photonic Solutions Inc. offers an Hg lamp similar to HBO lamp but with significantly improved power at the FITC excitation output. This results in a power of 34.8 $mW/cm^2$ at FITC excitation, and slightly reduced power of ~ 67.4 $mW/cm^2$ at TRITC. This affords a significant improvement in the contrast of FITC images without

compromising the quality of TRITC images. In many experiments, however, the power of 34.8 $mW/cm^2$ is not sufficient to produce a strong fluorescence in the FITC channel. Hence, the image acquisition time has to be increased. This can make difficult obtaining the high-contrast images for monolayers that move a lot at the interface (images C in Figure 2.10).

To further improve the contrast and crispiness of images as well as to enable their quantitative analysis, we have aligned the EFM setup with a laser providing the blue excitation output for FITC at a power of ~100 mW. The laser provides an output at ~100 mW with 473 nm excitation in our case. The laser was purchased from Laser Glow Technology Inc. ON. A schematic of the setup with the laser arm is shown in Figure 2.11. This excitation wavelength passes through the filter in the FITC channel and provides the energy at the excitation maximum peak for FITC fluorophore. The laser has the capacity to directly excite the fluorophore at the desired wavelength to provide the maximum excitation and subsequently the most efficient fluorescence emission. The setup has been further aligned with a lens that focused all of the 100 mW output power of the laser onto a spot of monolayer of ~500 μm in diameter. This significantly reduces the acquisition time and increases contrast and sharpness of the images (cf. Images B, C and D in Figure 2.10). Hence, this novel approach has indeed enabled us to better comprehend the membrane morphology as well as the mechanistic nature of insulin/membrane interactions.

In our study an upright, Nikon ECLIPSE FN1, epifluorescence microscope interfaced with Langmuir balance teflon NIMA trough (NIMA, Langmuir-Blodgett, model type 112D, Nima Technology Ltd. Coventry, U.K., was utilized for EFM imaging. This channel is equipped with a green excitation filter set (the Nikon TRITC HYQ filter combination, 545CWL excitation filter, 570LP dichroic mirror and 620CWL barrier filter). A blue excitation filter set (the Nikon B-1E

filter combination, 480CWL excitation filter, 505LP dichroic mirror, and 540CWL barrier filter) was employed to observe the fluorescence from the FITC fluorophore. Each of the two channels was equipped with a 10X objective. The images were captured by a CCD camera, ORCA ER(AG) (Hamamatsu, Japan) directly onto a computer screen using Simple PCI 6 software (Compix Inc., PA).

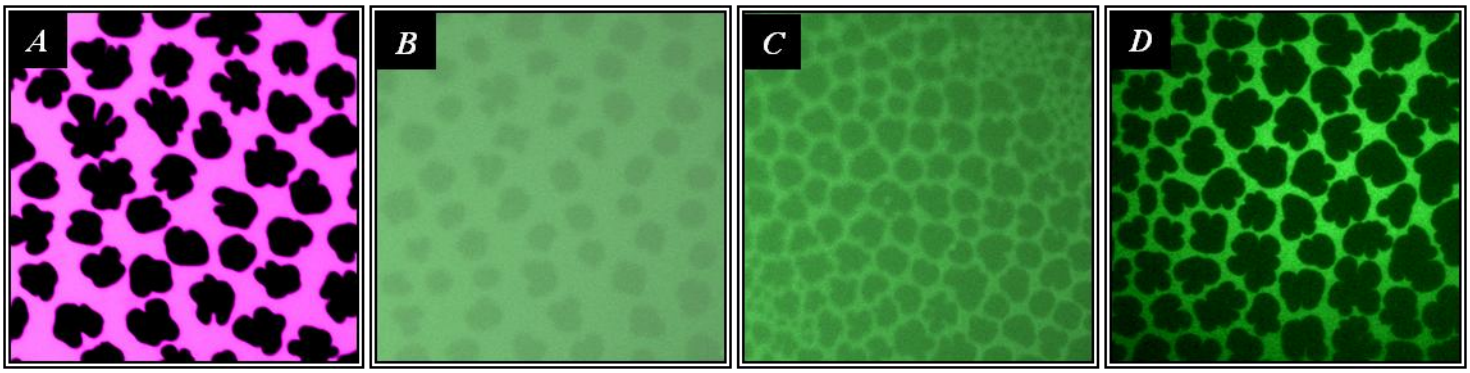


**Figure 2.10:** Image A of the monolayer was captured through TRITC channel using HBO lamp; Image B was captured by EFM via FITC channel using HBO lamp; Image C of the monolayer was captured using FIITC channel with X-Cite (120W) lamp; Image D was captured through the FITC channel using the Laser Glow Technology, laser and a lens focusing directly on the area of interest of about 500μm in diameter.

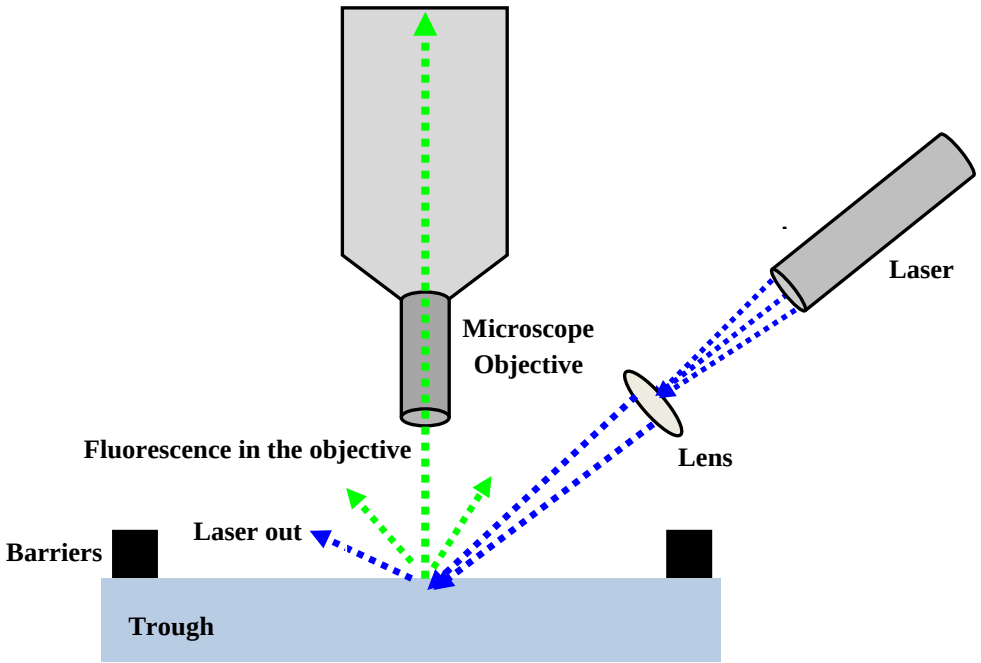


**Figure: 2.11:** Schematics of a laser arm with a focusing lens coupled with EFM. The blue dashed lines depict the excitation light passing through the lens onto the monolayer. Green dashed lines correspond to the emission light coming out of the monolayer and passing through the EFM objective.

### 2.2.4 Basic Principle of Circular Dichroism Spectroscopy, CD

Circular dichroism (CD), discovered by Biot, Fresnel and Cotton, works on the phenomenon of differential absorption of left and right handed circularly polarized light arising from a chiral molecule [Crone 1982]. CD is an advanced spectroscopic technique and is being used in numerous biological applications in particular for proteins structural analysis. Figure 2.12 outlines the basic components used in the instrument. Light from the lamp-house passes through the monochromator and gets dispersed into discrete wavelengths. The radiated beam then passes through the modulator, which produces left and right circularly polarized light. The circularly polarized light enters the sample in the sample compartment. The compartment can possess a variety of controlling systems including temperature control accessory. The light from the sample cell is then detected by a high speed and intensity photomultiplier tube. The output from the photomultiplier tube is converted to a voltage by a preamplifier and is sent to the electronic device where the signals get processed. The processed data is then sent to the computer system equipped with software that can communicate with the instrument and produce a spectrum for each sample, as can be seen in Figure 2.12 [Crone 1982].

In our study a Jasco J-810 spectropolarimeter equipped with a temperature controlled sample holder was used. Far-UV CD spectra were recorded from 260 to 200 nm with a scan rate at 10 nm/min and 1 nm bandwidth at 20 ˚C. Each spectrum was collected by averaging the signal at every 0.5 nm for 2 s. The CD measurements were performed with SUV models. Vesicle suspensions were prepared in PBS. For CD measurements, each vesicle suspension was placed into a rectangular cell with a path length of 10 mm. After recording CD spectra of SUV

suspension, insulin was injected in the cell. A thorough detail of methodology of CD measurements and spectra analysis will be discussed in chapter 7.

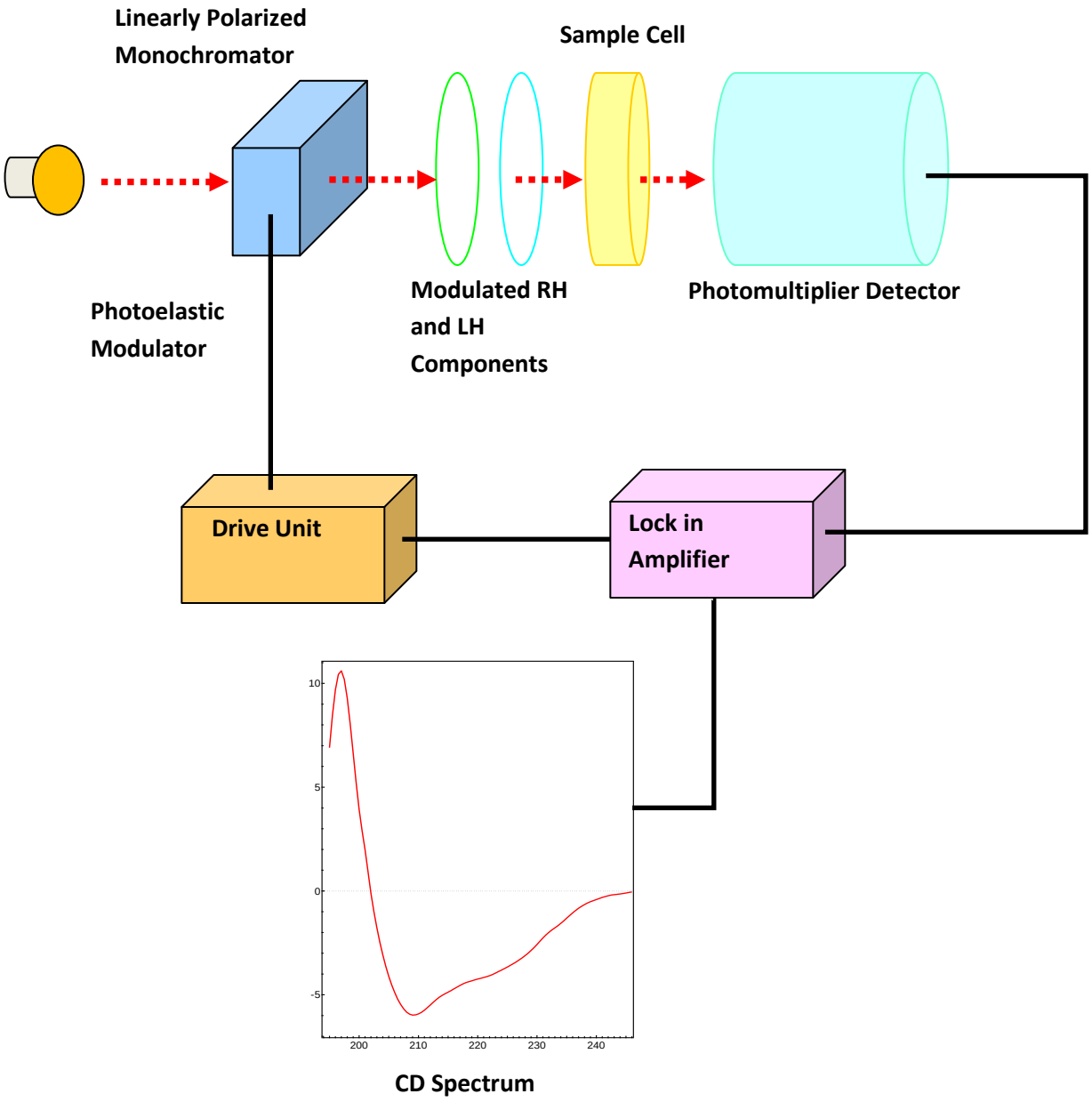


**Figure: 2.12:** Schematics illustrating the principle of Circular Dichroism Spectrophotometer. [The schematic is made based on Heard 2002].

## 2.3 References


Aumann, E. *PhD Dissertation, Stanford University* **2010**.

Birdi, K. S. *Lipid and Biopolymer Monolayers at Liquid Interfaces; Plenum Press: New York* **1989**.

Burner, H.; Winterhalter, M.; Benz, R. *J. Coll. and Inter. Sci.* **1994**, *168,* 183.

Bussieres, S.; Cantin, L.; Desbat, B.; and Salesse, C. *Langmuir,* **2012**, *28 (7),* 3516.

Chattopadhyay, A. *Chem. and phys.lip.***1990**, *53*, 1.

Crone, T. A. *PhD dissertation, Oklahoma State University* **1982**.

Dhruv, H. D. *PhD Dissertation, Utah State University* **2009**.

Gallier, S.; Gragson, D.; Jimenez-Flores, R.; and Everett, D. W. *J. Agric. Food Chem.* **2010**, *58,* 12275.

Gaines, G. L. Jr. *Insoluble monolayers at liquid-gas interfaces; Wiley: New York* **1966**.

Gudheti, M. V.; Mlodzianoski, M.; Hess, S. T. *Biophys. J* **2007**, *93*, 2011.

Heard, A. *PhD Dissertation, Georgia State University* **2002.**

Hentz, N. G.; Richardson, J. M.; Sportsman, J. R.; Daijo, J.; Sittampalam, G. S. *Anal. Chem.* **1997**, *69*, 4994.

Jebrail, M. J. *Masters Dissertation, York University* **2007**.

Kaganer, V. M.; Mohwald, H.; Dutta, P. *Rev. Mod. Phys*. **1999**, *71(3),* 779.

Losche, H.; Mohwald, H. *Coll. and Surf.***1984**, *10*, 217.

Maier, O.; Oberle, V.; Hoekstra, D. *Chem. and phys. of lip.***2002**, *116*, 3.

Mohwald, H. *Els. Sci. B. V.* **1995**, *41*, 441.

Mohwald, H. *Ann. Rev. Phys. Chem.* **1990**, *41*, 168.

Moy, V. T.; Keller, D. J.; Gaub, H. E.; McConnell, H. M. *J. Phys. Chem.* **1986,** *90,* 3198.

Myres, D. *Surfaces, Interfaces and Colloids (Principle and Applications); Wiley-VCH: New York* **1999**.

Na-Nakorn, P. *PhD Dissertation, University of Muenster, Germany* **2004**.

Ploem, J. S.; and Tanke, H. J. *Introduction to Fluorescence Microscopy, Oxford University Press; London* **1987**.

Shahid, M. N.; Tsoukanova, V. *J. Phys. Chem. B* **2011,** *115 (13),* 3303.

Shimshick, E. J.; McConnell, H. M. *Biochemistry* **1973**, *12(12),* 2351.

Tanwir, K.; Shahid, M. N.; Thomas, A.; Tsoukanova, V. *Langmuir* **2012**, *28(39),* 14000.

Tanwir, K.; Tsoukanova, V. *Langmuir* **2008,** *24*, 14078.

Tocanne, J-F.; Teissie, J. *Biochim. Biophys. Acta* **1990,** *1031*, 111.

Tsukanova, V.; Salesse, C. *J. Phys. Chem. B.* ***2004,*** *108(30),* 10754.

Tsukanova, V.; Grainger, D. W.; Salesse, C. *Langmuir* **2002**, *18*, 5539.

Vogel, V.; Mobius, D. *J. Coll. Inter. Sci.* **1988**, *126*, 408.

Wiedmer, S. K.; Jussila, M. S.; Riekkola, M. L. *Anal. Chem.* **2004**, *23*, 562.

Winterhalter, M.; Burner, H.; Marzinka, S.; Benz, R.; Kasianowicz, J. J. *Biophys. J.* **1995**, *69*, 1372.

# Chapter 3: Synthesis and Characterization of DPPE-PEG2000-FITC

A uniform distribution of polymer chains in the phospholipids membranes is considered one of the key factors in reducing the non-specific binding of dissolved biomolecules [Vermette 2003]. However, many studies have shown that the polymer chains are not always homogenously distributed which might create an uneven surface with insufficient PEG density and hence increase the exposure to dissolved biomolecules [Vermette 2003]. This has led us to study the lateral distribution of DPPE-PEG2000 in the DPPE-Succinyl matrix. EFM was chosen as the imaging tool to afford locating the PEG-phospholipid in model membranes. Based on the non-intrinsic fluorescence nature of phospholipid molecules, a FITC fluorophore was coupled to the distal end of the PEG chain of the DPPE-PEG2000 molecule to enable the EFM imaging. The chemical structures of DPPE-PEG2000 and DPPE-PEG2000-FITC are shown in Figure 3.1. The motivation behind the synthesis of DPPE-PEG2000-FITC was mainly due to the lack of its commercial availability. Although, a similar probe with longer aliphatic chains, DSPE-PEG2000-FITC is commercially available. According to Kinsinger et. al., the use of DSPE-PEG2000-FITC as a fluorescent probe for DPPE-PEG2000 does not introduce any artefacts or changes in the phase behaviour of binary phospholipid mixtures [Kinsinger 2010]. However, our latest studies, have suggested that the difference in the aliphatic chain lengths may have a substantial impact on the lateral organization and phase behaviour of PEG-grafted phospholipid mixtures (Tanwir 2012). Thus, to avoid artifacts in EFM imaging experiments DPPE-PEG2000-FITC was synthesized in our lab. This chapter will therefore deal with the synthesis and

characterization of DPPE-PEG2000-FITC using different analytical techniques including NMR and ESI-MS.

**Model Membrane Phospholipids:**

**a) The PEG-Phospholipid, DPPE-PEG2000**

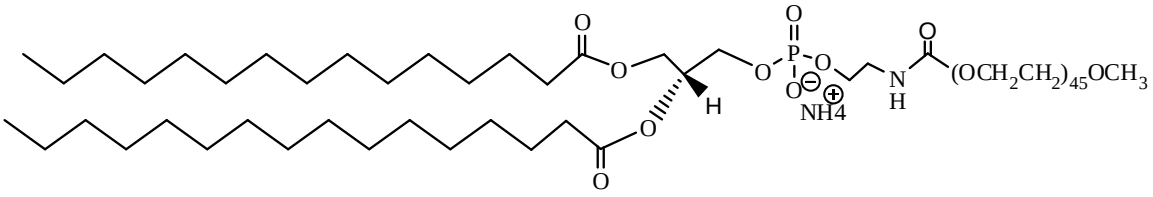

**b) FITC labelled PEG-Phospholipid, DPPE-PEG2000-FITC**

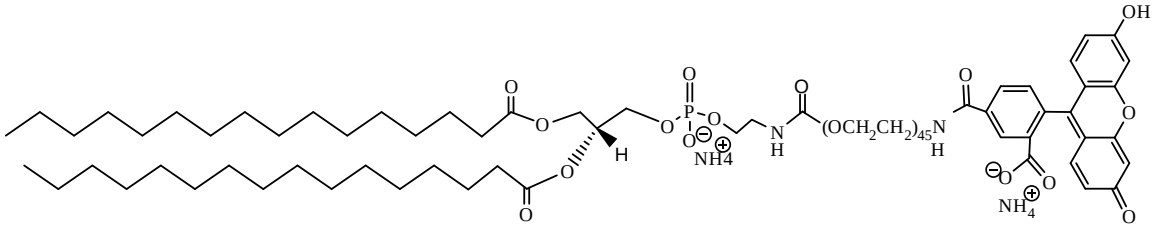

**Figure 3.1:** Chemical Structures of (**a**) DPPE-PEG2000 and (**b**) DPPE-PEG2000-FITC.

### 3.1 Synthesis of FITC Labelled DPPE-PEG2000

DPPE-PEG2000-FITC was synthesized by reacting the amino group of DPPE with the N-hydroxysuccinimidyl group of an NHS-ester, NHS-PEG2000-FITC, in the presence of TEA (triethylamine), as illustrated in Figure 3.2 [Mattson 1993; Miuraa 2006; Teramura 2009]. DPPE solution was prepared at a concentration of 0.036 mmol by dissolving 25 mg of DPPE in 2 mL of $CHCl_3$/MeOH (90:10%) mixture upon heating on a dry bath at ~30 °*C* for about 30 minutes. Triethylamine (5 μL) and 99 mg (0.043 mmol) of NHS-PEG2000-FITC in 1 mL of $CHCl_3$ were then transferred to the DPPE solution. The reaction mixture was stirred magnetically for 4 hrs at ~60 °*C* in the dark while connected to a condenser. The reaction mixture was then left overnight at ~30 °*C*. After 24 hrs, the remaining solvent was evaporated by roto-evaporation method at 70°*C* until the reaction mixture was reduced to 0.5 mL. The DPPE-PEG2000-FITC was precipitated in cold diethyl ether. To remove the excess of unbound NHS-PEG2000-FITC, the product was further washed three times with diethyl ether. The gel-like product was sonicated for 30 min followed by centrifugation for 5 min repeated three times. Then the product was dried under reduced pressure. DPPE-PEG2000-FITC was obtained as yellow orange solid crystals (0.035 mmol, yield 96%). Nuclear magnetic resonance spectroscopy (NMR) and electrospray ionization mass spectrometry (ESI-MS) were performed to characterize the product synthesized. NMR and MS data indicated the presence of traces of unreacted NHS-PEG2000-FITC in the product. The purity of the DPPE-PEG2000-FITC was then verified by measuring and comparing its $\pi - A$ isotherms with the pure DPPE-PEG2000 isotherms on water as subphase. This however, did not affect our monolayer measurements as discussed below. Finally, this product was used without any further purification for the EFM studies of DPPE-Succinyl/DPPE-PEG2000-FITC

binary mixtures to detect the fluorescence and lateral distribution of PEG chains in the phospholipid monolayers (discussed in detail in chapter 4).

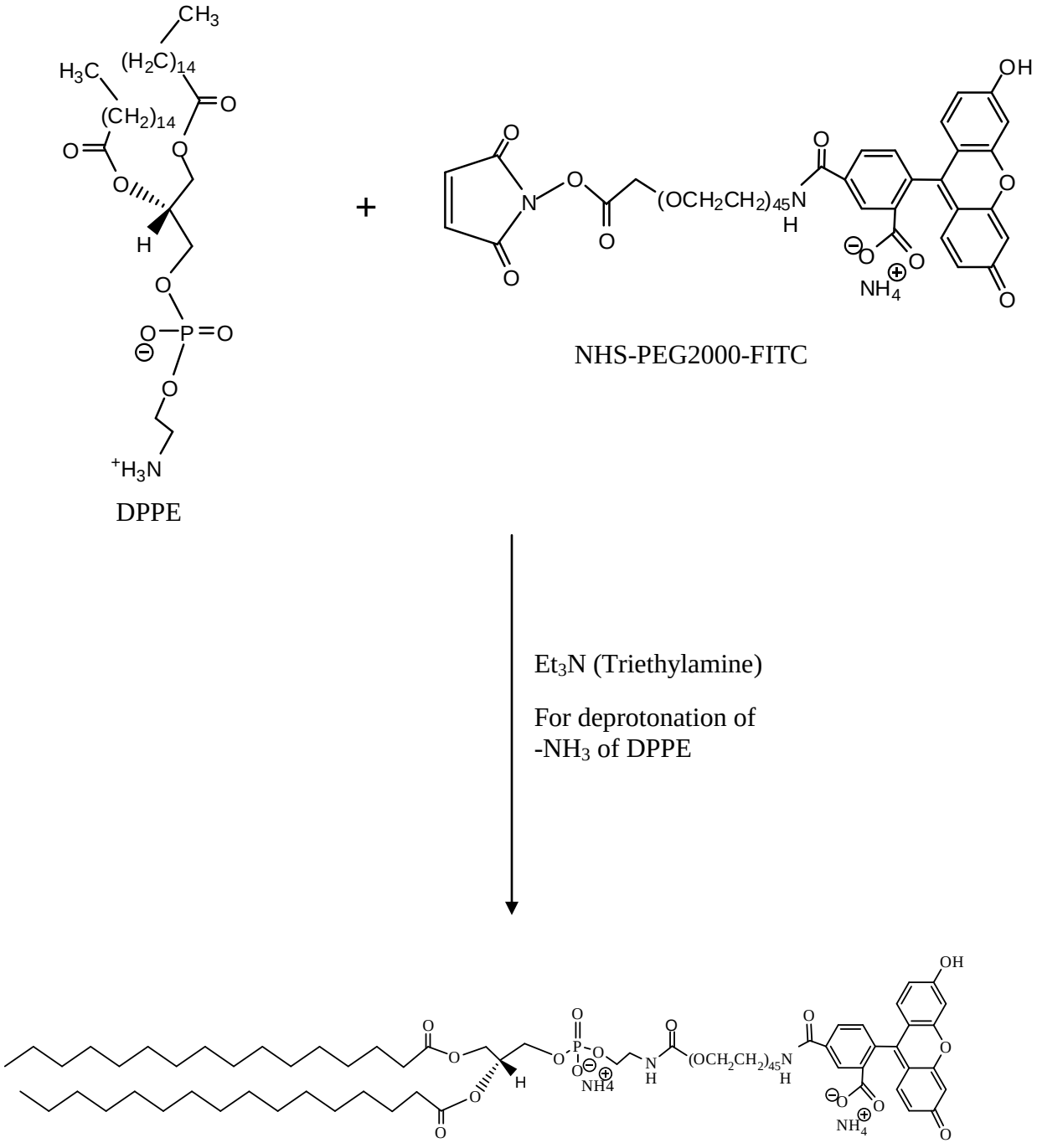


**Figure 3.2:** A chemical reaction scheme depicting the synthesis of DPPE-PEG2000-FITC by reacting DPPE with NHS-PEG2000-FITC.

## 3.2 Results and Discussions

### 3.2.1 Nuclear Magnetic Resonance (NMR) Spectroscopy Analysis of DPPE-PEG2000-FITC

Nuclear magnetic resonance (NMR) spectroscopy was conducted to ensure the complete coupling of DPPE and NHS-PEG2000-FITC. $^{1}H$, $^{13}C$, 2D $^{1}H$ - $^{1}H$ Correlation Spectroscopy (COSY), and 2D $^{1}H$ – $^{13}C$ Heteronuclear Multiple Quantum Correlation (HMBC)-NMR spectra were performed on a Bruker ARX 600 MHz NMR spectrometer (Department of Chemistry York University). The Bruker spectrometer is equipped with a 3-channel probe for $^{1}H$, $^{13}C$, $^{15}N$, xyz gradient and with a 2-channel probe for $^{1}H$ and broad band to cover several nuclei including $^{31}P$, $^{13}C$, $^{15}N$. The product was dissolved in $CD_2Cl_2$ for each run and every spectrum corresponds to an average of 32 scans. The chemical shifts for $^{1}H$ and $^{13}C$ are presented in **δ** (ppm). The signals are described as singlet, **s**, broad singlet, **brs**, doublet, **d**, doublet of doublet, **dd**, triplet, **t**, double triplet, **dt**, and multiplet as **m**. Briefly, peaks in $^{1}H$ NMR ($CD_2Cl_2$, 600 MHz, δ ppm) are categorized as; δ 0.85 [*t* - 6H, - $CH_3(CH_2)_{12}$], 1.23 [m - 9H, (- $C\mathbf{H_3}CH_2)_3N$], 1.23 – 1.39 [m – 48H, - $CH_3(C\mathbf{H_2})_{12}CH_2$], 1.62 [d – 4H, - 2 ($CH_3(CH_2)_{12}C\mathbf{H_2}CH_2CO$)], 2.33 [ t - 4H, - 2 ($CH_3(CH_2)_{12}CH_2C\mathbf{H_2}CO$)], 3.08 [t - 6H, - ($CH_3C\mathbf{H_2})_3N$], 3.3 [m – 6H –$CH_2CH_2N\mathbf{H}$], 3.5 – 3.7 [m – 206 H, - $O(C\mathbf{H_2}C\mathbf{H_2})_{45}NH$], 3.8[ s - 2H, - $OC\mathbf{H_2}$], 3.9 [ s - 2H, - $C\mathbf{H_2}PO_4$], 5.2 [s -1H, $CH_2CO\mathbf{H}CH_2$], 6.5 [d - 2H, –2(C**H**COH)], 6.6 [d – 2H, –2(C**H**CH)], 6.8 [s – 2H –2(C**H**CO)], 7 [s – 2H –C**H**CH], 7.8 [s – 2H –C**H**CHO], 9.2 [s – **H**NCO], and 11.75 [s –CO**H**] as displayed in Figure 3.3.

The purity of DPPE-PEG2000-FITC molecule was also confirmed using 2D $^{1}H$ - $^{1}H$ Correlation Spectroscopy (COSY), and 2D $^{1}H$ – $^{13}C$ Heteronuclear Multiple Bond Correlation (HMBC) NMR experiments. As shown in Figure 3.3 (Chemical Structure of DPPE-PEG2000-FITC), the

synthesized DPPE-PEG2000-FITC consists of two aliphatic chains (bearing two methyl groups at the terminal ends), a glycerol backbone, a polar head group, forty five monomers containing -$CH_2$ units and FITC attached to it through -NH linkage. As labelled in the NMR spectrum (Figure 3.3), the six protons of two terminal methyl groups, 48 protons of hydrophobic chains and protons of PEG monomers shows three big and several small resonances between 0 and 3.8 ppm. Similarly, the protons attached to the rest of the molecule exhibit resonances from 3.9 to 12 ppm. Starting from 0 ppm, the very first major peak at 0.85 ppm is a triplet (labelled as ***a*** in (Figure 3.3) and denote six protons of the two terminal methyl groups of hydrophobic chains. The second prominent resonance peak at 1.3 ppm labelled as ***b*** and $\boldsymbol{m_{TEA}}$ exists as a triplet and represents the methylene protons ($C_4$ to $C_{15}$) of the two aliphatic tails of DPPE-PEG2000-FITC as well as the TEA protons. The peaks ***a***, ***b*** and $\boldsymbol{m}_{TEA}$ were labelled based on the typical chemical shifts of methyl and methylene protons of saturated aliphatic chains [Biswas 2011; Fulmer 2010; Jebrail 2007]. The calculated integration value of peak ***b*** and $\boldsymbol{m}_{TEA}$ is 57, which is in good accord with an integral value of 57 as presented in Figure 3.3. The peaks ***c*** and ***d*** at 1.62 and 2.33 ppm correspond to the $C_{14}$ and $C_{15}$ of both aliphatic chains, respectively. The peak at 3.08 ppm represents the ethyl group of triethylamine ($\boldsymbol{n}_{TEA}$). Similarly, the theoretical integration value for the 45 –$CH_2$-$CH_2$- monomers of PEG2000 shows multiplet peak between 3.5 – 3.7 ppm (peak ***j***) that contains an integral value of 206, which is off from the recorded value of 182 (Figure 3.3). This discrepancy is normally due to large number of methylene protons in long hydrocarbon chains, which results from the difficulty experienced by the integrator while assigning each proton with an integration value of 1 [Knothe 2005]. Peaks at 3.8, 3.9, and 5.2 ppm correspond to glycerol protons as presented in the structure as ***e***, ***f***, and ***g***. Further, the protons present in the aromatic structure of FITC dye are labelled as ***l***, ***m***, ***n***, ***o***, ***p***, ***q*** and ***k*** fall at 6.5, 6.6, 6.8, 7, 7.8,

9.2, and 11.75 ppm, respectively, in the $^{1}$H NMR spectrum of DPPE-PEG2000-FITC (Figure 3.3).

2D $^{1}$H-$^{1}$H COSY was also employed to identify the coupling correlation of several protons in the synthesized product, DPPE-PEG2000-FITC. The 2D $^{1}$H-$^{1}$H COSY analysis is usually conducted by moving from a known diagonal peak, to a cross peak, and back to the diagonal for the assignment of a new peak. The $\boldsymbol{m_{TEA}}$ protons are the neighbouring protons of $\boldsymbol{n_{TEA}}$ and their coupling can be confirmed by the 2D COSY spectrum, as presented in (Figure 3.4). The coupling correlation of methyl and ethyl group protons (***a*** & ***b*)** in the aliphatic chains of DPPE-PEG2000-FITC as well as their bonding to the specific carbon ($^{13}$C) were identified using 2D COSY and 2D HMBC spectra (Figure 3.4 and 3.5). Protons labelled as ***c*** and ***d*** possess similar shifts and can be identified by their coupling correlation with each other. The higher chemical shift of protons ***d*** from ***c*** is due to the deshielding effect of carbonyl groups positioned close to the **d** protons. The coupling correlation of proton ***f*** with protons ***e*** and ***g*** in the glycerol backbone were also determined through 2D $^{1}$H-$^{1}$H COSY spectrum (Figure 3.4). Further, the attachment of proton ***f*** to the carbon of glycerol backbone can be clearly distinguished from the 2D HMBC spectrum. Moreover, correlation coupling of protons ***l***, ***n***, ***o***, and ***p*** corresponding to the protons of FITC probe were also identified through the 2D COSY spectrum (Figure 3.4). Moreover, the 2D $^{1}$H – $^{13}$C HMBC spectrum has also confirmed the correlation of PEG chain protons to their primary carbons (Figure 3.5).

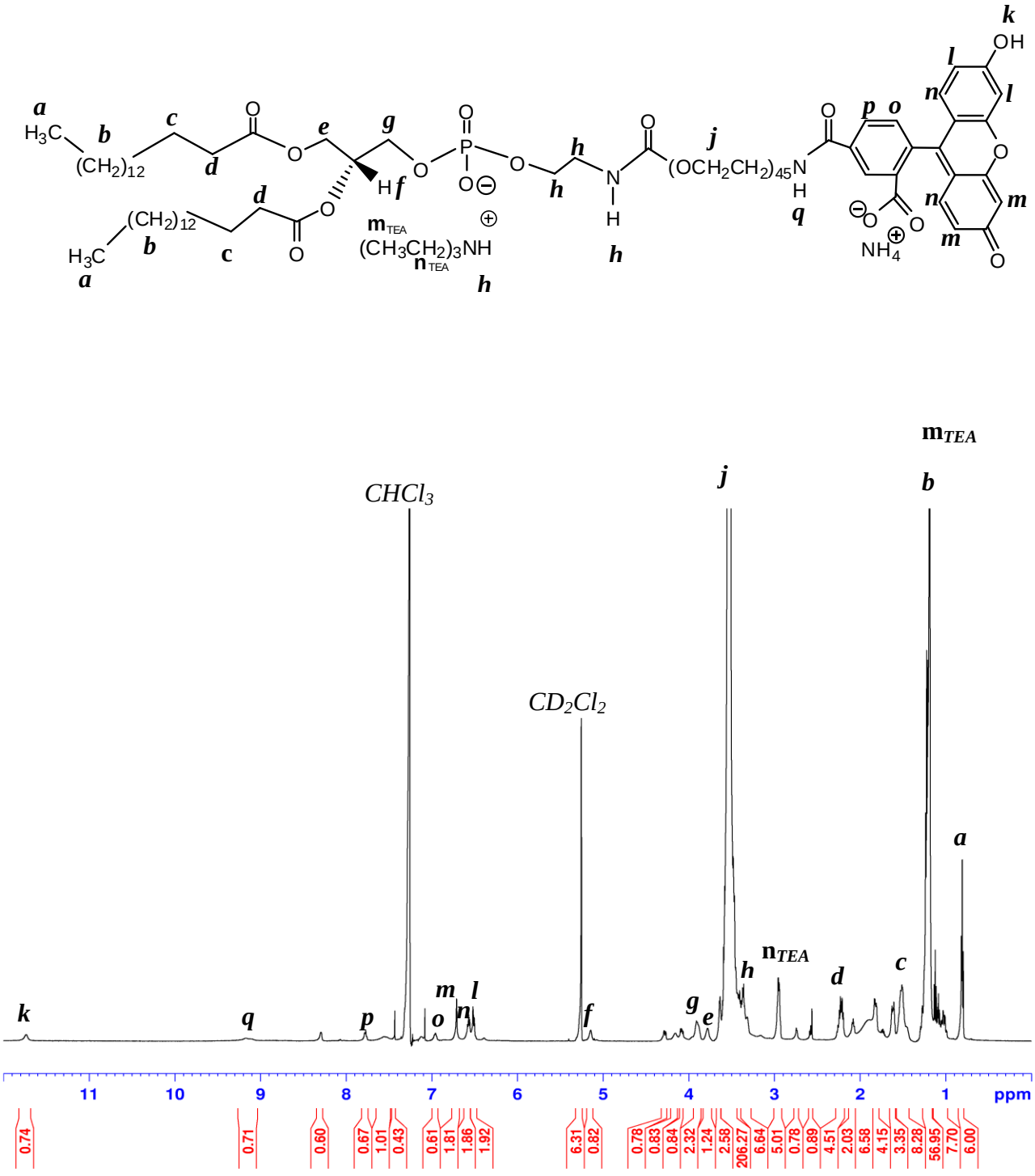


**Figure 3.3:** Chemical Structure and $^{1}H$ NMR Spectrum of DPPE-PEG2000-FITC in $CD_2Cl_2$. The letters on each peak corresponds to the protons present in the chemical structures of DPPE-PEG2000-FITC shown above.

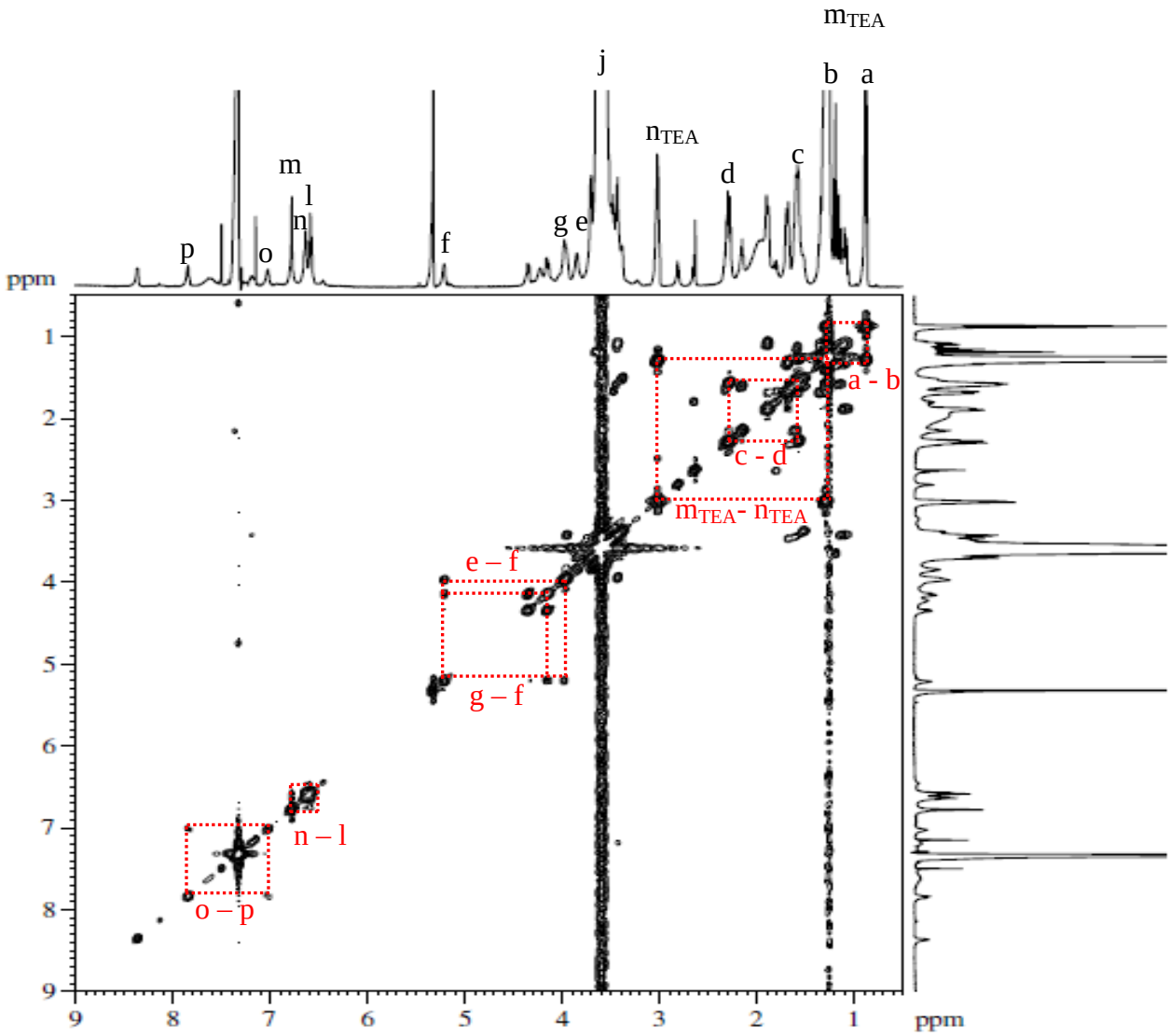


**Figure 3.4:** 2D $^{1}H$ -$^{1}H$ COSY Spectrum of DPPE-PEG2000-FITC in $CD_2Cl_2$ displaying the proton correlation with their adjacent proton.

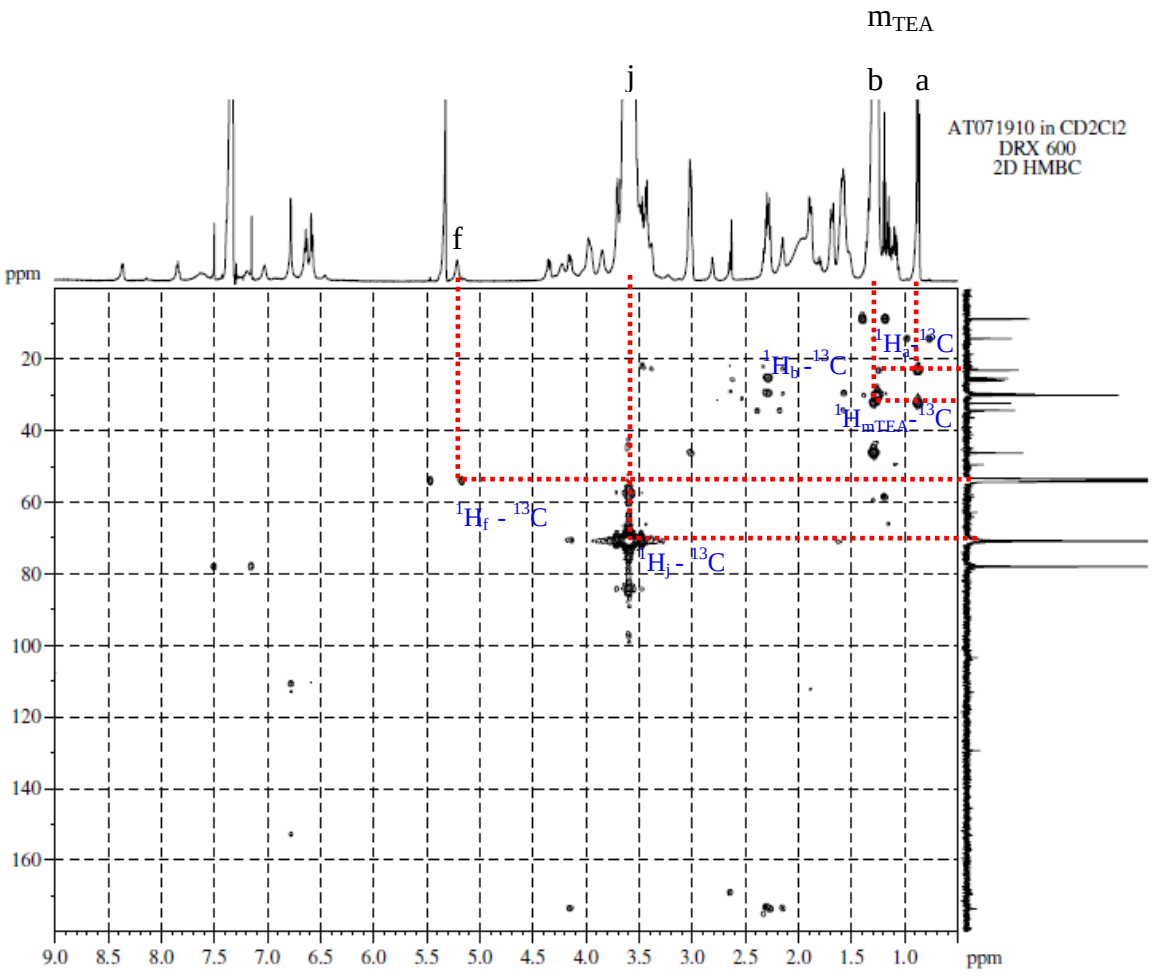


**Figure 3.5:** 2D $^{1}H$ – $^{13}C$ HMBC Spectrum of DPPE-PEG2000-FITC in $CD_2Cl_2$ exhibiting the proton correlation with their attached $^{13}C$.

### 3.2.2. ESI- Mass Spectroscopy (ESI-MS) Analysis of synthesized DPPE-PEG2000-FITC

Electrospray ionization mass spectrometry (ESI-MS) was also utilized to obtain the exact mass of our synthesized product. Experiments were conducted on QSTAR® Elite, a Sciex hybrid quadrupole time-of-flight mass spectrometer (QqTOF) from MDS Analytical Technologies. The instrument was run on an optimal condition of +5000V to +4800 V source. All measurements were done in positive ion mode and at an acquisition rate of $1s^{-1}$. The sample was scanned over 400 to 4000 m/z range to obtain the approximate mass of $C_{149}H_{273}N_2O_{60}$ P using turbo spray [Liuni 2010]. The mass spectrum of DPPE-PEG2000-FITC exhibits two major distributions first between 700 to 1050 Da with +3 charge state and the second between 1100 to 1500 Da with a charge state of +2 as shown in Figure 3.6 and 3.7. A quantitative analysis of both +2 and +3 charge distribution peaks yields an average mass close to ~ 2846.4 Da, which verifies the existence of our product, DPPE-PEG2000-FITC as can be seen from the enlarged view of +2 charge state peaks (Figure 3.6 and 3.7). In addition, a comparative analysis of most of the two large consecutive peaks between 1100 to 1500 Da gives rise to a value of 44 Da which corresponds to a fragment ion of a PEG ($O\text{-}CH_2\text{-}CH_2$) monomer. Thus, the ESI-MS analysis of our synthesized product confirms the complete coupling of DPPE-PEG2000 with FITC yielding an average molecular mass of ~2846.4 g/mol, which is in good agreement with the expected value for DPPE-PEG2000-FITC.

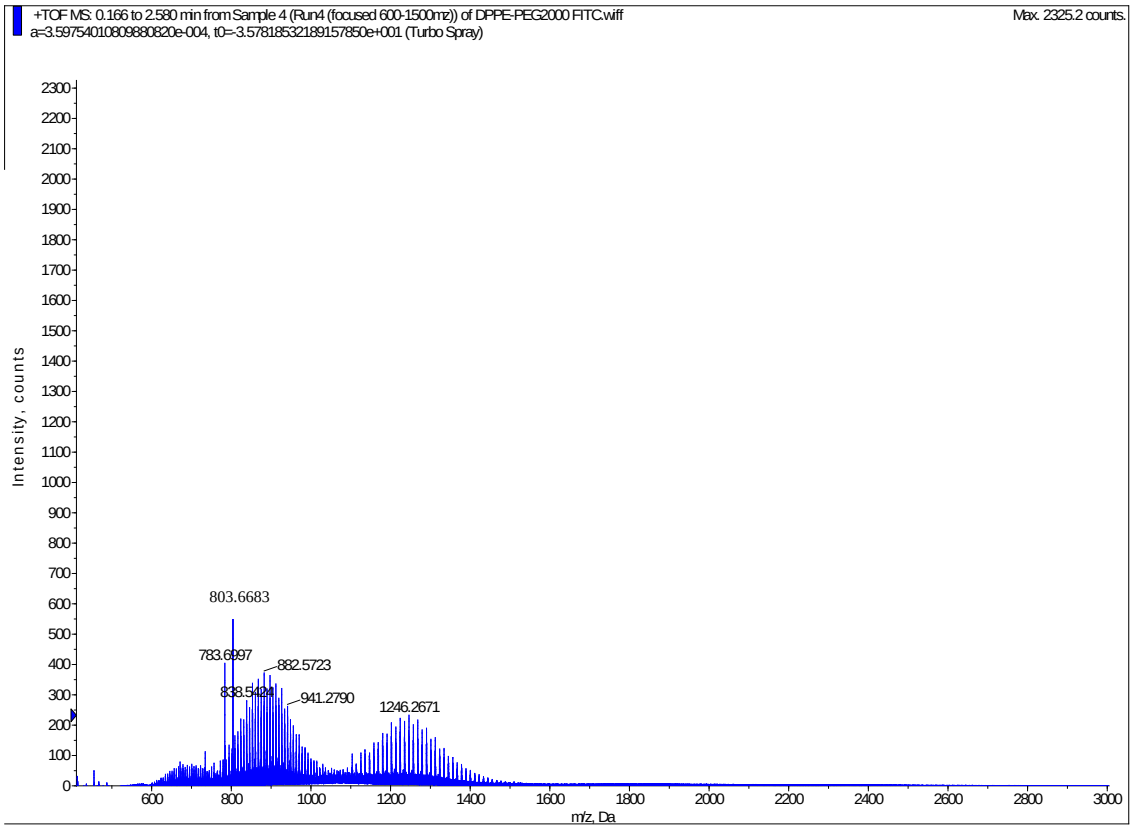


**Figure 3.6:** The ESI-MS spectrum of DPPE-PEG2000-FITC analyzed over an area of 400 to 3000 m/z. The peak area from 700 – 1050 m/z indicates a +3 charge distribution and from 1100 to 1500 m/z exhibits +2 charge distributions.

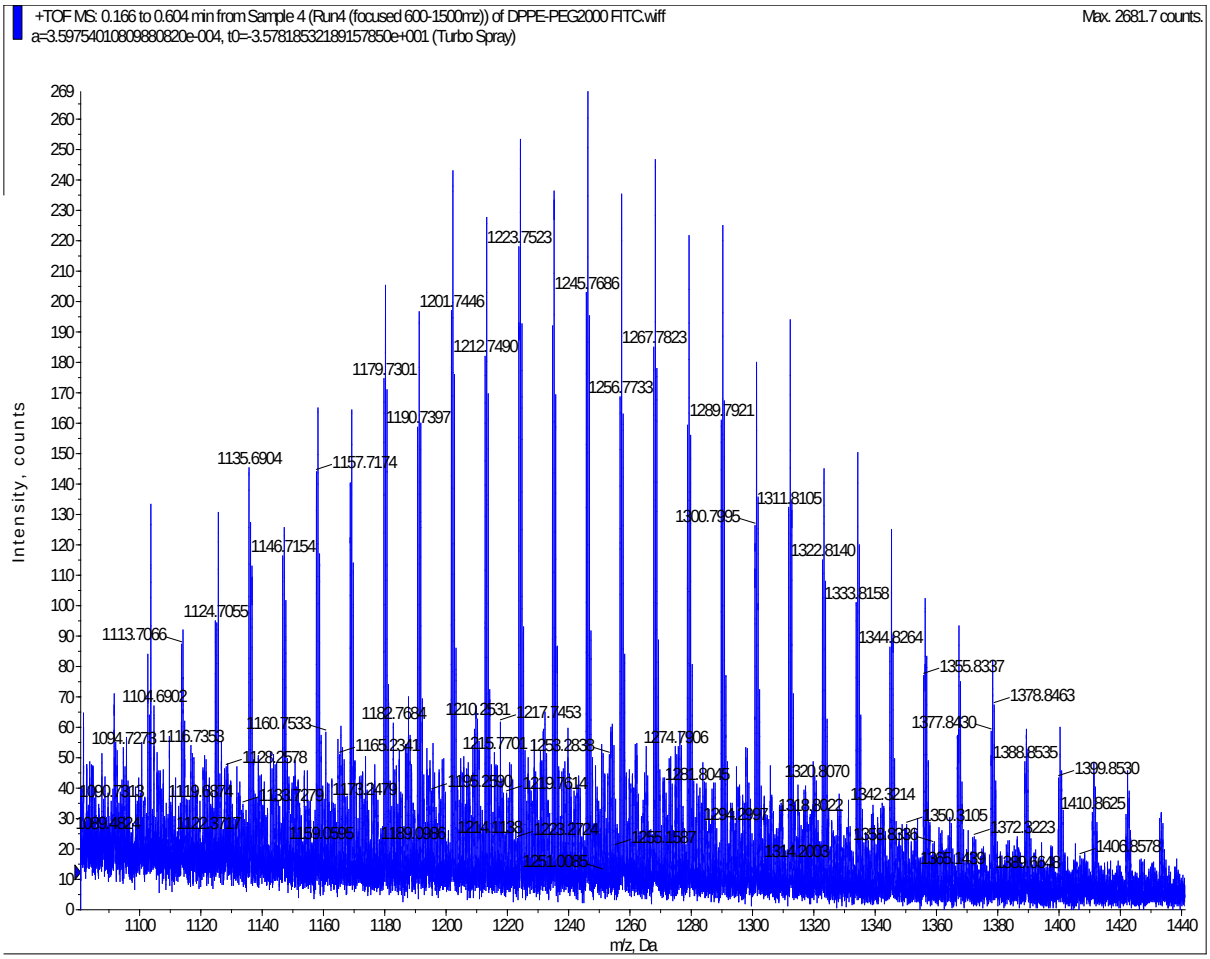


**Figure 3.7:** An enlarged view of the ESI-MS spectrum of DPPE-PEG2000-FITC analyzed over an area of 1100 to 1500 m/z (shown in Figure 3.5). The areas between two consecutive tall peaks give rise an average mass of 44 Da and the average of all +2 charge distribution peaks exhibit an average mass of 2846.4 Da.

### 3.2.3 Monolayer Properties of the DPPE-PEG2000-FITC Probe

The characterization of the synthesized DPPE-PEG2000-FITC probe by NMR and ESI-MS indicated the presence of some traces of unbound NHS-PEG2000-FITC along with the coupled product. Hence, before attempting any further purification, the $\pi - A$ isotherm of DPPE-PEG2000-FITC was measured at the air/water interface and compared with that of DPPE-PEG2000 isotherm to assess the impact of the unbound NHS-PEG2000-FITC traces on the imaging experiments. This was first examined by measuring and comparing the $\pi - A$ isotherms of pure DPPE-PEG2000, DPPE-PEG2000-FITC and NHS-PEG2000-FITC monolayers on water at 20 °C. The rationale behind measuring the $\pi - A$ isotherm of DPPE-PEG2000-FITC on water as a subphase was mainly due to the availability of results for comparative analysis in the literature [Jebrail 2007; Naumann 1999; Shahid 2011]. All three isotherms including DPPE-PEG2000, DPPE-PEG2000-FITC and NHS-PEG2000-FITC had shown the lift-off at an area of ~20 $nm^2$/molecule (Figure 3.8). The pseudo-plateau of all monolayers appeared in the same surface pressure range centered at ~10 mN/m (Figure 3.8). Interestingly, the $\pi - A$ isotherm of NHS-PEG2000-FITC did not go above 15 mN/m. By contrast, the isotherms of synthesized DPPE-PEG2000-FITC and DPPE-PEG2000 monolayers compressed all the way up to 56 mN/m with a mean molecular area of ~0.8 $nm^2$/molecule and exhibited a high-pressure transition at ~26 mN/m (1.6 –1.3 $nm^2$/molecule) as shown in Figure 3.8. Most importantly, the observed high pressure transition in both isotherms is in good accord with the literature data for DPPE-PEG2000 [Jebrail 2007; Naumann 1999; Shahid 2011]. For high-pressure transition to occur, both phospholipid and polymer parts have to be conjugated in the molecule. In fact, the superimposition of DPPE-PEG2000-FITC isotherm on DPPE-PEG2000 is a clear indication of a successful coupling of DPPE with PEG2000-FITC (Figure 3.8). Furthermore, the $\pi - A$ isotherm

of synthesized DPPE-PEG2000-FITC also confirms that the traces of unreacted NHS-PEG2000-FITC do not affect the phase behaviour of the monolayer. These observations also suggest that FITC probe has not altered the phase behavior of DPPE-PEG2000 monolayer and does not interfere with the molecular organization and intermolecular interactions to any significant extent [Tanwir 2008]. All the above findings thus suggest that the synthesized DPPE-PEG2000-FITC can be used without any further purification.

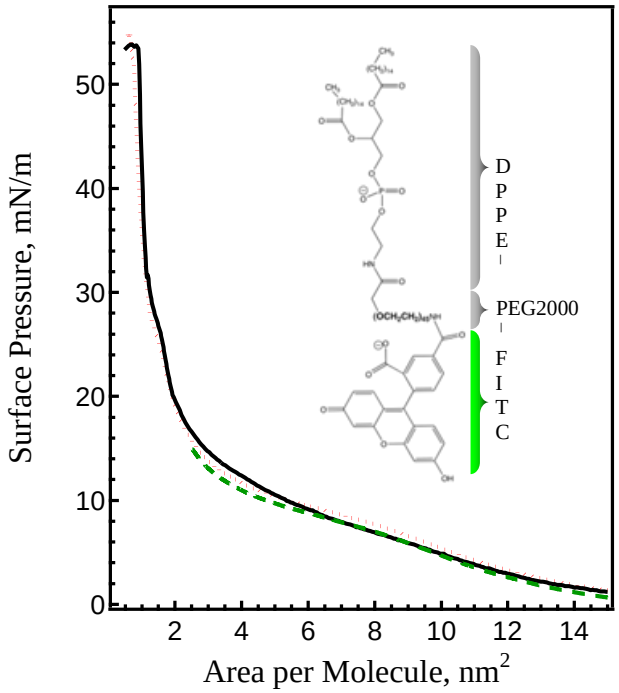


**Figure 3.8:** $\pi$ – $A$ isotherms of (red dotted line) DPPE-PEG2000, (black solid line) DPPE-PEG2000-FITC and (green dashed line) NHS-PEG2000-FITC measured on water as a subphase.

### 3.2.4 In-Situ EFM Imaging of DPPE-PEG2000 and DPPE-PEG2000-FITC Monolayers

The miscibility between DPPE-PEG2000 and DPPE-PEG2000-FITC was also examined using epifluorescency microscopy (EFM) at 20 *°C*. For this DPPE-PEG2000-FITC was added at a concentration of ~0.5 mol% to DPPE-PEG2000 spreading solution. As seen in images a and b in Figure 3.9, the DPPE-PEG2000 monolayers containing ~0.5 mol% DPPE-PEG2000-FITC exhibited a continuous liquid expanded (LE) phase throughout the compression both on water and PBS. At high pressure transitions, the monolayers exhibited even brighter LE phase. Further, no artifacts or phase separation were seen in the DPPE-PEG2000 monolayers containing 0.5 mol% DPPE-PEG2000-FITC throughout the compression. All the above findings, hence, suggest that both components are completely miscible with each other and can be used for further imaging analysis.

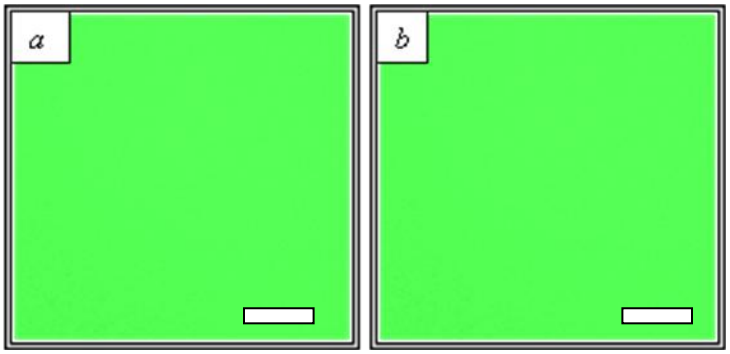


**Figure 3.9:** EFM images of DPPE-PEG2000 monolayer containing 0.5 mol % DPPE-PEG2000-FITC. Images were captured at 25 mN/m on water (*a*) and at 42 mN/m on PBS (*b*) at 20 ± 1 °C. Image size 250 x 250 $\mu m^2$. The scale bar is 50 $\mu m$.

### 3.3 Conclusion

Based on all the characterizations including TLC, NMR and ESI-MS it can be affirmed that DPPE-PEG2000-FITC was successfully synthesized with a yield of ~96%. $\pi - A$ isotherm measurements have also shown that the DPPE-PEG2000-FITC monolayer isotherm is completely super imposable to DPPE-PEG2000 isotherm without any significant changes caused by the FITC probe. The NMR spectra have also given a clear indication of the successful coupling of DPPE-PEG2000 with the FITC chromophore. More importantly, the molecular weight of the synthesized product was determined to be ~2846.4 Da which is very close to the actual molecular weight of DPPE-PEG2000-FITC and hence confirms that the molecule is completely and efficiently synthesized. Thus, the synthesized DPPE-PEG2000-FITC phospholipid conjugate was further used to analyze the lateral distribution of PEG chains throughout the host (DPPE-Succinyl) phospholipid matrix by epifluorescence microscopy.

## 3.4 References


Biswas, S.; Dodwadkar, N. S.; Sawant, R. R.; Torchilin, V. P. *Bioconj. Chem.* **2011**, *22*, 2005.

Fulmer, G. R.; Miller, A. J. M.; Sherden, N. H.; Gottlieb, H. E.; Nudelman, A.; Stoltz, B. M.; Bercaw, J. E.; Goldberg, K. I., *Organometallics* **2010**, *29*, 2176.

Jebrail, M. J. *Masters Dissertation, York University* **2007**.

Kinsinger, M. I.; Lynn D. M.; Abbott, N. L. *Soft Matter* **2010**, *6*, 4095.

Knothe, G, *1H-NMR Spectroscopy of Fatty Acids and their Derivatives, Saturated Fatty acids and Methyl Esters, Lipid library, Peoria, Illinois* **2005**.

Liuni, P.; Rob, T.; and Wilson, D. J., *Rapid Comm. Mass Spec.* **2010,** *24(3)*, 315.

Mattson, G.; Conklin, E.; Desai, S.; Nielander, G.; Savage, M. D.; Morgensen, S., *Mol. Bio. Rep.***1993**, *17*, 167.

Miuraa, S.; Teramura, Y.; Iwata, H., *Biomaterials* **2006**, *27*, 5828.

Naumann, C. A.; Brooks, C. F.; Fuller, G. G.; Knoll, W.; Frank, C. W. *Langmuir* **1999,** *15*, 7752.

Shahid, M. N.; Tsoukanova, V. *J. Phys. Chem. B* **2011,** *115(13)*, 3303.

Tanwir, K.; Shahid, M. N.; Thomas, A.; Tsoukanova, V. *Langmuir* **2012**, *28(39)*, 14000-14009.

Tanwir, K.; Tsoukanova, V. *Langmuir* **2008,** *24*, 14078.

Teramura, Y.; Iwata, H., *Biomaterials* **2009**, *30*, 2270.

Vermette, P.; Meagher, L. *Coll. and Sur. B* **2003**, *28*, 153.

# Chapter 4: Phase Behaviour of DPPE-Succinyl Monolayers

A negatively charged synthetic phospholipid, DPPE-Succinyl, has been chosen in our study as the matrix phospholipid to form model PEGylated membranes. As seen in the inset of Figure 4.1, DPPE-Succinyl is a carboxylated derivative of phosphatidylethanolamine that bears a negatively charged head group with $C_{16}$ aliphatic chains. One of the primary properties of DPPE-Succinyl includes the immobilization capacity of various ligands on its headgroup via covalent coupling to the *N*-carboxyacylamido-PE group [Immordino 2006; Kung 1986; Shahid 2011]. This makes DPPE-Succinyl molecule a promising candidate for the design of patterned PEG-phospholipid surfaces and tunable *pH*-sensitive colloidal lipid carriers [Cordeiro 2000; Immordino 2006; Karve 2010; Kung 1986; Lewis 2000; Shahid 2011; Vermette 2003; Zwaal 1998]. The use of *N*-carboxyacylamido-PEs however requires comprehensive understanding of the phase transitions and conformational behavior particularly for efficient and optimized biomedical applications.

Because of the anionic nature of DPPE-Succinyl molecule's head group, even a slight change in the pH of the medium can affect the phase transition(s) and subsequently the permeability of model membranes including monolayers, vesicles and lipoparticles. Hence, a comprehensive study was designed to investigate the effect of phosphate buffer saline with a physiological pH ~7.4 as well as each of its individual constituents including $Na_2HPO_4$, KCl, $KH_2PO_4$, and NaCl on the biophysical properties of DPPE-Succinyl monolayers as model membrane. The effect of each electrolyte's ionic strength on the phase state of DPPE-Succinyl membrane was also studied using lateral compression and epifluorescence microscopy (EFM).

## 4.1 Results

### 4.1.1 Surface Pressure – Area ($\pi - A$) Isotherms of DPPE-Succinyl Monolayers on Water and PBS

Monolayer properties of DPPE-Succinyl as well as the effect of PBS on the lateral organization and phase transition in the pure DPPE-Succinyl monolayer were first characterized by measuring $\pi - A$ isotherms at the air/water and air/PBS interface. The isotherms are presented in Figure 4.1 and indicate that DPPE-Succinyl forms an expanded type monolayer. On water, the $\pi - A$ isotherm of DPPE-Succinyl monolayer exhibits a first lift-off at 1.25 $nm^2$/molecule. The term lift-off refers to the area per molecule at which the adjacent phospholipid molecules begin to interact with each other. Upon further compression, the surface pressure rises to ~4.5 mN/m and levels off to a plateau with a midpoint at ~5.5 mN/m in a range of 1.25 – 0.98 $nm^2$/molecule. The plateau region is usually attributed to the two-dimensional coexistence of liquid expanded (LE) and liquid condensed (LC) phases [Rossie 2007]. For a typical membrane the term "liquid-disordered" (analogous to LE) and "gel" (analogous to LC) phase are generally used. The plateau region extends to ~0.55 $nm^2$/molecule and upon further compression a low compressibility region is rapidly attained. The low-compressibility region of the isotherm represents the region where surface pressure increases fast upon a slight change in area per molecule. Above this region the monolayer loses its physical stability and collapses at a molecular area of 0.38 $nm^2$/molecule and $\pi$ = 56 mN/m (Figure 4.1).

At the air/PBS interface, the $\pi - A$ isotherm of DPPE-Succinyl monolayer appears more expanded as compared to the monolayer spread on water. The isotherm shows the same regions, yet they appear shifted to either larger molecular areas or higher surface pressures than those for

the monolayer on water. The first lift-off of the isotherm was noticed at an area of ~1.6 $nm^2$/molecule. The plateau of the isotherm appears at a much higher surface pressure of ~25 mN/m as compared to the isotherm on water. However, the monolayer loses its stability and collapses at around the same mean molecular area, 0.39 $nm^2$/molecule as was observed on water but at slightly lower surface pressure of $\pi$ ~ 52 mN/m (isotherms in Figure 4.1). Based on the effect of PBS as compared to water, it will be really important to study the $\pi$ – A isotherms of DPPE-Succinyl on each individual constituent of PBS. Based on the effect of PBS as compared to water, it will thus be important to study the $\pi$ – A isotherms of DPPE-Succinyl on each individual constituent of PBS, which is discussed below.

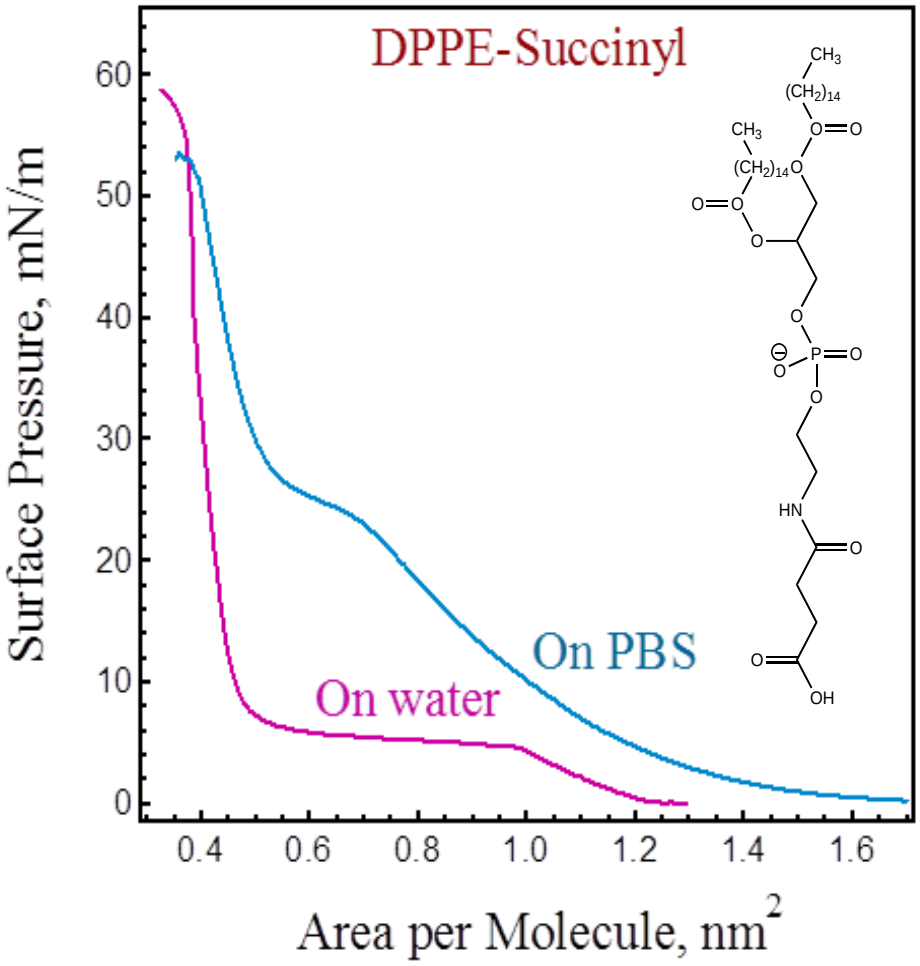


**Figure 4.1:** $\pi - A$ isotherms of DPPE-Succinyl monolayer on water and PBS as a subphase.

### 4.1.2 Surface Pressure – Area ($\pi - A$) Isotherms of DPPE-Succinyl Monolayers on Basic Constituents of PBS

A significant increase in the onset of the isotherm plateau from ~ 6 mN/m on water (pH ~ 6.2) to ~26 mN/m on PBS (pH of ~ 7.4) has led us to investigate the main contributing factors that are responsible for changing the monolayer behavior of DPPE-Succinyl when spread on PBS. The PBS used in our study is composed of different concentrations of potassium and sodium salts including $KH_2PO_4$, (1.47 mM), KCl (2.7 mM), $Na_2HPO_4$ (8.1 mM) and NaCl (138 mM). To study the effect of each electrolyte, an individual solution for each salt was prepared and used as a subphase to study the monolayer behavior of DPPE-Succinyl. Figure 4.2 displays the $\pi - A$ isotherms of DPPE-Succinyl monolayer measured at constituents' typical concentration present in PBS. Each component of the buffer has revealed a unique influence on the phase transitions of DPPE-Succinyl monolayers. Among all the PBS constituents, $KH_2PO_4$ solution containing 1.47 mM or 2.7 mM (isotherm not shown) exhibit the least pronounced effect on the monolayer behavior of DPPE-Succinyl monolayer as compared to water (Figure 4.2). On the contrary, as seen in the $\pi - A$ isotherms in Figure 4.2, NaCl solution containing 138 mM is the main contributing electrolyte altering the monolayer behavior of DPPE-Succinyl monolayer. The NaCl isotherm exhibits the onset of the plateau at about the same position as PBS (Figure 4.2). In fact, all the sodium salts containing subphases develop the LE – LC plateau in the upper portion of the graph with a midpoint at ~21 and 24 mN/m for $Na_2HPO_4$ and NaCl, respectively (Figure 4.2). By contrast, the isotherms of DPPE-Succinyl monolayer on the subphases containing potassium salts such as $KH_2PO_4$ and KCl show the onset of the plateau at lower pressures, at ~9 mN/m and ~18 mN/m, respectively (Figure 4.2). In the low-compressibility region the difference in the isotherms measured on various subphases diminishes. As seen in Figure 4.2 the DPPE-Succinyl

monolayers collapsed in the range of 53 – 58 mN/m, when spread on each individual PBS electrolyte subphase.

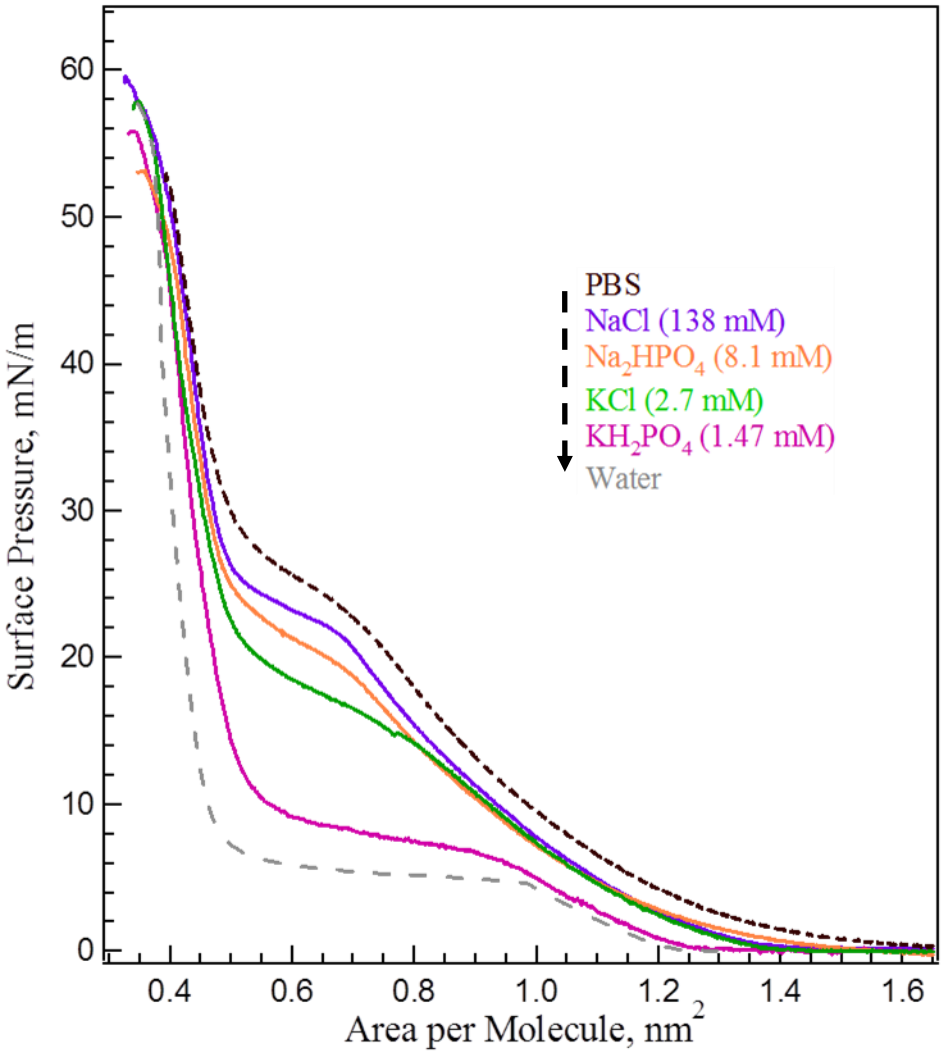


**Figure 4.2**: $\pi - A$ isotherms of DPPE-Succinyl monolayer on PBS (black dashed curve), NaCl (Blue), $Na_2HPO_4$ (Brown), KCl (green), $KH_2PO_4$ (Pink) and water (gray dashed curve) as a subphase, respectively.

### 4.1.3 In-Situ Imaging of DPPE-Succinyl Monolayer Morphology on Water and PBS

To gain further insight into lateral organization and phase transitions in pure DPPE-Succinyl monolayer and how they are affected by the subphase, an in-situ imaging study was performed. The EFM imaging was performed for monolayers on water, PBS and all the PBS constituents individually. First the images obtained on water and PBS will be discussed.

A rhodamine labeled phospholipid analog, DOPE-Rh, was added at a concentration of 0.5 mol% to visualize the phase transitions of pure DPPE-Succinyl monolayers by different partitioning between LE and LC phases, using TRITC channel of EFM. DOPE-Rh contains two unsaturated aliphatic chains due to which it has high affinity towards liquid-expanded phase and is excluded from the liquid-condensed phase [Shahid 2011; Tsoukanova 2008]. The dark domains in the TRITC images represent probe excluded areas and are considered as the LC phase of the monolayer both on water and PBS subphases whereas the bright fluorescence area corresponds to the LE phase with DOPE-Rh in it [Tsoukanova 2008]. The EFM images were captured at several points along the isotherms. Typical images are presented in Figure 4.3; they display the monolayer morphology before the plateau, at the middle of the plateau, and close to the collapse point of the isotherm on water and PBS (Figure 4.3). On water, the DPPE-Succinyl monolayer starts forming evenly distributed small circular domains at the onset of the plateau at ~ 4.5 mN/m. This correlates well with the plateau region of the $\pi - A$ isotherms obtained on water and can be described as the LE to LC phase transition [Nag 1998; Tsoukanova 2008; Worthman 1997;]. These dark circular domains persisted up to ~ 20 mN/m until the entire monolayer started converting into a single dark phase as shown in Figure 4.3. In contrast, on PBS, the domain size appeared to be relatively small, 2 – 8 $\mu m$, in diameter. Moreover, the domains remained virtually unchanged throughout the compression of the DPPE-Succinyl monolayer on the PBS subphase

(cf. images *e* and *f* Figure 4.3). Nevertheless, the DPPE-Succinyl monolayer converted to a single dark phase, yet at a relatively high surface pressure of ~ 45 mN/m.

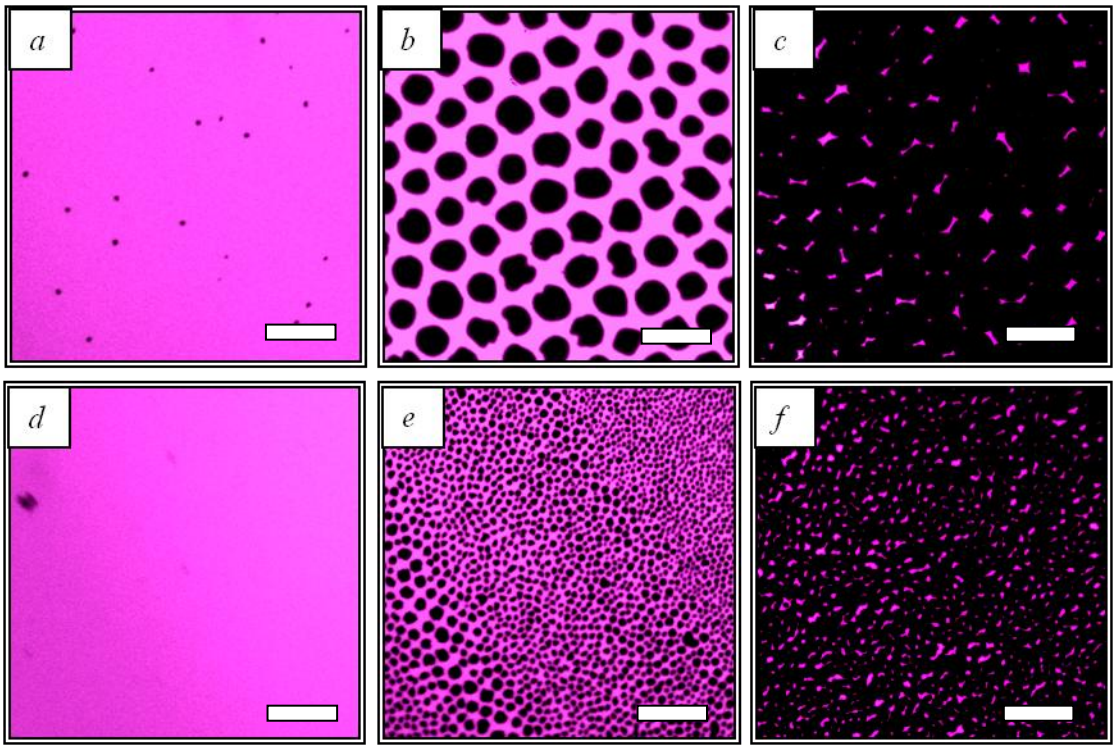


**Figure 4.3:** EFM images of DPPE-Succinyl monolayer captured on water (*a, b, c*) and PBS (*d, e, f*) at 20 ± 1°*C*. Images corresponds to the following regions in the isotherm: Before the plateau – 4 and 15 mN/m, on water and PBS, respectively; at the middle of the plateau – 6 and 26 mN/m, on water and PBS, respectively; close to the collapse point – 20 and 45 mN/m, on water and PBS, respectively. Image size 250 x 250 $\mu m^2$. The scale bar is 50 $\mu m$.

### 4.1.4 In-Situ Imaging of DPPE-Succinyl Monolayer Morphology on the PBS Constituents

A comparative analysis of pure DPPE-Succinyl monolayer data on water and PBS subphases showed a significant difference in terms of their morphology and phase behavior. This led us to investigate the lateral organization and phase transition behavior of DPPE-Succinyl monolayer with respect to change in pH and ionic concentrations. Hence, EFM imaging of DPPE-Succinyl monolayer was performed by spreading on each PBS constituent individually, including $KH_2PO_4$, (1.47 mM), KCl (2.7 mM), $Na_2HPO_4$ (8.1 mM) and NaCl (138 mM). The EFM images in Figure 4.4 correlate well with the different regions of the $\pi - A$ isotherms of DPPE-Succinyl monolayer in Figure 4.2 including expanded region, the LE – LC plateau, and the low-compressibility region. The morphology of DPPE-Succinyl monolayer on 1.47 mM solution of $KH_2PO_4$ as a subphase shows quite a resemblance with the one on water (cf. images *a* – *b* in Figure 4.4 and images *a* – *c* in Figure 4.3). The nucleation of dark circular domains commenced at a relatively low surface pressure of ~ 4 mN/m. However, the size of domains remained smaller throughout the compression on $KH_2PO_4$ as a subphase, as compared to water (cf. images *a* – *b* in Figure 4.4 and images *a* – *c* in Figure 4.3). At the end of the plateau, the monolayer started to attain a dark homogeneous phase which persisted until it reached the collapse point (Figure 4.4*b*).

The EFM images captured for DPPE-Succinyl monolayer on 2.7 mM solution of KCl (images *c* – *d* Figure 4.4) as a subphase show a somewhat different morphology with respect to the one on water (Figure 4.3 *a* – *c*) and $KH_2PO_4$ (images *a* – *b* Figure 4.4). Tiny dark domains started to appear at ~12 mN/m and later turned into rosette shape and persisted throughout the low compressibility region of the isotherm (images *c* – *d* Figure 4.4). As can be seen from the $\pi - A$ isotherm of DPPE-Succinyl monolayer on KCl (Figure 4.2), the plateau region has a midpoint at

~18 mN/m as compared to ~9 mN/m on $KH_2PO_4$ (Figure 4.2). Hence, the appearance of dark domains at an elevated surface pressure of ~18 mN/m on KCl correlates well with the plateau transition of its $\pi - A$ isotherm (cf. Figure 4.2 and Figure 4.4 *c* – *d*). Surprisingly, the EFM images captured for DPPE-Succinyl monolayer on KCl as a subphase showed a rather large size domains as compared to all other PBS constituent subphases, particularly in the low compressibility region of the $\pi - A$ isotherm (Figure 4.2). The DPPE-Succinyl monolayer converted to an almost complete LC phase at $\pi$ ~29 mN/m on KCl, as compared to only ~15 mN/m on $KH_2PO_4$ as a subphase. The continuous dark LC phase was attained at high surface pressures with small fluorescent spots harbouring the DOPE-Rh probe (images not shown).

The EFM measurements conducted for DPPE-Succinyl monolayer on $Na_2HPO_4$ (8.1 mM) as a subphase also shows interesting features throughout the compression. Among few of the unique properties of DPPE-Succinyl monolayer on $Na_2HPO_4$ subphase, the domain size was noticeably smaller and remained almost unchanged throughout the compression (images *e* – *f* in Figure 4.4). Unlike both $KH_2PO_4$ and KCl, DPPE-Succinyl monolayer on $Na_2HPO_4$ converted to a continuous LC phase close to the collapse point (images *e* – *f*, Figure 4.4).

For the DPPE-Succinyl monolayer on 138 mM solution of NaCl as a subphase, the dark circular domains began nucleating at ~15mN/m and persisted almost up to the collapse point. Upon further compression, the DPPE-Succinyl monolayer on NaCl attained an almost complete LC phase close to the collapse point, similar to the monolayer on PBS (c. f. images *d* – *f* Figure 4.3 and *g* – *h* in Figure 4.4). Hence, this behavior suggests that NaCl is the constituent of the PBS that contributes the most in changing the phase transition of DPPE-Succinyl on PBS as compared to that on water.

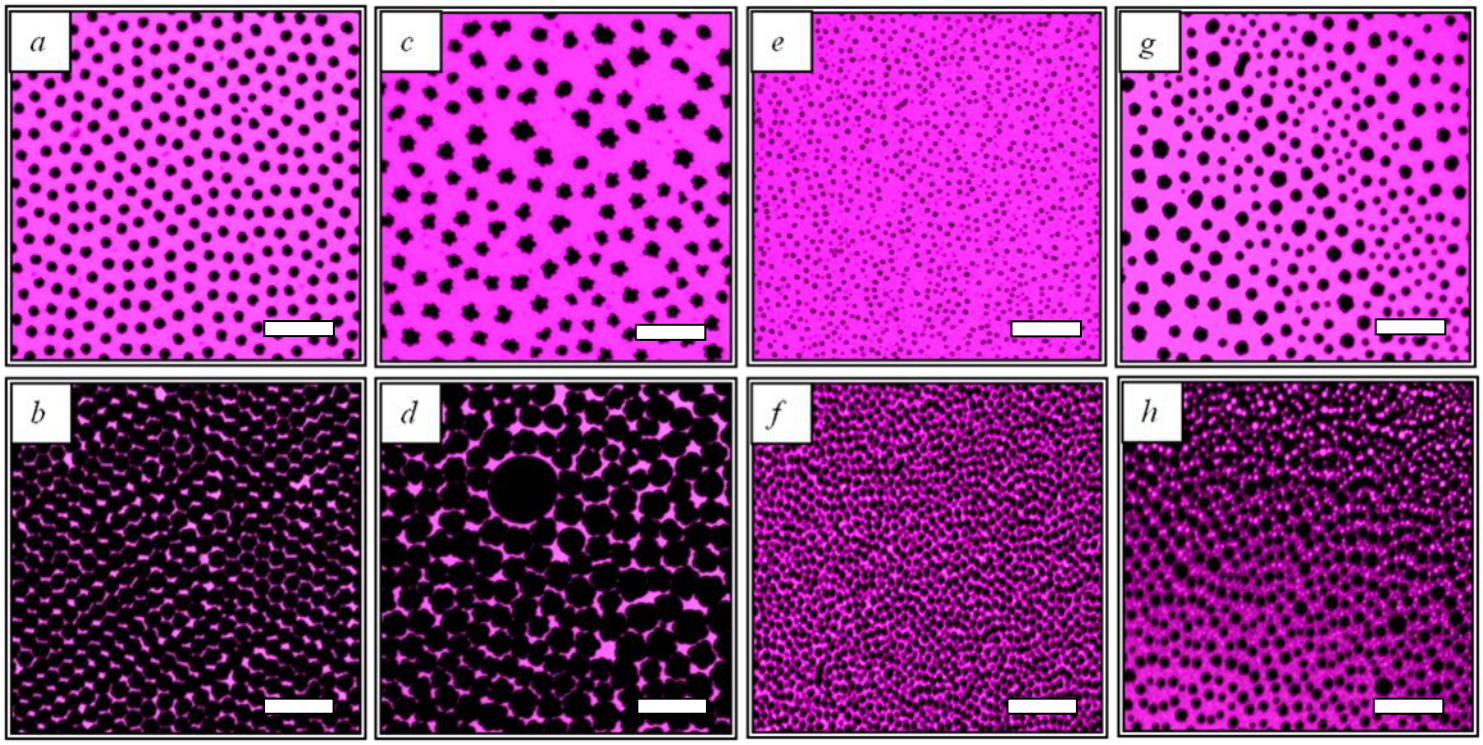


**Figure 4.4:** EFM images of DPPE-Succinyl monolayer containing 1 mol % DOPE-Rh as fluorescent probe, Images (*a, b)* captured at 9 and 15 mN/m on $KH_2PO_4$, (*c, d*) at 18 and 29 mN/m on KCl, (*e, f*) at 21 and 47 mN/m on $Na_2HPO_4$ , (*g, h*) at 24 and 49 mN/m on NaCl, respectively as subphases at 20 ± 1 °*C*. Image size 250 x 250 $\mu m^2$. The scale bar is 50 $\mu m$.

### 4.1.5 ΔV, and $\psi_0$ – Potential for DPPE-Succinyl Monolayer

Surface potential, $\Delta V$, measurements were performed in this study to assess the difference in $\psi_0$-potential of DPPE-Succinyl monolayer on water and PBS. As suggested by Demachak-Fort model, the surface potential for an ionized monolayer combines contributions from the group dipole moments, $\mu_i$ , and the electric double layer potential, $\psi_0$, as presented in equation 4.1 [Burner 1994].

$$\Delta V = \frac{1}{\varepsilon_o A}\sum\frac{\mu_i}{\varepsilon_i} + \psi_0 \text{ ---------- 4.1}$$

In this equation, $\boldsymbol{\varepsilon_0}$ is the permittivity of vacuum, $\boldsymbol{A}$ is the mean molecular area whereas $\boldsymbol{\varepsilon_i}$ is the local effective dielectric constant [Burner 1994; Tsukanova 2004; Tsukanova 2002]. The overall dipole contributions in DPPE-Succinyl monolayer comes from terminal $CH_3$ group, $\mu_{CH3}$, $C = O$ group, $\mu_{C=O}$, PE-Succinyl headgroup of DPPE-Succinyl, $\mu_{PE-Suc}$, as well as from the water molecules reorganized and polarized by the monolayer, $\mu_{H2O}$ [Burner 1994; Tocanne 1990; Tsukanova 2004; Tsukanova 2002].

The dipole moment, $\mu_i$, in equation 4.1 is a normal component of group dipole moment, which is taken as a projection of the group's dipole onto the normal to the monolayer plane [Knecht 2005; Tocanne 1990; Tsukanova 2004]. This implies that the same monolayer spread onto any subphase will have the same orientation of group dipole moments and their normal components, $\mu_i$, when phospholipids are in close–packed state and their group dipole orientational freedom is limited [Latka 2000; Tocanne 1990; Tsukanova 2002]. Further, variations in $\mu_{H_2O}$ will probably be negligible for closely packed monolayers on different subphases since the polarization and reorganization of water molecules` dipoles are only limited to the first layer of molecules of the

monolayer and hence phospholipid headgroups remain mainly dehydrated [Burner 1994; Latka 2000; Tocanne 1990; Tsukanova 2004; Tsukanova 2002; Winterhalter 1995]. However, the headgroup dissociation in the subphase may significantly affect the $\psi_0$ potential [Latka 2000; Tocanne 1990; Tsukanova 2002]. Hence, any difference in the monolayer`s surface potential measured on water and other subphases, in particular PBS, can be associated with the difference in $\psi_0$ potentials as shown below.

$$\Delta V_{PBS} - \Delta V_{H_2O} \approx \psi_{0,\,PBS} - \psi_{0,\,H_2O} \quad \text{---------- 4.2}$$

where $\Delta V_{PBS}$ is the monolayer surface potential measured on PBS, $\Delta V_{H_2O}$ is the monolayer surface potential measured on water, $\psi_{0,\,PBS}$ is the electric double-layer potential on PBS and $\psi_{0,\,H_2O}$ is the electric double-layer potential on water. The difference in electric double-layer potential of the monolayer on water ($\psi_{0,\,H_2O}$) and PBS ($\psi_{0,\,PBS}$) was thus assessed using equation 4.2 at monolayer`s mean molecular area of ~0.42 ± 0.04 $nm^2$. This area refers to the low-compressibility region of the $\pi - A$ isotherms as shown in Figure 4.1, where all DPPE-Succinyl molecules are in close-packed state in the monolayers. The $\Delta V$ recorded for pure DPPE-Succinyl monolayer, in close-packed state, spread on water was 385 ± 7 mV. By contrast, $\Delta V$ values attained for DPPE-Succinyl monolayer on PBS was 295 ± 6, which is ~90 mV lower than that for monolayers spread on water, which clearly indicates that $\Delta V_{PBS} - \Delta V_{H_2O} \approx \psi_{0,\,PBS} - \psi_{0,\,H_2O} \approx$ –90 mV . Based on the data obtained, it can be inferred that $\psi_0$ potential is more negative for monolayer spread on PBS than on water.

## 4.2 Discussion

A detailed study of DPPE-Succinyl monolayer on water, PBS and its basic constituents demonstrates an interesting trend in its phase transition behavior. As described by previous studies, the pH and electrolyte concentrations can enormously affect the lateral organization, molecular area and lateral compression of negatively charged phospholipid monolayers [Domingue 1998; Helm 1986; Shahid 2011]. This phenomenon might be attributed to the electrostatic interactions between dissociated headgroups and basic electrolytes of PBS in the monolayer of ionogenic amphiphiles with $C_{12} - C_{16}$ aliphatic chains [Angelova 1996; Helm 1986]. In particular Helm et al, have demonstrated for phosphatidic acids, that with an increase in the ionic strength of the subphase, the electrostatic contribution to the monolayer surface pressure can rise up to 10 – 15 mN/m due to a repulsion between dissociated head groups and inclusion of counterions in the monolayer [Aroti 2004; Chou 2000; Helm 1986; Patino 1996]. Indeed, the pure DPPE-Succinyl monolayer exhibited a similar trend. DPPE-Succinyl molecules carry a negative charge on their head group (inset in Figure 4.1). The isotherms in Figure 4.1 exhibit a great change in shape and surface pressure values when measured on subphases with different pH and ionic strength, in particular water and PBS. Moreover, upon spreading the DPPE-Succinyl monolayer on each individual buffer electrolyte, including $KH_2PO_4$, KCl, $Na_2HPO_4$ and NaCl, the plateau regions lie between ~6 mN/m (water) and 26 mN/m (PBS) in the isotherms (cf. Figure 4.1 – 4.2). This clearly shows a unique contribution from each electrolyte present in the PBS subphase on the DPPE-Succinyl monolayer and will be discussed later.

### 4.2.1 PBS-Induced Changes in Monolayer Properties of DPPE-Succinyl

The DPPE-Succinyl phospholipid molecule (inset in Figure 4.1) contains two $C_{16}$ aliphatic chains. The $C_{16}$ aliphatic chains of DPPE-Succinyl molecule are linked through a dual carbonyl bond to glycerol and a substituted phosphoethanolamine (PE) head group. The substitution in PE headgroup occurs by replacing two amine protons with a Succinyl group, which eliminates the positive charge from amino group and thus leaves PE headgroup with a single negative charge on the phosphate group. Further, the DPPE-Succinyl molecule possesses an ionogenic carboxyl group at its distal end which can provide another negative charge upon dissociation. Hence, our interpretation of DPPE-Succinyl monolayer behavior will be based on the headgroup dissociation and electrostatic interactions in the headgroup region since this appears to be the major cause for such considerable change in the isotherm spread on PBS (Figure 4.1).

The EFM image analysis of DPPE-Succinyl shows the coexistence of dark LC phase domains with the fluorescent LE background in the isotherms plateau region (Figure 4.1 and 4.3), which confirms that the plateau corresponds to the LE – LC phase transition [Nag 1998; Tsukanova 2002; Worthman 1997;]. LE – LC phase transition was observed on PBS as well. However, the transition appeared at higher surface pressures and with the formation of much smaller domains as compared to water (cf. Figure 4.1 and images *d* – *f* in Figure 4.3). This might point towards a higher barrier that hinders the LC phase growth in the monolayer on PBS subphase. [Angelova 1996; Helm 1986]. This barrier might be an indication of the PBS-induced electrostatic interactions with the headgroup region of the monolayer, as discussed in detail below [Angelova 1996; Helm 1986].

The summarized $\Delta V$ data shows a higher negative value of $\psi_{0,\ PBS}$ potential, which implies a higher negative surface charge density in the DPPE-Succinyl monolayer when spread on PBS compared to that on water. The surface charge density is a combined concentration of ionized carboxyl, $COO^{-}....H^{+}$, and phosphate, $-PO^{4-}....H^{+}$, groups [Tocanne 1990]. Hence, higher negative value of $\psi_{0,\ PBS}$ potential should signify that the DPPE-Succinyl monolayer headgroups dissociate on a somewhat larger scale on PBS than on the water subphase. Previous studies have also suggested that an increase in ionic strength of the subphase from water (~0 M, pH = 6.2) to PBS (~ 0.1 M, pH = 7.4) may increase the degree of dissociation of carboxyl and phosphate group by a factor of 6 and 10, respectively [Helm 1986; Tocanne 1990]. A higher degree of headgroup dissociation should consequently induce a stronger electrostatic repulsion in the DPPE-Succinyl monolayer on PBS [Helm 1986]. Interestingly, the dissociated headgroups in the monolayer also have a great tendency to get hydrated in the subphase [Boggs 1987; Tocanne 1990]. In addition, the negative charge on DPPE-Succinyl dissociated headgroups will tend to attract cations from the PBS subphase, which may trigger the formation of outer-sphere complexes and charge bridges between the carbonyl oxygen [Casares 2008; Tocanne 1990]. Overall, these factors might contribute to increase the effective headgroup area and lateral separation between DPPE-Succinyl molecules in the monolayer, which is in good agreement with the more expanded isotherm of DPPE-Succinyl spread on PBS subphase (Figure 4.1). The formation of smaller-diameter LC domains at much higher pressures on PBS, than on water, is also an evidence of a stronger repulsion in the headgroup region in the pure DPPE-Succinyl monolayer (cf. images in Figure 4.5). Indeed, the electrostatic repulsion created by charged phospholipids along the boundary of a dark LC phase domain will hinder the condensation of more of such phospholipids into a large domain on PBS. The latter will thus favour the

nucleation of a number of small domains, which do not tend to grow much in size upon compression [Helm 1986]. Therefore, in order to attain a complete LC phase for DPPE-Succinyl monolayer on PBS, a much higher surface pressure of ~45 mN/m, as opposed to ~20 mN/m on water, is required to overcome the electrostatic repulsion as well as to squeeze out cations and hydrated water molecules associated with the PE-Succinyl headgroups.

### 4.2.2 Effect of Saline: Contribution of Individual PBS Constituents to the Monolayer Behaviour of DPPE-Succinyl

A significant change in the monolayer properties of DPPE-Succinyl monolayer from water to PBS subphase led us to investigate the contribution of each individual electrolyte in PBS on the monolayer. The EFM images of DPPE-Succinyl monolayer also display distinct features in its morphology while spreading on water, PBS and each of PBS constituents (cf. Figure 4.3 and 4.5). As can be judged by the isotherms in Figure 4.2, adding electrolyte in the subphase has gradually increased the surface pressure and area per DPPE-Succinyl molecule. The increase in surface pressure is usually indicative of the electrolytes penetrating and perturbing the monolayer headgroup region [Aroti 2004; Helm 1986].The subphase with the lowest concentration of electrolyte used in our experiments was a ~1.47 mM solution of $KH_2PO_4$. As can be seen in Figure 4.2, the $\pi - A$ isotherm of DPPE-Succinyl spread on $KH_2PO_4$ lies in a very close proximity to that on water. The morphology of DPPE-Succinyl monolayer on $KH_2PO_4$ shows the appearance of LC domains at ~4 mN/m and converts to an entire LC phase at ~20 mN/m, which is also very similar to the monolayer on water (cf. images *a* and *b* in Figure 4.4 and images *b*

and *c* in Figure 4.3). This suggests that $KH_2PO_4$ component of PBS at a concentration of ~1.47 mM does not have a significant effect on the phase behaviour of DPPE-Succinyl monolayer.

Interestingly, while showing the morphological resemblance with the monolayer on $KH_2PO_4$ the isotherm of DPPE-Succinyl monolayer on a ~ 2.7 mM solution of KCl develops the plateau with a midpoint at ~18 mN/m (cf. 4.4 images *a –b* and *c – d* and Figure 4.2). This value is close to $Na_2HPO_4$ midpoint at ~21 mN/m (Figure 4.2). This effect of KCl electrolyte could be due to the mixed characteristics of $K^+$ and $Cl^-$ counter ions. As can be seen in Figure 4.2, the isotherms of the DPPE-Succinyl monolayers on $K^+$ and $H_2PO_4^-$ containing subphases display lower surface pressures than the isotherms of monolayers on $Na^+$ and $Cl^-$ containing subphases. Indeed, the latter show the expanded and plateau region in the upper portion of the graph in Figure 4.2. The EFM images captured for DPPE-Succinyl monolayer on KCl however shows rosette shaped LC domains quite similar in size to those on $KH_2PO_4$ subphase (cf. images *a –b* and *c – d* in Figure 4.4). This correlation in domain size may indicate less induced electrostatic interactions, between DPPE-Succinyl head group and the $K^+$ counter ions. Further, a delay in the onset of the plateau and LE – LC phase transition on KCl subphase may be due to greater electrostatic repulsion between dissociated head group of DPPE-Succinyl on KCl than on $KH_2PO_4$. This agrees well with Valtiner et. al and Domıinguez et. al findings suggesting that the monolayer may be affected by the increase in pH ($KH_2PO_4$ to KCl), which results in an increased electrostatic repulsion as well as change in the water dipole distribution and orientation that perturbs the hydrogen bonding between water molecules and the phospholipid headgroup [Dominguez 1998; Valtiner 2012].

The above interpretation can also be applied to discuss the isotherms obtained on $Na_2HPO_4$ and PBS subphases. 8.1 mM solution of $Na_2HPO_4$ has a pH of ~7.2, which is close to the pH ~7.4 of PBS and hence can explain the appearance of both plateaus at about the same surface pressure range (Figure 4.2).The late onset of the plateau region of DPPE-Succinyl monolayer isotherms on $Na_2HPO_4$ and PBS, with respect to water and $KH_2PO_4$, can thus be attributed to the subsequent increase in pH, higher degree of dissociation, and ionic strength of the subphase (Figure 4.2). DPPE-Succinyl monolayer on the $Na_2HPO_4$ subphase displays the LE – LC transition below the one on NaCl subphase, which is likely to suggest somewhat less repulsive forces as compared to NaCl and PBS (Figure 4.2). However, the EFM morphology of DPPE-Succinyl monolayer on $Na_2HPO_4$ subphase resembles that on PBS (cf. images d – f in Figure 4.3 and images e – f in Figure 4.4). This might be due to the effect of $Na^+$ ions, as discussed below.

Interestingly, NaCl subphase with a concentration of 138 mM showed the highest plateau transition for DPPE-Succinyl monolayer at ~24 mN/m. This value is closest to the one observed on PBS. The delay in the appearance of the LC phase domains from $KH_2PO_4$ (electrolyte concentration ~1.47 mM; dark domains start appearing at ~4 mN/m) to NaCl (electrolyte concentration ~138 mM ; dark domains start appearing at ~14 mN/m) might suggest a higher barrier to the LC phase growth which results in the expansion of monolayer, as can be seen in DPPE-Succinyl monolayer isotherms and morphology (Figure 4.2 and 4.4). On one hand, this delay can be due to the increased electrolyte concentration and/or ionic strength that promotes the dissociation of the phospholipid headgroup and induces a strong repulsion in the headgroup region, which results in the formation of smaller diameter LC domains seen in the EFM images (Figure 4.4) [Angelova 1996; Helm 1986; Shahid 2011].

On the other hand, $Na^+$ ions are also known to induce a restructuring of water molecules around the polar head groups of DPPE-Succinyl molecules [Patino 1996]. Hence, it can be suggested that the presence of more counter ions, in particular $Na^+$ and $Cl^-$, in the aqueous subphase can firmly anchor the polar head groups in the water molecules network and consequently create a more disordered monolayer system. The binding of hydrated $Na^+$ ions can also increase the hydration capacity of DPPE-Succinyl molecules, which results in repulsive interlayer hydration forces and expanded monolayer behaviour. As a result, $Na^+$ ions are likely to affect the DPPE-Succinyl monolayer more dramatically as compared to $K^+$ ions in the subphase as seen in Figure 4.2 and 4.4. Similarly, $Cl^-$ ions appear to affect the monolayer more significantly than the $H_2PO_4^-$ ions Figure 4.2 and 4.4. However, it can be suggested that the effect of all counter ions is not additive. Hence, it can be concluded that $Na^+$ and $Cl^-$ ions, when combined in the subphase, have the strongest impact on the phase behaviour of DPPE-Succinyl monolayer, as compared to all other constituents of PBS. More studies may be required to further comprehend the effect of counter ions on the phase behaviour of membrane models.

## 4.3 Conclusion

A comparative analysis of the $\pi$ – $A$ isotherms and EFM images has demonstrated an intricate behavior of DPPE-Succinyl on water, PBS and each of PBS constituents. Increased concentration of electrolytes in the subphase delayed the formation of a continuous LC phase in the DPPE-Succinyl monolayer. In fact, each of PBS constituents has shown a remarkable effect on the LE – LC phase transition of DPPE-Succinyl. However, the strongest effect has been observed for $Na^+$ and $Cl^-$ containing subphases, plausibly due to $Na^+$ and $Cl^-$ ions penetrating the head group region of the phospholipids. Thus, it can be suggested that saline has the most significant effect on the phase transition of pure DPPE-Succinyl monolayer.

The PBS-induced electrostatic interactions in the monolayer headgroup region may affect not only the LE – LC transition of DPPE-Succinyl. In mixed DPPE-Succinyl/DPPE-PEG2000 monolayers, the dissociated headgroups and cations from PBS penetrating the monolayer might compete with the grafted PEG2000 chains for hydration water molecules and thus affect their hydration and conformation, which will be investigated in the next chapter.

## 4.4 References


Angelova, A.; Vollhardt, D.; Ionov, R. *J. Phys. Chem.* **1996,** *100*, 10710.

Aroti, A.; Leontidis, E.; Maltseva, E.; Brezesinski, G. *J. Phys. Chem. B* **2004,** *108*, 15238.

Boggs, J. M. *Biochim. Biophys. Acta* **1987**, *906*, 353.

Burner, H.; Winterhalter, M.; Benz, R. *J. Coll. and Inter. Sci.***1994**, *168*, 183.

Casares, J. J. G.; Camacho, L.; Martin-Romero, M. T.; Cascales, J. J. L. *Chem. Phys. Chem.* **2008**, *9*, 2538.

Chou, T.-H.; Chang, C.-H. *Langmuir* **2000,** *16*, 3385.

Cordeiro, C.; Wiseman, D. J.; Lutwyche, P.; Uh, M.; Evans, J. C.; Finlay, B. B.; Webb, M. S. *Antimicro. Agen. and Chemo.***2000**, *44 (3)*, 533.

Dominguez, M. R.; Narvaez, I. G.; Patino J. M. R. *Ind. Eng. Chem. Res.* **1998,** *37*, 936.

Helm, C. A.; Laxhuber, L.; Losche, M.; Mohwald, H. *Coll. and Poly. Sci.***1986,** *264*, 46.

Immordino, M. L.; Dosio, F.; Cattel, L. *Inter. J. Nano.***2006**, *1 (3)*, 297-315.

Karve, S.; Bandekar, A.; Ali, Md. R.; Sofou, S. *Biomaterials* **2010**, *31*, 4409.

Knecht, V.; Muller, M.; Bonn, M.; Marrink, S-J.; Mark, A. E. *J. Chem. Phys.* **2005**, *122*, 024704.

Kung, V. T.; Redemann, C. T. *Biochim. Biophys. Acta* **1986**, *862*, 435.

Latka, P. D.; Dhanabalan, A.; Cavalli, A.; Oliveira-Jr, O. N. O. *J. Phys. Chem. B* **2000**, *104*, 1701.

Lewis, A. L., *Coll. Surf. B* **2000**, 18 *(3-4)*, 261.

Nag, K.; Perez-Gil, J.; Ruano, M. L. F.; Worthman, L.-A. D.; Stewart, J.; Casals, C.; Keough, K. M. W. *Biophys. J.* **1998**, 74, 2983.

Patino, J. M. R.; Dominguez, M. R. *Physicochem. and Eng. Asp.***1996,** *114*, 287.

Rossi, J.; Giasson, S.; Khalid, M. N.; Delmas, P.; Allen, C.; Leroux, J-C. *European J. of Pharm. and Biopharm.***2007,** *67,* 329.

Shahid, M. N.; Tsoukanova, V. *J. Phys. Chem. B* **2011,** *115 (13),* 3303.

Tocanne, J-F.; Teissie, J. *Biochim. et Biophys. Acta* **1990,** *1031*, 111.

Tsoukanova, V.; Salesse, C. *Langmuir* **2008,** *24*, 13019.

Tsukanova, V.; Salesse, C. *J. Phys. Chem. B* **2004,** *108*, 10754.

Tsukanova, V.; Grainger, D. W.; Salesse, C. *Langmuir* **2002**, *18*, 5539.

Valtiner, M.; Donaldson, S. H.; Gebbie, M. A.; and Israelachvili, J. N. *J. Am. Chem.Soc.* **2012,** *134*, 1746.

Vermette, P.; Gauvreau, V.; Pezolet, M.; Laroche, G. *Coll. and Surf. B* **2003**, *29(*4), 285.

Winterhalter, M.; Burner, H.; Marzinka, S.; Benz, R.; Kasianowicz, J. J. *Biophys. J.* **1995**, *69*, 1372.

Worthman, L.-A. D.; Nag, K.; Davis, P. J.; Keough, K. M. W. *Biophys. J.* **1997**, *72*, 2569.

Zwaal, R. F. A.; Comfurius, P.; Bevers, E.M. *Biochim. Biophys. Acta* **1998**, *1376*, 433.

# Chapter 5: Phase Behaviour of Binary Mixtures of DPPE-Succinyl/DPPE-PEG2000 Monolayers

Since cations from PBS have been found to significantly alter the phase behaviour of the matrix phospholipid, a detailed characterization of binary mixtures of DPPE-Succinyl/DPPE-PEG2000 phospholipids was performed on water and PBS. The characterization used the methodology as in the case of DPPE-Succinyl combining surface pressure, surface potential and EFM measurements. Additionally, the miscibility of the two phospholipids, DPPE-Succinyl and DPPE-PEG2000 in binary mixtures was assessed upon increasing PEG content. This was accomplished by combining $\pi - A$ isotherm analysis in terms of excess area with two channel EFM imaging.

## 5.1 Results

Prior to discussing the binary mixtures of DPPE-Succinyl and DPPE-PEG2000, the monolayer behavior of the PEG-phospholipid will be briefly characterized. Monolayer properties of DPPE-PEG2000 have been extensively studied at the air/water interface [Ahrens 2001; Jebrail 2008; Naumann 2002; Naumann 1999]. However, the effect of other subphases, such as PBS, on the monolayer behavior of DPPE-PEG2000 has rarely been discussed [Nosrati 2009; Shahid 2011]. Hence, in this study, $\pi$ – A isotherm and EFM measurements have been performed to assess the monolayer properties of DPPE-PEG2000 at the air/PBS interface.

### 5.1.1 Surface Pressure –Molecular Area ($\pi - A$) Isotherms for DPPE-PEG2000

The $\pi$ – $A$ isotherm of the PEG-phospholipid, DPPE-PEG2000, measured on water and PBS are presented in Figure 5.1. The isotherm measured on water is similar to the previously reported data [Ahrens 2001; Jebrail 2008; Naumann 2002; Naumann 1999]. The lift-off in the $\pi$ – $A$ isotherm on water is detected at ~20 $nm^2$/molecule as seen in Figure 5.1. Upon compressing the monolayer, the molecular area decreases gradually with a simultaneous increase in the surface pressure and attains a pseudo-plateau below ~8 $nm^2$/molecule. The pseudo-plateau correlates well with the literature data [Jebrail 2008; Naumann 1999].This plateau is attributed to a conformational transition in grafted PEG2000 chains from pancake to pseudo-brush conformation [Faure 1999; Jebrail 2008; Naumann 1999; Rex 1998;]. This is schematically shown in Figure 5.2. The plateau continues up to an area of ~3.5 $nm^2$/molecule with a midpoint at ~10 mN/m. Above the plateau, the surface pressure of the DPPE-PEG2000 monolayer isotherm increases rapidly until another discontinuity appears in its slope at a range of 1.6 – 1.3 $nm^2$/molecule at a $\pi$ of ~26 mN/m (Figure 5.1). This second transition has been referred to as a high-pressure transition and attributed to the formation of periodic DPPE-PEG2000 nanostructure depicted in Figure 5.3 [Ahrens 2001; Jebrail 2008; Naumann 1999; Shahid 2011]. The DPPE-PEG2000 phospholipid monolayer collapse is seen at an area of 0.8 $nm^2$/molecule and surface pressure of ~55 mN/m (Figure 5.1), which is in agreement with previously reported data [Jebrail 2008; Naumann 1999].

DPPE-PEG2000 monolayer spread on PBS also shows an expanded type isotherm, similar to the one on water as seen in Figure 5.1. The isotherm exhibits its lift-off at an area of ~22 $nm^2$/molecule. The pseudo-plateau and high pressure transition are also seen in the DPPE-PEG2000 isotherm on PBS similar to that on water. Indeed, the pseudo-plateau on PBS appears

in the same surface pressure of ~10 mN/m as on water although shifted to larger molecular areas. However, the high-pressure transition on PBS appears at a much higher surface pressure of ~42 mN/m but lies in the same range of molecular areas, 1.6 – 1.3 $nm^2$/molecule, as on water. Both monolayer isotherms, on water and PBS, converge above the high-pressure transition. DPPE-PEG2000 monolayer on PBS collapses at $A$ = 0.8 $nm^2$/molecule and $\pi$ = 57 mN/m.

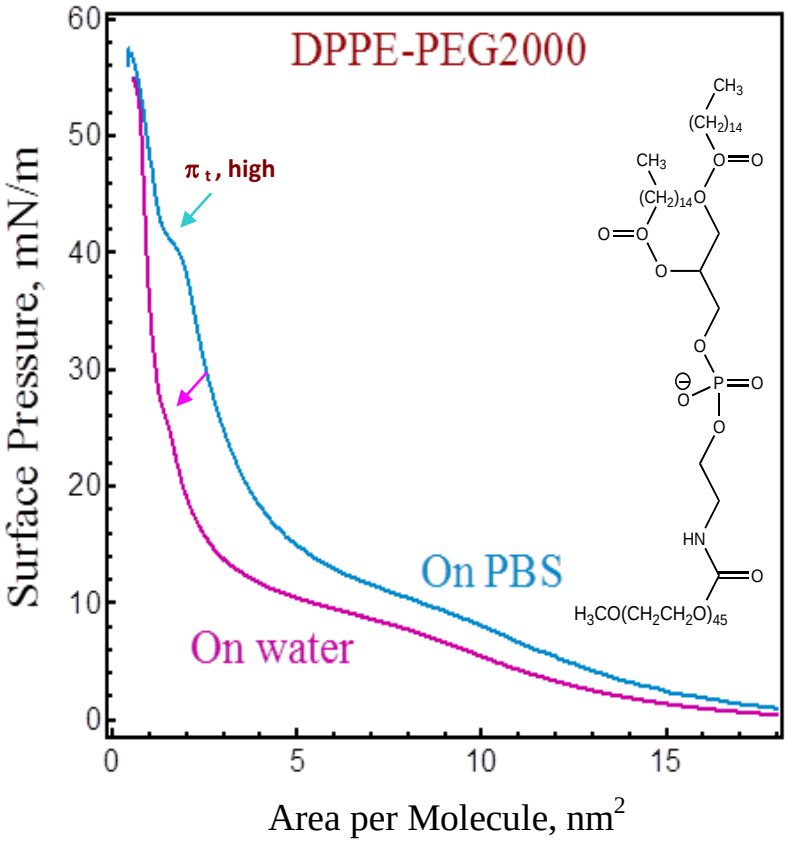


**Figure 5.1:** $\pi - A$ isotherms of DPPE-PEG2000 monolayer on water and PBS as a subphase.

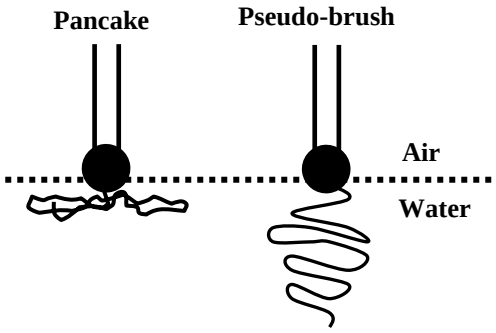


**Figure 5.2:** The schematics of PEG-phospholipid molecules conformational transition from pancake to pseudo-brush [Schematics made based on Baekmark 1995].

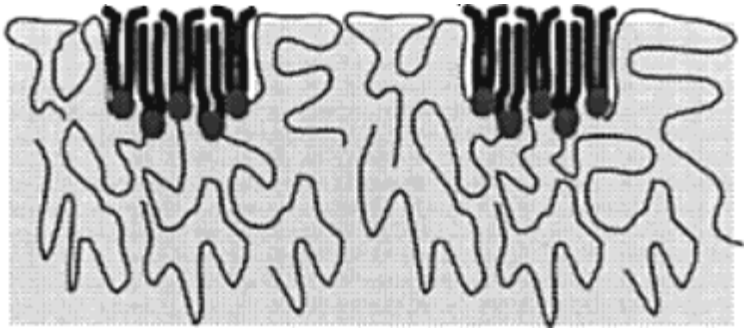

**Figure 5.3:** The schematics of PEG-phospholipid molecules arrangement, showing partially submerged PEG2000 chains in the subphase [Adapted from Ahrens 2001].

### 5.1.2 In-Situ EFM Imaging of DPPE-PEG2000 Monolayers on Water and PBS

Previous studies have suggested that, at high-pressure transition, the condensation of aliphatic chains of DPPE-PEG2000 occurs. This condensation is viewed as somewhat similar to LC phase formation [Ahrens 2001; Naumann 1999; Wiesenthal 1999], yet occurring on a much smaller scale with a periodicity of a few nanometers as seen in Figure 5.3. To verify whether this condensation may result in the formation of microscopic LC phase domains in DPPE-PEG2000 monolayers, an EFM study has been performed. For this, DOPE-Rh probe was added at a concentration of ~1 mol% to DPPE-PEG2000 spreading solution. Both on water and PBS, the DPPE-PEG2000 monolayer exhibited a continuous fluorescent field, starting from low surface pressure to the point of monolayer collapse, as displayed in images *a* – *b* in Figure 5.4. This is indicative of the LE phase and thus suggests that there is no microscopic LC phase formation. These observations confirm the prediction by Ahrens et al [Ahrens 2001] that the LC phase formation is likely to occur only at a nanoscale. Therefore, on a microscopic scale, the DPPE-PEG2000 molecules should appear as forming exclusively an LE phase that shows fluorescent in EFM images on both water and PBS.

EFM imaging was also performed to assess the miscibility between DPPE-PEG2000 and its fluorescent analog, DPPE-PEG2000-FITC, which has been discussed in detail in chapter 3.

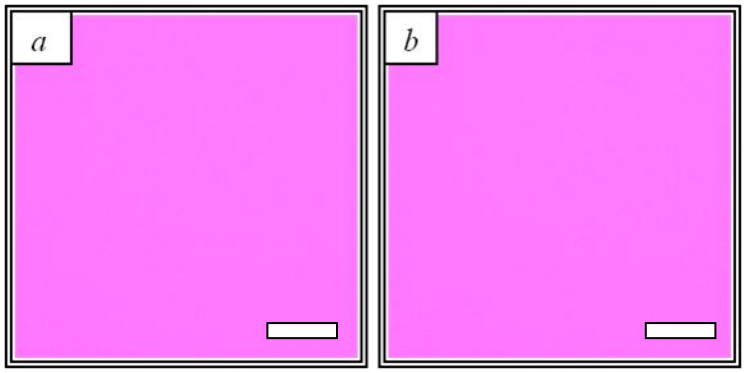


**Figure 5.4:** EFM images of DPPE-PEG2000 monolayer containing 1 mol % DOPE-Rh. Images were captured at 25 mN/m on water (*a*) and at 42 mN/m on PBS (*b*) at 20 ± 1 °C. Image size 250 x 250 $\mu m^2$. The scale bar is 50 $\mu m$.

### 5.1.3 Surface Pressure – Mean Molecular Area ($\pi - A$) Isotherms for Mixed DPPE-Succinyl/DPPE-PEG2000 monolayers

The $\pi - A$ isotherms of DPPE-Succinyl/DPPE-PEG2000 monolayers with varying PEG-phospholipid content, 1, 3, 6, 9 mol%, were measured on water and PBS subphases at 20 °C. On water, the $\pi - A$ isotherms of mixed DPPE-Succinyl/DPPE-PEG2000 monolayers clearly show the combined characteristics of both individual phospholipid isotherms. As seen in Figure 5.5a, all the mixed monolayer isotherms exhibit four major regions: (i) an expanded region below ~4.5 mN/m, corresponding to the liquid expanded phase, (ii) a plateau with a midpoint ~5.5 mN/m, typical of DPPE-Succinyl, (iii) a second plateau which resembles the DPPE-PEG2000 isotherm pseudo-plateau with a midpoint at ~10 mN/m and (iv) a collapse point at ~56 mN/m. Importantly, an increase in PEG content in the mixed monolayers results in a gradual increase in mean molecular area and broadening of the expanded region of the isotherm (Figure 5.5a). Moreover, the first plateau region of the isotherm shrinks significantly with increase in PEG content; yet, the second plateau of the isotherm becomes more apparent. Indeed, at 1 mol% PEG, the mixed monolayer isotherm exhibits an increased curvature between 6 and 12 mN/m, which was not seen in the isotherm of DPPE-Succinyl monolayer on water (cf. Figure 4.1 (chapter 4) and 5.5a). Upon increasing PEG content to 6 and 9 mol%, the second plateau becomes clearly seen in the mixed monolayer isotherms. Comparison with the DPPE-PEG2000 isotherm in Figure 5.1 shows that the second plateau in isotherms in Figure 5.5a resembles the pseudo-plateau of DPPE-PEG2000 monolayer isotherm on water. Interestingly, incorporation of PEG2000-phospholipid in the DPPE-Succinyl monolayers does not show any significant effect in the low-compressibility region of the isotherms, regardless of PEG content. Indeed, above ~30

mN/m all the mixed monolayer isotherms converge being less than 0.02 $nm^2$ apart from each other. All mixed monolayers collapse at ~56 mN/m on water.

On PBS subphase, the $\pi - A$ isotherms of the binary mixtures of DPPE-Succinyl/DPPE-PEG2000 also display characteristics of the two components, DPPE-Succinyl and DPPE-PEG2000, (cf. Figure 5.1, 5.5b with Figure 4.1 (chapter 4)). However, compared to the isotherms on water, the isotherms measured on PBS appear more expanded and shifted to larger areas and surface pressures. The two plateau regions, although observed in the isotherms of pure components, DPPE-Succinyl and DPPE-PEG2000, at different pressures, appear to overlap in Figure 5.5b. Indeed at, 1 and 3 mol% PEG, the mixed monolayer display a plateau with a mid point at ~25 mN/m. The plateau bears a striking resemblance to that seen in DPPE-Succinyl isotherm on PBS (Figure 4.1). However, at higher PEG content, mixed monolayers on PBS show a noticeable change in their isotherms. At 6 and 9 mol % PEG, monolayers exhibit a significant broadening in the plateau region. As seen in Figure 5.5b the onset of plateau decreases to ~17 and ~12 mN/m, respectively, as compared to ~23 mN/m for 1 mol % isotherm on PBS (cf. Figure 5.5b). Further, the low compressibility region of the monolayer isotherms containing 6 and 9 mol% PEG content display another discontinuity at ~42 mN/m, which resembles the high-pressure transition of the DPPE-PEG2000 monolayer on PBS (cf. Figure 5.1) [Baekmark 1999; Jebrail 2008; Shahid 2011; Naumann 1999]. An increase in PEG concentration from 1 to 9 mol% also results in an increase in the collapse pressure from 52 to 57 mN/m.

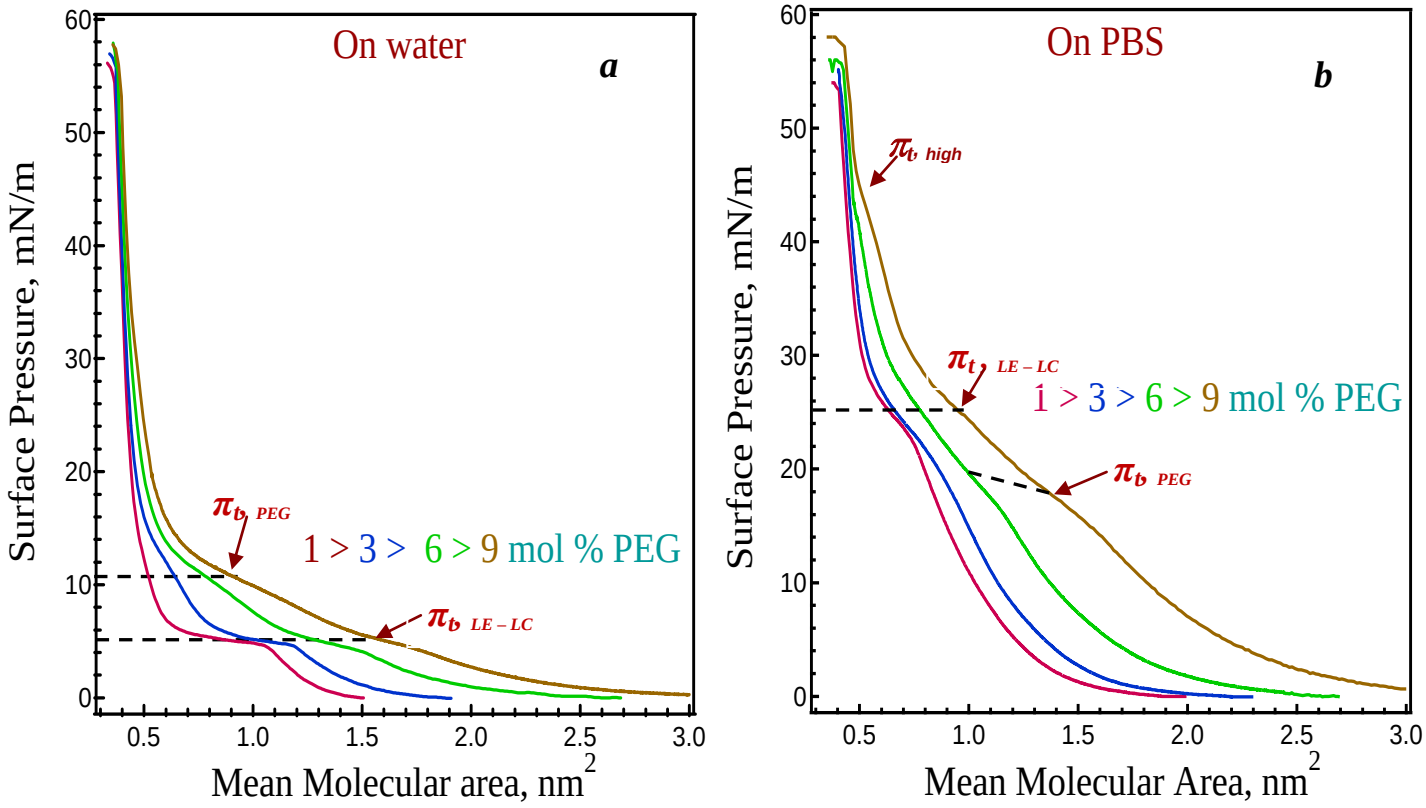


**Figure 5.5: (a)** $\pi$ - *A* isotherms of mixed DPPE-Succinyl/DPPE-PEG2000 monolayers on water (a) and PBS (b) subphase at 20 ± 1 °C. Arrows and dashed lines point at the surface pressure corresponding to the LE – LC transition, $\boldsymbol{\pi_{t,LE-LC}}$; the PEG2000 conformational transition, πt,PEG; and the high pressure transition, $\boldsymbol{\pi_{t,high}}$. For the monolayers at the air/water interface (***a***), the $\boldsymbol{\pi_{t,\,LE-LC}}$ transition occurs at ~5mN/m whereas $\boldsymbol{\pi_{t,PEG}}$ occurs at ~10 mN/m. For the monolayers on PBS (***b***), the $\boldsymbol{\pi_{t,\,PEG}}$ transition occurs at ~18-20 mN/m, $\boldsymbol{\pi_{t,\,LE-LC}}$ at ~25 mN/m, and $\boldsymbol{\pi_{t,high}}$ at ~42 mN/m.

### 5.1.4 Miscibility Analysis for Mixed DPPE-Succinyl/DPPE-PEG2000 Monolayers

To investigate the miscibility between the two components in mixed DPPE-Succinyl/DPPE-PEG2000 monolayers, the excess area, $A_{exc}$, of the mixture was calculated from quantitative analysis of $\pi - A$ isotherms in Figures 4.1, 5.1, and 5.5 [Shahid 2011].

$$A_{exc} = A - (\chi_{DPPE\text{-}Succinyl} A_{DPPE\text{-}Succinyl} + \chi_{DPPE\text{-}PEG2000} A_{DPPE\text{-}PEG2000}) \text{ ----------5.1}$$

where, $\boldsymbol{A_{exc}}$ , is the excess area of the mixture, $\boldsymbol{A}$ is the actual area per molecule in the mixed monolayers acquired from their isotherms in Figure 5.5, $\chi_{DPPE\text{-}Succinyl}$ *and* $\chi_{DPPE\text{-}PEG2000}$ are the mole fraction of the two components and $A_{DPPE\text{-}Succinyl}$ and $A_{DPPE\text{-}PEG2000}$ are the molecular area of DPPE-Succinyl and DPPE-PEG2000 in their pure monolayers at the same surface pressure which can be obtained from Figures 4.1(chapter 4) and 5.1, respectively. In general, if the two components form an ideal binary mixture, components are completely miscible, or are completely immiscible, $\boldsymbol{A_{exc}}$ is zero. Any deviation from zero, either positive or negative, points towards the non-ideal miscibility in the mixed monolayers [Tanwir 2008]. The calculated values of $\boldsymbol{A_{exc}}$ for the mixed DPPE-Succinyl/DPPE-PEG2000 monolayers on water and PBS are shown in table 5.1 and 5.2, respectively. The calculated values of $\boldsymbol{A_{exc}}$ for mixed monolayers on water are mostly negative, suggesting a closer packing between DPPE-Succinyl and DPPE-PEG2000 molecules in the mixture than among themselves (Table 5.1). The closer packing between monolayers thus indicates a favorable interaction between two components. In contrast, the mixed monolayers on PBS show quite a different trend. As seen in table 5.2, an increase in PEG content in the binary mixtures results in mostly positive $\boldsymbol{A_{exc}}$ values, which might indicate repulsive interactions and/or poor miscibility between the two components on PBS subphase. The calculated values of $\boldsymbol{A_{exc}}$ from both tables suggest a non-ideal mixing behavior of DPPE-

Succinyl and DPPE-PEG2000 in the binary mixtures on water and PBS subphases. Hence, it can be deduced that the components of mixed monolayers mainly exhibit negative $\boldsymbol{A_{exc}}$ values on water subphase suggesting a contraction of the mean molecular area as compared to mostly positive $\boldsymbol{A_{exc}}$ values on PBS subphase indicating an overall expansion of the mean molecular area.

**Table 5.1:** Excess area, $A_{exc}$, calculated using equation 5.1 for mixed monolayers containing 1, 3, 6 and 9 mol% DPPE-PEG2000 in DPPE-Succinyl at the air/water interface at various surface pressures.

| $A_{exc}$ nm$^2$ | | | | |
|---|---|---|---|---|
| $\pi, m$N/m | 1 mol% PEG | 3 mol% PEG | 6 mol% PEG | 9 mol% PEG |
| 6 | -0.02 | -0.02 | -0.02 | -0.02 |
| 12 | -0.03 | 0.0 | -0.04 | 0.0 |
| 15 | -0.04 | -0.03 | -0.06 | -0.05 |
| 35 | 0.0 | -0.01 | -0.03 | -0.02 |
| 50 | -0.01 | -0.01 | -0.02 | -0.01 |

Each value of $A_{exc}$ is an average over a set of five of five isotherm measurements. For all mixed monolayers, standard deviation for $A_{exc}$ were within ± 0.01 nm$^2$.

**Table 5.2:** Excess area, $A_{exc}$, calculated using equation 5.1 for mixed monolayers containing 1, 3, 6 and 9 mol% DPPE-PEG2000 in DPPE-Succinyl at the air/PBS interface at various surface pressures.

| $A_{exc}$ nm$^2$ | | | | |
|---|---|---|---|---|
| $\pi, m$N/m | 1 mol% PEG | 3 mol% PEG | 6 mol% PEG | 9 mol% PEG |
| 6 | -0.01 ± 0.01 | 0.01 ± 0.01 | 0.08 ± 0.01 | 0.13 ± 0.01 |
| 12 | 0.0 ± 0.00 | -0.01 ± 0.01 | 0.05 ± 0.01 | 0.10 ± 0.01 |
| 15 | 0.0 ± 0.00 | 0.0 ± 0.00 | 0.03 ± 0.01 | 0.07 ± 0.01 |
| 35 | -0.01 ± 0.01 | 0.01 ± 0.01 | 0.0 ± 0.00 | 0.02 ± 0.01 |
| 50 | 0.0 ± 0.00 | 0.02 ± 0.01 | 0.01 ± 0.01 | 0.02 ± 0.01 |

Each value of $A_{exc}$ is an average over a set of five of five isotherm measurements. For all mixed monolayers, standard deviation for $A_{exc}$ were within ± 0.01 nm$^2$.

### 5.1.5 In-Situ EFM Imaging of Mixed DPPE-Succinyl/DPPE-PEG2000 Monolayers on Water

The effect of increasing PEG-phospholipid content on the phase behavior and miscibility in mixed DPPE-Succinyl/DPPE-PEG2000 monolayers was further examined using the two channel EFM. The phase state imaging was performed through the TRITC channel. Contrast in the TRITC channel was derived due to DOPE-Rh probe, which has a high affinity towards the LE phase [Discher 1999; Shahid 2011; Tsoukanova 2008]. The FITC channel was used to monitor PEG-phospholipid distribution in the DPPE-Succinyl matrix and miscibility between the two components in binary mixtures. Contrast in the FITC channel was derived due to the fluorescence from FITC fluorophore attached to DPPE-PEG2000-FITC. As discussed in chapter 2, fluorescence from DPPE-PEG2000-FITC reports on the location of DPPE-PEG2000 molecules in the mixed monolayers since DPPE-PEG2000 and DPPE-PEG2000-FITC are ideally miscible. Hence, the fluorescence from DPPE-PEG2000-FITC stained green the areas where the PEG-phospholipid molecules were present while the dark domains indicated DPPE-PEG2000-FITC-excluded areas [Borden 2006; Kinsinger 2010; Tanwir 2008]. Most of the two channel EFM images shown were captured from the same area of the monolayer for comparative analysis.

The in-situ imaging was first performed for mixed monolayers on water. The EFM images were captured throughout the compression for mixed monolayers containing 1, 3, 6 and 9 mol% DPPE-PEG2000. However, only the images obtained just prior to the plateau, right after the plateau, and close to the collapse point are displayed for the clarity of presentation (Figures 5.6 – 5.9). One of the remarkable changes upon incorporation of PEG-phospholipid in the host DPPE-Succinyl matrix is the appearance of rosette-shaped DOPE-Rh-excluded LC domains as

compared to the circular domains of pure DPPE-Succinyl monolayer on water (cf. Figure 4.3 *a–c* and images *a–d* in Figure 5.6 – 5.9). Interestingly, a significant decrease in the size of domains was observed in both TRITC and FITC images with increasing PEG content in the binary mixtures of DPPE-Succinyl/DPPE-PEG2000 (cf. Figures 5.6 – 5.9). The domains ranged from 30 – 50 $\mu m$ in diameter for mixture containing 1 mol% PEG and reduced to 2 – 10 $\mu m$ for mixture containing 9 mol% PEG (cf. images *b* and *e* in Figure 5.6 with images *a – d* in Figure 5.9 captured at 6 mN/m). Regardless of the PEG-phospholipid content, three regimes including LE phase, LE – LC transition, and LC phase, were clearly distinguished in all the mixed monolayers on water. All the mixed monolayers spread on water appeared homogeneously fluorescent below 4 mN/m indicating the single LE phase, which correlates well with the observation of the expanded regions in their isotherms. The nucleation of dark DOPE-Rh-excluded LC phase domains in the mixed monolayers began at the onset of the first plateau in the isotherms, which is a typical feature of the pure DPPE-Succinyl monolayer spread on water (cf. Figure 4.3 *a – c* and images *a–d* in Figure 5.6 – 5.9). The fluorescent LE and dark LC phase then coexisted throughout the compression in the plateau region of the mixed monolayer isotherms, as can be seen in image *b* in Figures 5.6 – 5.9. Above ~12 mN/m, the domains began to fuse (images *c* and *g* in Figures 5.6 – 5.9). Upon further compression, a single dark LC phase was eventually observed for all the mixed monolayers in the low-compressibility region of their isotherms (images *d* and *h* in Figure 5.6 – 5.9). However, the surface pressure at which the single dark LC phase was attained varied depending on the DPPE-PEG2000 content in the mixed monolayers.

Figure 5.10 shows the analysis of % Dark Domains for 0, 1, 3, 6, and 9 mol% DPPE-PEG2000 in DPPE-Succinyl monolayers. Values for % Dark Domains were first calculated from EFM

images that were captured from several points along the isotherms of mixed monolayers and were then plotted with respect to the surface pressure. Percentage of dark DOPE-Rh-excluded LC phase domains gradually increased with increasing surface pressure in all mixed monolayers spread on water, as shown in Figure 5.10. Mixed monolayer containing 1 mol% PEG showed a value of 100% percentage of dark domains corresponding to the entire LC phase monolayer at $\pi \approx 25$ mN/m, which is slightly higher as compared to the pure DPPE-Succinyl monolayer (cf. Figure 5.10). The surface pressures at which the mixed monolayers containing 3, 6, and 9 mol% achieved a complete LC phase monolayer are 34, 41, and 52 mN/m, respectively (Figure 5.10). Interestingly, the successive increase of PEG2000 content in the mixed DPPE-Succinyl/DPPE-PEG2000 monolayers decreased the overall % Dark Domain, at any given surface pressure, $\pi$.

TRITC and FITC images displayed identical patterns for all binary mixtures at low and intermediate surface pressures (cf. images a – c and e – g in Figures 5.6 – 5.9). At high surface pressures, however, quite a different patterning was observed in both TRITC and FITC images, (images d and h in Figure 5.6 – 5.9). In TRITC images, the DOPE-Rh probe eventually becomes completely excluded from the LC phase monolayers at high surface pressure and harboured into tiny fluorescence spots sporadically appearing in the field of view and occupying less than 1% of the monolayer. The morphology where the monolayer becomes completely LC phase will be referred to as a "dark monolayer (images d in Figure 5.6 – 5.9). Conversely, in FITC images, a domain pattern is seen up to the monolayer collapse point (images h in Figure 5.6 – 5.9). Since the DPPE-PEG2000-FITC probe reports on the location of DPPE-PEG2000 in the monolayers, the non-uniform fluorescence patterns in FITC images indicates that the PEG-phospholipid does not achieve homogeneous distribution. Thus, it can be inferred that the binary mixtures of DPPE-

Succinyl/DPPE-PEG2000 did not achieve a homogenous distribution of PEG, regardless of the surface pressure or the PEG content.

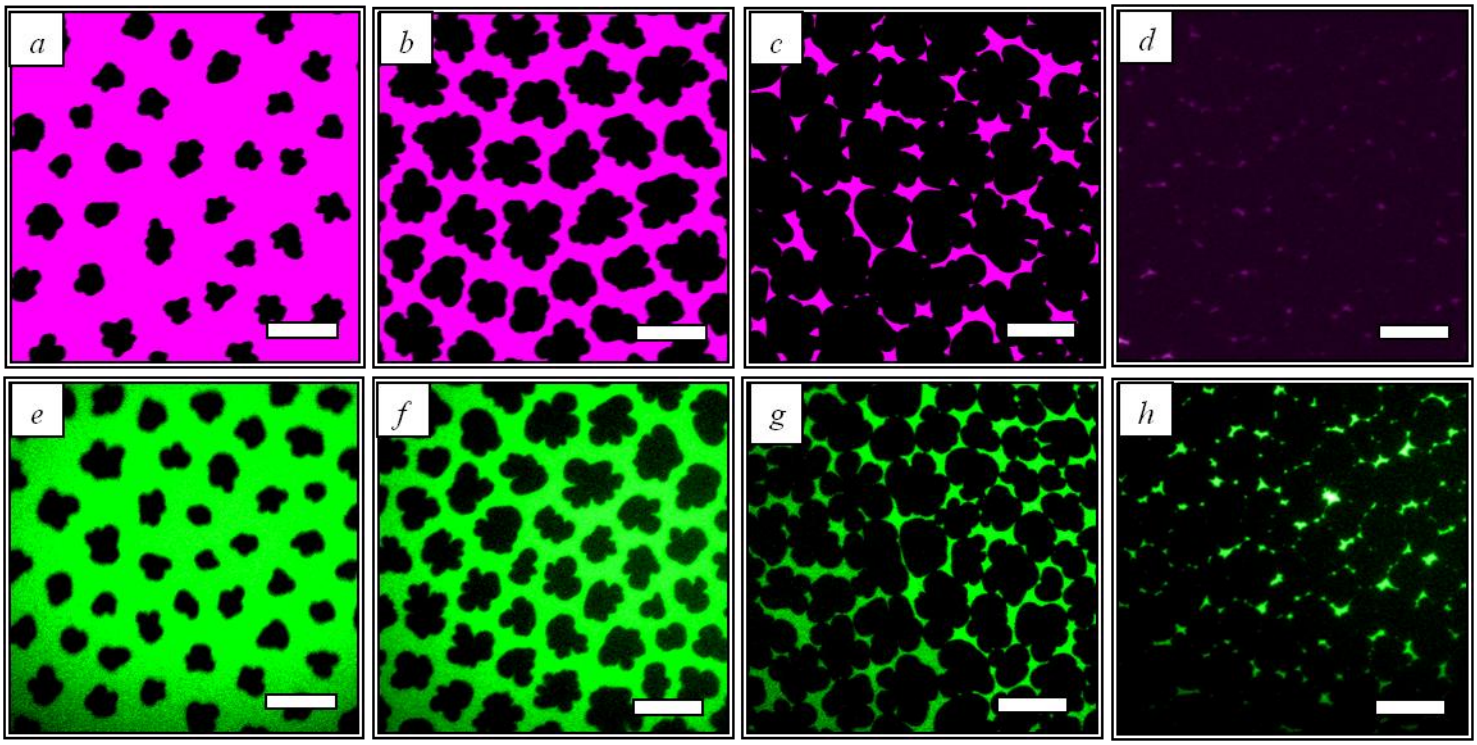


**Figure 5.6:** EFM images of 1 mol % DPPE-PEG2000 in DPPE-Succinyl monolayer on water as a subphase at 20 ± 1 °C. Images *a, b, c, d* were captured in TRITC channel and *e, f, g, h* in FITC channel at 4, 6, 12 and 49 mN/m. Image size 250 x 250 $\mu m^2$. The scale bar is 50 $\mu m$.

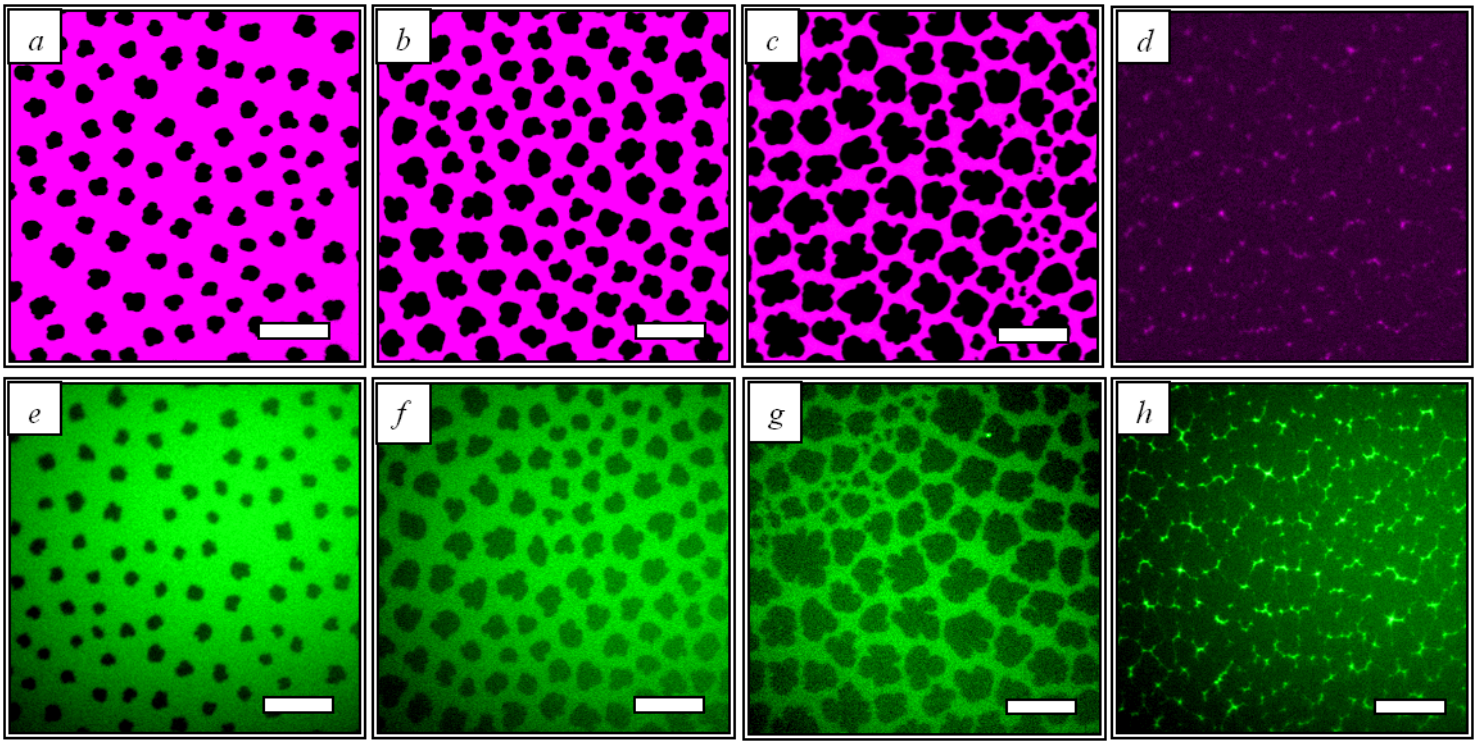


**Figure 5.7:** EFM images of 3 mol % DPPE-PEG2000 in DPPE-Succinyl monolayer on water as a subphase at 20 ± 1 °C. Images *a, b, c, d* were captured in TRITC channel and *e, f, g, h* in FITC channel at 4, 6, 12 and 50 mN/m. Image size 250 x 250 $\mu m^2$. The scale bar is 50 $\mu m$.

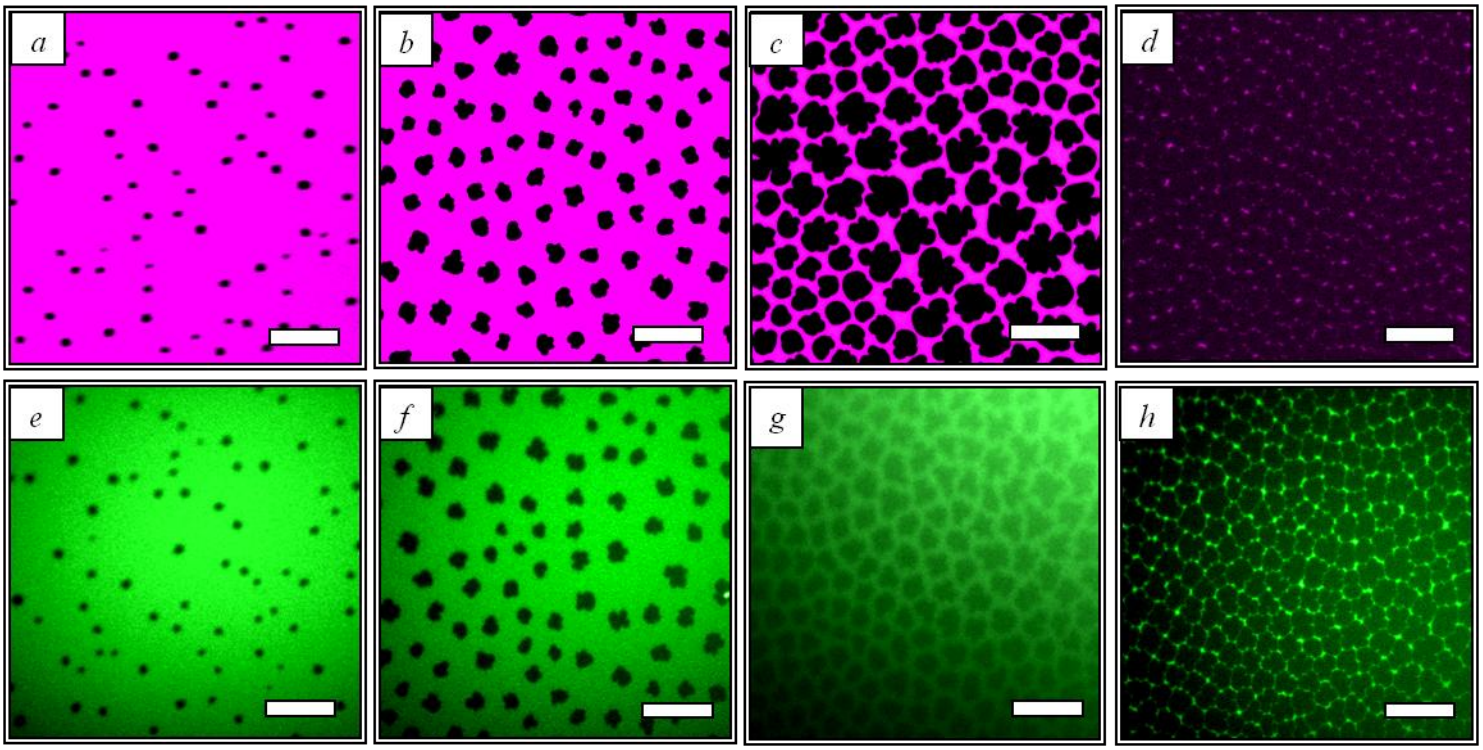


**Figure 5.8:** EFM images of 6 mol % DPPE-PEG2000 in DPPE-Succinyl monolayer on water as a subphase at 20 ± 1 °C. Images *a, b, c, d* were captured in TRITC channel and *e, f, g, h* in FITC channel at 5, 6, 12 and 50 mN/m. Image size 250 x 250 $\mu m^2$. The scale bar is 50 $\mu m$.

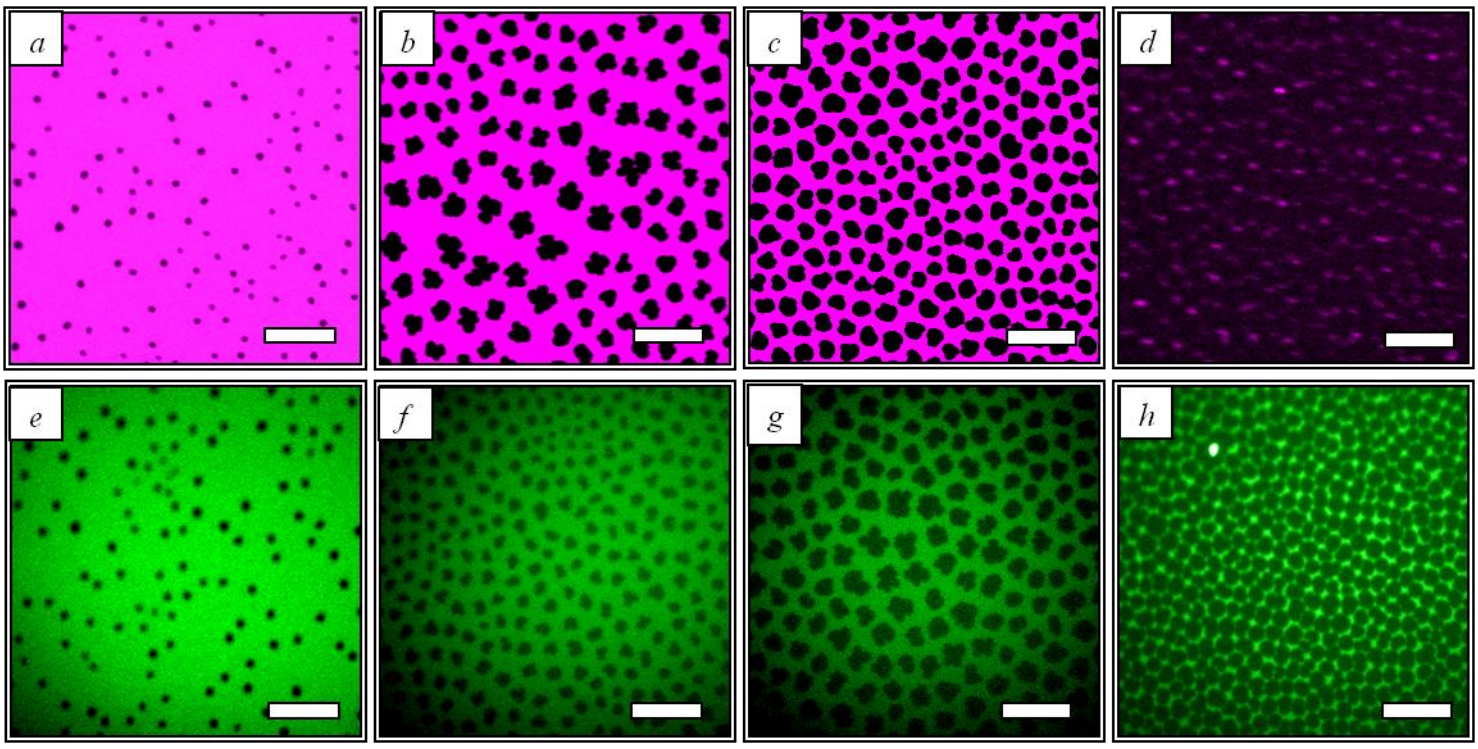


**Figure 5.9:** EFM images of 9 mol % DPPE-PEG2000 in DPPE-Succinyl on water as a subphase at 20 ± 1 °C. Images *a, b, c, d* were captured in TRITC channel and *e, f, g, h* in FITC channel at 6, 10, 12 and 52 mN/m. Image size 250 x 250 $\mu m^2$. The scale bar is 50 $\mu m$.

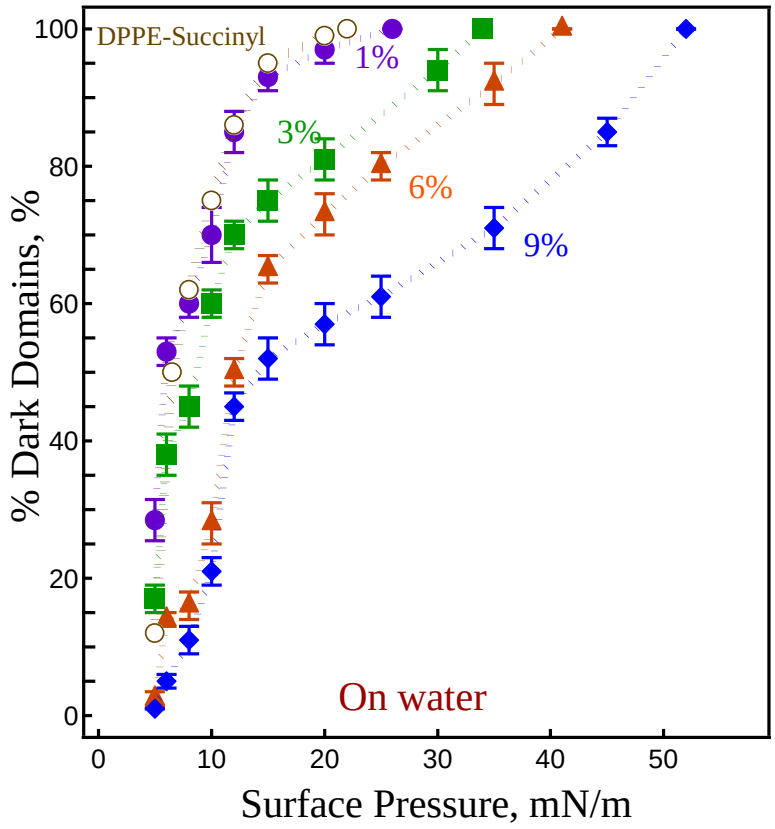


**Figure 5.10:** Percentage of Dark DOPE-Rh-excluded LC phase domains plotted against surface pressure for DPPE-Succinyl and mixed DPPE-Succinyl/DPPE-PEG2000 monolayers on water at 20 ± 1 ºC. Error bars indicate ± standard deviation. The data analysis and plots are courtesy of Dr. Tsoukanova.

### 5.1.6 In-Situ EFM Imaging of DPPE-Succinyl/DPPE-PEG2000 Monolayers on PBS

The lateral distribution of PEG chains and phase behaviour of DPPE-Succinyl/DPPE-PEG2000 binary mixtures on PBS were also visualized by switching between the two channels, TRITC and FITC. As compared to the mixed monolayers on water, only two regimes were observed in the mixed monolayers spread on PBS including LE phase and coexistence of LE and LC phase (Figures 5.11 – 5.14). A single fluorescent LE phase was observed at low surface pressures whereas tiny dark DOPE-Rh-excluded LC phase domains began to appear sporadically in all the mixed monolayers above 10 mN/m. However, a coordinated nucleation of the LC phase domains actually set in at ~23 mN/m (images not shown). The images of binary mixtures on PBS captured at different surface pressures resemble the rosette morphology of the LC phase domains on water but are quite smaller in size (cf. Figure 5.6 – 5.9 and 5.11 – 5.14). The domains ranged from 2 - 8 μm in diameter and did not change significantly upon compression. The coexistence of LE and LC phase persisted until the mixed monolayers collapsed. Interestingly, mixed monolayers spread on buffer never attained a complete LC phase as seen on water. This can be clearly seen from the % Dark Domains analysis of mixed DPPE-Succinyl/DPPE-PEG2000 monolayers on PBS, which shows quite a different mode in the morphology as opposed to monolayers spread on water (cf. Figure 5.10 and 5.15). All the mixed monolayers attained a maximum of 70% of the LC phase regardless of the PEG content, as can be seen by % Dark Domains data in Figure 5.15. A decrease in the % Dark Domains with an increase in PEG content in the binary mixtures on PBS was also observed, at any given surface pressure, similar to the monolayers on water (cf. Figure 5.10 and 5.15). Images *d* – *f* in Figure 5.11 and 5. 14 display the images depicting the lateral distribution of PEG visualized through the fluorescence from DPPE-PEG2000-FITC probe in all mixed monolayers on PBS. Images from FITC channel

exhibited fluorescence patterns similar to images seen in TRITC channel at all surface pressures (cf. images *a* – *d* and *e* – *h* in Figures 5.11 – 5.14). Hence, similarly to the observations on water, the binary mixtures of DPPE-Succinyl/DPPE-PEG2000 did not achieve uniform distribution of PEG, regardless of the surface pressure or the PEG content.

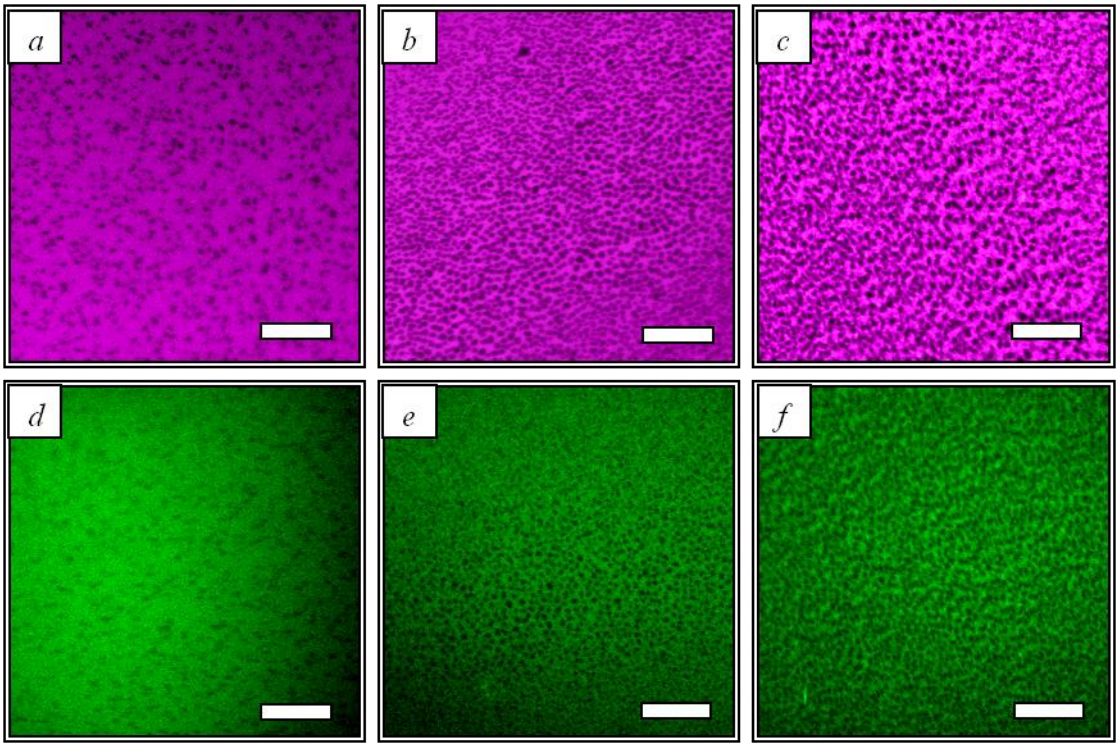


**Figure 5.11:** EFM images of 1 mol % DPPE-PEG2000 in DPPE-Succinyl monolayer on PBS as a subphase at 20 ± 1 °C. Images *a, b, c* were captured in TRITC channel and *d, e, f* in FITC channel at 25, 30 and 40 mN/m respectively. Image size 250 x 250 $\mu m^2$. The scale bar is 50 *μm.*

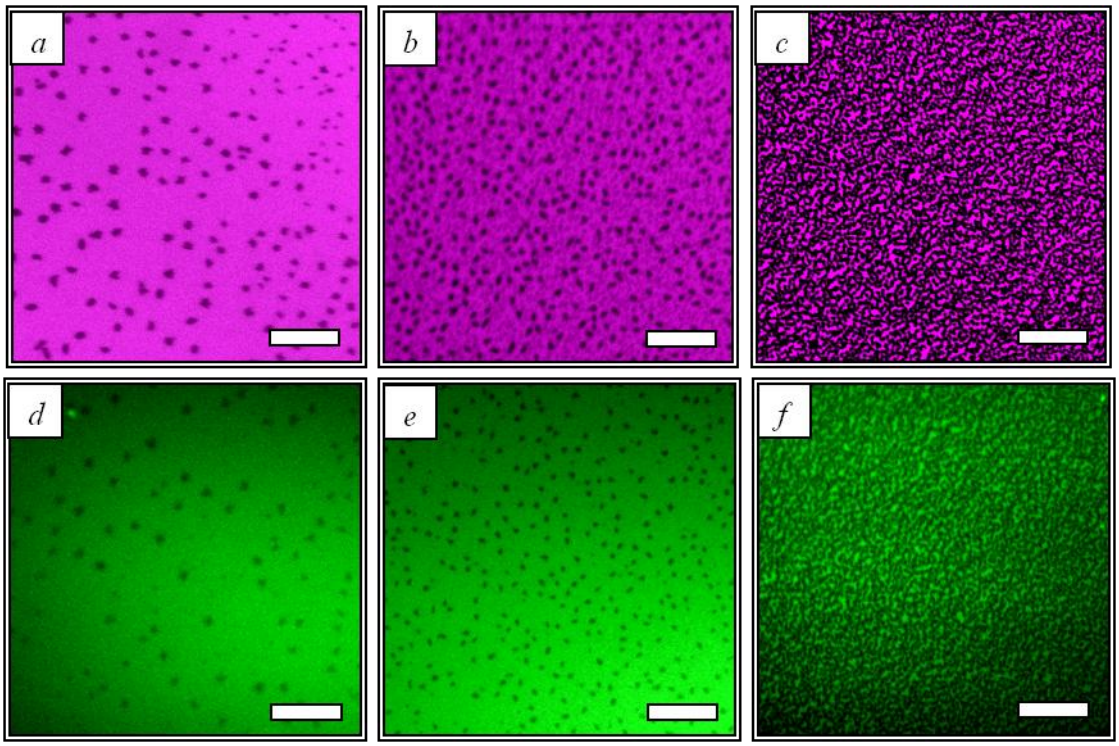


**Figure 5.12:** EFM images of 3 mol % DPPE-PEG2000 in DPPE-Succinyl monolayer on PBS as a subphase at 20 ± 1 °C. Images *a, b, c* were captured in TRITC channel and *d, e, f* in FITC channel at 25, 30 and 45 mN/m respectively. Image size 250 x 250 $\mu m^2$. The scale bar is 50 *μm.*

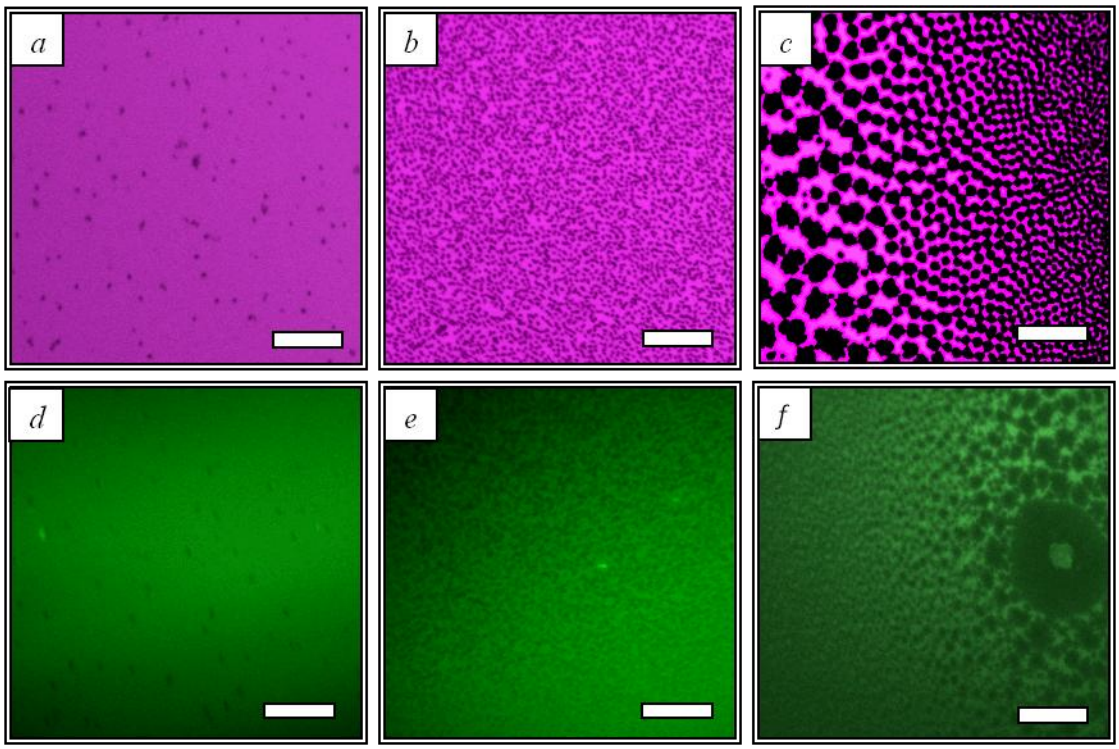


**Figure 5.13:** EFM images of 6 mol % DPPE-PEG2000 in DPPE-Succinyl monolayer on PBS as a subphase at 20 ± 1 °C. Images *a, b, c* were captured in TRITC channel and *d, e, f* in FITC channel at 25, 35 and 45 mN/m respectively. Image size 250 x 250 $\mu m^2$. The scale bar is 50 *μm.*

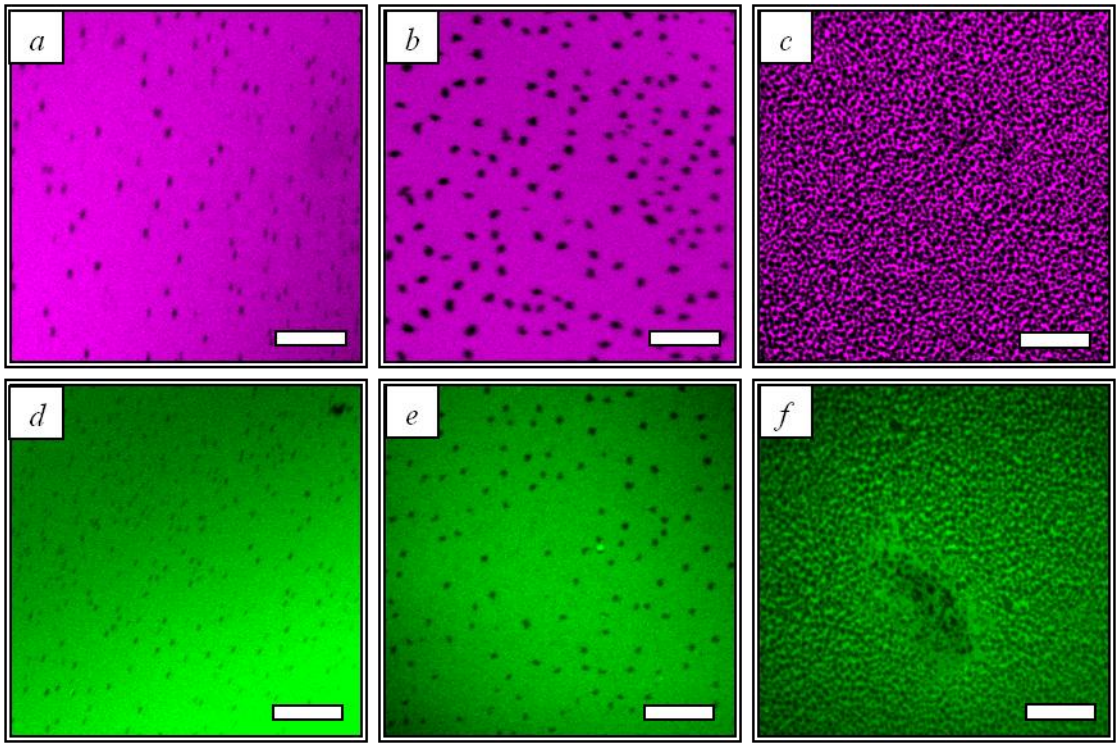


**Figure 5.14:** EFM images of 9 mol % DPPE-PEG2000 in DPPE-Succinyl monolayer on PBS as a subphase at 20 ± 1 °C. Images *a, b, c* were captured in TRITC channel and *d, e, f* in FITC channel at 25, 35 and 45 mN/m respectively. Image size 250 x 250 $\mu m^2$. The scale bar is 50 *μm.*

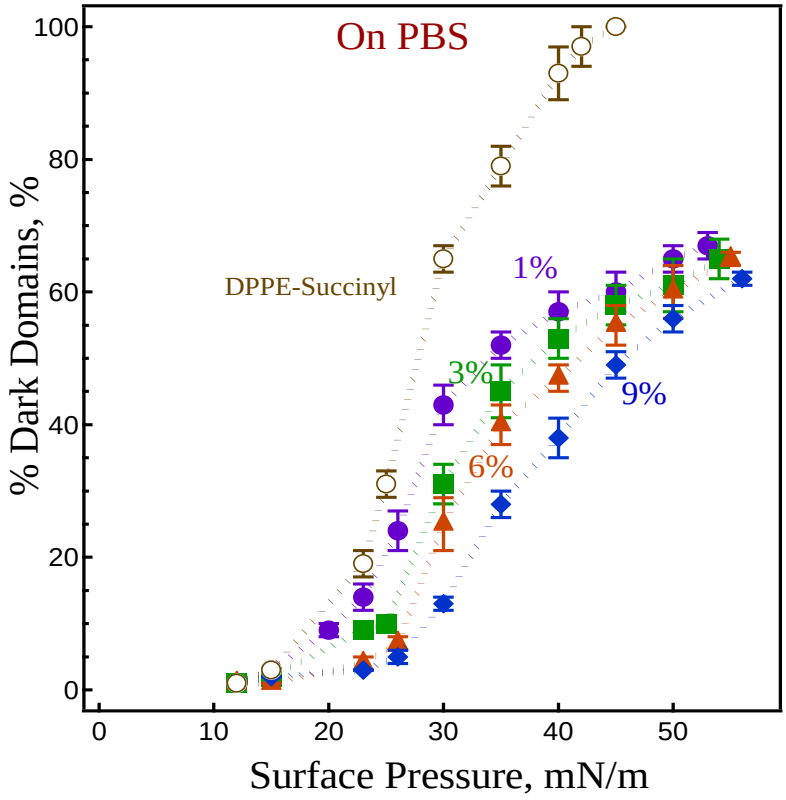


**Figure 5.15:** Percentage of Dark DOPE-Rh-excluded LC phase domains plotted against surface pressure for DPPE-Succinyl and mixed DPPE-Succinyl/DPPE-PEG2000 monolayers on PBS at 20 ± 1 ºC. Error bars indicate ± standard deviation. The data analysis and plots are courtesy of Dr. Tsoukanova.

### 5.1.7 Surface Potential Measurements for Mixed DPPE-Succinyl/DPPE-PEG2000 Monolayers

The surface potential, $\Delta V$, was measured for the binary mixtures containing 1, 3, 6, 9 mol% DPPE-PEG2000 in DPPE-Succinyl both on water and PBS subphases. As discussed earlier in detail (Chapter 4), the surface potential measurements are used in this study to assess the difference in electric double layer potential, $\psi_0$, between the monolayers on water and PBS. As discussed in the experimental section (Chapter 2) any difference in the monolayer`s surface potential measured on water and PBS, $\Delta V_{H_2O}$ and $\Delta V_{PBS}$ can be related to the difference in $\psi_0$ potentials as shown by equation 4.3 in Chapter 4. Similar to the pure DPPE-Succinyl monolayer, the difference in electric double-layer potential of the mixed monolayers on water ($\psi_{0,\ H_2O}$) and PBS ($\psi_{0,\ PBS}$) was assessed using equation 4.3 at monolayer`s mean molecular area of ~0.42 ± 0.04 nm$^2$. This area corresponds to the low-compressibility region of the $\pi - A$ isotherms, where all the phospholipids in the binary mixtures of DPPE-Succinyl and DPPE-PEG2000 are in close-packed state (Figure 5.5).

The $\Delta V$ data as a function of mol% PEG for pure DPPE-Succinyl and mixed DPPE-Succinyl/ DPPE-PEG2000 monolayers spread on water and PBS are shown in Figure 5.16. The values for $\Delta V$ in Figure 5.16 are the average values of $\Delta V$ for each monolayer and were obtained from the $\Delta V - A$ isotherms (not shown) that were measured simultaneously with $\pi - A$ isotherms. All the $\Delta V$ values were recorded in a narrow range of mean molecular areas at ~0.42 ± 0.04 nm$^2$ for the reason stated above. The $\Delta V$ recorded for pure DPPE-Succinyl monolayer, in a close-packed state, spread on water was + 385 ± 7 mV (Figure 5.16). When DPPE-PEG2000 was mixed in different proportions with DPPE-Succinyl, the $\Delta V$ values decreased on both water and PBS as

seen in Figure 5.16. This is in good accord with previously reported values [Burner 1994; Tocanne 1990; Winterhalter 1995]. Most importantly, $\Delta V$ values attained for all the monolayers on PBS were ~90 mV lower than those monolayers spread on water, which clearly indicates that $\Delta V_{PBS} - \Delta V_{H_2O} \approx \psi_{0,\,PBS} - \psi_{0,\,H_2O} \approx$ –90 mV (Figure 5.16). Based on the data obtained, it can be inferred that $\psi_0$ potential is more negative on PBS than on water for both DPPE-Succinyl and mixed DPPE-Succinyl/DPPE-PEG2000 monolayers.

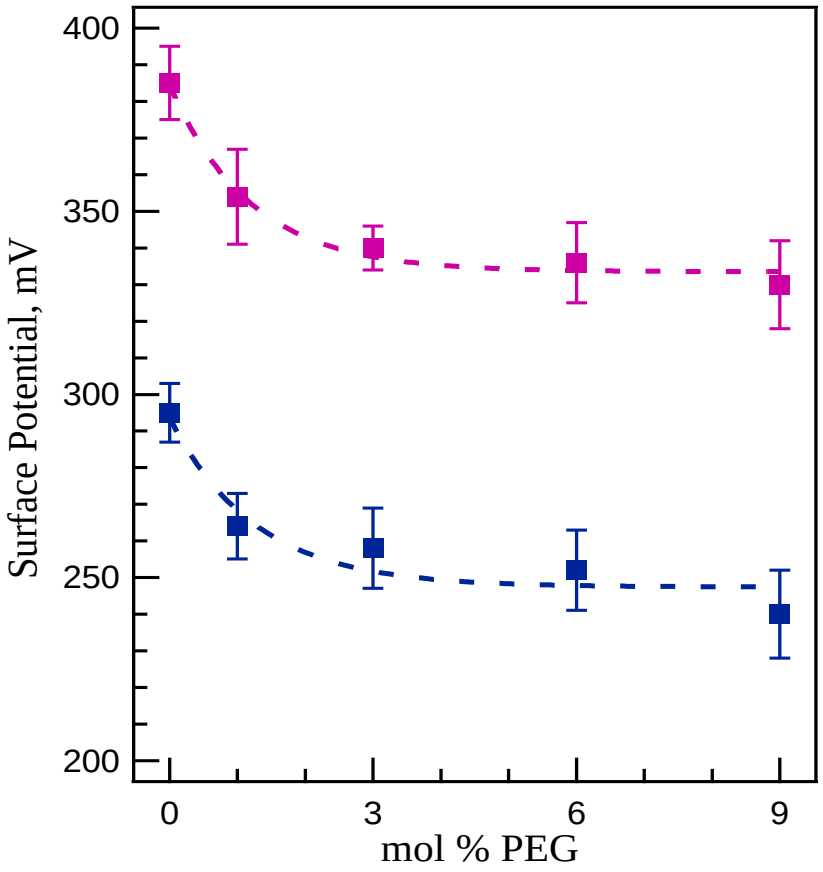


**Figure 5.16:** Surface potential, $\Delta V$, as a function of mol % PEG for monolayers spread on water ($\Delta V_{H2O}$) (pink curve) and PBS ($\Delta V_{PBS}$) (blue curve) at 20 ± 1°C. The values are for a mean molecular area of ~0.42 ± 0.04 nm$^2$. The dashed curves are guides to the eye. Error bars indicate ± standard deviation. The data analysis is courtesy of Dr. Tsoukanova.

## 5.2 Discussion

Previous studies have suggested that the subphase pH and presence of electrolytes can substantially affect the lateral organization of phospholipid monolayers [Angelova 1996; Dominguez 1998; Helm 1986]. This might be attributed to the electrostatic interactions between dissociated headgroups and basic electrolytes of PBS in the monolayer of phospholipids bearing charged headgroups and $C_{12} - C_{16}$ aliphatic chains [Angelova 1996; Helm 1986]. Both DPPE-Succinyl and DPPE-PEG2000 molecules carry a negative charge on their head groups (inset in Figure 4.1 and 5.1). However, the DPPE-Succinyl monolayer appears to show a greater change in its $\pi - A$ isotherm from water to PBS as compared to the DPPE-PEG2000 monolayer (cf. Figure 4.1 and 5.1). DPPE-PEG2000 monolayer isotherms in Figure 5.1 exhibits only an increase in the mean molecular area on PBS as compared to that on water but keeps the pseudo-plateau at about the same surface pressure range. By contrast, in mixed monolayers PBS subphase had a significant effect on the DPPE-PEG2000 component as compared to water (cf. Figure 5.1 and 5.5). This can be noticed from the disappearance of the PEG pseudo plateau at ~10 mN/m, which was clearly seen in mixed monolayers on water (cf. Figure 5.5 a and b). This makes it hard to identify the transitions in the mixed monolayers on PBS. Hence, our further discussion will be aimed at identifying and characterizing the transitions and conformational behaviour of PEG chains in mixed DPPE-Succinyl/DPPE-PEG2000 on PBS.

### 5.2.1 Lateral Compressibility in Identified Transitions in Mixed DPPE-Succinyl/DPPE-PEG2000 Monolayers

Changes in the $\pi$ – $A$ isotherm slope have been shown to correspond to various types of transitions in phospholipid monolayers [Conde 2011; El-Khouri 2011; Jebrail 2008]. The $\pi$ – $A$ isotherms of mixed DPPE-Succinyl/DPPE-PEG2000 monolayers exhibit two main slope changes upon compression at air/water interface as displayed in Figure 5.5a. A plateau with a midpoint at ~5.5 mN/m in the mixed DPPE-Succinyl/DPPE-PEG2000 monolayers (Figure 5.5a) is similar to the plateau observed in Figure 4.1, which corresponds to the LE–LC phase transition of DPPE-Succinyl monolayer. The EFM images are also in good agreement with the isotherm plateau and show the coexistence of two phases in mixed monolayers (Figure 5.6 – 5.9). The appearance of a second change in the slope of mixed monolayer isotherms at $\pi \approx 10$ mN/m is likely an indication of a conformational transition in PEG2000 chains [Jebrail 2008; Naumann 1999]. In general, this transition can be interpreted as a cooperative change in grafted PEG chains from 2D pancakes to a quasi-3D conformation. Quasi-3D conformation can be described as a conformational transition resembling a quasi-3D-structure of PEG chains [Bruzewicz 2006], which may be referred to as a mushroom, [Baekmark 1999; Baekmark 1995; Majewski 1997] a pseudobrush, [Faure 1999; Tsoukanova 2008] and a brush [Caro 2009; Chen 2005; Majewski 1997; Naumann 1999]. In this report, the term "quasi-3D conformation" will thus be used to refer to the PEG conformation adopted above the second change in the isotherm of mixed monolayers. Hence, the two transitions revealed by the changes in the slope of $\pi$ – $A$ isotherms of mixed DPPE-Succinyl/DPPE-PEG2000 monolayers on water can be identified as; (i) the LE – LC transition of DPPE-Succinyl with a midpoint at ~5mN/m, and (ii) the conformational transition in grafted PEG-chains with a midpoint at ~10mN/m. For monolayers on PBS however, it is rather difficult

to identify the transitions because the changes in the slope of isotherm in Figure 5.5b are not clearly distinguishable. Therefore, to identify the transitions in mixed DPPE-Succinyl/DPPE-PEG2000 monolayers on PBS, the $\pi - A$ isotherms of pure DPPE-Succinyl, DPPE-PEG2000 (Figure 4.1 and 5.1), as well as their mixtures (Figure 5.5) were analyzed in terms of lateral area compressibility, *C*, [Gaines 1966] as discussed below. The *C* values were calculated from the slope of the $\pi - A$ isotherms as given by the equation

$$C = -(1/A)\,(\partial A/\partial \pi)_T \quad \text{---------- 4.4}$$

As can be seen from the equation, the compressibility, *C*, is inversely proportional to the first derivative of $\pi$ with respect to *A*, and hence, is extremely sensitive to the changes in the isotherm slope upon compression. Hence, the $C - \pi$ compressibility plots made based on equation can be an ideal tool to detect and analyze even the slightest phase and conformational transition in monolayer on water and PBS subphase [Baekmark 1995; Jebrail 2008; Rossi 2007; Tsukanova 2004; Yu 2002]. The unique characteristic of the compressibility plot is the clear identification of LE–LC and conformational transition as distinct peaks. [Baekmark 1995; Tsukanova 2004; Yu 2002] The $C - \pi$ compressibility plots are usually attained from the numerical differentiation of $\pi - A$ isotherm datasets for the monolayers on water as presented in Figure 4.1(chapter 4). The compressibility plots of pure DPPE-Succinyl and DPPE-PEG2000 monolayers exhibit only single peaks (Figure 5.17). The $C - \pi$ peak for pure DPPE-Succinyl is centered at ~5 mN/m that appears to be in the surface pressure range corresponding to the plateau region of the $\pi - A$ isotherm. This peak thus represents the LE – LC phase transition in $C_{16}$ aliphatic chains of the DPPE-Succinyl monolayer at air/water interface. On the other hand, the $C - \pi$ plot for DPPE-

PEG2000 monolayer displays a peak, splitting into numerous sub-peaks, at ~10 mN/m that can be associated with the conformational transitions in grafted PEG2000 chains [Baekmark 1995] at the air/water interface as shown in Figure 5.17b. Interestingly, the compressibility plots for the mixed DPPE-Succinyl/DPPE-PEG2000 monolayers on water display two well defined peaks. For the clarity of presentation, each peak is presented in a separate graph (Figures 5.17a and b). The $C - \pi$ peaks appearing in the lower surface pressure range represent the first plateau transition, and are shown in Figure 5.17a. The peaks appearing at higher surface pressures are presented in Figure 5.17b. The peaks presented in Figure 5.17a, coincide well with the typical DPPE-Succinyl peak at 5 mN/m, which corresponds to the LE–LC phase transition. Increase in PEG content in the mixed DPPE-Succinyl/DPPE-PEG2000 monolayers reduces the sharpness of LE–LC transition peaks in the low surface pressure side (Figure 5.17a) but rather enhances the peaks towards the higher pressure range in the compressibility plots (Figure 5.17b). Among DPPE-Succinyl and DPPE-PEG2000 monolayers, only the later component shows its compressibility peak in the higher surface pressure range (Figure 5.17b). A comparative analysis of the mixed monolayers compressibility plots in Figure 5.17b reveals that the position of the second peak shifts towards the lower surface pressure range, ~12.5 mN/m at 1 mol% PEG to ~11 mN/m at 6 and 9 mol%, hence, approaching the typical surface pressure (~10 mN/m) of the PEG2000 conformational transition. Importantly, as can be confirmed from Figure 5.17b, the compressibility plot of DPPE-Succinyl monolayer does not exhibit any peak in the surface pressure of ~ 10 mN/m, which makes it safe to conclude that the second transition in the mixed monolayers is definitely due to the conformational transition of grafted PEG2000 chains. Interestingly, from the $C - \pi$ plots, the PEG transition can be easily seen for the mixed monolayers containing 1 and 3 mol% PEG, which was less apparent in the $\pi - A$ isotherms

(Figure 5.17b). Hence, a comparative analysis of $\pi - A$ isotherms, EFM images and $C - \pi$ plots enabled us to identify the two transitions as the LE – LC phase transition followed by the conformational transition in grafted PEG chains upon compression of mixed DPPE-Succinyl/DPPE-PEG2000 monolayers on water.

The most striking observation of this study is that the $\pi - A$ isotherms of mixed DPPE-Succinyl/DPPE-PEG2000 monolayers exhibit only one plateau on PBS as compared to two transitions on water (cf. Figure 5.5 a and b). As can be seen in Figure 5.5b the mixed monolayer isotherm containing 1 mol% PEG is quite similar to the pure DPPE-Succinyl monolayer isotherm on PBS (Figure 4.1). The EFM images also indicate a somewhat similar morphology in both monolayers in particular, the plateau region of the isotherm shows a coexistence of small dark LC domains with a fluorescent LE phase [cf. Images *e* –*h* Figure 5.6 to 5.9]. Based on the isotherm and EFM analysis, it can be said that the LE – LC phase transition is the primary cause for the appearance of the plateau in the isotherm of mixed monolayer containing 1 mol% PEG. However, for the mixed monolayers containing 3 – 9 mol% PEG, the plateau becomes broadened which might be due to the conformational transition of PEG chains. To identify the transitions in the mixed monolayers spread on PBS in Figure 5.5b, the lateral compressibility analysis discussed above was performed for $\pi - A$ isotherms in Figure 5.5b).

The $C - \pi$ plots for the mixed monolayers on PBS are shown in Figure 5.18 together with the compressibility plots of DPPE-Succinyl and DPPE-PEG2000. The compressibility plot for the pure DPPE-Succinyl monolayer shows a sharp peak centered at ~25 mN/m, which is consistent with the midpoint of the plateau in its $\pi - A$ isotherm in Figure 4.1. Hence, this peak is a clear evidence of the LE – LC phase transition in the DPPE-Succinyl aliphatic chains on PBS subphase. The LE – LC transition in all mixed DPPE-Succinyl/DPPE-PEG2000 monolayers is

also seen at about the same surface pressure (~25 mN/m) on PBS, which is quite high as compared to that on water at ~5 mN/m (Figure 5.18). Thus, it can be said that the buffer counter ions have a similar substantial impact on the LE – LC phase transition of both pure DPPE-Succinyl and mixed DPPE-Succinyl/DPPE-PEG2000 monolayers.

Increase in PEG content in mixed monolayers results in broadening of the LE – LC transition peak as well as the development of a shoulder at ~20 mN/m for 6 mol% PEG and a second peak at ~18 mN/m for 9 mol% PEG, respectively (Figure 5.18). To determine the origin of the second peak, compressibility plots of mixed monolayers are compared to the compressibility plot of DPPE-PEG2000 monolayer on PBS. The later displays a peak at ~12 mN/m as seen in Figure 5.18, which correlates well with the pseudo-plateau region of the DPPE-PEG2000 isotherm (Figure 5.1). This peak thus refers to the conformational transition of PEG chains on PBS subphase. The comparison shows that the second peak in the $C - \pi$ plot of the mixed monolayer containing 9 mol% PEG lies on the higher pressure side of the PEG2000 conformational transition peak. Thus, it can be suggested that the second peak in the mixed monolayer containing 9 mol% PEG together with the shoulder at 6 mol% PEG is likely the result of conformational transition in PEG2000 chains (Figure 5.18). The compressibility plot for mixed monolayer containing 3 mol % PEG on PBS indicates a slight broadening of the peak that can also be attributed to the conformational change in grafted PEG2000 chains followed by a LE – LC transition (Figure 5.18). However, this broadening seems very negligible as in the case of mixed monolayer containing 1 mol % PEG2000. Based on the $C - \pi$ analysis of all mixed DPPE-Succinyl/DPPE-PEG2000 monolayers on PBS, it can be suggested that the plateau region of the $\pi - A$ isotherms of mixed monolayers results from the two transitions superimposing on each other: (i) conformational transition of PEG2000 chains followed by (ii) the LE – LC phase

transition. Here, it can only be suggested that the conformational transition of PEG2000 chains in the mixed DPPE-Succinyl/DPPE-PEG2000 monolayers on PBS occurs at somewhat higher surface pressure between 18 – 20 mN/m as compared to the pure DPPE-PEG2000 monolayer on PBS at ~ 12mN/m and reported surface pressure on water between 8 – 10 mN/m [Baekmark 1999; Baekmark 1995; Faure 1999; Jebrail 2008; Majewski 1997; Naumann 1999]. Furthermore, as shown in Figure 5.5b, increase in PEG content in the mixed monolayers on PBS shifts the low-compressibility region of the $\pi - A$ isotherms towards higher mean molecular areas that correlates well with the positive $A_{exc}$ values (Table 5.2). This indicates that PEG2000 chains contribute in the mean molecular area even above the transition plateau when spread on PBS subphase.

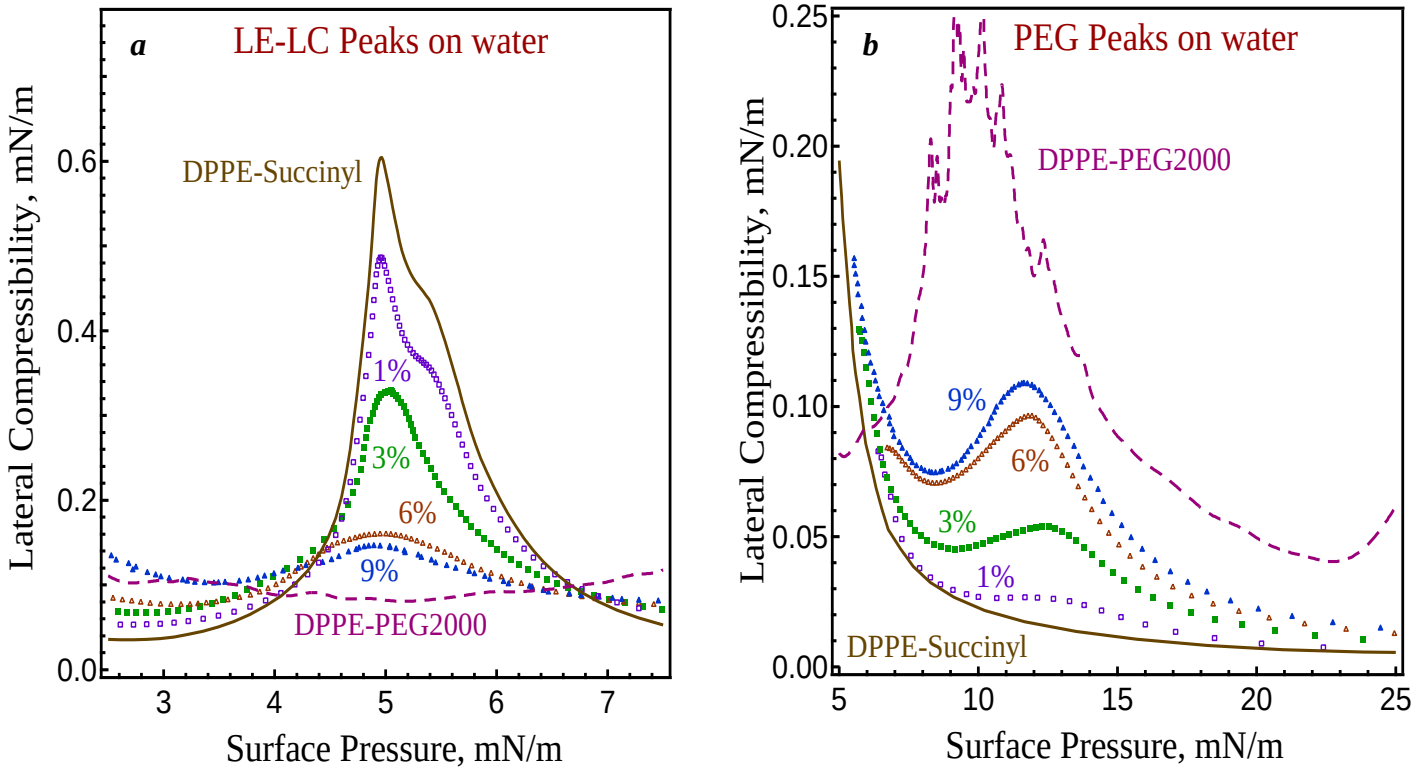


**Figure 5.17:** Lateral compressibility curves , *C*, with respect to surface pressure, $\pi$, for DPPE-Succinyl, DPPE-PEG2000 as well as their binary mixtures containing 1, 3, 6, and 9 mol % DPPE-PEG2000 in DPPE-Succinyl depicting (**a**) LE – LC phase transition peaks and (**b**) Pancake to Pseudobrush conformational transition peaks for PEG chains on water as a subphase. The data analysis and plots are courtesy of Dr. Tsoukanova.

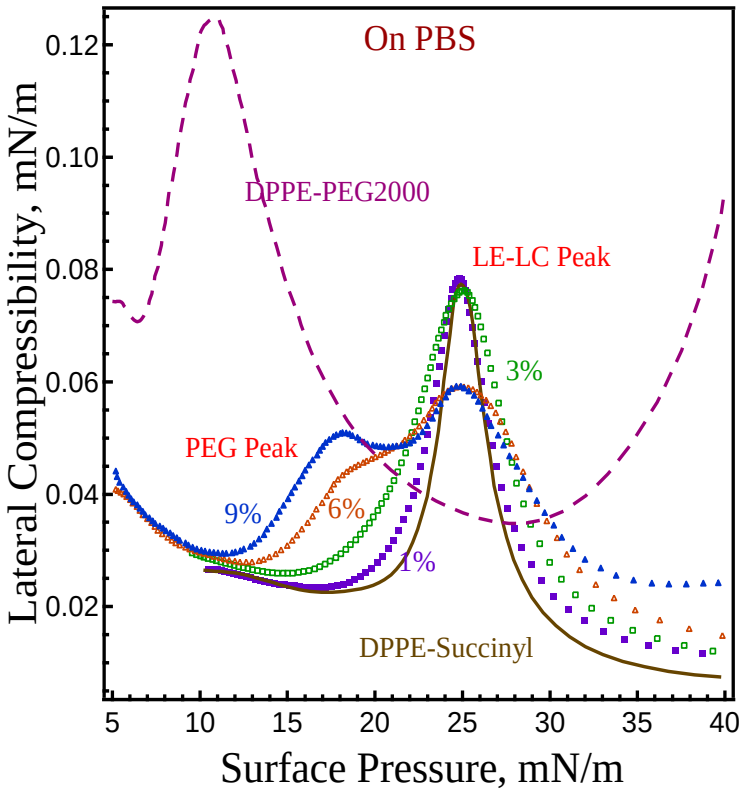


**Figure 5.18:** Lateral compressibility , *C*, with respect to surface pressure, $\pi$, for DPPE-Succinyl, DPPE-PEG2000 as well as their binary mixtures containing 1, 3, 6, and 9 mol % DPPE-PEG2000 in DPPE-Succinyl depicting (**a**) the LE – LC phase transition peaks and (**b**) the PEG conformational transition peaks on PBS as a subphase. The data analysis and plots are courtesy of Dr. Tsoukanova.

### 5.2.2 Effect of Saline on Phase and Conformational Transitions in DPPE-Succinyl/DPPE-PEG2000 Binary Mixtures

The morphology of pure DPPE-PEG2000 monolayer shows exclusively the LE phase on both water and PBS subphases, as presented in Figure 5.4. The primary reason for the formation of LE phase is the area mismatch between the bulky polymer moiety and the phospholipid part of the DPPE-PEG2000 molecule. As described by Ahren et al., DPPE-PEG2000 molecules can assemble in periodic structures with the LC type ordering of their aliphatic chains. However, the steric repulsion between PEG chains restricts this ordering to several nanometres [Ahrens 2001]. That is why only the LE phase monolayer is observed rather than a continuous LC monolayer. Thus, even upon mixing with DPPE-Succinyl, which is known to form the LC phase, DPPE-PEG2000 molecules are likely to be excluded from the LC phase DPPE-Succinyl domains because otherwise they would create disorder in the LC phase packing of DPPE-Succinyl [Shahid 2011; Tanwir 2008]. Hence, DPPE-PEG2000 should partition into the LE phase. This indeed is in good agreement with the progressive expansion of the area occupied by the LE phase observed upon increasing PEG content in the mixed DPPE-Succinyl/DPPE-PEG2000 monolayers both on water and PBS (red and green staining in the TRITC and FITC images, respectively in Figure 5.6 – 5.9 and 5.11 – 5.14).

In the LE phase, the bulky PEG2000 chains create large spatial separation which in turns tilts the $C_{16}$ aliphatic chains to a significant level whereas in the LC phase, the $C_{16}$ aliphatic chains remain perpendicular to the interface. [McConnell 1991; Yu 2002] The difference in aliphatic chains orientation in the LE and LC phase domains will create a barrier towards the LC phase growth and thus stabilize the separated phases [Frolov 2006; Kuzmin 2005; Tanwir 2008]. To overcome this barrier, which restricts the two phases to mix with each other, PEG2000 chains

have to undergo a conformational transition to pseudobrushes and submerge in the subphase, thus eliminating the large spatial separation and allowing to form an entire LC phase monolayer. In fact, several studies have reported the morphology change of many PEG-phospholipid monolayers from a phase-separated to a single LC phase monolayer. [Baekmark1995; Tsoukanova 2008; Tanwir 2008; Zhao 2002]. On water, the mixed DPPE-Succinyl/DPPE-PEG2000 monolayers also convert to a complete dark LC phase monolayer above ~20 mN/m, as can be seen from the values for the %Dark Domains in Figure 5.10. In addition, the convergence of $\pi - A$ isotherms in the low-compressibility region as well as the negative values of $A_{exc}$ (Table 5.1) for monolayers on water indicate that at high surface pressures, grafted PEG2000 chains do not contribute towards the mean molecular area of mixed monolayers on water [Tanwir 2008]. This implies that on water, grafted PEG chains undergo a conformational transition to a quasi-3D conformation and completely submerge underneath the monolayer upon compression thus enabling the mixed DPPE-Succinyl/DPPE-PEG2000 monolayers to form a complete LC phase on water.

In contrast to the mixed monolayers on water, none of the mixed monolayers achieved a single LC phase when spread on PBS, which can be seen from the EFM images and the values of %Dark Domains (cf. Figure 5.11 – 5.14 and Figure 5.15). This implies that LC phase growth in mixed monolayers on PBS might be hindered by a barrier associated with both PEG2000-induced disorder as well as PBS-induced electrostatic interactions in the headgroup region of the monolayer. However, the effect of PBS-induced electrostatic interactions on LC phase growth diminished for pure DPPE-Succinyl monolayer upon compression and a complete 100% LC phase was achieved at ~45 mN/m, as discussed above (Figure 5.15). In contrast, mixed DPPE-Succinyl/DPPE-PEG2000 monolayers only attained a maximum of ~70% Dark Domains, even at

high pressures, which clearly indicates that grafted PEG2000 chains might be contributing to the barrier hindering the LC phase growth by undergoing only a partial transition to a quasi-3D conformation. This conclusion is in fact supported by the $C - \pi$ plots in Figure 5.17b and 5.18. While, the $C - \pi$ plot of all mixed monolayers on water show a significant PEG2000 conformational transition peak at ~10 – 12.5 mN/m (Figure 5.17b), this peak is not obvious in Figure 5.18 for the mixed monolayers on PBS but rather appears at higher surface pressures (~18 – 20 mN/m). Moreover, given the shape of the peaks in Figure 5.18, the conformational transition of PEG in mixed DPPE-Succinyl/DPPE-PEG2000 monolayers is partial, which means that the PEG chains may still partially remain in the monolayers headgroup region. This can also be supported from Figure 5.15 that mixed monolayers never attained a 100% LC phase on PBS subphase even at higher surface pressures. Based on all the above mentioned factors, it can be postulated that the saline counter ions including $Na^+$ and $K^+$ may force some of the $-(CH_2CH_2O)-$ monomers of grafted polymer moiety to stay in the monolayer headgroup region even at high surface pressures. The grafted PEG2000 chains in the mixed monolayers on PBS are likely to undergo only a partial transition on a somewhat smaller scale, which differs from the ones mentioned in the literature [Baekmark 1999; Baekmark 1995; Faure 1999; Jebrail 2008; Majewski 1997; Naumann 1999; Tanwir 2008; Tsukanova 2004; Tsoukanova 2008]. The counter ions, including $Na^+$ and $K^+$ possibly penetrate the headgroup region of mixed DPPE-Succinyl/DPPE-PEG2000 monolayers and interact with the grafted PEG2000 chains while they are adopting the 2D pancake conformation. The water molecules, which are believed to cross-link the PEG monomers through hydrogen bonding via ether oxygen of $-(CH_2CH_2O)-$ monomers to undergo a quasi-3D conformation [Naumann 1999; Tsukanova 2004], may not be able to access the polymer chains that are complexed with $Na^+$ and/or $K^+$. Hence, grafted

PEG2000 chains conformational transition to a quasi-3D conformation might be partially suppressed by their interactions with $Na^+$ and/or $K^+$ counter ions and make them remain entangled in the monolayer. DPPE-PEG2000 molecules would probably form periodic nanostructures [Ahrens 2001] in the LE phase instead of participating in the formation of a LC phase.

An X-ray reflectivity study by Ahrens et al. has reported that, at high surface pressures, the hydrocarbon chains of DPPE-PEG2000 molecules tend to form LC type nano-assemblies embedded in grafted PEG2000 chains partially submerged into the subphase as seen in Figure 5.3 [Ahrens 2001]. The high pressure transition in $\pi - A$ isotherms of DPPE-PEG2000 monolayers at the air/water interface has been reported to correspond to the formation of these periodic nanostructures [Ahrens 2001]. Two of the mixed DPPE-Succinyl/DPPE-PEG2000 monolayer isotherms on PBS also exhibited quite a similar transition but at an elevated surface pressure of ~42 mN/m as described above (Figure 5.5b). Hence, it can be said that the growth of LC phase domains in mixed monolayers on PBS might be inhibited by the continuous formation of DPPE-PEG2000 nanostructures. However, further insight into the high-pressure transitions is beyond the scope of our study since we are primarily concerned with the range of membrane pressures up to 35 mN/m and the PEG nanostructures form on PBS above that range.

A phase diagram is sketched in Figure 5.19 to summarize the effect of saline on phase and conformational behaviour of mixed DPPE-Succinyl/DPPE-PEG2000 monolayers. The onset (below 20 mN/m) and completion (above 20 mN/m) of LC phase formation is represented by dotted black and solid blue curves, as deduced from % dark domain analysis Figure 5.10 and 5.15. These curves correspond to liquidus and solidus transitions, respectively [Lozano 2009; Spratte 1994]. The conformational transitions of PEG2000 chains in mixed monolayers are

represented by the solid red curves which illustrate the initial surface pressure range of PEG peaks in $C - \pi$ curves (Figure 5.17b and 5.18). The filled area in Figure 5.19 corresponds to a coexistence of two phases, $LC_{mix}$ and $LC_{DPPE\text{-}Succinyl}$ with grafted PEG2000 chains extending away from the monolayer surface. At higher surface pressures, the mixed DPPE-Succinyl/DPPE-PEG2000 monolayers on water exhibit a LC phase in TRITC images although displaying domain patterns in the FITC images. By contrast, the mixed monolayer on PBS never achieved a LC phase thus, completely eliminating the solidus transition from the phase diagram as shown in Figure 5.19. Moreover, mixed monolayers on PBS also did not exhibit homogenous distribution of PEG similar to those on water. Based on all the above discussed results as well as the schematic of Figure 5.19 it can be concluded that both "immiscible" phases including DPPE-Succinyl`s predominant LC phase and a mixed LE phase (possibly containing DPPE-PEG2000 nanostructures Ahrens 2001) are most likely to persist over the entire range of PEG 2000 contents on PBS.

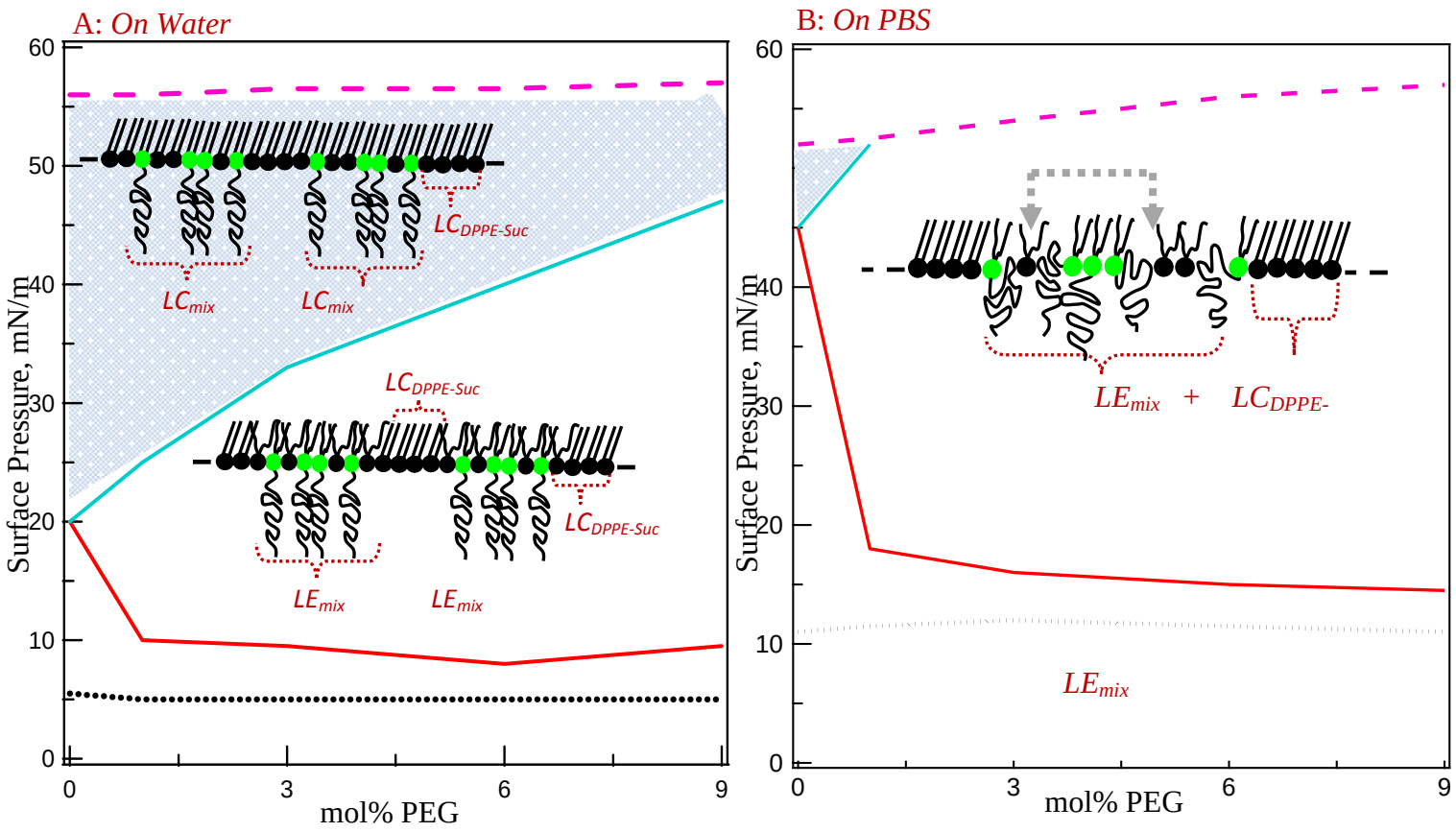


**Figure 5.19:** Phase diagrams for the binary DPPE-Succinyl/DPPE-PEG2000 mixtures at the air/water interface (A) and on the PBS subphase (B). Dotted black and solid blue curves correspond to the liquidus and solidus transitions. Solid red curves indicate the onset of PEG conformational transition. Filled areas show the mixed LC phases, $LC_{mix}$ + $LC_{DPPE\text{-}suc}$. The area between blue and red curves in both panels (A and B) display the coexistence of the two "immiscible" phases, $LE_{mix}$ + $LC_{DPPE\text{-}suc}$; that is, the LC phase of DPPE-Succinyl and a mixed LE phase. The schematics of binary mixtures with the grafted PEG chains completely submerged underneath the monolayer (filled area in panel A) and partially embedded between the phospholipid molecules (panel B) are made on the basis of results of previous studies [Baekmark 1995; Tsukanova 2004; Ahrens 2001; Lozano 2009]. The DPPE-Succinyl molecules are drawn in black; DPPE-PEG2000-FITC molecules shown with green head groups which are also used to represent DPPE-PEG2000 molecules. The dotted gray bracket with arrows indicates a motif of the periodic PEGphospholipid nanostructure [Ahrens 2001]. The data analysis is courtesy of Dr. Tsoukanova.

## 5.3 Conclusion

The $\pi - A$ isotherms, excess area parameters, and EFM imaging have demonstrated a non-ideal miscibility in the mixed DPPE-Succinyl/DPPE-PEG2000monolayers both on water and PBS. The two channel EFM imaging has shown immiscible phases from 1 – 9 mol% PEG content due to some unfavorable interactions between both phospholipids induced by PBS. This distinctive phase behavior on PBS subphase prevented the formation of a continuous LC phase in the mixed monolayers. These findings imply that grafted PEG2000 chains perhaps remain at the interface and undergo only a partial conformational transition to a quasi-3D conformation upon compression in monolayers on PBS. This partial conformational transition on PBS might be due to the interactions of $Na^+$ and $K^+$ counter ions penetrating the head group region of the phospholipids. In addition, the compressibility analysis has also confirmed that the PEG conformational transitions in mixed monolayers, on PBS subphase, occurs on a somewhat smaller scale. Hence, it can be concluded that saline has a substantial impact on both the conformation and phase transitions in PEG2000-grafted monolayers, which may have significant implications for understanding the behavior of PEG-grafted membrane-mimetic surfaces in aqueous media of biological relevance, in particular, non-specific interaction with dissolved proteins.

## 5.4 References


Ahrens, H.; Papastavrou, G.; Helm, C. A. *Langmuir* **2001**, *17*, 3113.

Angelova, A.; Vollhardt, D.; Ionov, R. *J. Phys. Chem.* **1996,** *100*, 10710.

Baekmark, T. R.; Wiesenthal, T.; Kuhn, P.; Albersdorfer, A.; Nuyken, O.; Merkel, R. *Langmuir* **1999,** *15*, 3616.

Baekmark, T. R.; Elender, G.; Lasic, D. D.; Sackmann, E. *Langmuir* **1995,** *11*, 3975.

Borden, M. A.; Martinez, G. V.; Ricker, J.; Tsvetkova, N.; Longo, M. L.; Gillies, R. J.; Bruzewicz, D. A.; Boncheva, M.;Winkleman, A.; Clair, J. M. St.; Engel, G. S.; Whitesides, G. M. *J. Am. Chem. Soc.* **2006**, *128*, 9314.

Burner, H.; Winterhalter, M.; Benz, R. *J. Coll. and Inter. Sci.* **1994**, *168*, 183.

Caro, A.; Humblot, V.; Methivier, C.; Minier, M.; Salmain, M. L.; Pradier, C.-M. *J. Phys. Chem. B* **2009**, *113 (7)*, 2101.

Chen, H.; Zhang, Z.; Chen, Y.; Brook, M. A.; Sheardown, H. *Biomaterials* **2005**, *26 (15)*, 2391.

Conde, M. M.; Conde, O.; Trillo, J. M.; J. Minones, Jr. J. *Langmuir* **2011**, 27, 3424.

Discher, B. M.; Schief, W. R.; Vogel, V.; Hall, S. B. *Biophys. J.* **1999**, *77*, 2051.

Dominguez, M. R.; Narvaez, I. G.; Patino J. M. R. *Ind. Eng. Chem. Res.* **1998,** *37*, 936.

El-Khouri, R. J.; Frey, S. L.; Szmodis, A. W.; Hall, E.; Kauffman, K. J.; Patten, T. E.; Lee, K. Y. C.; Parikh, A. N. *Langmuir* **2011**, *27(5)*, 1900.

Faure, M. C.; Bassereau, P. *Macromolecules* **1999,** *32*, 8538.

Frolov, V. A. J.; Chizmadzhev Y. A.; Cohen F. S.; Zimmerberg, J. *Biophys. J.* **2006**, *92*, 2842.

Gaines, G. L. *Jr. Insoluble Monolayers at Liquid-Gas Interfaces; Wiley:New York* **1966**.

Helm, C. A.; Laxhuber, L.; Losche, M.; Mohwald, H. *Coll. and Poly. Sci* **1986,** *264*, 46.

Jebrail, M.; Schmidt, R.; DeWolf, C. E.; Tsoukanova, V. *Coll. and Sur. A* **2008,** *321*, 168.

Kinsinger, M. I.; Lynn D. M.; Abbott, N. L. *Soft Matter* **2010**, *6*, 4095.

Kuzmin, P. I.; Akimov, S. A.; Chizmadzhev, Y. A.; Zimmerberg, J.; Cohen, F. S., *Biophys. J.* **2005**, *88*, 1120.

Lozano, M. M.; Longo, M. L. *Soft Matter* **2009**, *5*, 1822.

Majewski, J.; Kuhl, T. L.; Gerstenberg, M. C.; Israelachvili, J. N.; Smith, G. S. *J. Phys. Chem. B* **1997,** *101*, 3122.

McConnell, H. M. *Annu. Rev. Phys. Chem.* **1991**, *42*, 171.

Naumann, C. A.; Brooks, C. F.; Fuller, G. G.; Knoll, W.; Frank, C. W. *Macromolecules* **2002**, *34*, 3024.

Naumann, C. A.; Brooks, C. F.; Fuller, G. G.; Knoll, W.; Frank, C. W. *Langmuir* **1999,** *15*, 7752.

Nosrati, N., *Masters Dissertations, York University* **2009**.

Rossi, J.; Giasson, S.; Khalid, M. N.; Delmas, P.; Allen, C.; Leroux, J-C. *Eur. J. Pharm. and Biopharm.* **2007,** *67*, 329.

Shahid, M. N.; Tsoukanova, V. *J. Phys. Chem. B* **2011,** *115 (13)*, 3303.

Spratte, K.; Riegler, H. *Langmuir* **1994**, *10*, 3161.

Tanwir, K.; Tsoukanova, V. *Langmuir* **2008,** *24*, 14078.

Tocanne, J-F.; Teissie, J. *Biochim. Biophys. Acta* **1990,** *1031*, 111.

Tsoukanova, V.; Salesse, C. *Langmuir* **2008,** *24*, 13019.

Tsukanova, V.; Salesse, C. *J. Phys. Chem. B* **2004,** *108*, 10754.

Winterhalter, M.; Burner, H.; Marzinka, S.; Benz, R.; Kasianowicz, J. J. *Biophys. J.* **1995**, *69*, 1372.

Yu, Z-W.; Jin, J.; Cao, Y. *Langmuir* **2002**, *18*, 4530.

Zhao, H.; Dubielecka, P. M.; Soderlund, T.; Kinnunen, P. K. J. *Biophys. J.* **2002**, *83*, 954.

# Chapter 6: Binding Parameters of Insulin with Pure and Mixed DPPE-Succinyl/DPPE-PEG2000 Monolayers

Proteins are known to damage the phospholipid membrane-mimetic surfaces via non-specific penetration mechanism and hence can reduce the longevity and efficiency of these surfaces. The non-specific binding of proteins onto phospholipid monolayers may be driven by electrostatic interactions with the net charge in the monolayer headgroup region and/or by the tendency for hydrophobic residues on the outer surface of protein molecule to minimize their exposure to the aqueous environment through inserting themselves into the aliphatic chain region of the monolayer [Birdi 1976; Calvez 2009; Farias 1989; Hanakam 1996; Kozarac 1987; Nieto-Suarez 2008; Rahmati 2008; Vermette 2003; Zhao 2002; Zhao 2000]. This may result in a penetration of the protein molecules into the monolayer, anchoring/insertion of protein molecules to the monolayer via its hydrophobic residue, or accumulation of protein molecules on the monolayer surface by adsorption [Calvez 2009; Farias 1989; Hanakam 1996; Kozarac 1987; Rahmati 2008; Vermette 2003; Zhao 2002; Zhao 2000]. In the case of PEG-grafted monolayers, the latter may also be accompanied by the formation of intrapolymer complexes between polymer chains and protein molecules [Allen 2002; Sheth 1997]. Hence, the focus of this chapter will be aimed at elucidating the mechanisms involved in the interactions of insulin with pure DPPE-Succinyl and mixed DPPE-Succinyl/DPPE-PEG2000 monolayers. For that, monolayer area expansion techniques will be used [Seelig 1987]. The monolayer area expansion measurements upon monolayer interactions with insulin were performed on PBS at 20 °*C*. Upon expansion measurements, the morphology of

pure and mixed monolayers with insulin interactions was also visualized using two-channel EFM. The effect of varying the PEG content on the insulin/monolayer interactions is also analyzed. Based on all the experiments, insulin binding parameters including insulin penetration area, $A_p$, as well as its binding degree, $\chi_P$, for pure DPPE-Succinyl and mixed DPPE-Succinyl/DPPE-PEG2000 monolayers are determined.

## 6.1 Results

### 6.1.1 Area Expansion Measurements for Insulin/Monolayer Interactions

#### 6.1.1.1 Methodology for Area Expansion Measurements

The kinetics of insulin/monolayer interactions were measured by adopting area expansion, $\Delta A$, approach. In this method the monolayer was compressed to a preset surface pressure, $\pi$, value. The area expansion, $\Delta A$, of the monolayer was then monitored over time upon insulin injection, while holding the monolayer at a preset $\pi$. The surface pressure is maintained to the same value throughout the experiment by trough electronic feedback device, which controls the movement of the two barriers while the mean molecular area is recorded over time. Prior to the insulin injection into the subphase, the phospholipid monolayer was kept at the preset $\pi$ for about 20 min to detect any changes in the area with respect to time to ensure the stability of the monolayer. This is because the mean molecular area of a monolayer usually expands upon protein injection underneath the subphase, when protein molecules try to accommodate themselves within the monolayer [Hanakam 1996]. However, a contraction of the mean molecular area may also be observed due to a creep in the monolayer resulting from phospholipids'

conformational rearrangements with time [Xu 2000]. The creep in monolayers (and, consequently, the contraction of the mean molecular area) may occur before and/or after the interactions with proteins. Hence, the monolayer was examined for the creep before the area expansion measurements. The monolayer was considered stable, if the $\Delta A$ with respect to time was less than 3%. A pre-calculated concentration of insulin, ~75 ng/mL (~13 nM), was then injected in the subphase underneath the monolayer. A reference run was also performed for each monolayer to account for the contraction of the mean molecular area that might result from the creep in the monolayers over the 2 h experiment time. In the reference run, the mean molecular area was recorded for 2 h, at a preset $\pi$ value, without injecting insulin in the subphase underneath the monolayer. The $\Delta A - t$ curves were then obtained by subtracting the reference run from that with insulin run to account for the insulin- induced change in the monolayer mean molecular area ($\Delta A$) over time ($t$). Each measurement was performed three times to ensure the accuracy and reproducibility of the results. The difference between $\Delta A$ values attained from a series of measurements was within 15%.

#### 6.1.1.2 Area Expansion Measurements for DPPE-Succinyl and Mixed DPPE-Succinyl/DPPE-PEG2000 Monolayers upon Interactions with Insulin

To determine the binding parameters of insulin for pure DPPE-Succinyl and mixed DPPE-Succinyl/DPPE-PEG2000 monolayers, the monolayer area expansion upon interactions with insulin was measured for a surface pressure range of 13 – 45 mN/m with a surface pressure increment of 2 mN/m. Although the lateral pressure in the phospholipid bilayer membranes of liposomes, vesicles and lipoparticles cannot be

directly measured, it has been estimated to generally fall in the range of 25 – 35 mN/m [Calvez 2009; Konttila 1988; Vermette 2003]. For some membranes, values as low as 12.7 mN/m and as high as 50 mN/m has also been reported [Konttila 1988]. For PEG-grafted membranes, no estimate of the lateral pressure has been documented in the literature. Given that PEG-phospholipids tend to increase the fluidity of the host phospholipid matrix, [Hashizaki 20003] one may assume the lateral pressure in the membranes of PEG-grafted phospholipid carriers fall outside the "usual range" of 25 – 35 mN/m, presumably on the lower pressure side. Hence, in order to achieve a full characterization of DPPE-Succinyl and DPPE-Succinyl/DPPE-PEG2000 membranes as well as their interactions with insulin, the measurements in this study were performed for a monolayer surface pressure of 13 – 45 mN/m, i.e. for the entire range that might be relevant to the lateral pressure in the bilayer membranes of PEG-grafted phospholipid liposomes and lipoparticles.

The analyzed $\Delta A - t$ curves for pure DPPE-Succinyl and mixed DPPE-Succinyl/DPPE-PEG2000 monolayers are presented in Figure 6.2 – 6.6 and 6.7. For each pure DPPE-Succinyl and mixed DPPE-Succinyl/DPPE-PEG2000 monolayer, the $\Delta A - t$ curve was measured three times at each surface pressure and then averaged. Such an averaged $\Delta A - t$ curve is shown in Figure 6.1 for 1 mol% mixed DPPE-Succinyl/DPPE-PEG2000 at 13 mN/m. Reference runs for all monolayers were also recorded to determine the actual area expansion upon insulin injection, as illustrated in Figure 6.1. All the $\Delta A - t$ curves presented in Figure 6.2 to 6.6 correspond to the average subtracted curves for each monolayer at different surface pressures. As shown in Figures 6.2 – 6.6, the $\Delta A$ increases

rapidly upon insulin injection at $t \approx 0$ and levels off reaching a steady state value, $\Delta A_{ss}$, after 10 – 60 min depending on the preset $\pi$ value. Interestingly, the steady state was attained faster and the $\Delta A_{ss}$ value decreased, at higher preset $\pi$ value. For instance, the steady-state values in $\Delta A - t$ curves for DPPE-Succinyl monolayer at $\pi$ =13mN/m *is* ~0.28 $nm^2$ which decreased to about 0.02 $nm^2$ at $\pi$ =19mN/m (Figure 6.2). Similarly, the binary mixture of DPPE-Succinyl/DPPE-PEG2000 containing 9 mol % PEG displayed the $\Delta A_{ss}$ value of ~0.20$nm^2$ at $\pi$ =13mN/m that decreased to ~0.01$nm^2$ at $\pi$ =19mN/m (curves in Figure 6.2, 6.6 and Figure 6.7). The positive $\Delta A$ values in a surface pressure range of 13 to 19 mN/m for all the monolayers indicate that the monolayer area expansion is indeed the result of interactions between monolayer and the insulin molecules (Figure 6.2 – 6.6 and 6.7). As shown in Figure 6.2– 6.6, the steady state values of $\Delta A_{ss}$ also exhibited a similar decreasing trend at higher preset $\pi$ for pure DPPE-Succinyl and all the mixed DPPE-Succinyl/DPPE-PEG2000 monolayers. To better understand the effect of lateral surface pressure on the insulin/monolayer interactions, the $\Delta A_{ss}$ values for all the monolayers were obtained from the exponential fits to the $\Delta A - t$ data points, as shown by the solid curves in Figures 6.2– 6.6, and plotted with respect to $\pi$ as summarized in Figure 6.7. The plots shown in Figure 6.7 reveal a considerable monolayer area expansion induced by insulin molecules below 19mN/m, but the values for $\Delta A_{ss}$ vary depending on the PEG content in the mixed monolayers. This can be comprehended by relating the values of $\Delta A_{ss}$ found in the range of 0.28 – 0.20 $nm^2$/molecule at 13 mN/m (Figure 6.7) to the monolayer mean molecular area, *A*, varying at this surface pressure from 0.9 to 1.65 $nm^2$/molecule with PEG content increasing from 0 – 9 mol% (Figure 4.1 and 5.3b). This shows a significant change in insulin induced

monolayer area expansion from ~31% for DPPE-Succinyl monolayer to ~25% for the mixed DPPE-Succinyl/DPPE-PEG2000 monolayers containing 1 – 6 mol% PEG2000 and ~12% for the mixed monolayer containing 9 mol% PEG content. The dashed line in Figure 6.7, is drawn through the $\Delta A_{ss}$ data points to $\Delta A_{ss} = 0$, illustrates the surface pressure, $\pi$, at which insulin ceases to induce monolayer area expansion [Birdi 1976; Calvez 2009; Zhao 2002]. This $\pi$ lies at about 19.4 mN/m for pure DPPE-Succinyl and mixed DPPE-Succinyl/DPPE-PEG2000 monolayers (Figure 6.7). Indeed, the area expansion measurements done above this $\pi$ did not detect any change in the mean molecular area upon insulin injection underneath the monolayers (data not shown).

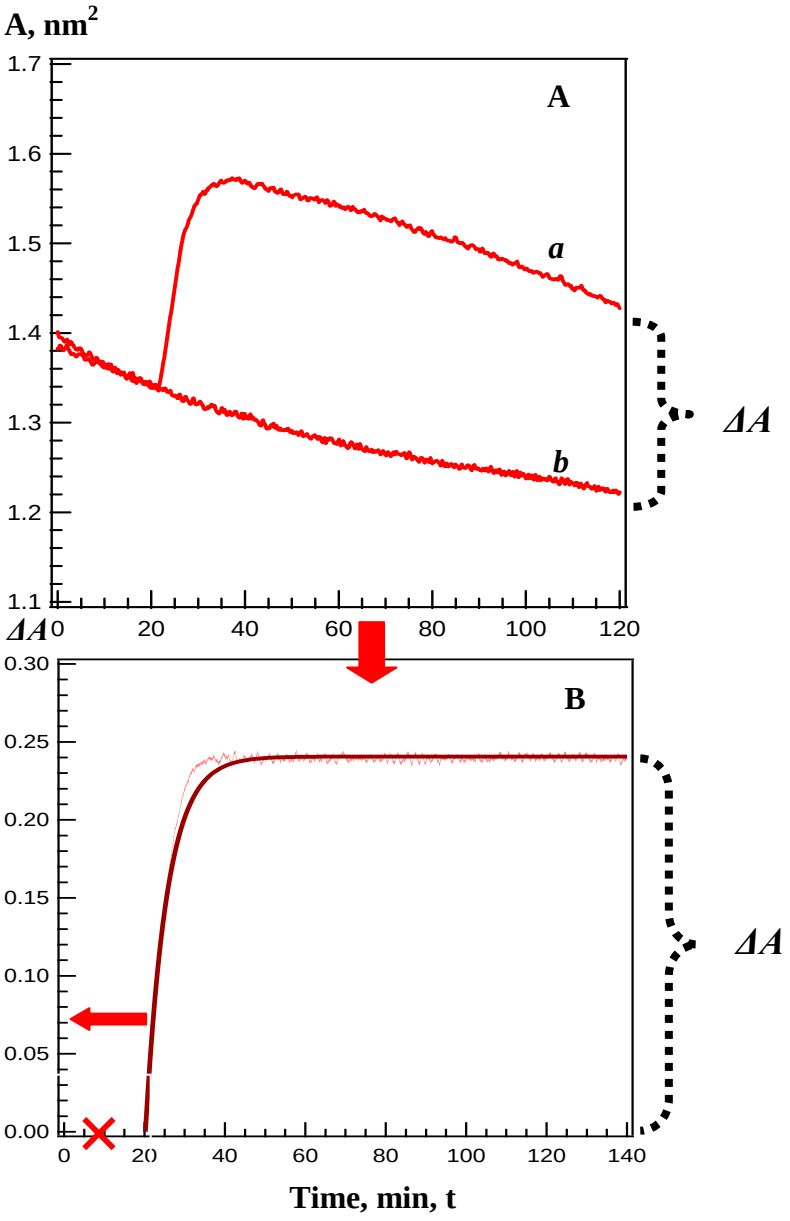


**Figure 6.1:** A **s**chematics illustrating the area expansion data analysis: (**A**) *A* – *t* curves obtained for a monolayer upon injecting insulin in the subphase at t ≈ min (***a***) and without insulin, i.e. reference run (***b***). Both curves are for a monolayer containing 1 mol% PEG held at a preset π of 13 mN/m. Curve "***a***" is the average of three runs. (**B**) *ΔA* – *t* curve obtained by subtraction of the reference run "***b***" from *A* – *t* curves for insulin/monolayer interactions. Dotted curve is the subtraction result whereas solid curve is the exponential fit were used to derive the steady-state $\Delta A_{ss}$ values. For clarity of presentation, the portion of the *ΔA* – *t* curve corresponding to the creep test (0 < t < 20 min) is then removed and the insulin injection point at t= 20 min is shifted to t = 0 min as indicated by the arrow in panel B. Therefore, *ΔA* – *t* curves in Figure 6.2 – 6.6 show *ΔA* rise at t = 0.

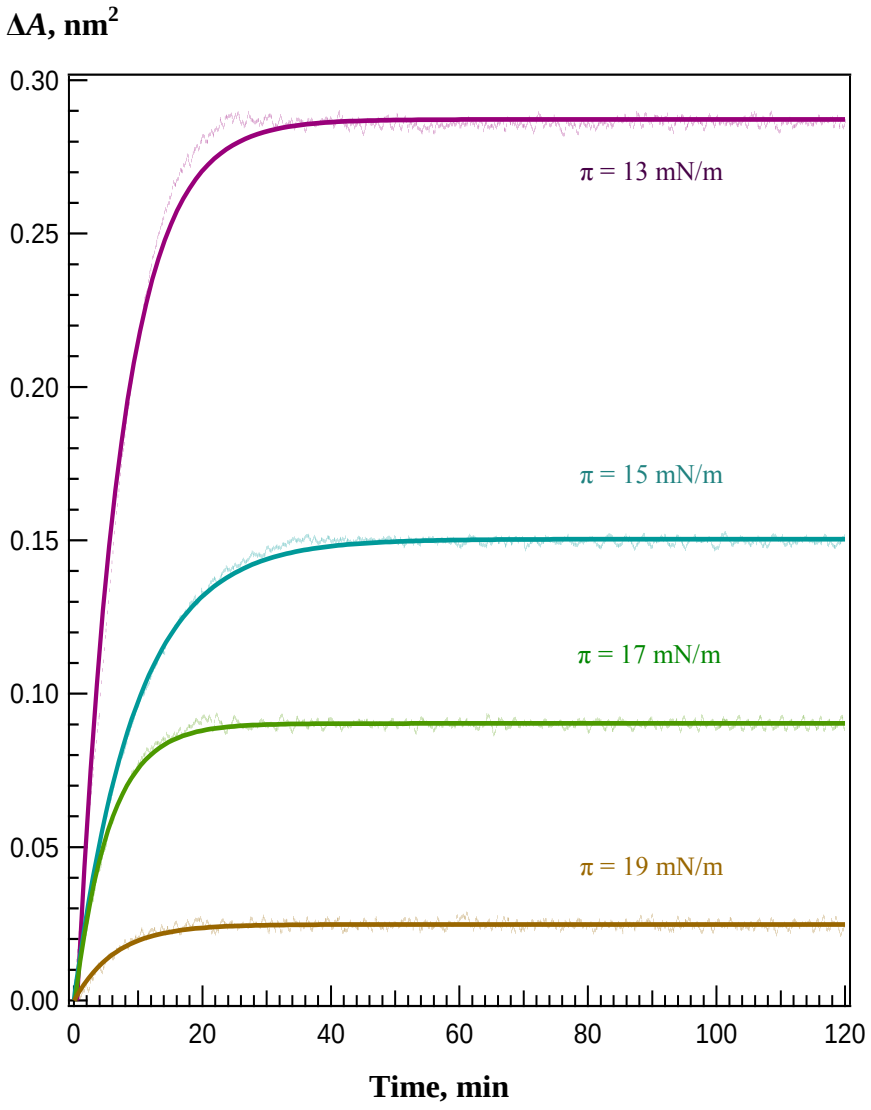


**Figure 6.2:** Insulin-induced changes in the pure DPPE-Succinyl monolayers mean molecular area as a function of time. Dotted curves shows typical *ΔA-t* curves measured upon the injection of insulin in the PBS subphase underneath the monolayer at preset $\pi$ values of 13, 15, 17, 19 mN/m. Solid curves are the exponential fit to the measured *ΔA-t* curves. The end values of *ΔA* in exponential fit were used to derive the steady-state $\Delta A_{ss}$ values. *All data are for insulin concentration in the PBS subphase of ~ 75 ng/mL (i.e. ~ 13nM).*

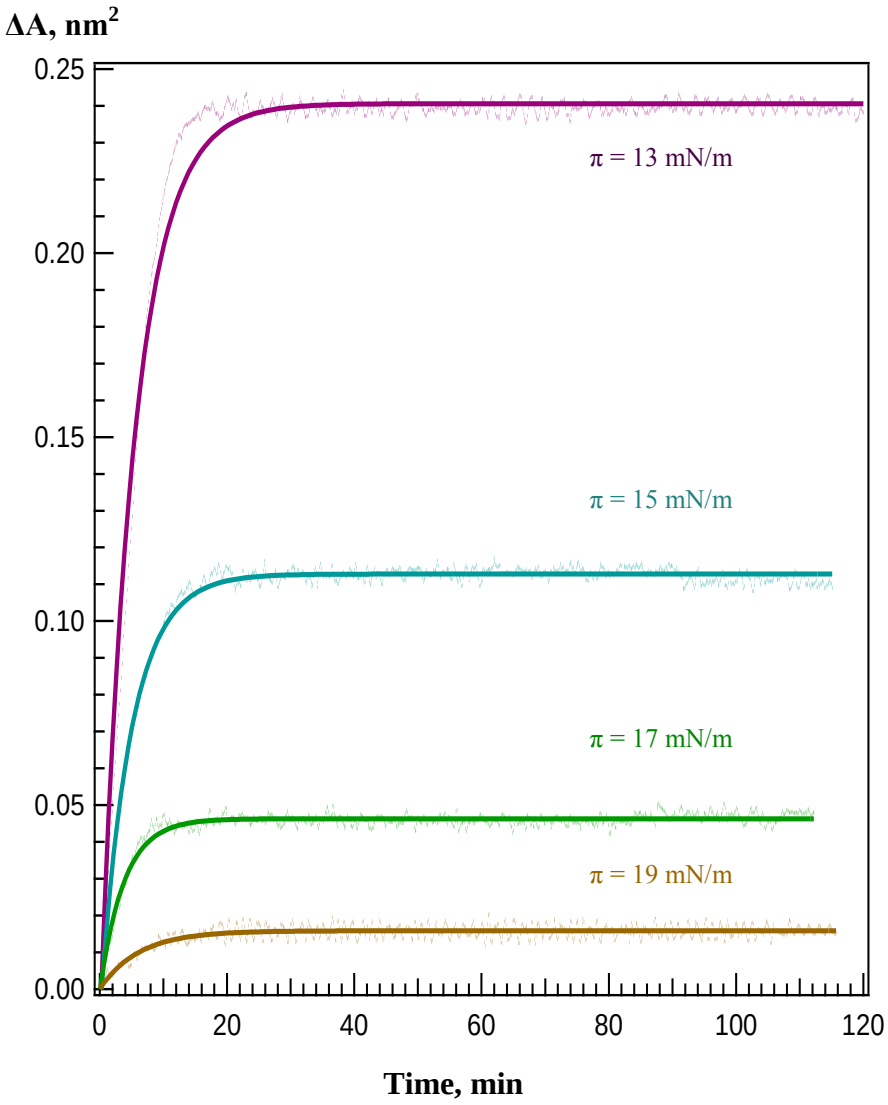


**Figure 6.3:** Insulin-induced changes in the 1 mol% DPPE-PEG2000 in DPPE-Succinyl monolayers mean molecular area as a function of time. Dotted curves shows average *ΔA-t* curves measured upon the injection of insulin in the PBS subphase underneath the monolayer at preset $\pi$ values of 13, 15, 17, 19 mN/m. Solid curves are the exponential fit to the measured *ΔA-t* curves. The end values of *ΔA* in exponential fit were used to derive the steady-state $\Delta A_{ss}$ values. *All data are for insulin concentration in the PBS subphase of ~ 75 ng/mL (i.e. ~ 13nM).*

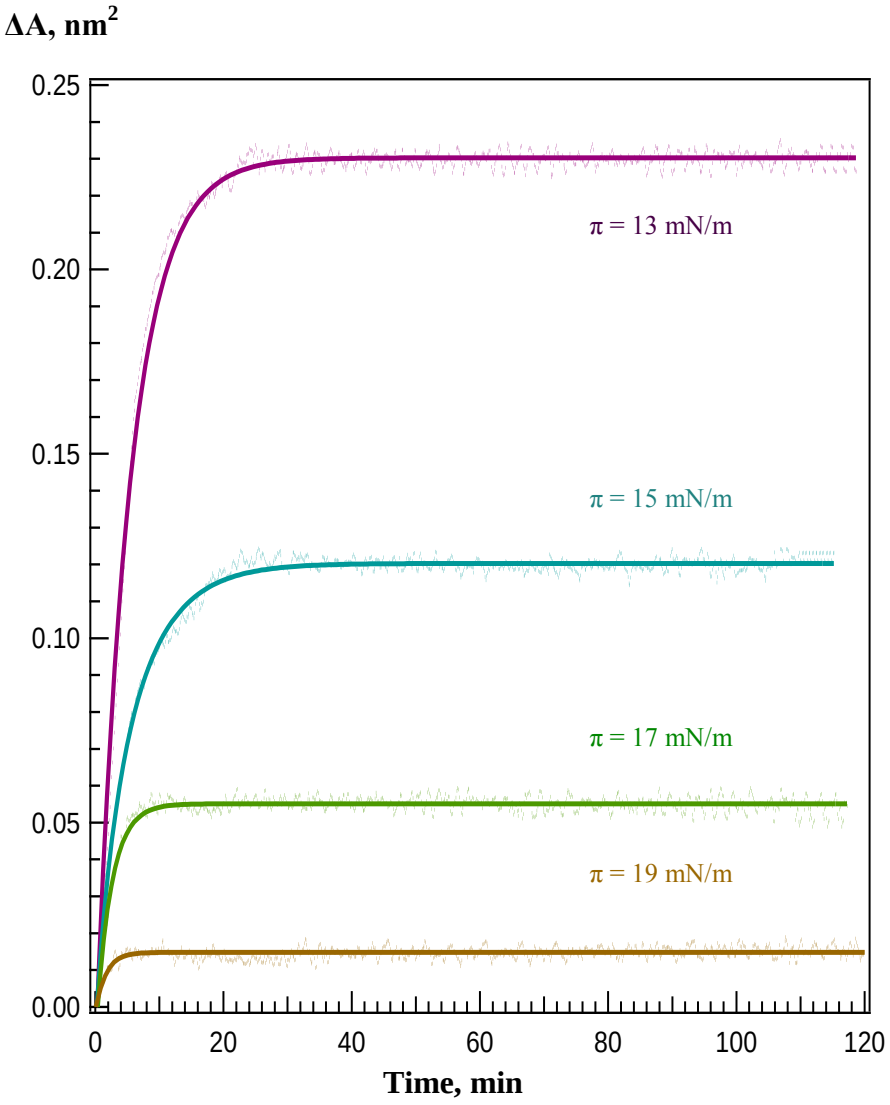


**Figure 6.4:** Insulin-induced changes in the 3 mol% DPPE-PEG2000 in DPPE-Succinyl monolayers mean molecular area as a function of time. Dotted curves shows average *ΔA-t* curves measured upon the injection of insulin in the PBS subphase underneath the monolayer at preset $\pi$ values of 13, 15, 17, 19 mN/m. Solid curves are the exponential fit to the measured *ΔA-t* curves. The end values of *ΔA* in exponential fit were used to derive the steady-state $\Delta A_{ss}$ values. *All data are for insulin concentration in the PBS subphase of ~ 75 ng/mL (i.e. ~ 13nM).*

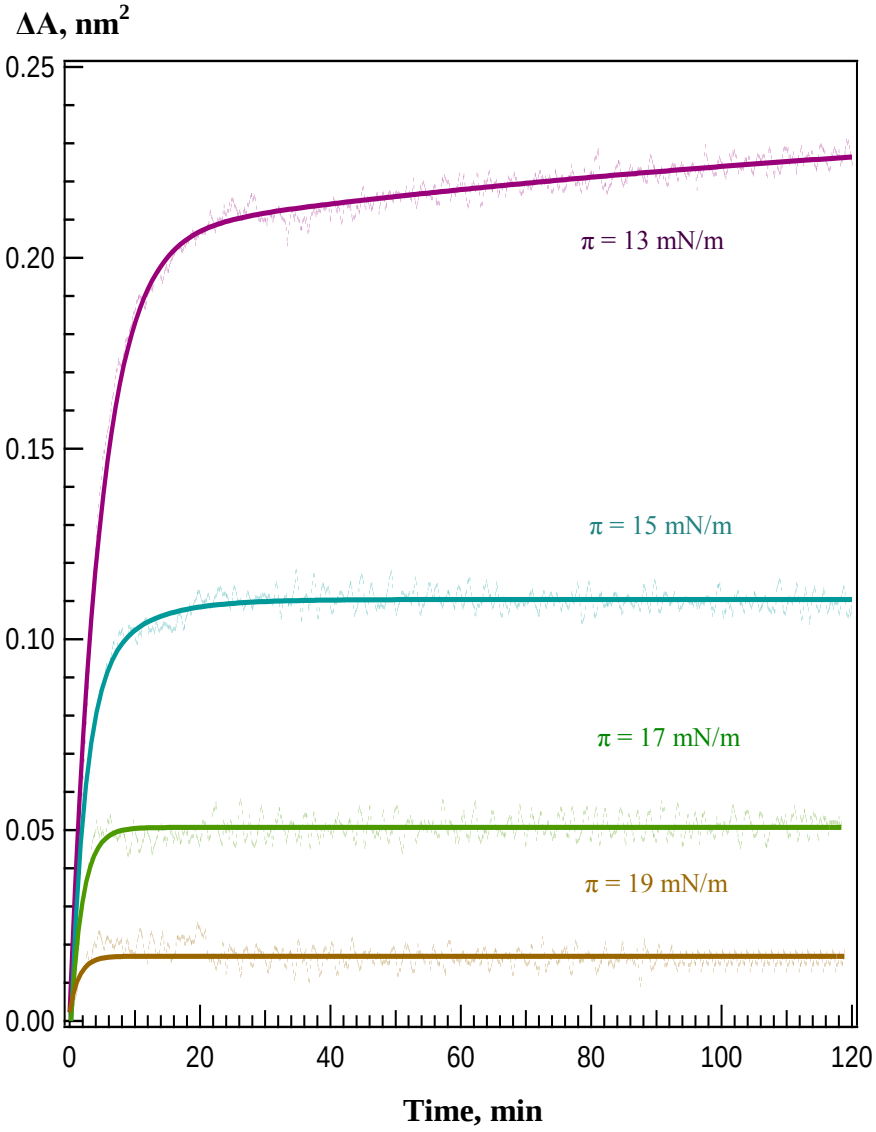


**Figure 6.5:** Insulin-induced changes in the 6 mol% DPPE-PEG2000 in DPPE-Succinyl monolayers mean molecular area as a function of time. Dotted curves shows average *ΔA-t* curves measured upon the injection of insulin in the PBS subphase underneath the monolayer at preset $\pi$ values of 13, 15, 17, 19 mN/m. Solid curves are the exponential fit to the measured *ΔA-t* curves. The end values of *ΔA* in exponential fit were used to derive the steady-state $\Delta A_{ss}$ values. *All data are for insulin concentration in the PBS subphase of ~ 75 ng/mL (i.e. ~ 13nM).*

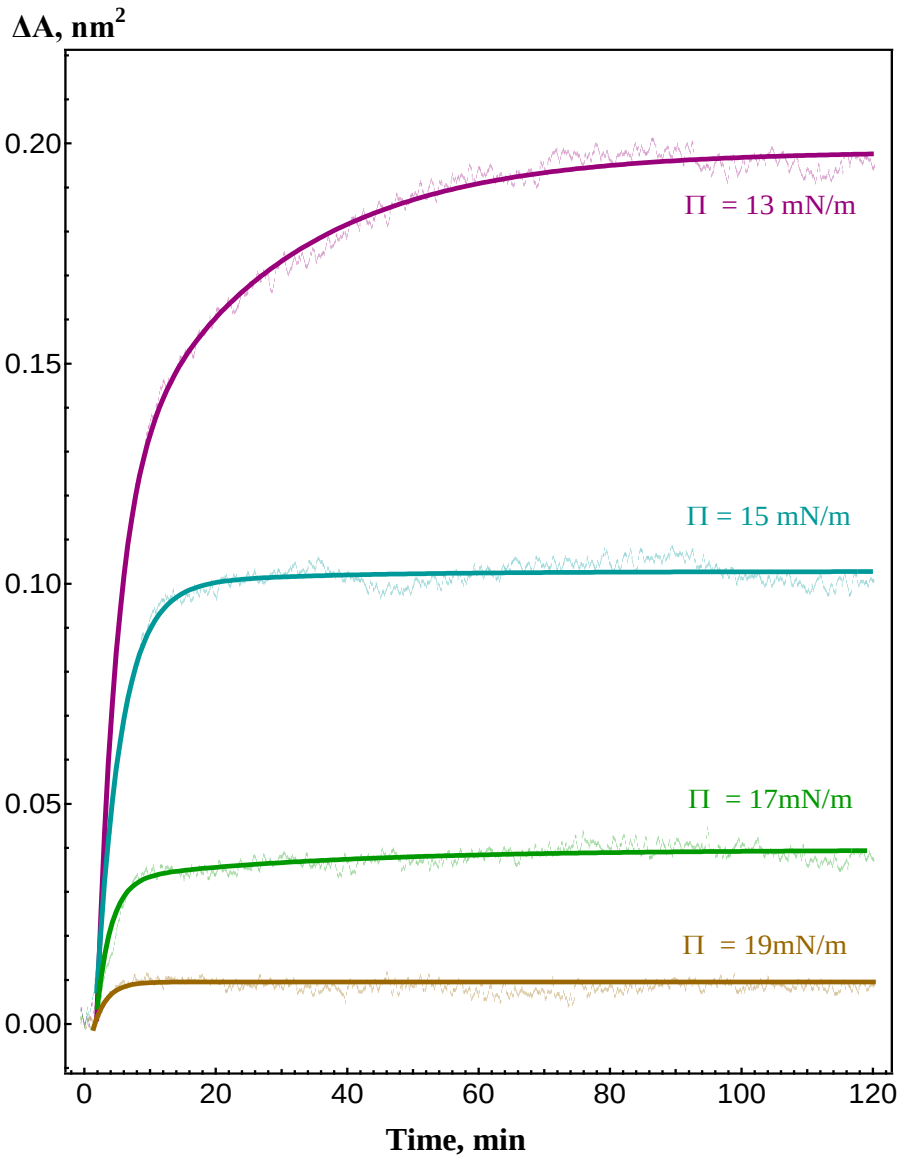


**Figure 6.6:** Insulin-induced changes in the 9 mol% DPPE-PEG2000 in DPPE-Succinyl monolayers mean molecular area as a function of time. Dotted curves shows average $\Delta A$-$t$ curves measured upon the injection of insulin in the PBS subphase underneath the monolayer at preset $\pi$ values of 13, 15, 17, 19 mN/m. Solid curves are the exponential fit to the measured $\Delta A$-$t$ curves. The end values of $\Delta A$ in exponential fit were used to derive the steady-state $\Delta A_{ss}$ values. *All data are for insulin concentration in the PBS subphase of ~ 75 ng/mL (i.e. ~ 13nM).*

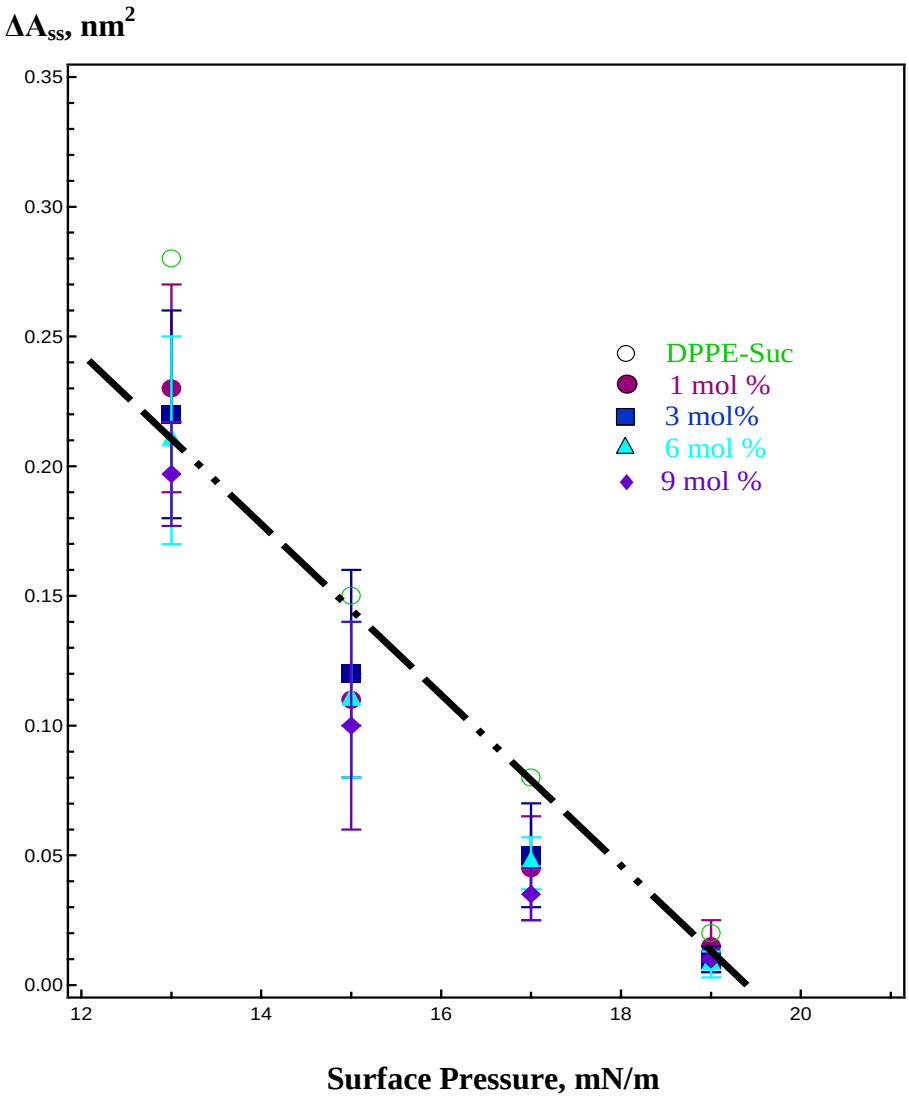


**Figure 6.7: S**ummarized data of the $\Delta A_{ss}$ values obtained for monolayers plotted with respect to π with different mol% PEG: (○) Pure DPPE-Succinyl, (●) 1, (■) 3, (▲) 6, (♦) 9 mol% PEG200. The dashed line shows the linear extrapolation to $\Delta A_{ss} = 0$. All data are for insulin concentration in the PBS subphase of ~75 ng/mL (i.e. ~ 13nM).

### 6.1.2 In-Situ Imaging of Insulin/Monolayer Interactions

#### 6.1.2.1 Methodology for In-Situ Imaging by EFM

The interactions of insulin with pure DPPE-Succinyl monolayer and binary mixtures containing 1, 3, 6 and 9 mol % DPPE-PEG2000 in DPPE-Succinyl were visualized by EFM at a preset π value. Upon gaining the required $\pi$, the compression was stopped and $A - t$ isotherms were measured by adjusting the barrier speed to a maximum value. The monolayer was tested for 20 min to assess its stability. Then, insulin was injected in the subphase as discussed above. EFM images were captured prior to insulin injection and after the insulin injection with an interval of 5 min until it reached the time period of ~2 hours of insulin interactions.

In this study, a rhodamine-labeled probe, DOPE-Rh, was used to image the monolayer morphology whereas FITC labeled insulin was injected underneath the PBS subphase to monitor the insulin/monolayer interactions. The fluorescence was detected by switching between TRITC and FITC channels. Thus, TRITC channel allowed the detection of DOPE-Rh fluorescence to monitor the insulin induced changes in the monolayer morphology and phase behavior. In contrast, fluorescence from FITC-insulin enabled monitoring the accumulation of insulin at the interface through the FITC channel. Both EFM imaging and area expansion measurements were carried out simultaneously. In each series of measurements, images most representative of the monolayer morphology were selected for analysis. Each measurement was performed three times to gain a maximum accuracy and reproducibility of the results.

#### 6.1.2.2 In-Situ Imaging of Insulin/DPPE-Succinyl Monolayer Interactions

The EFM imaging has revealed substantial changes in the monolayer morphology and a constant accumulation of insulin in the monolayers for the entire surface pressure range of 13 – 45 mN/m. A steady increase in the fluorescence intensity from FITC-insulin was observed through FITC channel for about 15 min period after injecting insulin underneath the monolayers. The FITC channel displayed a steady fluorescence from FITC-insulin in the monolayer that persisted over two hours interaction time, regardless of the surface pressure and PEG content.

The effect of insulin on monolayer morphology and physical state was first visualized for the DPPE-Succinyl. Figure 6.8 – 6.10 exhibit EFM images of the pure DPPE-Succinyl monolayer, at $\pi$ = 15, 25, and 35 mN/m, captured through TRITC and FITC channel 1 hour after the insulin injection. At 15 mN/m, the pure DPPE-Succinyl monolayer mainly exhibits a LE phase and hence, no significant change was observed in the monolayer after 1 h of insulin injection (Figure 6.8 A – C). At 25 mN/m, interactions with insulin caused some noticeable changes in monolayer morphology. Compared to image A in Figure 6.9 displaying the morphology of the pure DPPE-Succinyl monolayer on PBS before the insulin injection the percentage of the LC phase in image B in Figure 6.9 captured after 1 h interactions with insulin is higher by ~15% while the LC domains appear fused into worm-like structures and large irregularly-shaped islands. Moreover, the areas close to the large LC islands sporadically showed an increased fluorescence from insulin as seen in the FITC image C in Figure 6.9 featuring high fluorescence patches corresponding to the areas along the boundary of the large LC island in image B (Figure 6.9). The FITC-

insulin depleted patches were also observed in the FITC channel that appeared mimicking the shape of some LC phase islands visualized in TRITC channel (images not shown). At 35 mN/m, the DPPE-Succinyl monolayer appeared quite condensed (image A, Figure 6.10), but after 1 h insulin interaction time, the monolayer exhibited somewhat similar type of morphology in both TRITC and FITC channel as the one seen at 25 mN/m (cf. images B and C in Figure 6.9 and 6.10).

The effect of insulin interaction on the binary mixtures of DPPE-Succinyl and DPPE-PEG2000 was also examined for a typical range of membrane lateral pressures. For the clarity of presentation, the images captured for the binary mixtures containing 9 mol % PEG at 15, 25 and 35 mN/m will only be presented. The mixed monolayer containing 1 mol% PEG behaved quite similar to the pure DPPE-Succinyl monolayer. For higher PEG contents, three distinct types of morphology changes were noticed. (1) The mixed DPPE-Succinyl/DPPE-PEG2000 monolayers in the expanded region of their isotherm retained their mostly uniform fluorescence appearance seen in image A in Figure 6.11, yet irregular flow patterns and large dark stripes seen in image B in Figure 6.11 for the monolayer containing 9 mol% PEG at $\pi$ = 15 mN/m were invariably observed through the TRITC channel for these monolayers upon interactions with insulin. In the FITC channel, these stripes appeared brighter than the background as displayed by image C in Figure 6.11. (2) At the intermediate surface pressures corresponding to the plateau in the isotherms in Figure 5.3b and the coexistence of LE phase with tiny LC domains seen in image A Figure 6.12 for the monolayer containing 9 mol% PEG at $\pi$ = 25 mN/m, interactions of mixed monolayers with insulin resulted in segregation of the LC domains

out of the LE phase into large, irregularly-shaped islands displayed by images B and C in Figure 6.12. FITC channel showed mostly homogenous distribution of FITC-insulin throughout the monolayers, yet both FITC-insulin-depleted and FITC-insulin-rich islands resembling the morphology of the LC islands in the TRITC channel were sporadically observed in the FITC channel (cf. images B and D, C and E in Figure 6.12). (3) At high surface pressures, when the mixed monolayers are made up of mostly LC phase domains as seen in Figure 6.13A for the monolayer containing 9 mol% PEG at $\pi$ = 35 mN/m, the interactions with insulin result in a localized "dissolution" of the LC domains in a fast expanding LE phase (bright areas) that cuts through the LC phase network (dark lace-like-pattern) as displayed by image B in Figure 6.13. In the FITC channel, FITC-insulin-depleted networks identical to those seen in the TRITC channel were observed (cf. image B and D in Figure 6.13). Images C and E in Figure 6.12 taken from a different part of the monolayer have revealed that the expansion of the LC phase occurred at the expense of the LC phase forced to form more densely packed LC islands (images C and E in Figure 6.13). Based on the results, it can be suggested that, overall, insulin interactions cause significant morphology changes in both pure DPPE-Succinyl and mixed DPPE-Succinyl/DPPE-PEG2000 monolayers.

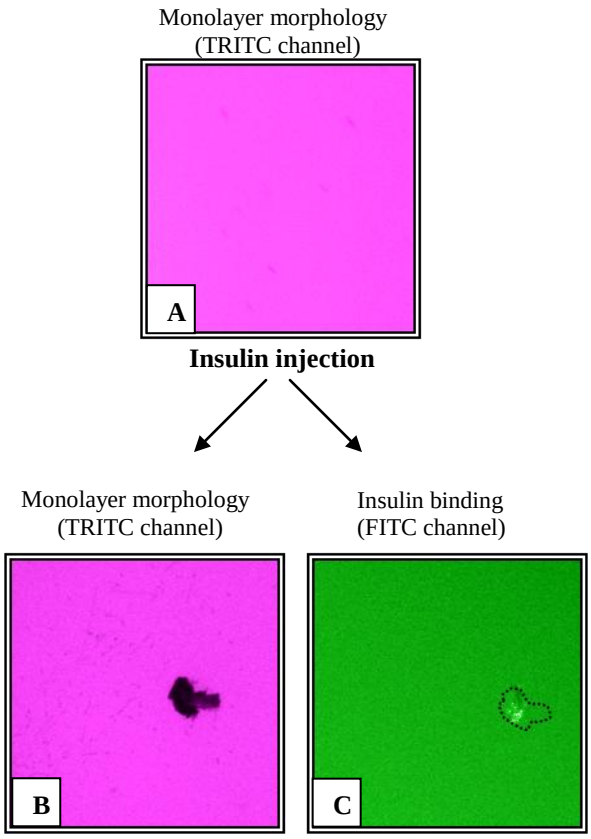


**Figure 6.8:** (A) EFM image displaying the monolayer morphology of DPPE-Succinyl monolayer on PBS subphase at $\pi \approx 15$mN/m. Typical EFM images captured through TRITC (B) and FITC (C) channel for the Pure DPPE-Succinyl monolayer at a preset π of 15mN/m. Both images (B, C) were captured at the same area, 1 h after insulin injection in the subphase underneath the monolayer. The dashed line in image C outlines the boundary of the dark LC phase island in image B. The image size is $250 \times 250$ μm$^2$.

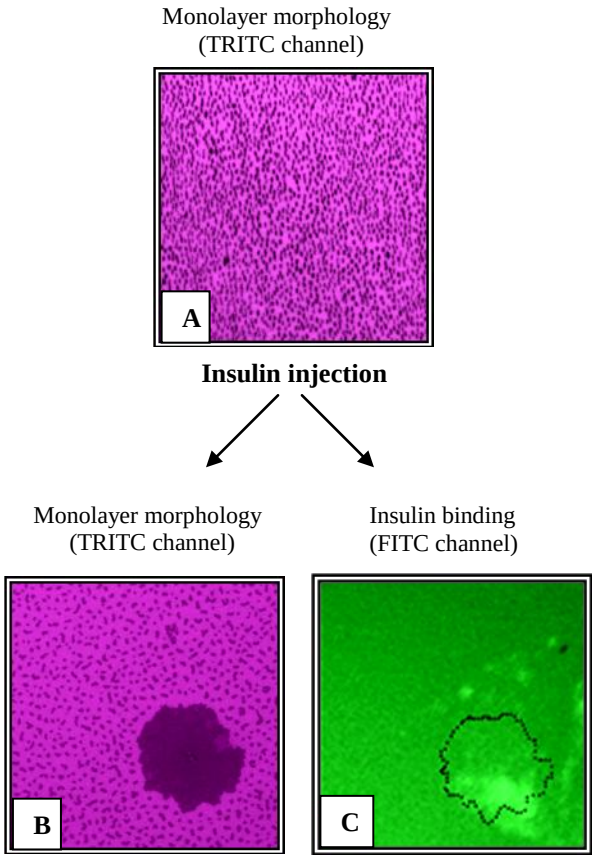


**Figure 6.9:** (A) EFM image displaying the monolayer morphology of DPPE-Succinyl monolayer on PBS subphase at $\pi \approx 25$mN/m. Typical EFM images captured through TRITC (B) and FITC (C) channel for the Pure DPPE-Succinyl monolayer at a preset π of 25mN/m. Both images (B, C) were captured at the same area, 1 h after insulin injection in the subphase underneath the monolayer. The dashed line in image C outlines the boundary of the dark LC phase island in image B. The image size is $250 \times 250$ μm$^2$.

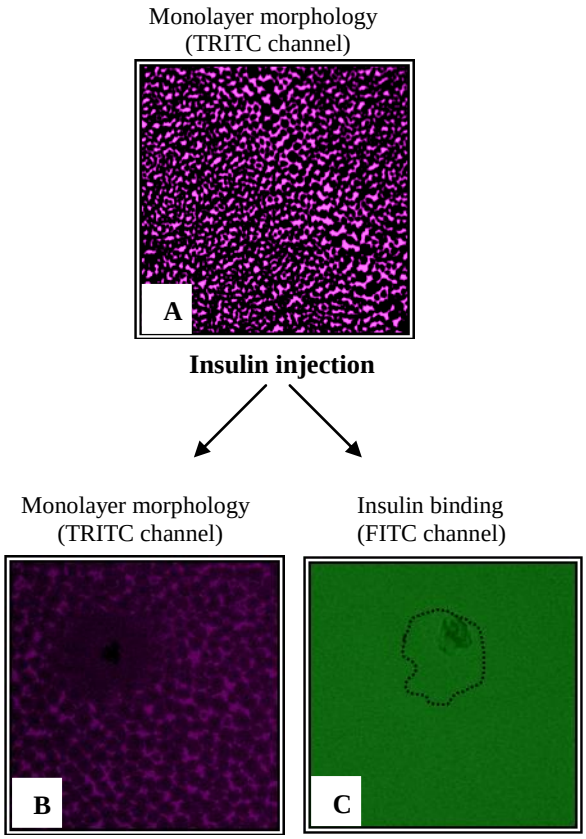


**Figure 6.10:** (A) EFM image displaying the monolayer morphology of DPPE-Succinyl monolayer on PBS subphase at $\pi \approx 35$mN/m. Typical EFM images captured through TRITC (B) and FITC (C) channel for the Pure DPPE-Succinyl monolayer at a preset π of 35mN/m. Both images (B, C) were captured at about the same area, 1 h after insulin injection in the subphase underneath the monolayer. The image size is $250 \times 250$ μm$^2$.

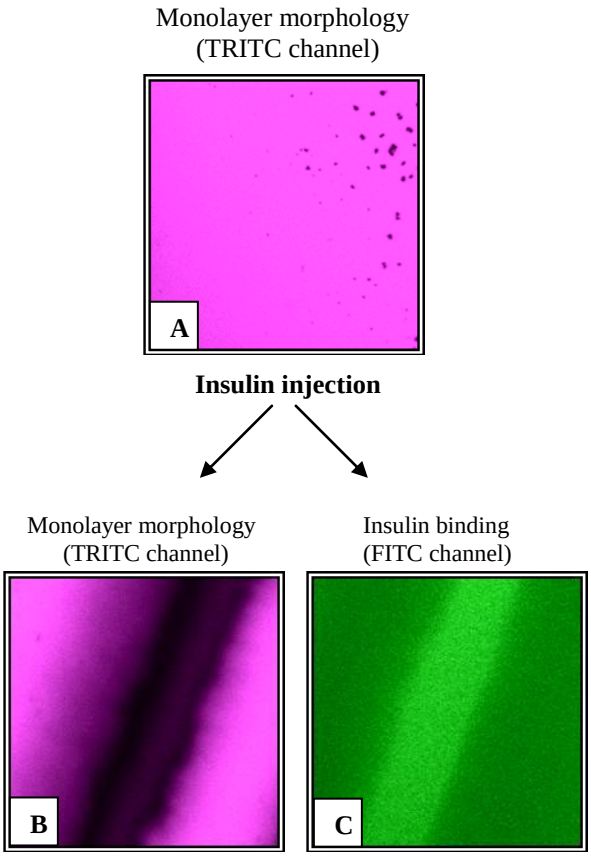


**Figure 6.11:** Typical EFM images captured through TRITC (A, B) and FITC (C) channel for the mixed DPPE-Succinyl/DPPE-PEG2000 monolayer containing 9 mol% PEG at a preset π of 15mN/m. Image A was captured right before the insulin injection. Images B and C were captured from the same area 1 h after insulin injection in the subphase underneath the monolayer. The image size is 250 × 250 $\mu m^2$.

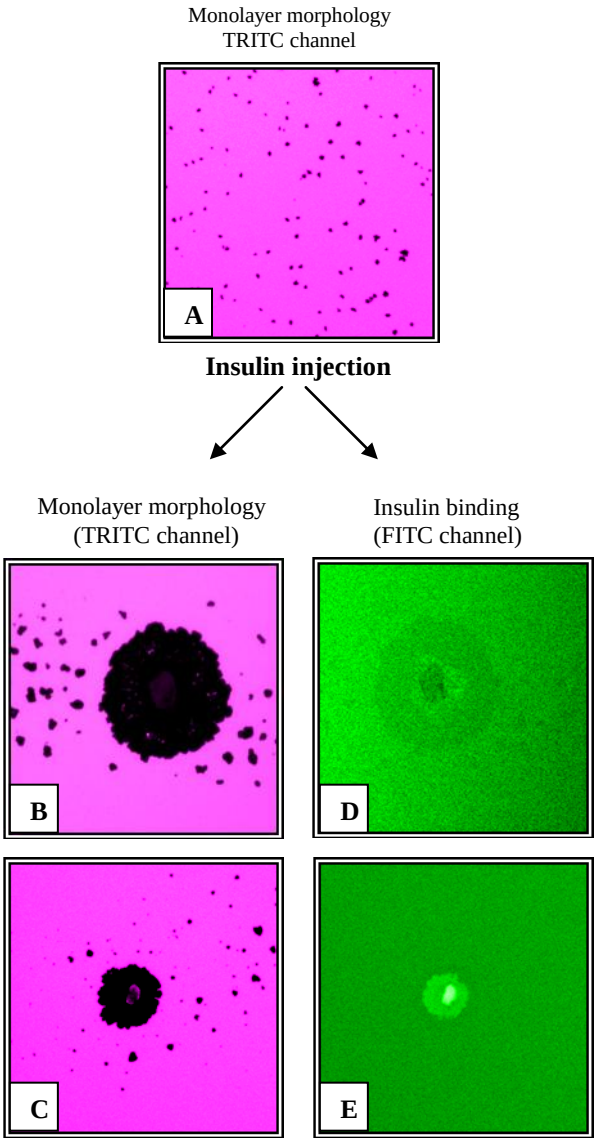


**Figure 6.12:** Typical EFM images captured through TRITC (A, B, C) and FITC (D, E) channel for the mixed DPPE-Succinyl/DPPE-PEG2000 monolayer containing 9 mol% PEG at a preset $\pi$ of 25mN/m. Image A was captured right before the insulin injection. Images B – E were captured after 1 h of insulin injection in the subphase underneath the monolayer. The phospholipid probe (TRITC) and insulin probe (FITC) shows similar patterns in images B and D obtained from the same area while images C and E captured from a different area shows similar patterns which are opposite in contrast. The image size is 250 × 250 $\mu m^2$.

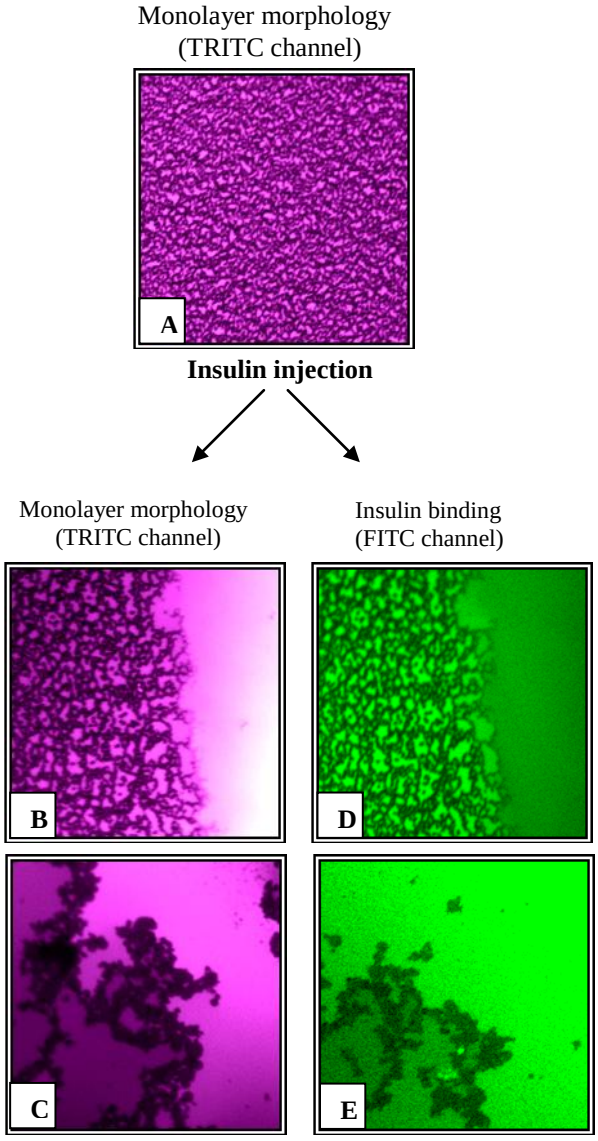


**Figure 6.13:** Typical EFM images captured through TRITC (A, B, C) and FITC (D, E) channel for the mixed DPPE-Succinyl/DPPE-PEG2000 monolayer containing 9 mol% PEG at a preset $\pi$ of 35mN/m. Image A was captured right before the insulin injection. Images B – E were captured after 1 h of insulin injection in the subphase underneath the monolayer. The phospholipid probe (TRITC) and insulin probe (FITC) shows similar patterns. Image pairs B, D and C, E visualize different parts of the monolayer. The image size is 250 × 250 $\mu m^2$.

## 6.2 Discussion

The DPPE-Succinyl monolayer and binary mixtures of DPPE-Succinyl and DPPE-PEG2000 bear negative charge as discussed in chapters 4 and 5. Insulin is known to be an acidic protein with an isoelectric point of ~5.3 and is believed to bear an overall negative charge in PBS subphase with a pH of ~7.4 [Farias 1989; Vermette 2003]. The negative charge distribution on the monolayers and insulin molecules is, hence, expected to introduce repulsive electrostatic interactions between them [Farias, 1989; Taneva 1995]. As suggested by many studies, the PEG chains in the membranes should also aid in creating a steric repulsive barrier against the insulin molecules [Bianco-Peled 2001; Shahid 2011; Vermette 2003; Xu 2000; Zhao 2002]. However, an enhanced adsorption of both acidic and basic proteins on some negatively charged phospholipids membranes with high surface charge density have also been observed at a physiological pH of ~ 7.4 [Vermette 2003]. Some previous studies have also reported that grafted polymeric chains in the outer segment of the membrane are not always efficient in repelling proteins but in contrast play a role in attracting proteins and change their confirmation from the *trans-gauche-trans* (protein-repulsive) to *gauche* (protein-attractive) configuration [Allen 2002; Efremova 2000; Sheth 1997; Vermette 2003; Xu 2000]. The area expansion measurements as well as the accumulation of insulin in monolayers in our study indeed suggest a penetration mechanism of insulin interactions with pure DPPE-Succinyl and mixed DPPE-Succinyl/DPPE-PEG2000 monolayers (Figure 6.2 – 6.13) [Kozarac 1987] . A comparison of $\Delta A_{ss}$ values further demonstrates that the incorporation of DPPE-PEG2000 seems to have a minimal impact on the insulin penetration behavior. As can be seen in Figure 6.7, the pure DPPE-Succinyl and mixed DPPE-Succinyl/DPPE-PEG2000

monolayers only have a slight difference in the area expansion due to insulin interactions. Further, a steady accumulation of insulin for all the monolayers at higher surface pressures without causing any expansion in the monolayers' mean molecular area, above 19.4 mN/m, may suggest that the number of insulin molecules binding onto the monolayers decreases with increasing surface pressure (Figure 6.2 – 6.12). This makes the insulin-induced change in the monolayer mean molecular area undetectable as can be seen in Figure 6.2 – 6.6 and 6.7. This trend might also points towards a somewhat different mechanism between insulin and monolayer interactions above 19.4 mN/m. Thus, at higher pressures, insulin molecules may bind onto the monolayers by the adsorption mechanism without penetrating into the aliphatic chain region and inducing any expansion in the monolayer area [Kozarac 1987]. Our discussion will hence focus on verifying the above interpretive scheme by determining the protein binding parameters, insulin penetration area, $A_p$, as well as the binding degree, $\chi_p$, from the results. The impact of surface pressure and PEG2000 content on these parameters will also be assessed. Furthermore, we will discuss the effect of insulin interactions on the morphology of pure DPPE-Succinyl and mixed DPPE-Succinyl/DPPEPEG-2000 monolayers using EFM.

### 6.2.1 Insulin Penetration Area, $A_p$, for DPPE-Succinyl and Mixed DPPE-Succinyl/DPPE-PEG2000 Monolayers

Monolayer area expansion technique has been used to estimate the penetration area, $A_p$, of various biomolecules and proteins such as hisactophilin and phospholipase C isoforms for various neutral and negatively charged phospholipid membranes [Boguslavsky 1994; Hanakam 1996; Seelig, 1987; Wang 2006]. The results of these studies, in terms of $A_p$

values, have been reported to be in good accord with the NMR and other data for the structural parameters of these molecules [Boguslavsky 1994; Hanakam 1996]. As explained by Boguslavsky et. al., the expansion of monolayer mean molecular area, $\Delta A$, upon protein penetration with an area, $A_p$, is proportional to the Boltzmann factor, $exp(-\pi A_p/kT)$, as shown below

$$\Delta A/A \approx K\, exp(-\pi A_p/kT) \text{ ---------- } 6.1$$

where $A$ is the area per molecule of phospholipid monolayer without protein at a surface pressure $\pi$, $K$ is constant, $k$ is Boltzmann constant and T is the absolute temperature.

Re-arrangement of the equation 6.1 gives

$$\text{Ln}(\Delta A/A) \sim -(A_p/kT)\pi \text{ ---------- } 6.2$$

If a semi-logarithmic plot of $\Delta A/A$ as a function of surface pressure, $\pi$, yields a straight line then indicates that the protein penetrates the monolayer with a constant area known as $A_p$. The slope can then be used to calculate the penetration area of the protein since $A_p = -kT \times slope$. Hence, the insulin penetration area for pure DPPE-Succinyl and mixed DPPE-Succinyl/DPPE-PEG2000 monolayers can be determined by plotting the $\Delta A/A$ data on a semi-logarithmic scale with respect to surface pressure, $\pi$ (Figure 6.14). $\Delta A_{ss}$ values were obtained from Figure 6.7 whereas values of $A$ were obtained from the isotherms in Figure 4.1 and 5.5b (chapter 4) for the same surface pressures to calculate the $\ln(\Delta A_{ss}/A)$. The plot in Figure 6.14 shows a straight line for all the monolayers which suggests that $\ln(\Delta A_{ss}/A)$ is a linear function of $\pi$ from 13 – 19 mN/m. As seen in Figure

6.14, the slope of all plots remains the same, which indicates that insulin penetration remains almost unchanged in monolayers regardless of the PEG content. The insulin penetration area, $A_p$, for DPPE-Succinyl and all mixed DPPE-Succinyl/DPPE-PEG2000 monolayers, using the slope of the $\ln(\Delta A_{ss}/A) - \pi$ plots, is determined to be 1.84 ± 0.07 $nm^2$. In comparison to the results reported in the literature, the penetration area of insulin calculated in the present study is quite small. According to Birdi's results, the area of completely unfolded insulin can be estimated as approximately 9 $nm^2$ in 0.4 M NaCl at air/PBS interface and 25 $^oC$ [Birdi 1976]. Moreover, based on the Browne et al. data, the area of tightly packed insulin molecules at the decane/PBS interface is found to be 7.24 $nm^2$, which is in good agreement with the X-ray data of insulin dimer's structural parameters [Browne 1973]. The lateral dimensions of insulin hydrophobic binding domain have also been determined to be in a range of about 2 × 3 $nm^2$ [Yip 1998]. However, due to different experimental conditions, a direct comparison might not be valid between the data available in the literature and results obtained in the present study.

Nevertheless, two interpretive schemes can be proposed to justify the relatively small value of $A_p$ as 1.84 ± 0.07 $nm^2$. (1) Insulin molecules may conform to a compact size to minimize the area occupied by each molecule in order to penetrate the phospholipid monolayers. In fact, insulin molecules, like other proteins, have shown to change their conformation by partially submerging the hydrophilic residues into the subphase when the area available per insulin molecule in the monolayer decreases [Jorgensen 2011; Nieto-Suarez 2008; Wang 2002]. This conformational change may justify the area of insulin molecule to be 1.84 ± 0.07 $nm^2$ where the polar residues on the A chain and the

protein's helical chains with associated water molecules are displaced down to the phospholipid headgroup region, underneath the subphase, while the hydrophobic residues of the B chain might embed in the monolayer's aliphatic chain regions mainly due to hydrophobic interactions [Gerebtzoff 2004; Mihajlovic 2006]. On the contrary, (2) the insulin molecule interactions with the pure and mixed DPPE-succinyl/DPPE-PEG2000 monolayers can be attributed to the insertion of a small hydrophobic residue loop or domain into the membrane, which is one of the main driving forces of non-specific binding [Gerebtzoff 2004; Hanakam 1996; Mihajlovic 2006]. Based on the above analysis, the value of $1.84 \pm 0.07$ nm$^2$ may correspond to the cross sectional area of such a domain/loop that anchors the insulin molecule to the monolayer. Further investigations would be required to find the most likely scenario. Hence, the value of $A_p$ determined in this report can be beneficial for the system setup in future molecular modeling designs.

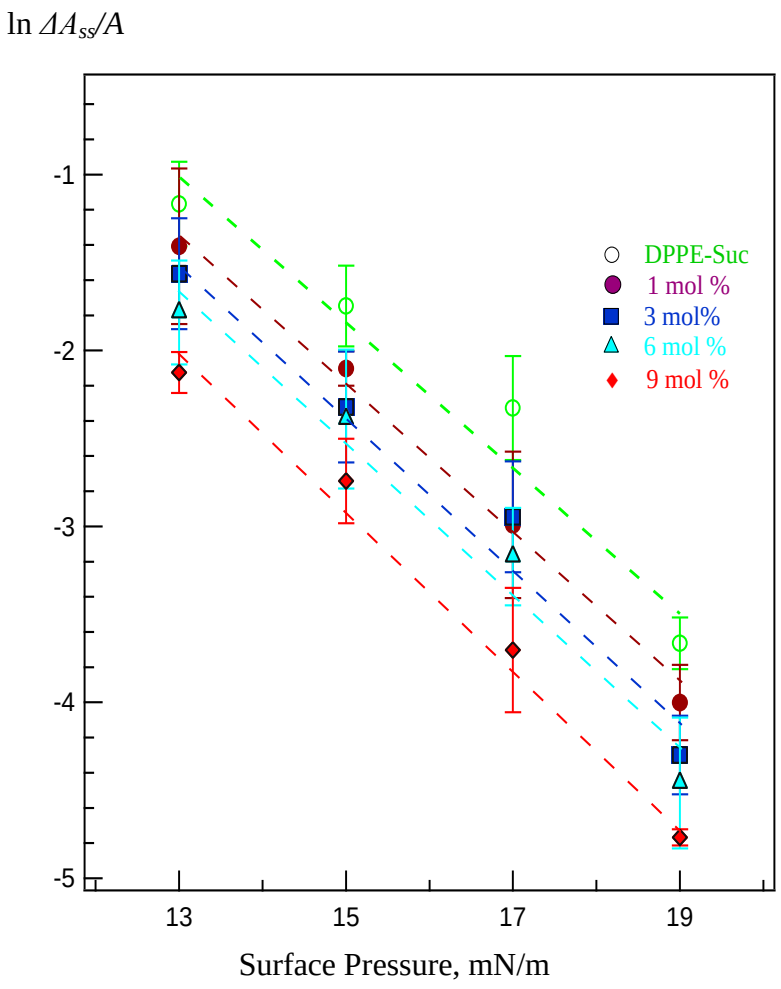


**Figure 6.14:** A Semilogarithmic plot of $\Delta A_{ss}/A$ with respect to surface pressure, $\pi$, with different mol % PEG. (○) Pure DPPE-Succinyl, (●) 1, (■) 3, (▲) 6, (♦) 9 mol% PEG2000. The dashed lines depict the linear fits to the $\ln(\Delta A_{ss}/A) - \pi$ values. A value of 1.84 $nm^2$ is obtained from the slopes of the linear fits illustrating the penetration area of insulin, $A_p$ (see text for more detail). All data are for insulin concentration of ~75 ng/mL (i.e. ~13 nM) in the PBS subphase.

### 6.2.2 Binding Degree of Insulin, $\chi_p$, for DPPE-Succinyl and Mixed DPPE-Succinyl/DPPE-PEG2000 Monolayers

The degree of protein binding, $\chi_p$, can further be estimated from the area expansion measurements after determining the $A_p$ [Boguslavsky 1994; Hanakam 1996; Seelig 1987]. $\chi_p$ is defined as the ratio between the number of moles of protein binding onto the monolayer, $n_p$, and number of moles of phospholipid molecules in the monolayer, $n_{pl}$. The degree of protein binding, $\chi_p$, can further be related to the measured mean molecular area expansion, $\Delta A$ [Hanakam 1996], as

$$\chi_p = n_{p/} n_{pl} = (\Delta A/A)(A_{pl}/A_p) \quad \text{---------- 6.4}$$

where $A_{pl}$ is the effective area of phospholipid in a closely packed state and can be determined from the monolayer's $\pi - A$ isotherm by extrapolating its low compressibility region to $\pi$ = 0 mN/m [Cheng 1999]. The effective area of DPPE-Succinyl molecule from its pure monolayer isotherm is determined to be 0.57 $nm^2$/molecule (Figure 4.1). Similarly, the effective area of phospholipid, $A_{pl}$, in mixed monolayers containing 1, 3, 6, and 9 mol% PEG is found to be 0.58, 0.59, 0.62, and 0.67 $nm^2$/molecule, respectively (Figure 5.5b). Hence, the degree of insulin binding, $\chi_p$, for all the monolayers were calculated using $A_p$ of 1.84 $nm^2$, $A_{pl}$ values, and $\Delta A_{ss}$ data from Figure 6.7 in a surface pressure range of 13 – 19 mN/m (Table 6.1). As can be seen from the table, the degree of insulin binding, $\chi_p$, decreases upon increasing the DPPE-PEG2000 content in the monolayers. Indeed, the number of moles of insulin bound to the monolayer decreases by a factor of ~2 with increasing PEG content in the monolayer from 1 to 9 mol%.

Strikingly, the $\chi_p$ seems to be more affected by the monolayer surface pressure than by the PEG content. As seen in Table 6.1, the $\chi_p$ values for all the monolayers decrease ten times at 19 mN/m as compared to those at 13 mN/m. Indeed, the values of $\chi_p$ are in a range of 0.043 – 0.096 at 13 mN/m indicating that 43 – 96 insulin molecules bind per 1000 phospholipids in the monolayer depending on the PEG content, which drops down to 3 – 8 insulin molecules at 19 mN/m. This suggests that the number of insulin molecules interacting with the monolayers decreases at higher surface pressures. This might explain negligible changes in the mean molecular area expansion above 19 mN/m although a steady accumulation of insulin in monolayers was continuously monitored through EFM imaging.

Table 6.1: Degree of insulin binding, $\chi_p$, for DPPE-Succinyl and mixed DPPE-Succinyl/DPPE-PEG2000 monolayers calculated from $\Delta A_{ss}$ data by using equation 6.4.

| Degree of Insulin Binding, $\chi_p$ | | | | | |
|---|---|---|---|---|---|
| π, mN/m | DPPE-Succinyl | 1 mol% PEG | 3 mol% PEG | 6 mol% PEG | 9 mol% PEG |
| 13 | 0.096 ± 0.010 | 0.078 ± 0.008 | 0.067 ± 0.006 | 0.057 ± 0.006 | 0.043 ± 0.005 |
| 15 | 0.054 ± 0.008 | 0.039 ± 0.006 | 0.038 ± 0.004 | 0.032 ± 0.004 | 0.023 ± 0.003 |
| 17 | 0.030 ± 0.004 | 0.017 ± 0.003 | 0.017 ± 0.002 | 0.014 ± 0.002 | 0.009 ± 0.002 |
| 19 | 0.008 ± 0.002 | 0.006 ± 0.002 | 0.004 ± 0.001 | 0.003 ± 0.001 | 0.003 ± 0.001 |

Standard deviations for $\chi_p$ were calculated based on series of three measurements.

### 6.2.3 Effect of Grafted PEG2000 Chains on Insulin/Monolayer Interactions

A detailed analysis of penetration area, $\boldsymbol{A_p}$ and binding degree, $\chi_p$, of insulin have revealed that increasing the DPPE-PEG2000 content in the binary mixtures certainly decrease the binding of insulin onto the monolayer but do not have a significant impact on the insulin penetration area. Therefore, the mechanism of insulin/monolayer interactions is likely to remain the same regardless of PEG content. EFM imaging also support this conclusion. As can be seen in Figure 6.8 – 6.10, the nucleation of LC phase in DPPE-Succinyl monolayer is mainly induced by the penetration mechanism of insulin and is considered as a typical feature of protein/monolayer interactions [Wang 2002; Wang 2001; Zhao 2000]. The stimulation of LC phase formation might be attributed to insulin molecules, which compress and bring the phospholipid aliphatic chains closer together, while inserting their hydrophobic residues in the monolayer. This type of morphology change at all surface pressures suggests that the penetration mechanism occurs over the entire surface pressure range of 13 – 45 mN/m. However, the number of insulin molecules inserting into the pure DPPE-Succinyl monolayer aliphatic chain region decreases upon monolayer compression and thus no monolayer area expansion is detected above ~19.4 mN/m.

An increased nucleation of the LC phase in the mixed DPPE-Succinyl/DPPE-PEG2000 monolayers containing 3 – 9 mol% PEG upon insulin interactions was also seen at intermediate surface pressures around 25 mN/m (Figure 6.12). However, at higher surface pressures, all the mixed monolayers exhibited somewhat different morphology indicating an expansion of the LE phase upon interactions with insulin. The EFM images of mixed monolayer containing 9 mol% DPPE-PEG2000 at a surface pressure of 35

mN/m (Figure 6.13) reveal that a uniform dense lace-like network of the LC phase domain (image A) turned into a "diluted" phase (image B) after 1 hour of insulin interactions. Most importantly, large portions of the LC network begin to disappear in the increasing expanded LE phase (bright field on the right-hand side in image B of Figure 6.13). Indeed, the expansion of the LE phase and the binding pattern of insulin to the monolayer coincide well with each other, as can be compared in image B and D of Figure 6.13. Interestingly, insulin binding effect on the morphology of the mixed DPPE-Succinyl/DPPE-PEG2000 monolayers seems to be more dramatic at lower surface pressures. As can be seen in Figure 6.11, the penetration of insulin cleaves the mixed monolayer containing 3 – 9 mol% PEG producing a few-micrometer-wide "slit" free of phospholipid molecules, seen as dark stripe in image B, and yet populated with insulin molecules, displayed as bright stripe in image C. The "cleavage" patterns and expansion of LE phase are indicative of monolayer perturbation by protein molecules, which might be resulting from a localized phospholipid packing disruption in the mixed monolayers. This type of cleavage phenomenon correlates well with the morphological patterns observed by Wang et. al specifically for negatively charged monolayers [Haas 1989; Wang 2002]. The disruption in phospholipid packing, however, may not be due to the insulin hydrophobic residues insertion into the hydrophobic region of the monolayer but rather the result of competitive interactions of protein molecules with PEG-grafted phospholipids to stay at the air/PBS interface, entrapment of insulin in the PEG chains, and/or adhesive contacts between insulin molecules and PEG outer segment region [Allen 2002; Dhruv 2006; Cheng 1999; Efremova 2000; Halperin 2007; Sheth 1997]. Hence, the steady accumulation of insulin molecules in monolayers impels us to conclude

that the interactions between insulin and mixed DPPE-Succinyl/DPPE-PEG2000 monolayers can be well defined as penetration mechanism at all surface pressures, which is quite similar to the pure DPPE-Succinyl monolayer, but somewhat changed due to the incorporation of grafted PEG chains.

### 6.3 Conclusion

A comparative analysis of $\Delta A - t$ measurements and EFM imaging studies has revealed that the area of DPPE-Succinyl monolayers and binary mixtures of DPPE-Succinyl/DPPE-PEG2000 expands upon interactions with insulin. The incorporation of PEG does not seem to suppress the penetration mechanism of insulin/monolayer interactions as can be seen from the calculated insulin penetration area of $1.84 \pm 0.07$ nm$^2$ for both pure DPPE-Succinyl and mixed DPPE-Succinyl/DPPE-PEG2000 monolayers. The relatively small value of $A_p$ suggests that the insulin molecule indeed inserts into the monolayers through the same domain or in a compact conformation regardless of the PEG content.

## 6.4 References


Allen, C.; Santos, N. D.; Gallagher, R.; Chiu, G. N. C.; Shu, Y.; Li, W. M.; Johnstone, S. A.; Janoff, A. S.; Mayer, L. D.; Webb, M. S.; Bally, M. B. *Biosci. Rep.* **2002**, *22 (2)*, 225.

Bianco-Peled, H.; Dori, Y.; Schneider, J.; Sung, L. P.; Satija, S.; Tirrell, M. *Langmuir* **2001**, *17*, 6931.

Birdi, K. S. *J. Coll. and Inter. Sci.* **1976**, *57(2)*, 228.

Boguslavsky, V.; Rebecchi, M.; Morris, A. J.; Jhon, D-Y.; Rhee, S. G.; Maclaughlin, S. *Biochemistry* **1994**, *33*, 3032.

Browne, M.; Cecil, R.; Miller, J. C. *Eur. J. Biochem.* **1973**, *33*, 233.

Calvez, P.; Bussieres, S.; Demers, E.; Salesse, C. *Biochimie* **2009**, *91*, 718.

Cheng, Q.; Fu, J. A.; Burkard, R. Wang, W.; Yamamoto, M.; Yang, J.; Stevens, R. C. *Thin Solid Films* **1999**, *345*, 292.

Dhruv, H.; Pepalla, R.; Taveras, M.; Britt, D. W. *Biotech. Prog.* **2006**, *22*, 150.

Efremova, N. V.; Bondurant, B.; O'Brien, D. F.; Leckband, D. E. *Biochemistry* **2000**, *39*, 3441.

Farias, R. N.; Vinals, A. E. L.; Posse, E.; Morero, R. D. *Biochem. J.* **1989**, *264*, 285.

Gerebtzoff, G., Li-Blatter, X., Fischer, H., Frentzel, A. and Seelig, A. *Chem. Bio. Chem.* **2004**, *5*, 676.

Haas, H., and Mohwald, H. *Thin Solid Films* **1989**, *180*, 101.

Hanakam, F.; Gerisch, G.; Lotz, S.; Alt, T.; Seelig, A. *Biochemistry* **1996**, *35*, 11036.

Hashizaki, K.; Taguchi, H.; Itoh, C.; Sakai, H.; Abe, M.; Saito, Y. ; Ogawa, N. *Chem. Pharm. Bull.* **2003**, *51*, 815.

Halperin, A.; Fragneto, G.; Schollier, A.; Sferrazza, M. *Langmuir* **2007**, *23*, 10603.

Jorgensen, L., Bennedsen, P., Hoffmann, S. V., Krogh, R. L., Pinholt, C., Groenning, M., Hostrup, S., Bukrinsky, J. T. *Eur. J. Pharm. Sci.* **2011**, *42*, 509.

Konttila, R.; Salonen, I.; Virtanen, J. A.; Kinnunen, P. K. J. *Biochemistry* **1988**, *27*, 7443.

Kozarac, Z.; Dhathathreyan, A.; Mobius, D. *Eur. Biophys. J.* **1987**, *15*, 193.

Lozano, M. M.; Longo, M. L. *Soft Matter* **2009**, *5*, 1822.

Mihajlovic, M., and Lazaridis, T. *J. Phys. Chem. B* **2006**, *110*, 3375.

Nieto-Suarez, M.; Vila-Romeu, N.; Dynarowicz-Latka, P. *Coll. and Sur.A* **2008**, *321*, 189.

Rahmati, K.; Koifman, J.; Tsuokanova, V. *Coll. and Sur. A* **2008**, *321*, 181.

Seelig, A. *Biochim. Biophys. Acta* **1987**, *899*, 196.

Shahid, M. N.; Tsoukanova, V. *J. Phys. Chem. B* **2011,** *115(13)*, 3303.

Sheth, S. R.; Leckband, D.; *Proc. Natl. Acad. Sci. USA* **1997**, *94*, 8399.

Taneva, S.; McEachren, T.; Stewart, J.; Keough, K. M. W. *Biochemistry* **1995**, *34*, 10279.

Vermette, P.; Meagher, L. *Coll. and Sur. B* **2003**, *28*, 153.

Wang, Z-G. *Ind. Eng. Chem. Res.* **2006**, *45*, 5538.

Wang, X., Zhang, Y., Wu, J., Wang, M., Cui, G., Li, J., and Brezesinski, G. *Coll. and Sur. B* **2002**, *23*, 339.

Wang X., Zhang, H., Cui, G., and Li, J. *J. Mol. Liq.***2001**, *90*, 149.

Xu, Z.; Marchant, R. E. *Biomaterials* **2000**, *21*, 1075.

Yip, C. M.; Yip, C. C.; Ward, M. D. *Biochemistry* **1998**, *37*, 5439.

Zhao, H.; Dubielecka, P. M.; Soderlund, T.; Kinnunen, P. K. J. *Biophys. J.* **2002**, *83*, 954.

Zhao, J.; Vollhardt, D.; Brezesinski, G.; Siegel, S.; Wu, J.; Li, J. B.; Miller, R. *Coll. and Sur. A* **2000**, *171*, 175.

# Chapter 7: Insulin Conformation in Non-Specific Interactions with DPPE-Succinyl/DPPE-PEG2000 Model Membranes: CD Spectroscopy Study

Based on our insulin monolayer studies (chapter 6) it is concluded that insulin may interact with the model membranes (monolayers) either by inserting a loop, domain or as a monomer in a compact conformation. In this chapter, we will perform a study focusing on possible changes in the conformation of insulin upon interacting with the model membranes. CD spectroscopy is employed to obtain information about insulin conformation and secondary structure, in particular α-helical content, upon the non-specific interactions with model membranes. Small unilamaller vesicles (SUVs) were selected as model membranes for insulin/membrane interaction studies. Hence, the preparation techniques for SUVs and their imaging analysis will also be discussed in this chapter.

### 7.1.1 Molecular Dimensions of Insulin Molecule

Insulin is a small, hydrophobic protein and is primarily composed of α – helical chains [Zlatica 1998]. Insulin is a 51 amino acid long polypeptide consisting of two chains A and B that are connected to each other via two disulfide bridges [Henry 2008; Hong 2012]. Chain A made up of 21 residues is mainly hydrophilic and forms two antiparallel α−helices as well as bears two negative charges at pH of ~7. Conversely, chain B made up of 30 amino acid residues is hydrophobic and forms α−helix, turn, as well as β−strand conformation [Hong 2012; Perez-Lopez 2011; Zlatica 1998]. Insulin molecule in the

crystalline form is known to possess $A_1 – A_4$ amino acid residues in a loose helical turn with $A_{12} – A_{19}$ residues forming a helical structure whereas $B_9 – B_{20}$ residues in a very stiff α−helical conformation [Pocker 1980]. Among all these three peptide regions of the insulin molecule, only the two A-chain helical segments can undergo helix to random coil transitions due to their less compact and loose structure [Pocker 1980]. Moreover, insulin bears a net charge of −2 per monomer at a physiological pH of ~7.4 [Henry 2008].

Insulin is known to exhibit an intricate self-association behavior in the blood stream, where it mainly exists in three structural levels as monomer, dimer and hexamer [Liu 2012; Henry 2008]. The presence of these species depends on different environmental conditions such as temperature, pH, concentration of insulin and other factors [Liu 2012]. Insulin monomer appears as a wedge in shape with a molecular dimension of about 20 × 25 × 20 $Å^3$ [Henry 2008]. The dimer (composed of two monomers) exists as an oblong shape with an estimated cross sectional area of 20 × 25 × 40 $Å^3$ whereas the hexamer (composed of six insulin molecules) is a flattened spheroid with an approximate diameter of 49 Å and height of ~ 34 Å [Henry 2008]. A monomer is considered as the biologically active form while hexamer is inactive but the most stable form of insulin [Perez-Lopez 2011; Pocker 1980]. The structural level of insulin mainly depends on the concentration of the solution [Nylander 2003]. For instance, insulin is likely to exist in the monomer conformation at a concentration range between 0.1 – 1 μM [Pocker 1980]. Hence, the insulin concentration of 0.7 μM, used in our study, lies within this range.

### 7.1.2 Conformational Dynamics of Insulin Molecule

At certain destabilizing conditions, insulin may change its conformation, self-association and aggregation states [Hong 2012; Perez-Lopez 2011]. In particular, these conditions may include the non-specific interactions with phospholipid membranes. The non-specific binding of insulin onto membranes may be driven by electrostatic interactions with the net charge in the monolayer headgroup region and/or by the tendency for hydrophobic residues on the outer surface of insulin to minimize their exposure to the aqueous environment through inserting themselves into the aliphatic chain region of the membrane [Birdi 1976]. Figure 7.1 exhibits the secondary structure of insulin monomer depicting chain B highlighted as brown color (mainly hydrophobic region) whereas chain A highlighted as white color ( mainly hydrophilic region). It has been suggested that the presence of different hydrophobic environments, such as the physical state of phospholipid membranes, can substantially influence the conformational behavior and aggregation rate of insulin during the non-specific interactions [Birdi 1976; Boisselier 2012; Nosrati 2009; Perez-Lopez 2011]. Interestingly, a partial unfolding or loss of native conformation of insulin has been reported while interacting with a negatively charged phospholipid DOPS membrane [Grudzielanek 2007]. Several other studies have reported a partial unfolding of various proteins including cytochrome *c*, phospholipase $A_2$, acetylcholinesterase and recombinant human prion protein in the membrane environment [Gorbenko 2006]. A decrease in the activation energy barrier for protein upon interactions with the phospholipid bilayers is believed to be the contributing factor for the subsequent loss of native conformation or partial unfolding of proteins [Gorbenko 2006]. A complementary structural analysis of insulin, in terms of the α-

helical content, is thus largely required to address its conformational changes upon the non-specific binding to membranes. Numerous microscopic and spectroscopic techniques have been utilized to study the protein-membrane interactions. Among the techniques, Fourier transform infrared spectroscopy (FTIR), differential scanning calorimetry (DSC) and circular dichroism spectroscopy (CD) have been used to structurally characterize proteins while interacting with membrane models [Tamm 1997]. However, there are some potential limitations associated to the FTIR technique. The major pitfall is the assignment of FTIR absorption bands due to amide vibrational overlapping with vibrations arising from other hydrocarbons [Jackson 1995; Tamm 1997]. CD was, hence, employed to determine the secondary structure and orientation of proteins upon interactions with membrane due to its relative simplicity and reproducibility.

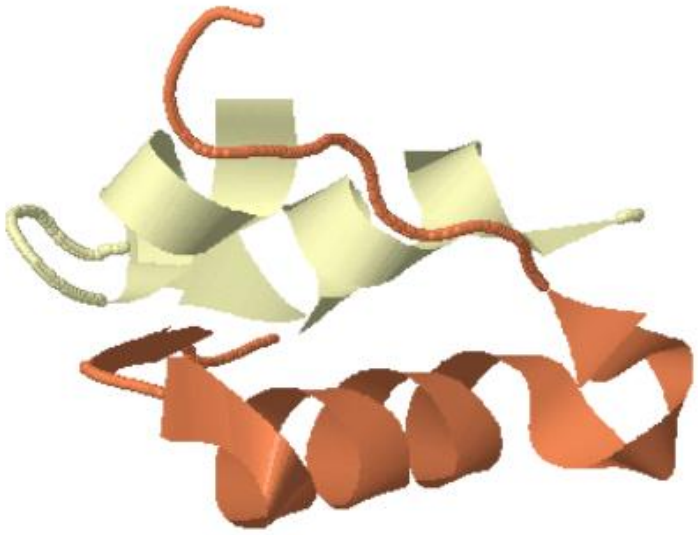

**Figure 7.1:** Secondary structure of an insulin monomer (PDB ID: 2JV1) indicating brown colour segment as B-chain containing mostly α−helices and β−strand (mainly hydrophobic region) as well as white segment as A-chain bearing mostly α−helices (mainly hydrophilic region) [adapted from PDB: Bocian 2008].

### 7.1.3 CD Spectroscopy for Insulin-Membrane Interactions

The CD spectroscopy is generally employed for the structural analysis of proteins including their secondary, tertiary structures, conformational changes, folding/unfolding states as well as binding properties [Greenfield 2006]. CD works on the principle of measuring the unequal absorption of left- and right-handed circularly polarized light that arise from an optically active asymmetrical (chiral) molecule, at a given wavelength [Greenfield 2006; Sadhale 1999; Solomon 2006; Whitnore 2007]. The presence of dextrorotary and levorotary components in the protein molecules rotates the circularly polarized light differently, which gives rise to a CD spectrum representing the unique signature of each individual protein structure. The CD spectrum of a typical protein is primarily divided into three distinctive regions (i) a far-UV range, between 190 – 250 nm, (ii) a near-UV range between 250 – 350 nm and (iii) a near UV-visible range from 300 – 700 nm as sketched in Figure 7.2. The far-UV range of spectrum provides information about the secondary structure of a protein molecule using peptide contributions [Sreerama 2004]. The near-UV range exhibits information about the tertiary structure, folding/unfolding as well as the contributions from the aromatic side-chains (Figure 7.2) [Sreerama 2004]. Furthermore, the near UV-visible range reveals information about ligand binding and metal-protein interactions using contribution from extrinsic chromophores [Sreerama 2004]. A typical example of far-UV CD spectra exhibiting three different conformations of secondary structure of poly-lysine is shown in Figure 7.3. These conformations include α−helix, β−sheet and random coil (unordered structure) in the poly-peptide chain. The CD-spectrum of α−helix is characterized by a positive band at about 192 nm and two negative bands at ~209 and 222 nm that are usually used for the

CD analysis [Pourhosseini 2007; Sreerama 2004]. The main focus of this analysis is to monitor the changes in the α−helical content of insulin upon non-specific interactions with the membrane models. Hence, this report will only cover the far-UV CD spectrum of insulin to examine the conformational change, aggregation states, with respect to its α−helical content, upon interactions with membrane models (SUVs).

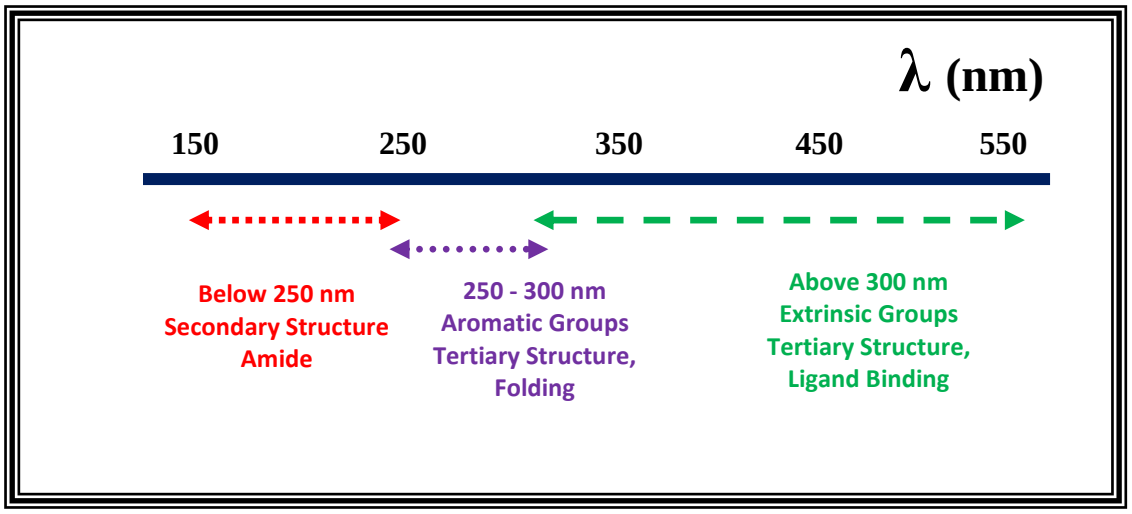


**Figure 7.2:** Spectral Regions of CD and Chromospheres contributions from proteins. [The schematic is made based on the results by Sreerama 2004].

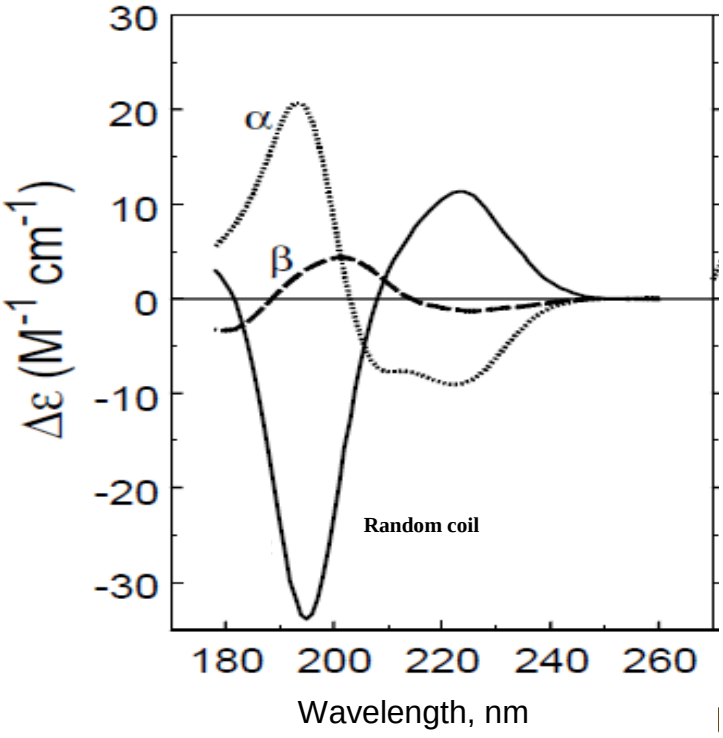


**Figure 7.3:** A typical CD spectra of polypeptide indicating α−helix, β−sheet and random coil [The schematic is made based on the results by Sreerama 2004].

### 7.1.4 Preparation of Small Unilamellar Vesicles (SUVs)

The CD measurements of insulin were performed upon interactions with SUVs as model membranes. The SUVs were prepared by mixing 1, 3, 6 and 9 mol % DPPE-PEG2000 in DPPE-Succinyl by using a typical method of hydrating the dry phospholipid film [Jesorka 2008]. The stock solutions of DPPE-Succinyl and DPPE-PEG2000 were prepared in chloroform/methanol, ~20 mg/mL and 2 mg/mL, respectively, and their binary mixtures containing 1, 3, 6 and 9 mol% PEG in DPPE-Succinyl were obtained by mixing their appropriate molar ratios. The phospholipid solutions were prepared in flat 6 mL vials. The organic solvents were evaporated at 60 – 70 *°C* for about 30 min and the remaining phospholipid film was dried under vacuum overnight followed by its hydration in PBS, pH ~7.4, to make a solution with a total phospholipid concentration of ~ 0.4 mM. The solution was then stirred for 30 min at ~70 *°C* and then sonicated for 30 min at 50 *°C* in a bath-type sonicator. The sonication step was important to produce a suspension of SUVs $\leq$ 10 μm in diameter. The size distribution of SUVs were analyzed by visible light microscopy prior and following the CD measurements.

### 7.1.5 Methodology of CD Measurements

Circular Dichroism (CD) spectroscopy was performed for native insulin and insulin interacting with SUVs in PBS. The PBS baseline was first measured, which was later used to subtract from all the final average CD scans. Secondly, the CD spectrum of native insulin was measured in PBS at a concentration of 0.7 μM. The insulin was then injected in vesicle suspension to a concentration of 0.7 μM and the far-UV CD spectra were

measured. The spectra were obtained every hour after the insulin injection into SUVs suspensions over 3 hours of interaction time. The CD measurements were performed within 5 hours of SUVs preparation. The wavelength scanning range was 190 – 250 nm which is the range for far-UV of the CD spectrum. A rectangular cell with a path length of 1 cm was used for all measurements. The scanning rate was 50 nm/min with a bandwidth of 1.0 nm. Each scan took 3 min and three consecutive scan were obtained for an average CD plot. Each CD measurement was performed three times for maximum reproducibility. The spectra of insulin interacting with SUVs were obtained by subtracting the spectra of vesicles in PBS. The data for CD were recorded as ellipticity in millidegrees.

## 7.2 Results and Discussion

### 7.2.1 In-Situ EFM Visualization of Insulin Interactions with DPPE-Succinyl/DPPE-PEG2000 Vesicles

Visible light microscopy was utilized to monitor the size of small unilamellar vesicles upon interactions with insulin. Figure 7.4 exhibits typical EFM images of pure DPPE-Succinyl vesicles before and after interactions with insulin. The size of SUVs before interactions with insulin ranged 1 – 2 μm in diameter. The size of most of the DPPE-Succinyl SUVs increased after two hours of insulin interactions to approximately 2 – 6 μm in diameter. Interestingly, the numbers of SUVs in the images appear to increase after two hours of insulin interaction time (cf. Figure 7.4 A and B). This can be attributed to

the fact that before interaction with insulin, the diameter of a majority of SUVs was very small, below the resolution limit of the microscope objective of 1 – 2 μm. However, after interactions with insulin the vesicles appeared noticeably bigger. Hence, more of them became clearly visible in the image (cf. Figure 7.4 A and B]. Most importantly, the SUVs without adding insulin did not grow in size over two hours period (data not shown). This indicates that an increase in the size of SUVs can only be due to insulin penetrating the membrane and eventually making them appear larger. This correlates well with the observations of model membrane expansion in the monolayer studies (chapter 6).

The binary mixtures of DPPE-Succinyl and DPPE-PEG2000 exhibited a very similar trend. However, for the clarity of presentation, the binary mixtures of DPPE-Succinyl and DPPE-PEG2000 containing 9 mol% PEG will only be presented. As can be seen in Figure 7.5, the size and quantity of SUVs containing 9 mol% PEG also increased after 2 hours of insulin interaction. As can be seen in the image in Figure 7.5A, the SUVs were barely seen before insulin interaction suggesting that most of them were probably <1 μm in diameter. The size of SUVs, however, increased to about 1 – 3 μm in diameter and became noticeably bigger after interactions with insulin (cf. Figure 7.5 A and B). Increase in SUV size after insulin interactions points towards insulin interacting with membrane phospholipids and PEG chains and expanding the membrane. Thus, examining the insulin/SUVs interactions using CD spectroscopy can provide valuable information about the conformational behavior of insulin upon expanding the membrane.

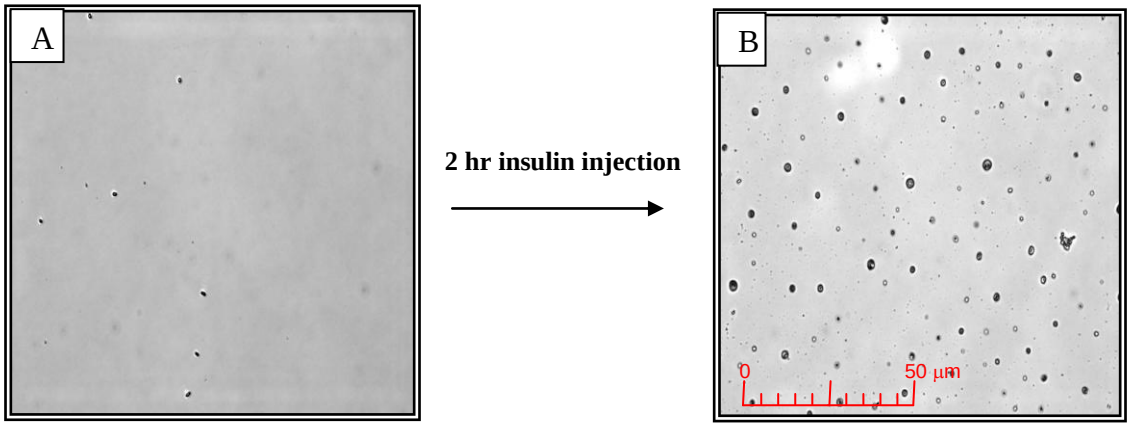


**Figure 7.4:** Snapshots of DPPE-Succinyl small unilamellar vesicles (SUV) (A) before the insulin (B) 2 hr after the insulin injection. The images were captured before and after CD measurements were performed. T = 20 ºC.

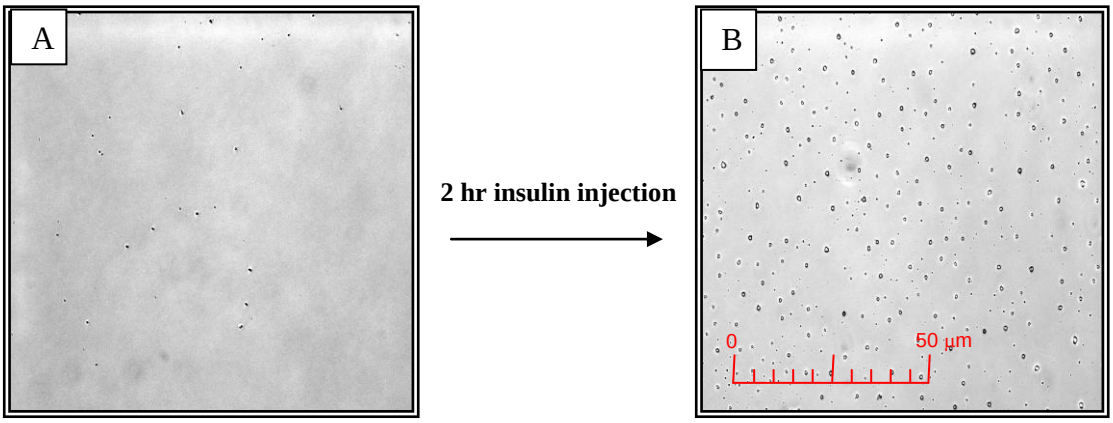


**Figure 7.5:** Snapshots of binary mixture containing 9 mol% DPPE-PEG2000 and DPPE-Succinyl small unilamellar vesicles (SUV) (A) before the insulin (B) 2 hr after the insulin injection. The images were captured before and after CD measurements were performed. T = 20 ºC.

### 7.2.2 Far-UV CD Spectrum of Native Insulin Molecule

The far-UV CD spectrum of native insulin was first obtained in PBS at 20 °C as a reference for the comparative analysis (Figure 7.6). The CD spectrum of insulin in Figure 7.6 exhibits a positive band at ~196 nm and two negative bands at 209 and 222 nm crossing over at ~202 nm to a positive band. This characteristic is typical of a native insulin monomer exhibiting an appreciable amount of α-helical structure, as discussed below [Ahmed 2005; Ettinger 1971; Jorgensen 2011; Pourhosseini 2007]. There are two electronic transitions in the far-UV spectrum that correspond to the α-helical polypeptides. The first one appears as the negative ~209 nm band and is described as the $n \rightarrow \pi^*$ transition, which occurs due to the large dipole moment besides the carbonyl bond whereas the second one appears as the negative 222 nm band and corresponds to the $\pi \rightarrow \pi^*$ transition next to the peptide bond [Ahmed 2004; Iwanga 1997; Nosrati 2009; Whitnore 2007; Wu 1981]. In addition, the positive peak at 196 nm as well as negative peaks at 209 and 222 nm in the insulin spectrum are believed to be due to the presence of phenylalanine, tyrosine and cysteine amino acids, respectively [Ahmed 2004; Nosrati 2009; Iwanga 1997]. Some previously reported data suggest that the positive band below 200 nm might be due to the contributions of phenylalanine residues transitions [Ettinger 1971]. Moreover, the appearance of positive extremum at ~196 nm in the CD spectrum of insulin has also been associated with the strong contributions originating from the β-conformation [Ettinger 1971]. The presence of negative band at ~200 nm, however, refers to the disulfide bonds between cysteine amino acids residues whereas the negative band at ~225 nm corresponds to the tyrosine residues as sketched in Figure 7.6 [Beychok 1964; Coleman 1968; Ettinger 1971]. Based on our CD analysis, it can be suggested that

the positive extremum at 196 nm might be due to either presence of phenylalanine residues or β-conformation and negative band at 209 nm might be due to the three disulfide bonds between cysteine-cysteine amino acids of insulin's A and B chains (Figure 7.6). While the peak at 222 nm could refer to the tyrosine residues present in the insulin structure (Figure 7.6). Hence, any changes occurring in the insulin's secondary structure upon increasing PEG content in the vesicles will be shown as changes in the CD spectra intensity in between the two wavelengths from ~195 to 250 nm.

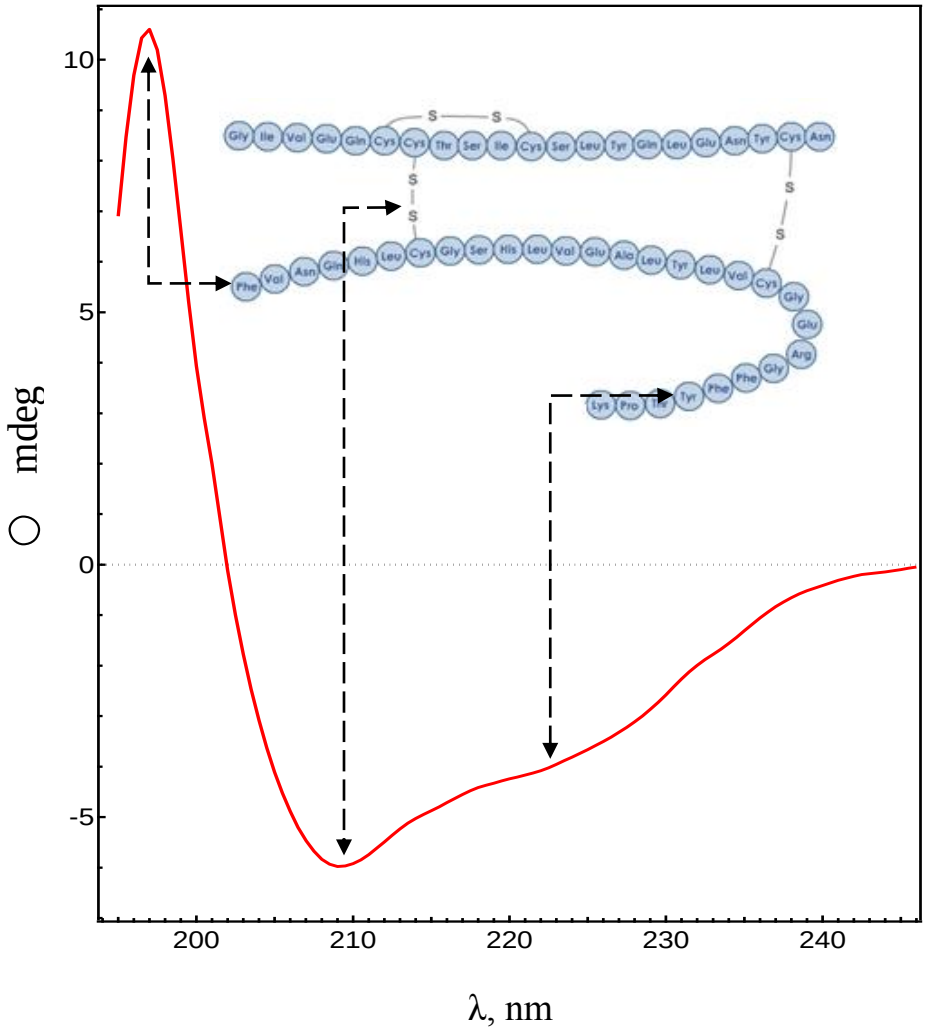


**Figure 7.6:** Far-UV CD spectrum of native insulin in PBS, pH~7.4 at 20 ˚C. The positive band at 196 nm with negative bands at 222 nm and 209 nm show typical feature of α-helical structure of insulin. The positive peak at 196 nm refers to the phenylalanine or β-conformation contributions. The negative peak at 209 nm corresponds to the three disulfide bonds between cysteine-cysteine amino acids whereas the negative peak at 222 nm refers to the tyrosine residues present in the insulin structure.

### 7.2.3 Monitoring Changes in the Secondary Structure of Insulin upon Interactions with DPPE-Succinyl/DPPE-PEG2000 Membrane (SUVs) by CD

The far-UV CD spectra of native insulin and upon interactions with pure DPPE-Succinyl and DPPE-Succinyl/DPPE-PEG2000 SUVs were collected in PBS at 20 °C (Figure 7.7). Black dashed line in the figure displays the CD spectrum of native insulin as a reference whereas the other ones refer to the insulin spectra in the presence of SUVs. Interactions of insulin with pure DPPE-Succinyl and mixed DPPE-Succinyl/DPPE-PEG2000 SUVs, within the two hours of interactions, caused noticeable changes in the CD spectra. A relative shift and broadening of the insulin's CD spectra was observed in the presence of SUVs (Figure 7.7). Furthermore, a decrease in the mean residue ellipticity, [θ], at the positive band of 196 nm as well as both negative bands centering at 209 and 222 nm, was also observed in the presence of SUVs (Figure 7.7). It can be seen from the figure that the intensity of the positive peak centering at 196 nm for insulin with vesicles of pure DPPE-Succinyl and SUVs containing 1 mol% PEG decreased as compared to the native insulin spectrum. Moreover, the negative peak at 209 nm shifted to 205 nm whereas the band at 222 nm decreased in the magnitude in the presence of either DPPE-Succinyl or 1 mol% PEG containing SUVs. A shift of the minimum band at 209 nm can account for the increase in random coil in the insulin structure [Bouchard 2000]. This can also be correlated with the CD spectrum of polypeptide in Figure 7.3 where a shift in the α–helix (209 nm) band would fall within the range of random coil structure. Furthermore, the loss of intensity of the 222 nm peak can be attributed to a reduction in the α–helix in the insulin structure [Bouchard 2000]. However, upon increasing PEG content (3, 6 and 9 mol %) in the SUVs, the intensities of all three bands at ~196, 209 and 222 nm

approached the CD spectrum of native insulin. This may suggest that insulin monomer needs only a little adjustment in its conformation in order to penetrate the SUVs with higher PEG content as opposed to the ones containing lower PEG contents. Most importantly, the CD spectra of insulin with all kinds of SUVs showed a considerable α-helix (secondary structure) throughout the curve indicating that only a slight change in insulin's conformation might occur during the interactions [Ahmed 2004]. This slight adjustment in the conformation, however, possibly favors the insertion and subsequently the process of accumulation in the membrane, which was also seen in insulin/monolayer studies for all the monolayers (Figure 6.1 – 6.12) [Gorbenko 2006; Grudzielanek 2007].

Analyzing the CD spectra in terms of estimating the percentage of α-helix (secondary structure) can provide an even better explanation of the changes occurring in the insulin molecule with increasing PEG content in SUVs. Percentage of α-helix can be calculated as described by Seelig et al. using equation below [Seelig 2000],

$$f_h = \frac{[\theta]_{222}}{\theta_h^n} \times 100\,\% \quad \text{---------- 7.1}$$

where [θ] is the mean residue ellipticity measured at 222 nm, in units of degrees (deg) $cm^2$ $dmol^{-1}$, and can be calculated by equation, described by Sreerama et al., below [Sreerama 2004],

$$[\theta] = 100\theta / Cl \quad \text{---------- 7.2}$$

where *C* is the molar concentration, *l* is the pathlength in (cm) of the cuvette, and θ is the ellipticity which can be directly taken from the curve in Figure 7.7. Molar ellipticity can either be expressed as deg.$M^{-1}$.$m^{-1}$ or as deg.$cm^2$.$dmole^{-1}$, and these units are equivalent. $\theta_h^n$ in equation (1) represents the maximum absorption of an α-helix with n amino acid residues and can be calculated by equation shown by Seelig et al. as follows.

$$\theta_h^n = (1 - k/n)\theta_h^\infty \quad \text{---------- 7.3}$$

Where *k* shows the wavelength-dependent constant ($k_{222}$ = 2.57), $\theta_h^\infty$ depicts the maximum ellipticity of an α-helix with infinite length of -39,000 deg $cm^2$ $dmol^{-1}$, and n represents the number of amino acid residues in the α-helix portion of the protein, which is 22 for insulin [Seelig 2000; Yan 2003]. The values for percentage of α-helix, as summarized in Table 7.1, were calculated from CD spectra in Figure 7.7 by using equations 7.1 – 7.3 for insulin after 2 h interactions time with pure DPPE-Succinyl and mixed DPPE-Succinyl/DPPE-PEG2000 vesicles. As can be seen from the Table, the α-helical content is about 32% for native insulin monomer in PBS, which is in good agreement with previously published reports [Ettinger 1971; Pocker 1980; Rawitch 1980 ; Sadhale 1999; Stretton 2002]. The change in α-helical conformation of insulin varies depending on the PEG content in the vesicles. As can be seen from table 7.1, the α-helical content of insulin in the presence of pure DPPE-Succinyl and binary mixtures containing 1 mol% PEG SUVs are 24.1% and 22.8% respectively, which increased to 27% in the presence of SUVs containing 9 mol% PEG. Most importantly, the change in α-helical

conformation of insulin does not vary significantly upon interacting with SUVs from pure to binary mixtures DPPE-Succinyl/DPPE-PEG2000 containing 9 mol% (Table 7.1). This correlates well with our insulin-monolayer studies where the insulin penetration area, $A_p$, remains almost unchanged of about 1.84 ± 0.07 $nm^2$, regardless of the PEG content. Hence, it can be suggested that the conformation of insulin does not change significantly upon interacting with the pure DPPE-Succinyl and DPPE-Succinyl/DPPE-PEG2000 membrane vesicles.

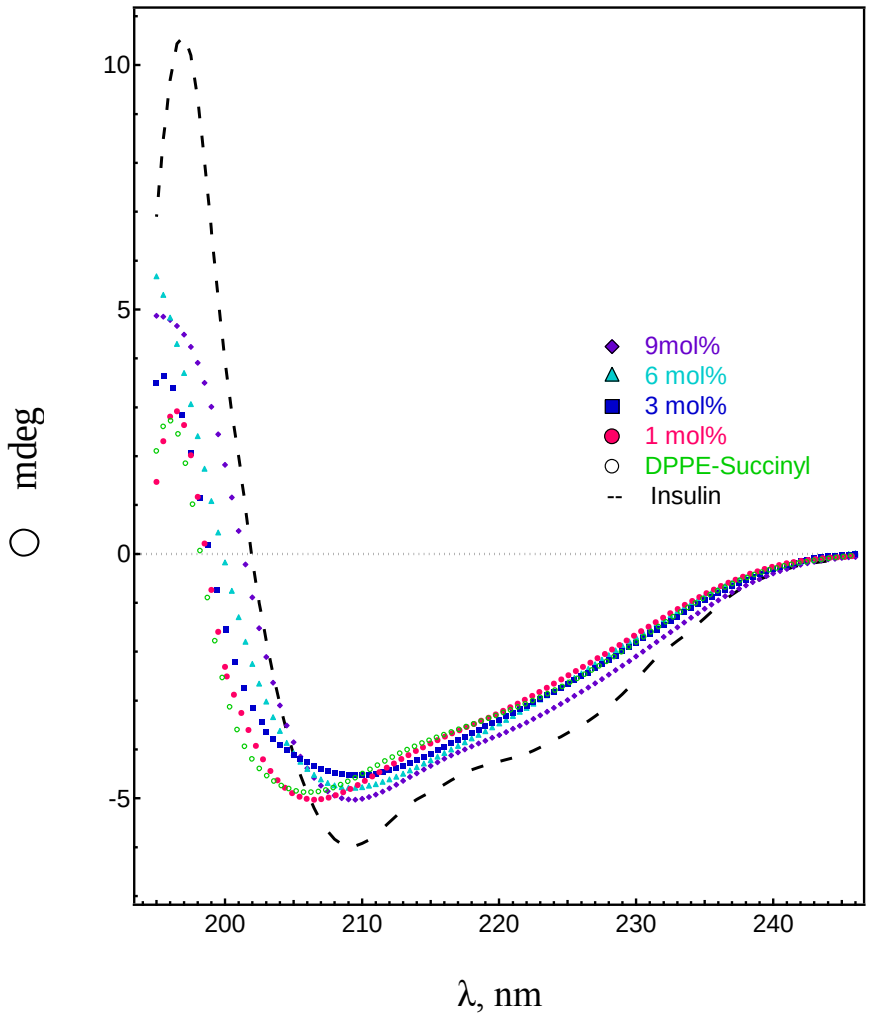


**Figure 7.7:** Far-UV CD spectra beginning from (♦) 9 mol% (▲) 6 mol%, (■) 3 mol%, (●) 1 mol%, (○) DPPE-Succinyl and (--) the native insulin interacting with DPPE-Succinyl/DPPE-PEG2000 vesicles in PBS. Negative bands at 222 nm and 209 nm show typical feature of α-helical structure. T = 20 ˚C.

**Table 7.1**: Changes in the α-helical structure content of insulin due to PEG increment in vesicles

| Mixtures | Vesicles Present | Helix insulin (%) |
|---|---|---|
| Native Insulin | No | 32 ± 3 |
| Pure DPPE-Succinyl | Yes | 24.1 ± 2 |
| 1 mol% | Yes | 22.8 ± 2 |
| 3 mol% | Yes | 24.4 ± 2 |
| 6 mol% | Yes | 25.1 ± 1 |
| 9 mol% | Yes | 27.0 ± 2 |

## 7.3 Conclusion

Analysis of insulin interactions with pure DPPE-Succinyl and DPPE-Succinyl/DPPE-PEG2000 membranes containing 1 – 9 mol% PEG revealed that upon interaction with insulin, the size of SUVs expands. The expansion of the vesicles might be due to the steric repulsion and redistribution of the PEG chain volume upon the compression exerted by insulin. CD spectroscopy results have revealed that insulin inserts in model membranes as a monomer with a slight decrease in the helical content but with minimal changes in its conformation. Our findings suggest that the percentage of α–helical content of insulin varies depending on the amount of PEG content present in the model membranes but the difference is not big. This is in good agreement with our insulin-monolayer interaction studies where the insulin penetration area has been found to be almost the same at about $1.84 \pm 0.07$ $nm^2$ for all the model membranes.

**7.4 References**


Ahmed, A.; Uversky, V. N.; Hong, D.; Fink, A. L. *J. Bio. Chem.* **2005**, *280 (52)*, 42669.

Ahmed, A.; Millets, I. S.; Doniach, S.; Uversky, V. N. ; Fink, A. L. *Bio. Chem.* **2004**, *279(15)*, 14999.

Beychok, S.; Fasman, G. D. *Bio. Chem.* **1964**, *3*, 1675.

Birdi, K. S. *Journal of Coll. and Inter. Sci.* **1976**, *57(2)*, 228.

Bocian, W.; Sitkowski, J.; Bednarek, E.; Tarnowska, A.; Kawecki, R.; Kozerski, L.; *J. Biomol. NMR.* **2008**, *40(1)*, 55.

Boisselier, E.; Calvez, P.; Demers, E.; Cantin, L.; Salesse, C. *Langmuir* **2012**, *28*, 9680.

Bouchard, M.; Zurdo, J,; Nettleton, E. J.; Dobson, C. M.; Robinson, C. V. *Pro. Sci.* **2000**, *9*, 1960.

Coleman, D. L.; Blout, E. R. *J. Am. Chem. Soc.* **1968**, *90*, 2405.

Ettinger, M. J.; Timasheff, S. N. *Biochemistry* **1971**, *10(5)*, 824.

Goldman, J., and Carpenter, F. H. C. *Biochemistry* **1974**, *13*, 4567.

Gorbenko, G. P.; Kinnunen, P. K. J. *Chem. and Phys. Lip.* **2006**, *141*, 72.

Greenfield, N. J. *Nat. Protoc*. **2006**, *1(6)*, 2876.

Grudzielanek, S.; Smirnovas, V.; Winter, R. *Chem. and Phys. Lip.* **2007**, *149*, 28.

Henry, M.; Dupont-Gillain, C.; Bertrand, P. *Langmuir* **2008**, *24*, 458.

Hong, Y.; Meng, L.; Chen, S.; Leung, C. W. T.; Da, L.-T., Faisal, M.; Silva, D-A.; Liu, J.; Lam, J. W. Y. ; Huang, X.; Tang, B. Z. *J. Am. Chem. Soc.* **2012**, *134*, 1680.

Iwanga, K.;Ono, S,; Narioka, K.; Morimoto, K,; Kakemi, M.; Yamashita, Sh,; Nango, M.; Oku, N. *Inter. J. Pharm.* **1997**, *157*, 73.

Jackson, M.; Mantsch, H. M. *Crit. Rev. Biochem. and Mol. Bio.* **1995**, *30(2)*, 95.

Jeffrey, P. D., and Coates, J. H. *Biochim. Biophys. Acta* **1965**, *109, 551*.

Jorgensen, L., Bennedsen, P., Hoffmann, S. V., Krogh, R. L., Pinholt, C., Groenning, M., Hostrup, S., Bukrinsky, J. T. *Eur. J. Pharm. Sci.* **2011**, *42*, 509.

Jesorka, A.; Orwar, O. *Ann. Rev. Anal. Chem.* **2008**, *1*, 801.

Liu, W.; Johnson, S.; Micic, M.; Orbulescu, J.; Whyte, J.; Garcia, ;A. R.; Nosrati, N., Masters Dissertations, *York University* **2009**.

Nylander, T. In *Biopolymers at Interfaces, 2nd ed., New York* **2003**.

Pekar, A. H., and Frank, B. H. *Biochemistry* **1972**, *11, 4013.*

Perez-Lopez, S.; Blanco-Vila, N. M.; Vila-Romeu, N. *J. Phys. Chem. B* **2011**, *115*, 9387.

Pocker, Y.; Biswas, S. B. *Biochemistry* **1980**, *19*, 5043.

Pourhosseini, P. S.; Saboury, A. A.; Najafi, F.; Sarbolouki, M. N. *Biochim. Bioph. Acta* **2007**, *1774*, 1274.

Rawitch, A. B.; Moore, W. V. *Int. J. Biochem.* **1980**, *11*, 357.

Sadhale, Y.; Shah, J. C. *Inter. J. Pharm.* **1999**, *191*, 51.

Seelig, A; Blatter, X. L.; Frentzel, A.; Isenberg, G. *J. Bio. Chem.* **2000**, *275(24)*, 17954.

Solomon, I.; Lever, A. P. *Wiley* **2006**, *1*, 78.

Sreerama, N.; Woody, R. *Methods in Enzymology* **2004**, *383*, 318.

Stretton, A. O. W. *Genetics* **2002**, *162*, 527.

Tamm, L.; Tatulian, S. *Quar. Rev. Biophys.* **1997**, *30(4)*, 365.

Whitnore, L.; Wallace, B. A. *Biopolymers* **2007**, *89(5)*, 392.

Wu, C.; Yang, J. T. *Biochim. Biophys. Acta.* **1981**, *66*, 285.

Yan, H.; Guo, Z-Y.; Gong, X-W.; Xi, D.; Feng, Y-M. *Protein Science* **2003**, *12(4)*, 768.

Zlatica, K.;Dhathathreyan, A; Mabius, D. *Coll. and Sur.***1998**, *33*, 11.

## Summary

In this work, different approaches were adapted to examine the negatively charged PEG-grafted phospholipid membrane models. First, the miscibility, conformational and phase behavior of mixed DPPE-Succinyl/DPPE-PEG2000 were investigated in the aqueous media of physiological relevance, PBS pH ~7.4. In the second approach, the effect of non-specific insulin interactions on the binary mixtures membrane models of DPPE-Succinyl and DPPE-PEG2000 was examined. Further, the effect of non-specific insulin interactions with membrane on the insulin secondary structure was also studied.

The Langmuir technique and EFM studies have demonstrated an intricate behavior for DPPE-Succinyl on water, PBS and each of PBS electrolytes. PBS and each of its individual constituents have shown a remarkable effect on the phase behavior of DPPE-Succinyl monolayers. Importantly, $Na^+$ and $Cl^-$ containing subphases have shown to cause the strongest effect on the monolayers, plausibly due to $Na^+$ and $Cl^-$ ions penetrating the head group region of the DPPE-Succinyl molecule.

Aqueous media of physiological relevance, PBS, has also shown to cause significant effect on the phase and conformational behavior of binary mixtures of DPPE-Succinyl and DPPE-PEG2000. The $\pi$ – $A$ isotherms, excess area parameters, and EFM imaging studies have also revealed a non-ideal miscibility in the mixed monolayers on PBS. Immiscible behavior of binary mixtures containing 1 – 9 mol% PEG as well as prevention of a continuous LC phase formation might be due to some unfavorable interactions between both phospholipids induced by PBS. This suggests that on PBS, grafted PEG2000 chains in the mixed monolayers perhaps undergo only a

partial conformational transition to a quasi-3D conformation, due to the interactions of $Na^+$ and $K^+$ electrolytes penetrating the head group region of the phospholipids.

In the second investigation, the non-specific insulin/membrane interactions have revealed that insulin indeed penetrates and expands the area of membrane models (monolayers and SUVs) of DPPE-Succinyl as well as binary mixtures of DPPE-Succinyl and DPPE-PEG2000. The expansion of the vesicles might be due to the steric repulsion and redistribution of the PEG chain volume upon the compression exerted by insulin. Incorporation of PEG, however, does not seem to suppress the penetration mechanism of insulin/monolayer interactions since the insulin penetration area remains $1.84 \pm 0.07$ $nm^2$ for all monolayers regardless of the PEG content. Furthermore, CD spectroscopy results have illustrated that insulin inserts in the model membranes as a monomer with a slight decrease in the helical content but with minimal changes in its secondary structure.

# Future Directions

In this work, the phase behavior, lateral organization, compressibility and the morphology of pure and mixed monolayers as well as their interactions with insulin have been demonstrated in aqueous media of physiological relevance. However, further investigations on surface characterization of lipid-lipid and lipid-protein interactions on air/solid interface using Atomic Force Microscopy (AFM) will be very helpful to better comprehend the lateral organization, structural and morphological properties of phospholipid membranes at nanoscale. These findings would prove to play a significant role in both fundamental and applied research.

It was also demonstrated that each salt of phosphate buffered saline (PBS) had a distinctive effect on the DPPE-Succinyl monolayer. Based on these findings, it would be beneficial to further investigate the effect of each individual PBS constituent on the miscibility, phase transition and conformational behavior of binary mixtures of DPPE-Succinyl and DPPE-PEG2000.

As suggested by our previous research group work that a change in the temperature has a significant impact on the miscibility and phase transitional behavior of PEG-grafted monolayers bearing different aliphatic chain length and headgroups [Tanwir 2012; Nosrati 2010; Abdelsyed 2007]. Hence, studying the miscibility, phase and conformational behavior of pure DPPE-Succinyl and mixed DPPE-Succinyl and DPPE-PEG2000 monolayers at temperature of physiological relevance, 37 *°C*, may lead to gain insight to develop efficient and controlled membrane-mimetic surfaces for numerous biomedical applications.

As demonstrated in our study that compressibility plots are very sensitive to transitions, particularly for PEG conformation transitions. Hence, the effect of insulin penetration on the lateral compressibility of binary mixture of DPPE-Succinyl and DPPE-PEG2000 can also be studied using compressibility analysis. A proposed plot is shown in the schematic below to illustrate the compressibility for different transitions with respect to lateral surface pressure. This may aid in understanding the PEG conformational behavior upon interactions with insulin.

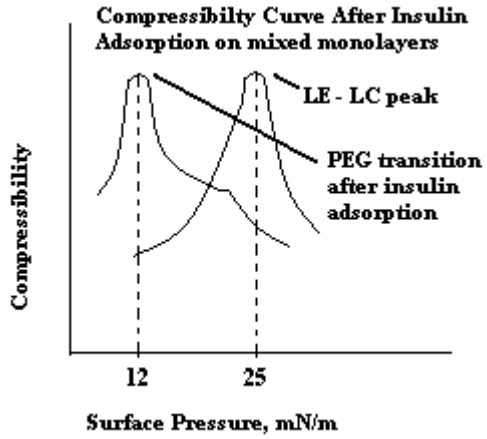


Most importantly, the anionic nature of DPPE-Succinyl molecule's head group can be of great interest for targeted therapeutic delivery systems due to the immobilization capacity of various ligands. This unique approach can thus be used to modify the DPPE-Succinyl headgroups with antibodies and/or ligands of interest and study their phase behavior at aqueous media and temperature of physiological relevance.

**References:**

Abdelsyed, H. Masters Dissertation, *York University* **2007**.

Nosrati, N. Masters Dissertation, *York University* **2010.**

Tanwir, K.; Shahid, M. N.; Thomas, A.; Tsoukanova, V. *Langmuir* **2012**, *28(39)*, 14000-14009.